ENGINEERING OF OLIGOPEPTIDE-MODIFIED SURFACE FOR METAL ION ADSORPTION AND SENSING APPLICATIONS

BI XINYAN

NATIONAL UNIVERSITY OF SINGAPORE

2009

ENGINEERING OF OLIGOPEPTIDE-MODIFIED SURFACE FOR METAL ION ADSORPTION AND SENSING APPLICATIONS

BI XINYAN

(*M. Eng.*)

A THESIS SUBMITTED

FOR THE DEGREE OF DOCTOR OF PHILOSOPHY

DEPARTMENT OF CHEMICAL AND BIOMOLECULAR ENGINEERING

NATIONAL UNIVERSITY OF SINGAPORE

ACKNOWLEDGEMENTS

First of all, I would like to thank my parents and my husband for their infinite love and support. They have been the source of courage when I was down and the reason why I cannot give up.

I am especially grateful to my supervisor, Dr. Kun-Lin Yang, for his guidance, patience, continuous encouragement, invaluable suggestions, and considerable understanding throughout the period of this project. In addition to giving me the interesting and challenging research projects, he gave me freedom to express my ideas and instructed me how to write scientific papers and PhD thesis. His enthusiasm, sincerity, and dedication on scientific research have greatly impressed me and will benefit me in my future career.

I would also like to thank Dr. Ajay Agarwal and the members of Institute of Microelectronics (A*STAR) for their strong supports in silicon nanowire experiments. The research scholarship funded by NUS is also gratefully acknowledged.

I want to give many thanks to all people in our group: Deny, Siok Lian, Laura, Vera, Xu Huan, Yadong, Maricar, Chih Hsin, Zhang Wei, and Xiaokang (in the order that I got to know them). I not only obtained lots of their help but also shared fun and joy with them.

I would like to take this opportunity to acknowledge Prof. Chen Shing Bor and Dr. Yung Lin-Yue Lanry, the members of my oral qualification examination committee, for their inspired suggestions and comments on this topic, together with my thesis

reviewers for their time, assistance and examination on this thesis.

Acknowledgement also goes to Mr. Boey, Ms. Lee Chai Keng, Dr. Yuan Zeliang, Dr. Rajarathnam D., Ms. Chew Su Mei Novel, Ms. Goh Mei Ling Evelyn for their kind supports in my experiments.

Finally, I would like to thank Chinese government for giving me the award for outstanding self-financed students abroad in 2008. I would also like to appreciate the people who have contributed either directly or indirectly to this thesis work but have not been mentioned above.

TABLE OF CONTENT

SUMMARY

Surfaces presenting unique functionalities have found tremendous applications, such as separation and sensor design. Unlike traditional self-assembled monolayers (SAMs) offering limited choices, the surfaces modified with custom-made oligopeptides are versatile, because the sequences of oligopeptides can be tailored for binding metal ions and biomolecules with high specificity. First, past studies have demonstrated that oligopeptides with particular side groups are able to complex metal ions with high sensitivity and selectivity, hence, silica gel modified with Gly-Gly-Gly or Gly-Gly-His can adsorb Cu^{2+} with high selectivity, even in the presence of Zn^{2+}. This principle was also applied to modify silicon nanowire (SiNW) to create a sensitive Cu^{2+} sensor. Secondly, it is known that to fabricate metal ion sensors, the oligopeptides with specific sequences need to be immobilized on the surface with a well-defined orientation to keep their functions. In this thesis, we demonstrated that an N-terminal cysteine label lead to well-oriented immobilized oligopeptides. Thus, SiNWs modified with a Pb^{2+}-sensitive oligopeptide can be used to detect Pb^{2+} in the presence of Cu^{2+}. Finally, we exploited interactions between liquid crystals (LCs) and immobilized oligopeptide for creating real-time enzyme biosensors. The detection principle is based on the changes of the anchoring of LCs supported on surfaces, because the anchoring of LCs can be easily affected by the chemical compositions and molecular-level structures of surfaces. Our results show that the enzymatic cleavages of oligopeptide substrates can lead to changes in the optical appearance of LCs.

Moreover, because anchoring of LCs is controlled by a fine scale of energetics, it is possible to couple the orientations of LCs to surfactants, lipids, proteins, and synthetic polymers adsorbed at the aqueous/LC interface. Based on this principle, we sought to design a new LC based pH sensor and study the feasibility of using the LC based pH sensor for monitoring H^+ released from enzymatic reactions in real time. These new principles may offer tremendous opportunities for developing next-generation biosensors.

LIST OF TABLES

LIST OF FIGURES

LIST OF SCHEMES

LIST OF SYMBOLS

SAMs	self-assembled monolayers
3D	three-dimensional
SiNWs	silicon nanowires
FETs	field-effect transistors
LCs	liquid crystals
MES	4-morpholinoethanesulfonic acid
APES	3-aminopropyltriethoxysilane
DMOAP	*N*,*N*-dimethyl-n-octadecyl-3-aminopropyltrimethoxysilyl chloride
TEA	triethoxysilane aldehyde
5CB	4-cyano-4’-pentylbiphenyl
PEI	poly(ethylene imine)
PBA	4’-pentyl-biphenyl-4-carboxylic acid
PBS	phosphate buffer saline
SDS	sodium dodecyl sulfate
FITC	fluorescein isothiocyanate
FTIR	Fourier Transformation Infrared
HATR	horizontal attenuated total reflectance
MCT	mercury-cadmium-telluride
XPS	X-ray photoelectron spectroscopy
QCM	quartz crystal microbalance

E (%)	copper adsorption percentage
Q	adsorption capacity
G%	percentage of change in conductance
β	overall equilibrium constant
K_d	dissociation constant
D	diffusion coefficient
r_0	generation rate
k_{cat}	catalytic rate constant
K_m	Michaelis constant

CHAPTER 1
INTRODUCTION

Surfaces presenting unique functionalities have tremendous applications in separation and sensor design. To prepare such functional surfaces, one of the most popular methods is by using self-assembled monolayers (SAMs) (Love et al., 2005). Currently, research of SAMs is focused on self-assembly of organothiols on gold surfaces or organosilanes on silica surfaces. Although SAMs have a number of useful properties, there are only a limited number of organothiols and organosilanes available for preparing SAMs with desired functionalities. Oligopeptides, on the other hand, are more versatile. For a simple oligopeptide with 10 amino acid units, the number of available sequence will be 20^{10} (from 20 naturally occurring amino acids). By rearranging the sequence of amino acids, one can tailor the properties of oligopeptides to prepare wide varieties of molecular receptors for different applications. In addition, oligopeptides have many interesting features: they can be used to mimic biological activities of proteins, they are easy to synthesize and manipulate, and they are usually highly stable and inexpensive. Therefore, modifying surfaces with oligopeptides has attracted considerable attention in a number of fields such as bioassays, biosensors, and metal ion sensing applications.

1.1 Adsorption of Metal Ions

The presence of heavy metal ions in the environment is a major concern due to their high toxicity. One of the most popular methods for removing metal ions is based on

the adsorption of metal ions onto a sorbent, which is usually modified with some functional groups (ligands) to form complexes with the metal ions in solution. In the past, many functional groups such as amine, carboxylate, thiol, hydroxyl, ether, and nitrile, have been used as ligands to adsorb metal ions (Jal et al., 2004). However, these ligands can complex many different metal ions without much selectivity. In contrast, oligopeptides readily form complexes with metal ions through terminal primary amine, carboxylate groups, amide groups along the peptide backbones, and various side groups (Sigel et al, 1982; Yang et al., 2001a,b). Past studies have reported that oligopeptides with particular side groups are able to complex metal ions with high sensitivity and selectivity. One of such example is Gly-Gly-His, which is a famous copper-binding oligopeptide. Other well-known examples include His-Ser-Gln-Lys-Val-Phe and Asp-Arg-Val- Tyr-Ile-His-Pro-Phe-His-Leu, which have high specificity for binding Cd^{2+} and Pb^{2+}, respectively (Chow et al., 2005a). These examples suggest that one can design unique oligopeptide sequences for complexing metal ions with high specificity.

Unfortunately, when ligands are immobilized on surfaces, they often experience strong steric hindrance, which may affect their binding capabilities. To avoid the steric hindrance, appropriate distance must be maintained between two ligands. A powerful technique to control the distance between two ligands is molecular imprinting. Up to date, most of the molecular imprinting techniques are based on three-dimensional (3D) polymer networks, where the template molecules bound to functional monomers are copolymerized to form highly cross-linked polymers. After the removal of the

templates, cavities which match the molecular structure of target analytes are formed (Wulff G., 1995). 3D imprinting methods have been used to selectively remove heavy metal ions in the presence of other metal ions. However, these molecularly imprinted materials have poor site accessibility because the templates are embedded deep inside the polymer matrices. In contrast, in 2D imprinting method, the ligands are self-assembled on the surface of an inorganic matrix in the presence of metal ions (templates) (Liu et al., 1998). After the removal of the templates, the resulting cavities on the monolayers can be used to re-adsorb the metal ions. Although the 2D imprinting method has been applied in many systems to adsorb metal ions, the choice of surface modifying agents is often limited to organosilanes containing primary amine, secondary amine or thiol.

Because oligopeptides are versatile ligands for complexing metal ions with good selectivity, in this thesis, we use the 2D imprinting method to create functional surfaces modified with oligopeptides for the adsorption of metal ions. Both complexation capability and specificity for the target metal ions are increased significantly. This technique may shed light on the complexation of metal ions with immobilized peptides on surfaces and provides a useful guideline for increasing the sensitivity of metal ion sensors by using ion-selective peptides.

1.2 Metal Ion Sensors

The detection and quantification of metal ions in aqueous solutions is an important analytical problem. Although atomic adsorption spectrometry and inductively coupled

plasma mass spectrometry have been used to detect and quantify metal ions with high sensitivity, they are not real-time and the instruments are usually expensive. Therefore, the development of a real-time metal ion sensor has attracted considerable interest.

Generally speaking, a metal ion sensor consists of two major components: a recognition element that binds the metal ion specifically and a transducer which transduces metal-ion binding events into measurable signals. Because of the highly specific complexation between oligopeptides and metal ions, oligopeptides are ideal recognition elements. For example, Chow et al. modified the gold electrodes with Asp-Arg-Val-Tyr-Ile-His-Pro-Phe-His-Leu to detect Pb^{2+} with a detection limit of 1 nM (Chow et al., 2005a). They also employed Gly-Gly-His-modified gold electrodes to detect Cu^{2+}. In these studies, the oligopeptide-modified electrodes were coupled to cyclic voltammetry or Osteryoung square wave voltammetry to transduce the oligopeptide-metal binding events (Chow et al., 2006). Although the electrodes can detect metal ions with high sensitivity and selectivity, they are difficult to be miniaturized. In contrast, recent studies have reported novel electrical properties of silicon nanowires (SiNWs) and their applications as nanometer-scale sensors (Cui, et. al., 2001a; Li et al., 2004). The SiNWs-based sensors have various advantages such as biocompatibility, vast surface-to-bulk ratio, tunable electrical properties, and fast response. In addition, an attractive feature of the SiNW-based sensors is that the chemical binding can be monitored directly by using the changes in conductance or related electrical properties. Until now, SiNWs have been used for the detection of metal ions, small molecules (e.g. Adenosine triphosphate (ATP)), viruses, cells, DNA,

and proteins.

In the past, metal ions were detected by using calmodulin-modified SiNWs (Cui et al., 2001a). Although the SiNWs showed high sensitivity and specificity for Ca^{2+}, the stability of protein may limit its application. To overcome the stability issue, we explore the concept of using SiNWs modified with oligopeptide ligands to detect metal ions in this thesis. Because metal ions are positively charged, the binding of metal ions on the modified SiNWs act as positive gate potential and thus result in changes in the conductance of SiNWs, which can be measured and correlated with the concentration of metal ions.

1.3 Oligopeptides Immobilization

One common element in the applications of oligopeptide-modified surfaces for the adsorption of metal ions and the fabrication of metal ion sensors is that oligopeptides with specific sequences need to be immobilized on the surface with a well-defined orientation to keep their functions. However, controlling the orientations of immobilized oligopeptides remains a big challenge because most immobilization strategies rely on the crosslinking of reactive residues, such as lysine or cysteine, in a nonspecific manner. In contrast, several reactions, such as Staudinger ligation or Diels-Alder reaction can be used to immobilize oligopeptides with high specificity (Soellner et al., 2006; Houseman et al., 2002). However, these immobilization strategies require labeling oligopeptides with an unnatural moiety, such as phosphinothioester or cyclopentadiene. Meanwhile, some other methods only require

natural amino acid labels, such as histidine or cysteine, because the former is able to complex with nickel ions and the latter can form an Au-S bond on a gold surface (Zhu et al., 2001). The use of natural amino acids is advantageous because additional amino acids can be introduced into target proteins or peptides through genetic engineering. However, these methods are not site-specific since any histidine or cysteine residues, regardless of their positions in the oligopeptides, can bind nickel ions or react with gold. Because understanding how to control the orientations of oligopeptides is an important step to prepare oligopeptide-modified surfaces for various applications, an objective of this thesis is to study the potential utility of a highly specific reaction between aldehyde and N-terminal cysteine for oligopeptide immobilization. When an oligopeptide with an N-terminal cysteine label and multiple lysines is immobilized on the aldehyde-terminated surface, the N-terminal cysteine quickly reacts with surface aldehydes to form a stable thiazolidine ring, which prevents lysines from reacting with aldehydes. This immobilization strategy can lead to well-defined orientations of immobilized oligopeptide.

1.4 Biosensors for Monitoring Enzymatic Activities

Protease enzymes, which can selectively cleave peptide bonds in polypeptides or proteins, are abundant in nature and essential for cellular function and viability. Because oligopeptides with well-defined sequences and lengths can be custom-made by using solid-phase synthesis, immobilized oligopeptides on solid surfaces are often used as protease substrates.

When the immobilized oligopeptides are exposed to a solution containing proteases, they are recognized and cleaved by proteases. Afterwards, the surfaces can be detected by using several analytical methods, including Matrix-Assisted Laser Desorption/Ionization Time-of-Flight (MALDI-TOF) mass spectrometry, liquid chromatography-mass spectrometry (LC-MS), surface plasmon resonance (SPR) and quartz crystal microbalance (QCM) (Karlsson et al., 2000; Rich et al., 2000). Although these methods are highly sensitive, they usually require expensive instrumentations and trained personnel. Alternatively, several past studies have demonstrated that liquid crystals (LCs) can be used to image chemical species adsorbed on surfaces (Gupta et al., 1998; Shah et al., 2001). The detection principle is based on the changes of the anchoring of LCs supported on surfaces, because the anchoring of LCs can be easily affected by the chemical compositions and molecular-level structures of surfaces. Therefore, subtle changes caused by adsorbed molecules can lead to different orientations of LCs near the surface, and that can be amplified rapidly through the bulk of LCs up to 100 μm away. In addition, the orientational changes of LCs can be easily observed under crossed polarizers with the naked eye as different optical textures.

Recently, Park et al. reported a LC-based sensor to monitor the protease activity of trypsin acting on an oligopeptide substrate (Ser-Asn-Lys-Tyr-Arg-Ile-Asp-Glu-Ala-Asn-Asn-Lys-Ala-Tyr-Lys-Met-Leu) (Park et al., 2008), which was covalently immobilized at an aqueous/LC interface. It was found that when the oligopeptide was cleaved by trypsin, the optical textures of the LCs underneath changed from bright to

dark. Despite the promise of this method, the exact mechanism that leads to the disruption of LCs was not fully understood. As reported by the authors, cleavage of some well-known trypsin substrates, such as poly-lysine, did not cause any response in the LCs. Moreover, the sensor was built upon aqueous/LC, which precluded the use of microarray techniques for preparing a high density array with hundreds or thousands of oligopeptide probes. In this thesis, we create an oligopeptide microarray with oligopeptides having well-controlled orientations. By using trypsin or chymotrypsin as model proteases, we study the feasibility of uisng LCs to transduce the cleavage events into optical images. The LC-based protease assay opens up possibilities for detecting toxins such as botulinum neurotoxins.

Furthermore, because anchoring of LCs at the aqueous/LC interface is controlled by a fine scale of energetics (10^{-2} to10^{-3} mJ/m^2), it is possible to couple the orientations of LCs to surfactants, lipids, proteins, and synthetic polymers adsorbed at the aqueous/LC interface. Moreover, when these surfactants or polymers contain pH sensitive functional groups, orientations of LCs become sensitive to pH of the aqueous phase. For example, Kinsinger et al. (2007) designed a polymer-functionalized aqueous/LC interface (by conjugate addition of poly(ethylene imine) to *N*-[3-(dimethylamino)propyl] acrylamide) and obtained a LC sensor that responded reversibly to pH changes in the aqueous phase. They demonstrated that the pH-dependent changes in the orientation and optical appearance of LC arose from the changes in the ordering of the polymer at the interface. However, they only observed different optical appearance of LC at pH = 9.0 and 5.0. Thus, whether this system is

suitable for detecting very small pH changes is unclear. Moreover, the response time was very long (10 h). To address the need for detecting small pH changes and the issue of slow response time, we sought to design a new LC based pH sensor and study the feasibility of using the LC based pH sensor for monitoring H^+ released from enzymatic reactions in real time. The challenge is that because only a small amount of H^+ is released during an enzymatic reaction, it only causes a very small pH change in the bulk solution, especially when the buffer capacity is high. However, the small amount of H^+ still can lead to localized and temporal pH changes which can be detected by a highly sensitive LC based pH sensor with a good spatial resolution.

1.5 Research Objectives

The objectives of this thesis are four-fold.

1) To prevent the surface crowdedness and to provide a moderate surface density of oligopeptides (such that an oligopeptide-metal complex with the preferential tetragonal geometry can be formed on the surface), a 2D ion imprinting technique is employed. Briefly, the oligopeptides are immobilized on the surface in the presence of target metal ions (templates). **Chapter 3** reports a copper-imprinted sorbent by modifying the surface of silica gel with glycine, diglycine and triglycine with copper ion as the templates. The adsorption capacity and specificity for copper ions on the copper-imprinted and nonimprinted silica gel are compared. The conformational changes of immobilized triglycine during the immobilization procedure are investigated by using FTIR. In **Chapter 4**, we

compare the complexation properties of two copper-selective tripeptides, Gly-Gly-His and His-Gly-Gly. We also study whether the surface crowding effects of Gly-Gly-His-modified surface can be overcome by employing the 2D ion imprinting technique.

2) **Chapter 5** and **6** demonstrate the potential utility of oligopeptide-modified SiNWs as metal ion sensors. In **Chapter 5**, the surface of SiNWs is functionalized with a His-containing tripeptide, which serves as a copper sensitive layer. Because the complexation between copper ions and His-containing tripeptides leads to an increase in the SiNW conductance, copper ions can be detected through the changes in the conductance. In **Chapter 6**, we describe the preparation and applications of oligopeptide-modified SiNW arrays as multichannel metal ion sensors. Two different SiNW clusters are modified with Pb^{2+}-selective and Cu^{2+}-selective oligopeptide, respectively. Therefore, concentrations of Pb^{2+} and Cu^{2+} in aqueous solutions can be detected simultaneously and selectively in two different channels.

3) To keep the function of immobilized oligopeptides, immobilization of oligopeptides on surfaces with well-defined orientations is required. **Chapter 7** reports a strategy of using N-terminal cysteine labels for controlling the immobilization of oligopeptides on aldehyde-terminated surfaces through the formation of stable thiazolidine rings. Four oligopeptides, including Cys-Gly-Gly, Gly-Gly-Cys, Cys-Gly-Gly-Gly-Lys, and Cys-Ser-Asn-Lys-Tyr-Arg-Ile-Asp-Glu-

Ala-Asn-Asn-Lys-Ala-Tyr-Lys-Met-Leu, are employed to study the immobilization strategy. Subsequently, whether these oligopeptides are immobilized on the surface with well-defined orientations is evaluated by using ellipsometry, FTIR, and XPS, etc.

4) The final objective of this thesis is to develop a simple and sensitive LC-based biosensor for monitoring enzymatic activities. First of all, in **Chapter 8**, we determine the feasibility of using LC for optical detection of surface immobilized oligopeptides. It is hypothesized that when glycine oligomers with different molecular lengths are immobilized on the surface, they form monolayers with different thicknesses. As a result, the orientations of LC may be disturbed, which is dependent on the thickness. Because the cleavage of oligopeptides by protease may decrease the length of oligopeptides, the results obtained in **Chapter 8** is further exploited to develop a protease assay when immobilized oligopeptides are used as the substrate. Then, in **Chapter 9**, we create an oligopeptide microarray and immerse it in a protease solution. When a thin layer of LC is supported on the microarray, the oligopeptide cleavage by protease can be transduced into an optical image, which is easily observed by naked eye. This result provides an easy method for detecting toxins such as botulinum neurotoxins which are known to cleave proteins and affect the docking and fusing synaptic vesicles. Finally, **Chapter 10** reports a LC based sensor for real-time monitoring changes in local pH values near a solid surface and its application for monitoring activities of enzymes immobilized on the solid surface. As a proof of concept, the hydrolysis

of penicillin G by enzyme penicillinase, which is immobilized on a TEM copper grid, is monitored by using the system. This type of LC-based sensor may find utilities in high throughput screening of potential enzyme substrates and enzyme inhibitors.

CHAPTER 2
LITERATURE REVIEW

In this chapter, an overview of recent research and development is provided in adsorption of metal ions on oligopeptide-modified surfaces, immobilization of oligopeptides on surfaces, SiNWs based sensors and LCs-based optical sensors.

2.1 Interactions Between Metal Ions and Oligopeptides

2.1.1 Formation of oligopeptide-metal complex in solution

Of all the possible model systems involving metal ions and biological ligands, the interactions between metal ions and amino acids have been the longest and the most investigated. It is well-known that amino acid is a good ligand because it can coordinate with different transition metal ions and forms a 5-membered chelate ring (Burger et al., 1990) via the terminal amino and carboxylate groups. Besides these two groups, most of the essential amino acids contain side-chain groups. Generally, the side-chain groups of amino acids are classified into three categories based on their abilities to bind metal ions: (1) non-coordinating (Ala, Val, Leu, Ile, Phe, Trp), (2) weakly coordinating (Ser, Thr, Tyr, Lys, Arg, Asp, Glu, Asn, Gln, Met), and (3) strongly coordinating (His and Cys).

When the amino group of one amino acid reacts with the carboxylic acid group of another, an amide linkage (known as peptide bond) is formed. The resulting short oligomers are called oligopeptides and long polymers are called polypeptides or

proteins. With at least 20 naturally occurring amino acids combinations available, the number of peptides that can be synthesized by using simple amino acid is infinite. Therefore, peptides are versatile and effective ligands for binding metal ions (Sigel et al., 1982). However, the common terminal amino and carboxylate groups in peptides are too far from each other, and thus the steric hindrance exclude the formation of 5-membered chelate rings. On the other hand, it is obvious that carbonyl-O and amide-N in the peptide bond are also the potential donor atoms for binding with metal ions. Therefore, for the simplest oligopeptide, diglycine, at least four donor atoms (amino-N, carbonyl-O, amide-N, and carboxylate-O) are present. The general feature of the complex ability of diglycine is that the terminal amino group is the primary ligating group for various metal ions.

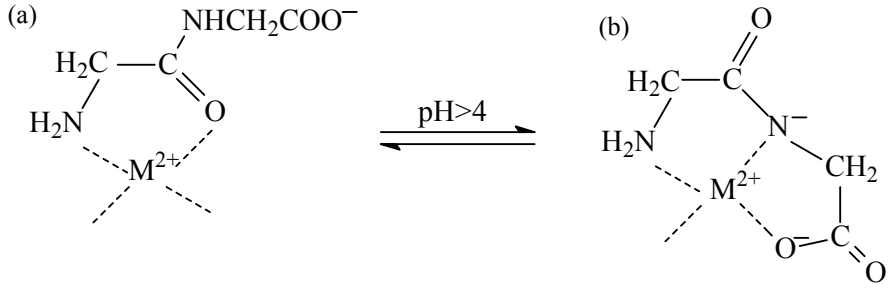

Figure 2.1 Complexation of metal ions to diglycine.

As shown in Figure 2.1a, via the coordination of the amino nitrogen and neighboring carbonyl oxygen, a 5-membered ring with moderate stability can be formed. As pH increases, some metal ions, such as Cu^{2+}, are able to deprotonate the amide nitrogen and thus coordination is accomplished by the possibility of the formation of a second 5-membered ring, with the participation of terminal carboxylate group, which results

in an enhanced stability of the complex (Figure 2.1b). It should be noted that the occurrence of this process highly depends on the nature of the metal ions, and only a few of them are able to deprotonated the amide- N.

Because the amide-N leads to significantly stronger binding metal ions than carboxylate-O (Sigel et al., 1982), the extending of diglycine to triglycine and tetraglycine will result in more stable complexes. For triglycine, the coordination occurs via amino-N, two deprotonated amide-N, and carboxylate-O, while copper complex of tetraglycine occurs via amino-N and three deprotonated amide-N.

One of the disadvantages of the complex between metal ions and oligopeptides through the terminal amino and carboxylate and amide groups is that it is nonselective. However, as mentioned above, the side-chain groups of amino acid contain the potential sites for the binding with metal ions. Therefore, the oligopeptides with different amino acid sequences may increase their specificity for particular metal ions. The first example was Gly-Gly-His (Gooding et al., 2001), known as copper binding oligopeptide. Because the imidazole moiety in His residue contains a pyridine-like nitrogen atom, it is a good ligand for metal ions. As shown in Figure 2.2, the complexation proceeds with the formation of three fused chelate rings and thus saturates the coordination site. However, the position of His residue in the oligopeptide motif is very important to keep the

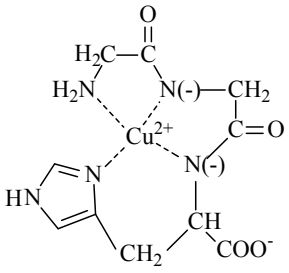

Figure 2.2 Structures of major copper complexes with Gly-Gly-His in aqueous solutions.

stability of the metal complexes. If the His residue is in the first or second position, there is more than 10-fold reduction in complex stability. This is because the imidazole-N can hinder the deprotonation of the amide-N. A second interesting example is the specific interaction between Cd^{2+} and a hexapeptide, His-Ser-Gln-Lys-Val-Phe (Mejare et al., 1998). Although the hexapeptide does not contain Cys residue (which has strong binding preference for Cd^{2+}), it is capable of binding Cd^{2+} with high specificity. The last example is an oligopeptide, Asp-Arg-Val-Tyr-Ile-His-Pro-Phe-His-Leu, which binds Pb^{2+} selectively. Loo and coworkers have demonstrated that the His residues at position 6 and 9 are involved in metal coordination (Loo et al., 1994; Hu et al., 1995). It was also suggested by them that metal ions are only coordinated to one of the His residues and to the two immediate carbonyl groups, imparting minimum constraints on the oligopeptide. All examples discussed above demonstrate that there is great potential for using oligopeptides as recognition elements to detect metal ions.

2.1.2 Formation of oligopeptide-metal complex on solid surfaces

The strong interactions between oligopeptides and metal ions provide an incentive of using oligopeptide-modified surfaces to detect metal ions. In the past, Takehara et al. (1994) used Glu-Cys-Gly-modified gold electrodes as ion gates for detecting lanthanide ions. The Glu-Cys-Gly-modified surface functioned as an "on/off" switching gate for the permeation of ions. In the absence of lanthanide ions and at pH > 5.7, a barrier of negatively charged carboxylate groups prevents the movement

of redox active $Fe(CN)_6^{4-}$ to the electrode. Upon lanthanide binding to the carboxylate groups, the oligopeptide Glu-Cys-Gly changed its conformation to a more compact form, thus opening up channels for $Fe(CN)_6^{4-}$ to access the electrode surface. The detection limit was about 1 μM La^{3+}. In addition, self-assembly of Gly-Gly-His on the gold electrode surface was used to detect copper ions (Yang et al., 2001a,b). Figure 2.3 shows the tetragonal coordination between Cu^{2+} and the surface immobilized Gly-Gly-His. Osteryoung square wave voltammetry was employed for the detection of Cu^{2+} with sub-ppt detection limits. Minimal interference from other metal ions (except nickel ions) was observed.

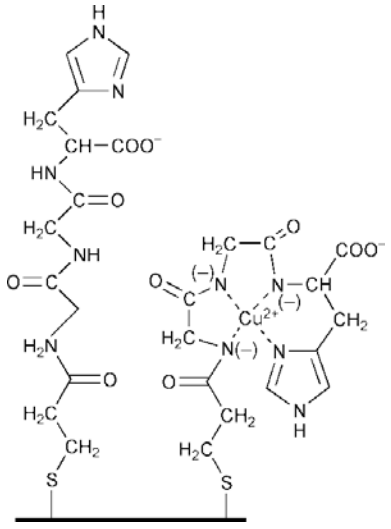

Figure 2.3 Schematic illustrations of the Gly-Gly-His-modified electrode with and without complexed Cu^{2+}.

Detection of Cd^{2+} was made possible by using His-Ser-Gln-Lys-Val-Phe as the ligand attached to a gold surface. The hexapeptide was identified through a phage display library. Therefore, although it does not possess any cysteine residues, it can detect Cd^{2+} with a low detection limit (0.9 nM) and high selectivity (Chow et al., 2005b).

Cu^{2+} did not affect the detection of Cd^{2+}, but Pb^{2+} causes minor interference. Another example of using surface immobilized oligopeptide as the recognition element for the metal ion detection was Asp-Arg-Val-Tyr-Ile-His-Pro-Phe-His-Leu, which could detect Pb^{2+} with a detection limit of 1.9 nM (Chow et al., 2005a). The high selectivity of Asp-Arg-Val-Tyr-Ile-His-Pro-Phe-His-Leu for Pb^{2+} is probably because Pb^{2+} complexes with one of the His residues and two adjacent carbonyl groups. Another possible mechanism is that both His6 and His9 are responsible for complex with Pb^{2+}.

2.1.3 Molecular imprinting

Although the above mentioned surface immobilized oligopeptides may bind metal ions, the high sensitivity and specificity were only provided by using the oligopeptides with specific sequences. There are only a few examples of such oligopeptides and they are often expensive to apply. Moreover, the reactivity of immobilized oligopeptides can be significantly reduced as a consequence of steric hindrance, transport limitations, etc. A simple solution is to create an artificial binding site by using molecular imprinting technique.

Molecular imprinting is a technique used to create recognition sites for a template molecule in a polymeric matrix (Mosbach et al., 1994; Wulff et al., 1995). The artificially generated recognition sites are complementary in shape, size, and functionality with respect to the templates and favor the binding of template molecules to other compounds with similar structures. Molecularly imprinted polymers (so called three-dimensional (3D) molecular imprinting) have already been

successfully used to create artificial receptors for small molecules (Vlatakis et al., 1993; Wulff et al., 2002; Haupt et al., 2003; Zimmerman et al., 2004). It generally involves three steps (Dai et al., 1999; Wulff et al., 1995): (1) selecting one target molecule as the template, (2) incorporating the template into solid networks through copolymerization, and (3) removing the template to leave cavities which can selectively rebind the molecules with the same shape and size of the template molecules. The 3D molecular imprinting technique has been successfully exploited to resolve racemates (Wulff et al., 1995), to design bio-mimetic sensor devices (Piletsky et al., 1995) and to separate mixtures of metal cations (Kuchen et al., 1988). One major drawback of this technique is that the kinetics of the adsorption/desorption process are unfavorable because the template molecules are deeply embedded in the matrices. This issue can be addressed by the development of 2D molecular imprinting (Yang et al., 2005a; Fang et al., 2005) where the functional groups are introduced onto the surface through imprinting coating. The key is to coat the surface with complexes of the ligands and target molecules rather than the free ligands. After removal of the target molecules, the resulting imprinted sites are more accessible, the mass transfer is faster, and the binding kinetics is more rapid. Thus, 2D molecular imprinting is very attractive for sensor applications (Hillberg et al., 2005).

The first 2D molecularly imprinted surface was created by Sagiv (1980). In his method, mixed monolayers of trichloro-*n*-octadecyl-silane and a dye modified with a detergent as the template were adsorbed on the surface of glass. The modified dye molecule that was not covalently bound could be dissolved out. This left holes

showed preferential adsorption of the template used. Recently, several approaches have been investigated for sensor applications. Piletsky et al. (1999) used hexadecylmercaptan to form molecularly imprinted monolayers (MIMs) on gold electrodes, which show high specificity for cholesterol. In their approach, hexadecylmercaptan and cholesterol (template) were adsorbed simultaneously on the gold surface. Because the simultaneous adsorption may suffer from competitive binding between hexadecylmercaptan and cholesterol during imprinting procedure, the density of imprinting sites are difficult to control over. Moreover, Au-S bond strength is stronger than the interaction between cholesterol and gold (van der Waals or hydrophobic interaction). Therefore, if the imprinting time is long enough, hexadecylmercaptan will cover the entire surface preferentially.

To overcome this problem, Li and coworkers (Li et al., 2006) developed a two-step imprinting process involving pretreatment of the gold surface by a solution containing only the template followed by backfilling with thiol. In this case, the gold surface was first covered by an equilibrium deposition of template molecules, and then thiols were immobilized around the template molecules by backfilling. Removal of the templates by a washing step leaves the thiol layer patterned with cavities that match the templates geometrically. Following this procedure, we developed a quartz crystal microbalance (QCM) sensor decorated with 2D MIMs for identification and quantification of thiacloprid and imidacloprid in a real-time manner (Bi et al., 2009). The 2D molecularly imprinted technique can also be applied for creating a metal ion imprinted surface. That is, the oligopeptides, such as triglycine, were immobilized on

the surface in the presence of copper ions. After the removal of copper ions from the surface, multiple hydrogen bonds are formed between adjacent triglycine molecules and stabilize the loop structure (so the copper imprinted surface is created) as shown in Figure 2.4. The resulting surface has been shown to selectively bind with copper even in the presence of zinc or nickel.

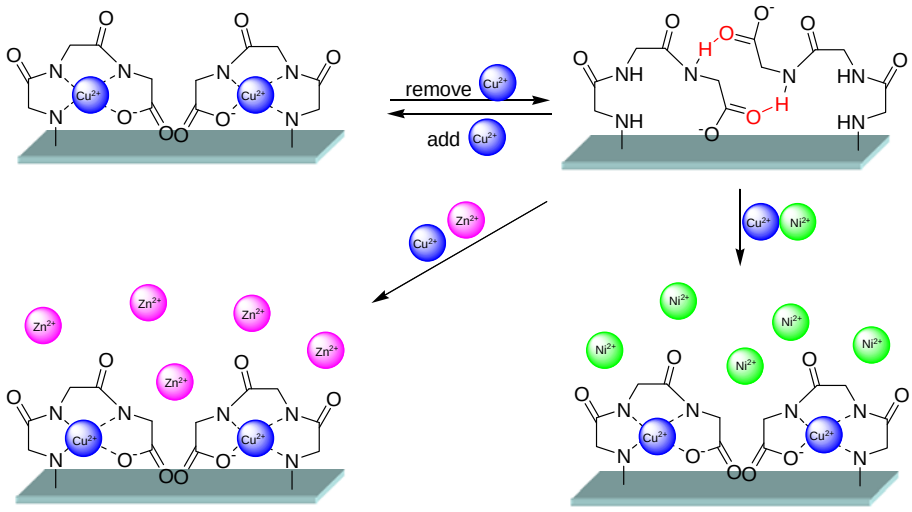

Figure 2.4 Schematic illustrations of copper-selective surface binding sites created by using 2D molecular imprinting techniques.

2.2 Immobilization of Oligopeptides on Surfaces

One of the important elements in Chapter 2.1 is that the oligopeptides need to be immobilized on the solid surfaces. To immobilize oligopeptides on surfaces, several methods are readily available. For example, immobilization of oligopeptides by using physical adsorption, ionic binding, physical entrapment, and covalent attachment have been reported before. The simplest approach is through adsorption of the oligopeptide molecules either by electrostatic forces on charged surfaces (Haab et al., 2001), by hydrophobic attraction, or by van der Waals interaction (Bussow et al., 1998). In spite

of its simplicity, the adsorption method is not desirable because the attached peptides can be removed under stringent washing conditions. In contrast, covalent attachment of peptides on the substrate represents a more robust system. To link oligopeptides covalently to the surface, the presence of suitable functional groups such as amino groups, carboxylic acids, epoxides, or aldehydes (Zammatteo et al., 2000) on the surfaces is required.

2.2.1 Reaction between primary amine and surface aldehyde

It is well known that aldehyde can react with primary amine to form Schiff base under mild conditions (Lemieux et al., 1998; Miller et al., 1983). In the past, several papers have evaluated the performance of oligonucleotide arrays on aldehyde-modified substrates. Horton et al. reported the preparation of aldehyde-terminated gold surface by exploiting the equilibrium between 2-hydroxypentamethylene sulfide and its open-chain aldehyde isomer. The surface aldehyde group was reacted with alkylamines to form a Schiff base (Horton et al., 1997). Because typical proteins display many lysine residues on their surfaces as well as the generally more reactive primary amine at their NH_2-termini, they can attach to the aldehyde-terminated surface in a variety of orientations, permitting different sides of the protein to interact with other proteins or small molecules in solution (MacBeath et al., 2000). Although appropriate for most applications, aldehyde-terminated surfaces cannot be used when oligopeptides or small molecules are immobilized, presumably because the Schiff base formed from the coupling of aldehyde with amine in small molecules readily

undergoes hydrolysis in an aqueous environment and reverses back to free amine and aldehyde groups. As a result, this instability issue needs to be addressed by reducing the Schiff base with a reducing agent, such as sodium cyanoborohydride, to generate a stable secondary amine linkage (Peelen et al., 2005). The surface modification of an aldehyde-terminated glass slide with oligopeptides (such as glycine oligomers) through the formation of Schiff base, which was further reduced to a stable secondary amine by a reducing agent $NaBH_3CN$, is shown in Figure 2.5.

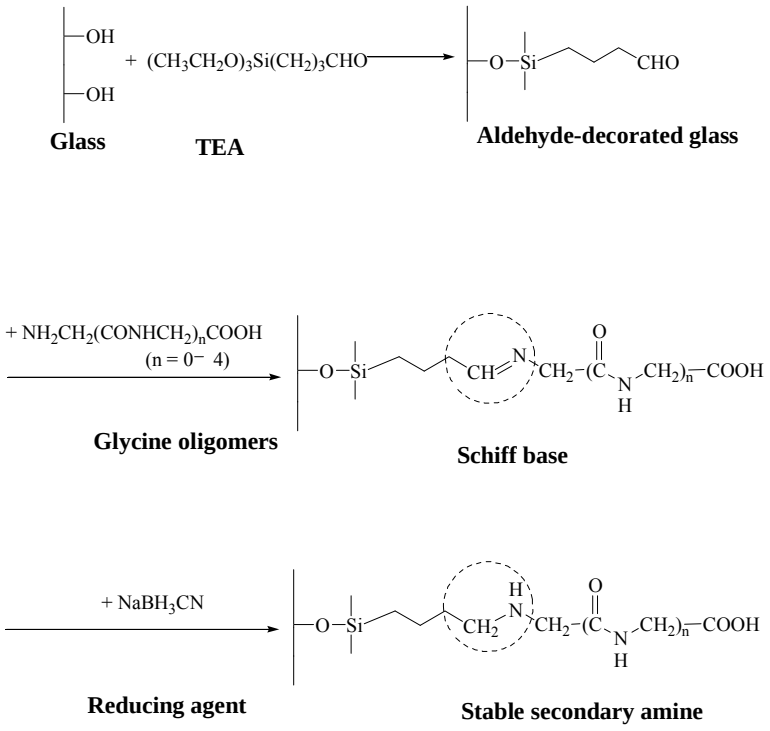

Figure 2.5 Schematic illustration of a glass slide surface modified with an aldehyde-containing organosilane TEA and the reaction of glycine oligomers with aldehyde groups through the formation of Schiff base, which was further reduced to a stable secondary amine by a reducing agent $NaBH_3CN$.

2.2.2 Reaction between primary amine and surface carboxylate

Another linker group for covalent immobilization of oligopeptides is carboxylate

group. In general, the oligopeptides are immobilized on the carboxylate-modified surface using water-soluble carbodiimides, such as 1-ethyl-3-(3-dimethylaminopropyl) carbodiimide hydrochloride (EDC), to form covalent conjugates via amide bonds (Sehgal et al., 1994). The reaction involves the intermediate formation of the activated *O*-acylurea derivative of the carbodiimide (Figure 2.6). A subsequent attack by the amino-N in the oligopeptides brings about the formation of the amide linkage. The formation of *O*-acylurea occurs optimally at pH 4-5. On the other hand, *N*-hydroxysuccinimide (NHS) reacts with carboxylate to produce aminoacyl esters under facile conditions. The resultant esters hydrolyze slowly in aqueous media compared with their rates of reaction with amino groups and thus enhance the coupling efficiency of carbodiimides for conjugating carboxylate with amino groups in oligopeptides.

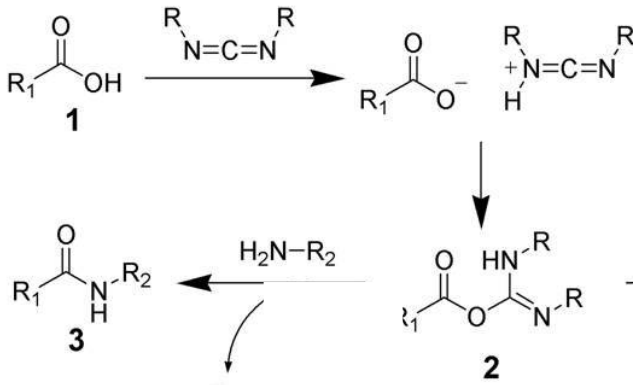

Figure 2.6 The reaction between primary amine and carboxylic acid via the carbodiimide coupling agent.

2.2.3 Immobilization of oligopeptides through single anchoring point

One major disadvantage of the above immobilization methods is that they are not

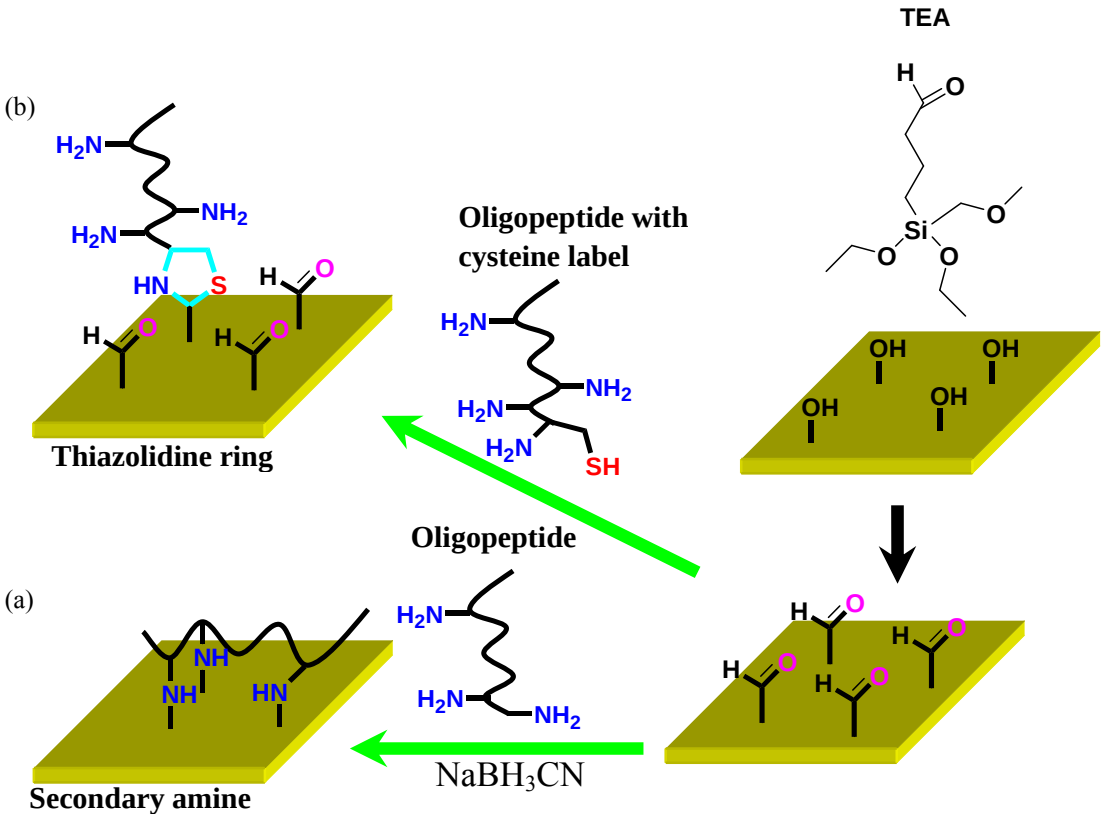

Figure 2.7 Schematic illustrations showing the immobilization of TEA and oligopeptides on the surfaces through (a) multiple anchoring points and (b) single anchoring point.

site-specific. Any primary amines in oligopeptides may react with aldehydes and carboxylates (Figure 2.7a). However, because oligopeptides often lack a well-defined three-dimensional structure, a correct orientation is essential to keep their interaction with the target (Seong et al., 2004; Lesaicherre et al., 2002a,b; Luk et al., 2004a). Up to date, several reactions, such as Staudinger ligation (Köhn et al., 2003; Soellner et al., 2003 and 2006) and Diels-Alder reaction (Houseman et al., 2002) have been used to immobilize proteins or peptides on the surface with high site-specificity. Nonetheless, these immobilization strategies require labeling peptides with an unnatural moiety, such as phosphinothioester or cyclopentadiene. In contrast, some

methods only require natural amino acid labels, such as histidine (Zhu et al., 2001; Cha et al., 2004) or cysteine (Shen et al., 2005; Lee et al., 2007), because the former is able to complex with nickel ions and the latter can form an Au-S bond on a gold surface. The use of natural amino acids is advantageous because additional amino acids can be introduced into target proteins or peptides through genetic engineering (Sambrook et al., 1989). The disadvantage of these methods is that they are not site-specific because any histidine or cysteine residues, regardless of their positions in the peptides or proteins, can bind nickel ions or react with gold.

To address these issues mentioned above, a site-specific immobilization reaction between aldehyde and N-terminal cysteine (Liu et al., 1994a,b; Shao et al., 1995), in which free aldehyde group reacts with the mercaptoethylamine moiety of cysteine and forms a stable thiazolidine ring (Zatsepin et al., 2002; Spetzler et al., 1995) has been proposed. The oligopeptide only requires to be labeled with an N-terminal cysteine and then it can be immobilized on the aldehyde-terminated surface through the formation of a thiazolidine ring and the orientation of immobilized oligopeptides is well-defined (Figure 2.7b).

2.3 Silicon Nanowire-Based Sensors

Recently, semiconductive structures have been used as building blocks for detecting and quantification of chemical and biological species. Until now, significant processes have been made (Hafeman et al., 1988). An example is the chemically sensitive field-effect transistor (CHEMFET) (Janata et al., 1994; Domansky et al., 1993), in

which the gate oxide is modified with molecular receptors or selective membranes. If charged analytes bind with the receptors or membranes, the gate potential may change and thus target analytes can be detected (Zemel et al., 1975; Blackburn et al., 1987; Seker et al., 2000). Although the detection of analytes by CHEMFET can be monitored by a direct change in conductance or other electrical properties, the main limitations of the system include the low sensitivity and the difficulties in integration (Cui et al., 2001a,b). In contrast, numerous past studies have demonstrated that these limitations can be overcome by using nanoscale FETs (Tans et al., 1999; Collins et al., 2001; Cui et al., 2000 and 2001a,b; Duan et al., 2001). Because binding of the chemical or biological species to the surface of a nanowire or nanotube (NT) will result in the depletion and accumulation of carriers in the "bulk" of the nanometer diameter structure, the sensitivity can be increased. Dai and coworkers have shown NT FETs to function as gas sensors (Kong et al., 2000). However, there are two main limitations of NTs. First, the specific growth of metallic or semiconducting tubes is not possible. Second, controlled doping of NTs is not possible. On the other hand, SiNWs do not have these limitations because they are always semiconducting independent of diameter and the dopant type and concentration can be controlled (Morales et al., 1998; Duan et al., 2000a,b,c; Hu et al., 1999).

2.3.1 Semiconductor physics

To better understand the operation of FETs, it is necessary to know energy bands of semiconductor materials. For semiconductor materials, the band with high energy

level is known as conduction band while valence band is the low energy band (Blackburn et al., 1987; Seker et al., 2000). The energy difference between conduction band and valence band is called band gap. When electrons exist in conduction band, the material is capable for electronic conduction, but electrons in valence band cannot. Therefore, in order to cause electron movement for conduction, electrons need to be freed from valence band to conduction band. However, at room temperature, only small amount of electrons can jump across the band gap; therefore, no conduction of electrons can be observed. One of the easiest methods to promote electrons from valence band to conduction band is by introduction of dopants, that is, adding impurity from group III or V of the periodic table into the semiconductor materials to create free holes or electrons. If an atom from the semiconductor, such as silicon is substituted by a group III element, the group III atom is satisfied to bind itself with only 3 of the 4 neighboring silicon atoms. The remaining silicon will seek an electron from elsewhere to complete the bond, and thus results in the creation of a hole. The same principle can be applied when silicon atoms are substituted by a group V element and a free electron for conduction will be created. When electrical potential is applied, the charged species (either electron or hole) move under the influence of an electronic field which results in the occurrence of electrical current.

2.3.2 Fabrication of SiNWs-based FETs

To fabricate SiNW FET devices for sensing applications, one can either follow a "bottom-up" or a "top-down" approach. Most of the reported studies are based on the

"bottom-up" approach in which the synthesis of SiNWs involves nanoparticle-catalyzed vapor-liquid-solid (VLS) growth on an oxidized silicon substrate by using gold nanoparticles the catalyst. The diameter of gold nanoparticle catalyst defines the diameter of the resulting SiNWs. The separation process involves washing off SiNWs from the substrate into an ethanolic solution. Then, by combining the self-assembly of SiNWs on a chip and a one-step photolithography to make contacts, a FET device can be fabricated. A flow chart of the fabrication of SiNW devices is shown in Scheme 2.1 (Patolsky et al., 2006a).

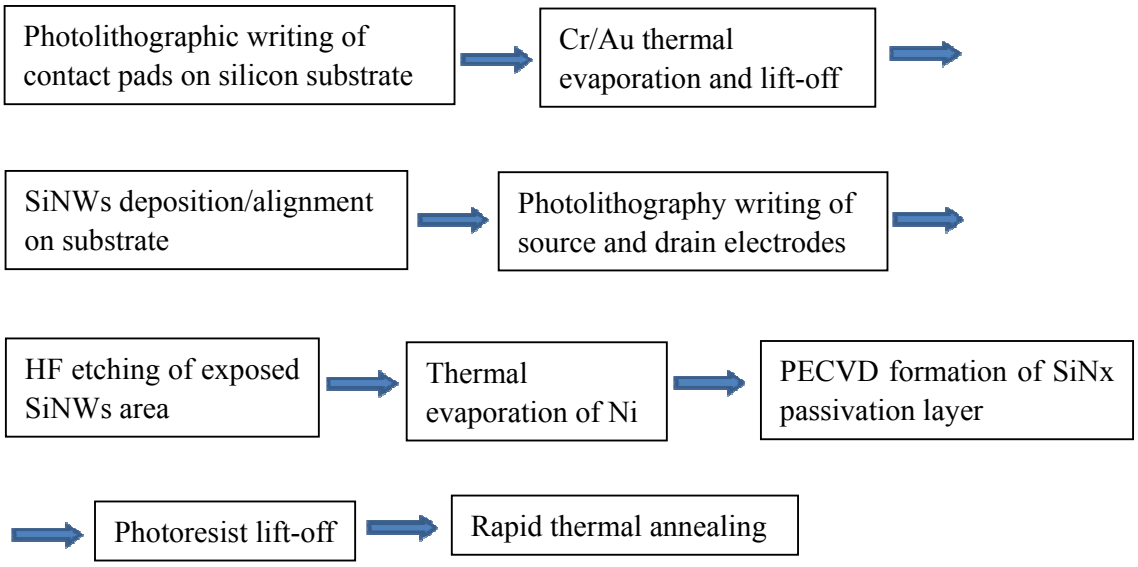

Scheme 2.1 Steps for fabrication of SiNW devices following bottom-up method (Patolsky et al., 2006a).

However, the bottom-up processing procedure is often limited by the complex processes of transferring and positioning of SiNWs and making reliable ohmic contacts with them. Furthermore, the control of doping concentrations in self-assembled

semi-conducting nanostructures remains a challenge, and the fabrication of high-density sensor arrays is very difficult (Li et al., 2005). In contrast, the "top-down" approach takes the full advantages of current semiconductor technologies and permits the production of hundreds of SiNWs in an array format simultaneously. It also creates a pathway for designing high-density, high-quality nanoscale sensors that can be fully integrated with the manufacturing processes of the SiNWs (Li et al., 2004). The synthesis of SiNWs is realized on silicon-on-insulator (SOI) wafers, which are doped with *p*-type (boron) or *n*-type (phosphorous) impurities using an ion implanter. The dopants are then activated in rapid thermal annealing furnace and nanowire-fins are patterned (using standard DUV lithography) in the array format; silicon/poly-silicon is etched in reactive ion etcher and resulting fins are oxidized in O_2 to realize nanowire array. The two ends of the nanowires are further doped to obtain *n*+ or *p*+ regions, followed by connecting to contact metal and alloying to realize Ohmic contacts. The device is then passivated by silicon nitride film except for the active nanowire sensor area and metal pads. A typical SiNW FET structure is shown in Figure 2.8.

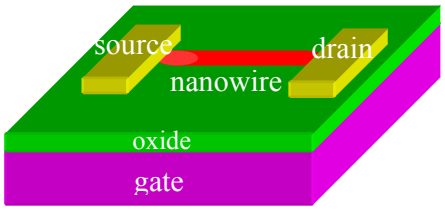

Figure 2.8 Schematic illustration of a SiNW FET showing metal source and drain electrodes with the NW and contacts on the surface of SiO_2 substrate.

2.3.3 Sensing applications

In the literatures, it has been demonstrated that SiNWs-based FETs can be used for the detection of ions (Cui et al., 2001a), proteins (Zheng et al., 2005; Stern et al.,

2007), virus (Patolsky et al., 2004), and cells (Patolsky et al., 2006b). The fundamental detection principle of these applications is that the conductivity changes due to the variations in the electric field or potentials on the surface (Cui et al., 2001a). For a typical FET, a semiconductor such as *n*-type silicon (*n*-Si) is connected to a metal source and a drain electrode, and the conductance is controlled by a third gate electrode. In the case of *n*-Si, a positive gate voltage depletes carriers (electrons) and increases the conductance while a negative gate voltage accumulates carriers and decreases the conductance. However, for *p*-Si, a positive gate voltage depletes carriers (holes) and decreases the conductance. In the following, a few applications of SiNW-based FET sensor will be reviewed.

Firstly, because the conductance of SiNW is modulated by an applied gate, the SiNW-based FET can be used as a pH nanosensor if the SiNW surface is modified with an organosilane, 3-aminopeopyltriethoxysilane (APTES), which contains a pH-sensitive amine group. As shown in Figure 2.9a, at low pH, the $–NH_2$ group is protonated and becomes $–NH_3^+$, which acts as a positive gate (Vezenov et al., 1997). However, at high pH, -SiOH is deprotonated and becomes $–SiO^-$, which acts as a negative gate. Figure 2.9b shows a typical plot of the conductance versus pH. It was found that the pH dependence is linear over the pH 2 to 9 and hence the APTES-modified SiNWs can be used as nanoscale pH sensors.

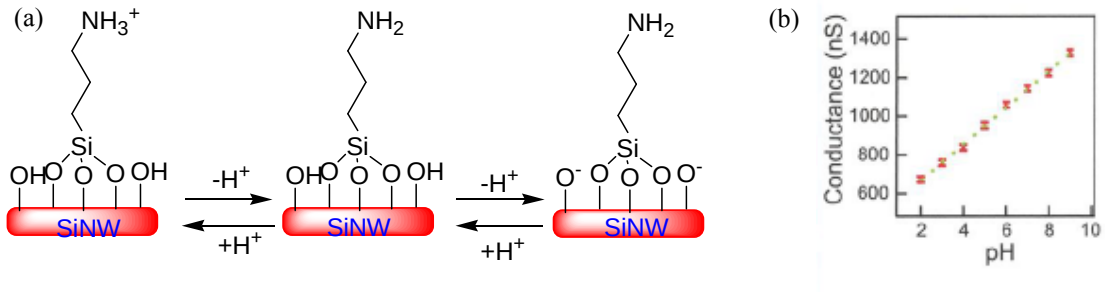

Figure 2.9 (a) APTES-modified SiNW surface changes surface charges with pH. (b) Plot of the conductance versus pH (Cui et al., 2001a).

Secondly, the conversion of SiNW FETs into sensors for protein detection was carried out by attaching protein antibodies to the NW surface after device fabrication. As shown in Figure 2.10, Cui et al. explored the sensitivity of biotin-modified SiNWs and found that it is possible to detect streptavidin down to 10 pM (Cui et al., 2001a). With a similar concept, recent literatures have reported the detection of prostate specific antigen (PSA), which is used as a protein marker of prostate cancer, by immobilizing anti-PSA on the SiNW surface (Li et al., 2005; Kim et al., 2007). The results in these studies suggest that the detection limit of PSA depends on both FET dimension and doping concentrations. Meanwhile, modification of distinct SiNWs with receptors in an array format allows the multiplexed detection of PSA, PSA-α1-antichymotrypsin, carcinoembryonic antigen and mucin-1 with good sensitivity and selectivity (Zheng et al., 2005). This technique has the potential for diagnosis and treatment of cancer and other diseases.

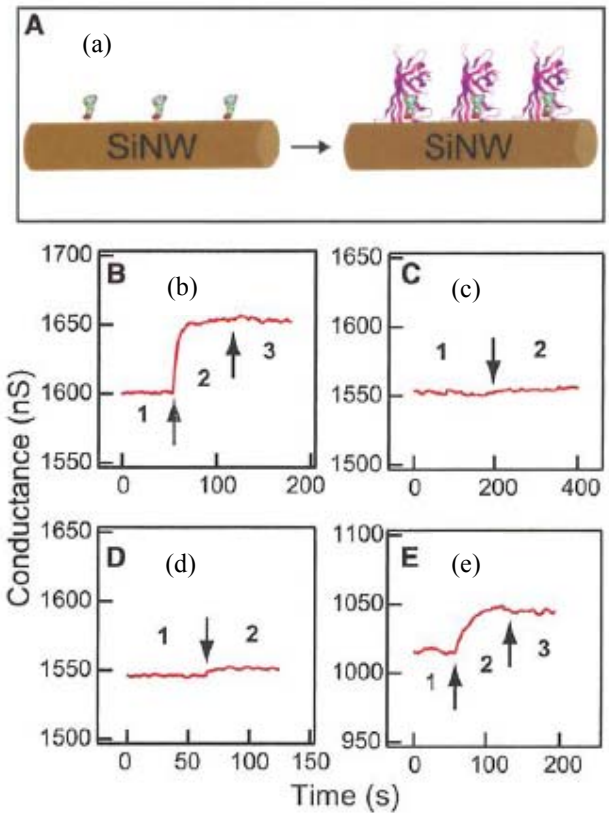

Figure 2.10 Real-time detection of protein binding. (a) Schematic illustrating a biotin-modified SiNW (left) and subsequent binding of streptavidin to the SiNW surface (right). (b) Plot of conductance versus time for a biotin-modified SiNW. (c) Conductance versus time for an un-modified SiNW. (d) Conductance versus time for a biotin-modified SiNW. (e) Conductance versus time for a biotin-modified SiNW (Cui et al., 2001a).

Thirdly, the identification of small organic molecules that bind specifically to proteins is known to be central to the discovery and development of new drug molecules. For example, the identification of inhibitors to ATP may be of substantial importance to treat diseases linked to a tyrosine kinase (Wang et al., 2005). In this paper, Wang et al. modified the SiNWs with tyrosine kinase Abl and used them to detect ATP binding and small-molecule inhibition of ATP binding. It was found that ATP binding to Abl can be distinguished above background at concentrations as low as 100 pM. Moreover, the results of competitive inhibition of ATP binding to Abl-modified SiNWs shows

that Gleevec, *N*-(3-amino-6-methylphenyl)-4-(3'-pyridyl)-2-pyrimidi-neamine, *N*-(3-nitro-6-methylphenyl)-4-(3'-pyridyl)-2-pyrimidine- amine, methyl 4-(2,5-dihy-droxy-benzylamino)benzoate exhibit a linear increase in the inhibition at low concentrations, followed by saturation at higher values.

Viruses are the causes of many human diseases and potential biological warfare agents (Stadler et al., 2003; Niiler et al., 2002). Thus, the ability to detect a virus particle rapidly and accurately is very important. The underlining concept of virus detection is similar to that of protein detection: when a virus particle binds to the antibody receptor on a nanowire device, the conductance of that device increases or decreases. Patolsky et al. (2004) showed that single viruses can be detected directly, including parallel detection of different viruses by modifying SiNWs with specific antibody receptors in an array, using SiNWs FET. The capability for real-time monitoring viruses opens up possibilities for the detection of distinct viral threats at the single virus level.

Another application of SiNWs-based sensors is to detect oligonucleotides. However, because SiNWs detect the local charge density change, high ionic strength solutions will screen (via Debye screening) the change. For example, in a 0.14 M electrolyte (which represents physiological environments such as serum) the screening length is about 1 nm (Israelachvili et al., 1985; Bunimovich et al. 2006). Therefore, to allow DNA hybridization to take place at low ionic strength and thus minimize the background response, peptide nucleic acid (PNA) was usually chosen as a recognition

element to detect DNA since PNA can bind to DNA with much greater affinity and stability than corresponding DNA (Nielsen et al., 1991; Jensen et al., 1997; Wang et al., 1996). By comparison of PNA-functionalized SiNWs (Li et al., 2005) and DNA-functionalized SiNWs (Li et al., 2004) for the same doping type and dimension, PNA-functionalized device was about 4 times more sensitive than the DNA-functionalized one. Hahm et al. (Hahm et al., 2004) has demonstrated that p-type SiNWs functionalized with PNA receptors can detect DNA at concentrations down to tens of femtomolar range. Furthermore, the SiNWs can distinguish the wild type versus mutant DNA sequences associated with the ΔF508 mutation site in the cystic fibrosis transmembrane receptor gene. Compared to other DNA assays, the SiNWs-based biosensor is ultrasensitive, label-free, cost-effective, portable, robust and easy-to-handle (Gao et al., 2007; Zhang et al., 2008).

The concept of using SiNW-based FETs for specific detection can also be extended to metal ions detection (Cui et al., 2001a). In this study, Ca^{2+} was detected by using by using calmodulin-modified SiNWs. Although the SiNWs showed high sensitivity and specificity for Ca^{2+}, the stability of protein may limit its application. The stability issue can be addressed by using small molecules with functional groups to construct the sensitive layer. For example, phosphate-containing molecules have been exploited in the past study for the design of calcium sensors (Moss et al., 1978; Jaffrezic-Renault et al., 1991). Unfortunately, to incorporate the phosphate moiety onto the sensitive layer requires multiple chemical reactions, which usually results in low yields and low sensitivities.

On the other hand, our recent study shows that a nature-occurring amino acid phosphotyrosine can be used to construct the sensitive layer for calcium sensing (Bi et al., 2008). Because phosphotyrosine also plays an important role in cell signaling processes, the proposed sensor may also give insights into the role of calcium in the cell signaling processes. The results show that the average conductance of phosphotyrosine-modified SiNWs increases with the increasing calcium-ion concentration up to 10 μM. Although the SiNW-based sensor also responds to magnesium, the threshold concentration required to cause measurable change of conductance is approximately 10 times higher than that of calcium. Meanwhile, this sensor shows high selectivity for calcium ions in the presence of sodium and potassium as interfering ions. Moreover, since oligopeptides with optimal amino acid sequences are considered as attractive molecular receptors for metal ion recognition, histidine-containing oligopeptides modified SiNWs are used to detect copper ions. Outstanding copper binding ability was reported for the X-Y-His sequence. By immobilizing Gly-Gly-His on the SiNWs surface, a highly sensitive and selective copper ions sensor was created (please see **Chapter 5**).

2.4 Liquid Crystals (LCs)

2.4.1 Definition of LCs

LC is an intermediate state between crystalline solid and an isotropic liquid. Although the molecules in the LC state are free to move about in the same way as the molecules in liquid, they tend to remain oriented in a certain direction. However, the orientations

are not as perfect as that in solid. Small organic molecules that exhibit liquid crystallinity in the absence of solvent phases are described as thermotropic LCs thanks to their temperature-dependent phase properties. In the presence of solvent, liquid crystalline phases are described as lyotropic LCs and they show a phase behavior that is dependent on the concentration of mesogen within the solvent. The lyotropic LCs are found throughout many biological systems and represent an important subsection of LCs, but we focus here on thermotropic LCs.

The most common thermotropic LC phase is nematic, where the bulk system has an orientational order, but lacks positional order. Up to date, more than 20 000 compounds with nematic phase are known. Among them, two typical LCs are 4-cyano-4'-pentylbiphenyl (5CB) and 4-methoxybenzylidene-4'-*n*-butylaniline (MBBA) (Their molecular structures are shown as Figure 2.11).

5CB MBBA

Figure 2.11 Molecular structures of 5CB and MBBA.

The molecular shape of nematic LCs is rod-like. Contrary to isotropic liquids, the molecular long axes of nematic LCs stay in parallel in one direction commonly known as director, as shown in Figure 2.12. Because of that, nematic LCs also show intrinsic optical anisotropy (birefringence or double refraction) (Collings et al., 2002), meaning that the light polarized along the director propagates at a different velocity

from the light polarized perpendicular to the director.

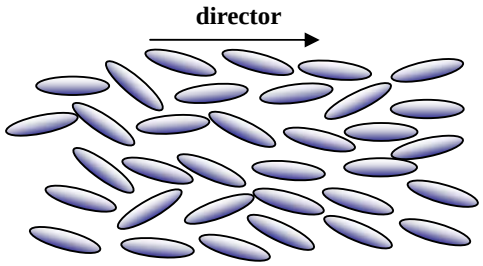

Figure 2.12 Structure of the nematic phase aligned in a single direction.

2.4.2 Anchoring of LC on solid surfaces

When LC is in contact with a confining medium, it will tend to reorient to minimize its free energy, which is determined by the chemistry and geometry of the interfacial region. This phenomenon is referred to as the anchoring of LCs by surfaces. Surface induced ordering of LCs typically is a direct consequence of the long range orientational ordering of molecules within the LCs. Therefore, LCs can be well aligned using surface alignment techniques. On a clean glass slide, LC molecules lie on the surface, and thus result in planar alignment. In contrast, homeotropic alignment can be achieved by coating the glass slide with a surfactant containing an aliphatic tail. The polar head groups of such surfactants bind to the glass slide surface, creating an aliphatic tail-modified surface; it becomes energetically favorable for a LC molecule to stand up amongst these tails. Previous studies also showed that when an organosilane, *N*,*N*-dimethyl-*n*-octadecyl-3-aminopropyl-trimethoxysilyl chloride (DMOAP) is covalently bound to the surface of glass slides, the hydrocarbon chains are orientated perpendicular to the surface (Kahn et al., 1973). As a result, the director

of 5CB is perpendicular to the surface (Figure 2.13a) and the orientation of 5CB is homeotropic as shown in Figure 2.13b.

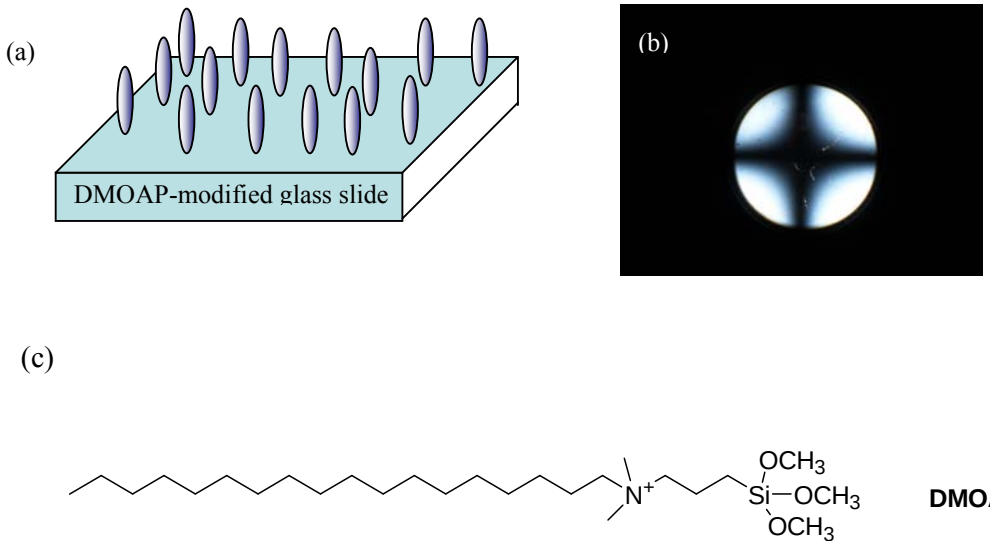

Figure 2.13 (a) Alignment of 5CB supported on DMOAP-modified glass slides. (b) Homeotropic orientation of 5CB supported on DMOAP-modified glass slides. (c) Molecular structure of DMOAP.

2.4.3 Optical properties of LC

The birefringent property of a LC molecule has been exploited in nearly all LC-based devices. The optical appearances of LCs were usually observed by fabricating a LC cell. Typically, a LC cell is fabricated by confining a thin layer (~ 2 - 20 μm) of LC between two glass slides. Normally, no light emerges from crossed polarizers if no material or isotropic material is inserted between two glass slides. This is because the light emerging from the polarizer is completely absorbed by the analyzer and the polarization of the light does not change as it travels through the isotropic material (Figure 2.14a). In the case where the polarized light from the polarizer is orientated with the director of LCs (the director of LCs makes an angle other 0° or 90° with the

direction of polarization), we can consider this light to be composed of light polarized along the director and perpendicular to the director. When passing through the LCs, the two polarizations emerge as elliptically polarized light (Figure 2.14b).

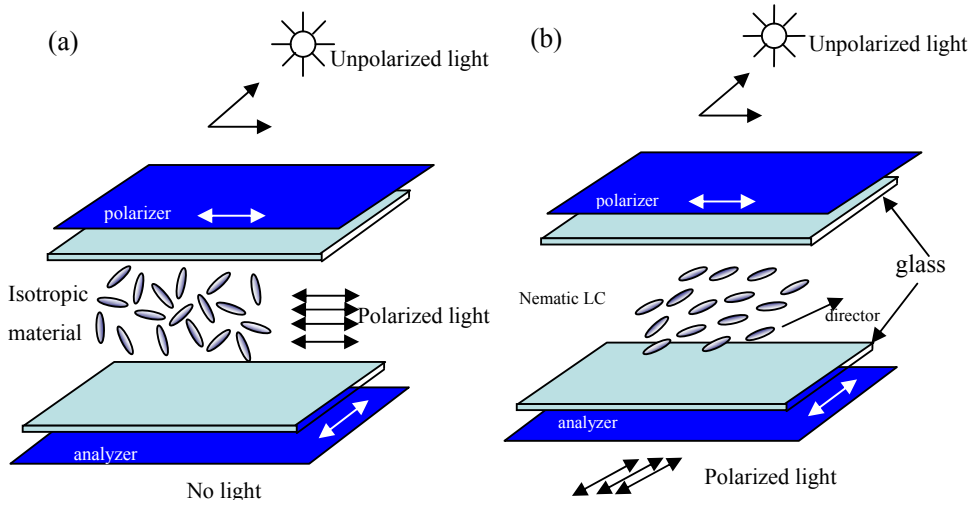

Figure 2.14 The effect of polarizing filters on the LC cells inserted with (a) isotropic material; (b) nematic LCs with the director not oriented parallel to the polarizer or analyzer. The polarizer allows only light polarized along the x-axis to pass, while the analyzer allows only light polarized along the y-axis to pass.

Since the electric field of elliptically polarized light is constantly rotated, it is parallel to the analyzer twice during one rotation. Thus, some light will emerge from the analyzer. Introduction of LCs between crossed polarizers causes the field to appear bright, while no LCs between the crossed polarizers causes the field to appear dark. If a hybrid cell is fabricated by a chemical functionalized surface (bottom surface) and a DMOAP-modified surface (top surface), the regions which are chemically modified would appear bright or dark under crossed polarizers. If the hybrid cell is rotated to any angles to the axes of the polarizers, and the image viewed under crossed polarizers remains dark, the orientations of LCs supported on the chemically modified

surface are homeotropic. In contrast, if the image viewed under crossed polarizers is not homogeneously colored, it means the orientations of LCs supported on the chemically modified surface are planar or titled.

2.4.4 LCs-based sensors

In the past, orientations of mesogens in the LC phase, including their response to temperature, pressure, and external stimuli have been widely studied and exploited for the applications of chemical sensors (Novak et al., 1972; Poziomek et al., 1973). For example, past studies have shown that the pitch of cholesteric LCs may increase when the temperature is raised, or when organic vapors diffuse into the layers of cholesteric LC. As a result, the color of LC changes according to the environmental temperature, or the concentration of organic vapors (Winterbottom et al., 2003).

Recently, more studies have demonstrated an alternative of using LCs to report chemical and biomolecular binding events occurring on solid surfaces (Gupta et al., 1998; Shah et al. 2001; Brake et al. 2003a,b; Luk et al., 2004). The detection principle, however, is based on the changes of the anchoring of LCs supported on surfaces, rather than the changes of their bulk properties. Because the orientations of LCs are determined by interactions between mesogens and surfaces (Shah et al., 1999), the chemical compositions and the molecular-level structures of surfaces will affect the anchoring of LCs (Jerome et al., 1991). Based on the correlations between the anchoring energies and surface properties, subtle changes of the surface properties can lead to the different orientations of LCs supported on the surface. Moreover, these

orientations of LCs near surfaces can be propagated and amplified rapidly through the bulk of LCs up to 100 μm away, thanks to the liquid-like mobilities of mesogens. This LC based detection method has been exploited to report the protein binding events on nanostructured surfaces and low-level of chemical analytes in the vapor phase (Yang, 2005). Compared to other detection techniques, the LC-based detection method does not require the use of complicated instrumentation. It also provides good spatial resolution, and is sufficiently simple.

Optical amplification of protein binding events

Because the orientations assumed by LCs near surfaces reflect the molecular-level or mesoscale structure of a surface, surfaces have been designed such that the binding of macromolecules, such as proteins, can be amplified and transduced into optical signals. Abbott's group (Gupta et al., 1998) created surfaces with nanometer scale topographies (Figure 2.15) which could be erased or marked by the specific binding of proteins to surface immobilized ligands. For example, they formed a mixed SAMs formed from biotin-$(CH_2)_2[(CH_2)_2O]_2NHCO$-$(CH_2)_{11}SH$ and $CH_3(CH_2)_7SH$. When the mixed SAMs were exposed to avidin, the orientations of LCs supported on these surfaces were changed. Because the size of the topography is approximately matched to the size of the proteins that bind to the receptors, LCs can report whether or not proteins are bound to the receptors. Two conclusions can be obtained from their studies. First, it is possible to control the anisotropy within the surfaces such that the immobilization of ligands does not disturb the uniform orientations of LCs. Second,

the specific adsorption of target protein to the surface may change the orientations of LCs.

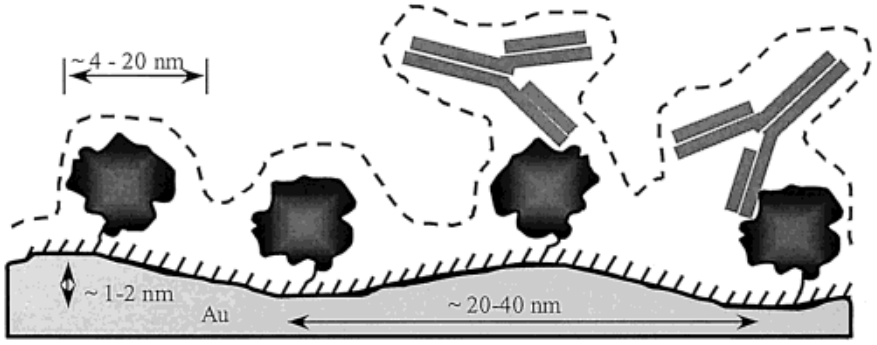

Figure 2.15 Schematic illustration of surface topography with and without protein bound to a SAM supported on a surface possessing nanometer scale topography (Gupta et al. 1998).

Detection of vaporous analytes

Recent studies have demonstrated that the orientational transitions of LCs were also triggered by exposure to parts-per-billion (ppb) vapor concentrations of chemical analytes, such as organoamine and organophosphorus (Shah et al., 2001). The design of the detection system involved the following principles (Figure 2.16). First, the solid surface was modified with chemical receptors that weakly bound molecules of LCs and oriented LCs in a well-defined direction. Second, the receptors bound targeted vapor analytes more strongly than they bound the molecules of LCs such that the analytes released LCs from their receptor-enforced orientation. However, the non-targeted species bound the receptors more weakly than LCs. Therefore, they would not change the orientations of LCs. This competitive interaction provided a level of specificity for

the targeted analyte that was substantially greater than schemes based on non-competitive binding of analytes to receptors.

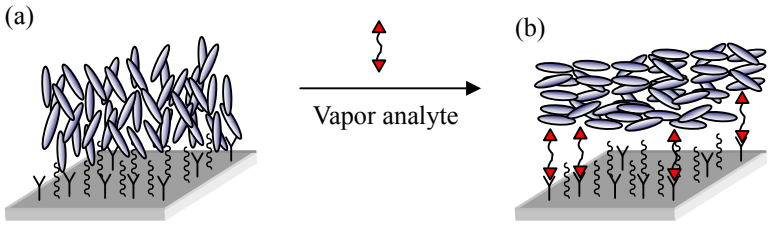

Figure 2.16 Schematic illustrations of orientations of LCs supported on a surface modified with molecular receptors (a) before and (b) after exposing to the targeted vapor analytes.

For the detection of organoamines, carboxylic acid (-COOH) groups were used as the molecular receptors and 5CB as the LC. The nitrile group of 5CB formed a hydrogen bond with a –COOH and thus 5CB assumed an orientation that was parallel to the surface. In contrast, exposure of the surface to a vapor of hexylamine caused 5CB to assume a different orientation because the stronger acid-base interaction displaced 5CB from its hydrogen bond with –COOH group. If the bound –COOH groups were treated with 100 mM $Cu(ClO_4)_2$, the complexation of the nitrile group of 5CB with Cu^{2+} gave rise to the perpendicular orientation of 5CB. After the exposure of an organophosphorus $(H_3CO)_2POCH_3$, the orientations of 5CB changed because of the competitive binding of $(H_3CO)_2POCH_3$ to Cu^{2+}.

Controlling orientations of LCs at aqueous/LC interface

The design of interfaces is critical for most applications of LC materials. Unlike the orientational behaviors of LCs on solid surfaces, the deformable and fluid nature of

the interfaces between LCs and aqueous phases leads to new types of interfacial and anchoring phenomena. The experimental geometry for the study of interfacial orientations of LCs involves an interface between an aqueous phase and the water-immiscible LC. Typically, LC is hosted in the pores of an electron microscopy gird (copper or grid) that is supported on a glass slide treated with DMOAP. Immersion of this system into an aqueous phase leads to the formation of a stable interface between the aqueous phase and LC. Past studies have demonstrated that the experimental geometry provides a general scheme for the study of the adsorption of surfactants and other amphiphiles at the aqueous/LC interface (Brake et al., 2002). For example, self-assembly of ionic surfactants at the aqueous/LC interface using the experimental geometry induced the orientational transitions of LCs (Figure 2.17).

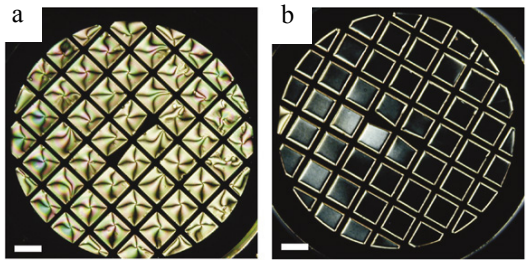

Figure 2.17 Anchoring of 5CB by aqueous solutions of SDS. Optical images (crossed polars) of 5CB hosted in a copper grid supported on an OTS-coated glass slide and placed into contact with (a) water or (b) a 2.2 mM aqueous solution of SDS (Brake et al., 2002).

Figure 2.17b shows that SDS causes the dark appearance of 5CB, which is consistent with homeotropic anchoring of 5CB. An advantage of this experimental system is that it is straightforward to increase or decrease the surfactant concentration within the aqueous phase, and thus characterize the change in orientation of the LC with

concentration of adsorbed surfactants. Therefore, this system has been used for monitoring enzymatic activity, self-assembly of polyelectrolyte multilayer, and self-assembly of protein-based films (Lockwood et al., 2008).

CHAPTER 3
OLIGOGLYCINES-MODIFIED SURFACES FOR Cu^{2+} ADSORPTION

This chapter reports a copper-imprinted sorbent by modifying the surface of silica gel with glycine, diglycine and triglycine with Cu^{2+} as the templates. The adsorption capacity and specificity for Cu^{2+} on the copper-imprinted and nonimprinted silica gel are compared. The conformational changes of immobilized triglycine during the immobilization procedure are investigated by using FTIR.

3.1 Ion-Imprinted Silica Gels Functionalized With Oligoglycines For Cu^{2+} Adsorption

3.1.1 Introduction

Molecular imprinting is an effective technique to form artificial receptors for molecular recognitions (Wulff, 1995; Mosbach, 1994; Li and Husson, 2006; Lotierzo et al., 2004). Up to date, most of the molecular imprinting techniques are based on three-dimensional (3D) polymer networks (Piletsky et al., 1995, 1997 and 1998; Wang et al., 1997; Ramström et al., 1996; Andersson et al., 1995), where the template molecules bound to functional monomers are copolymerized to form highly cross-linked polymers. After the removal of the templates, cavities which match the molecular structure of target analytes are formed. Although these molecularly imprinted materials exhibit high affinity and selectivity for target molecules, they

have poor site accessibility because the templates are embedded deep inside the polymer matrices. In contrast, in two-dimensional (2D) imprinting method, the ligands (usually organosilanes or thoils) are self-assembled on the surface of an inorganic matrix in the presence of templates (Chidsey et al., 1990; Chailapakul et al., 1993; Mirsky et al., 1999; Liu et al., 2000). After the removal of the templates, the resulting cavities on the monolayers can be used to adsorb molecules with similar size and shape as the templates. Recently, 2D imprinting method has attracted a lot of attention because the templates can be removed completely to create imprinted sites that can be reached by the target molecules more easily and quickly (Yang et al., 2005; Fang et al., 2005).

One of the major applications of molecular imprinting is to prepare sorbents which can be used to selectively remove heavy metal ions in the presence of other metal ions. In the past, 3D imprinting methods were often used for this purpose (Dai et al., 1999, 2000 and 2001; Fang et al., 2005; Lu et al., 2004). However, as discussed above, sorbents prepared by using 3D imprinting method are limited by slow mass transfer; it is difficult for target metal ions to reach adsorption sites. More recently, several studies have demonstrated that 2D imprinted sorbents can be used to adsorb metal ions with high affinity and selectivity. Mass transfer of metal ions inside the 2D imprinted sorbents is also faster. In these studies, however, the choice of surface modifying agents is often limited to a range of organosilanes containing primary amine, secondary amine or thiol. For example, 3-aminopropyltrimethoxysilane and 3-mercaptopropyltrimethoxysilane (Liu et al., 1998) were used to functionalize the

surfaces of mesoporous materials in the presence of target metal ions to create selective adsorption sites for them. Despite of these successful examples, we believe other ligands without the silane functionality can also be used in the 2D imprinting procedures to enhance our capabilities of designing 2D imprinted sorbents.

The candidate ligands to be examined in this study are simple amino acids, dipeptides and tripeptides because past studies have shown that they readily form complexes with metal ions through terminal primary amine, carboxylate groups, amide groups along the peptide backbones, and various side groups such as imidazole and thiol (Burger et al., 1990; Sigel et al., 1982; Chow et al., 2006). Unfortunately, the binding of metal ions through terminal functional groups and peptide backbones is relatively nonselective. Recently, some groups have demonstrated the use of oligopeptides with particular side groups to complex metal ions with high selectivity (Yang et al., 2001). However, there are only a few examples of such oligopeptides (Takehara et al., 1994; Arrigan et al., 1999; Liu et al., 1999) and they are often expensive to apply. A simple solution to provide selectivity for metal ions with nonselective amino acids or oligopeptides is the development of a 2D ion-imprinting method. The hypothesis is that by following the 2D ion-imprinting method, even simple amino acid or oligopeptides such as glycine, diglycine and triglycine can form recognition sites for selective adsorption of metal ions when they are immobilized on the surface of silica gel.

3.1.2 Experimental Section

Materials

Silica gel (pore size 150 Å, BET surface area ~ 320 m^2/g), 4-morpholinoethanesulfonic acid (MES) (98%), copper sulfate, copper chloride, calcium chloride, magnesium sulfate, dithizone (99%), Triton X-100 (ultrapure), 3-aminopropyltriethoxysilane (APES) (99%), and glutaraldehyde solution (50%, photographic grade) were purchased from Sigma Aldrich (Singapore) and used as received. Water was purified through a Milli-Q system (Millipore).

Surface modification of silica gel

First, 5.0 g of silica gel was stirred in 30 mL of aqueous solution containing 10% (v/v) of APES at 50°C for 1 h. After the silanization, the APES-modified silica gel was washed with copious amounts of deionized water and acetone to remove residual silanes. Then, it was dried at 100°C for 3 h to allow the cross-linking of silanol groups. Next, the APES-modified silica gel was stirred in 100 mL of aqueous solution containing 5% (w/w) of glutaraldehyde at room temperature for 1 h. The aldehyde-decorated silica gel was washed with excessive deionized water and acetone sequentially to remove residual glutaraldehyde. Then, it was dried at 100°C for 2 h.

Functionalization of silica gel with glycine oligomers

For nonimprinted silica gel, 1.0 g of glutaraldehyde-modified silica gel was stirred in 100 mL of 0.5 M carbonate buffer (pH = 10) containing 50 mM of $NaBH_3CN$ and 10

mM of glycine, diglycine, or triglycine at 50°C for 2 h. After the reaction, the modified silica gel was washed with copious amounts of deionized water and dried at 100°C for 2 h. For copper-imprinted silica gel, copper sulfate was dissolved in an aqueous solution containing 50 mM of $NaBH_3CN$ and 10 mM of glycine, diglycine, or triglycine to a final concentration of 10 mM. Then, 1.0 g of glutaraldehyde-modified silica gel was added and reacted at 50°C for 2 h. After the reaction, Cu^{2+} were removed from the imprinted silica gel by rinsing the silica gel with 10 mM of hydrochloric acid for 20 min. Subsequently, the silica gel was cleaned in an ultrasonic bath for 2 min. The Cu^{2+} removal procedure was repeated for 5 times. The eluates were measured with a UV-vis spectrometer to ensure there was no Cu^{2+} left in the silica gel. Finally, the silica gel was dried at 100°C for 2 h.

Elemental analysis

The contents of carbon, hydrogen, and nitrogen on the surface of silica gel were analyzed by using a CHNS/O Elemental Analyzer (Perkin Elmer 2400 series II, Waltham, MA, USA). After running five instrument blanks, three acetanilide samples (~ 1.0 mg) as K-factors, one acetanilide as the standard sample, and about 1.0 mg of each sample was loaded onto a carousel for analysis to obtain the weight percentage of carbon, hydrogen, and nitrogen. The density of functional group on the surface was calculated from the weight percentage of carbon and the surface area of the silica gel.

Adsorption of metal ions with silica gel

First, 50 mM of MES buffer containing 4.0 μg/mL of Cu^{2+} was buffered to a specific pH. In a typical run, 10 mg of silica gel was stuffed in the barrel of a 3-mL syringe with a polyethylene frits having a pore size of 20 μm (Varian, Palo Alto, CA, USA), and 2 mL of MES buffer containing metal ions was passed through the column by gravity. The eluates were collected and analyzed via UV-vis spectroscopy to quantify the change of Cu^{2+} concentration after passing through the adsorption column. The copper adsorption percentage E (%) is defined as follows.

$$E\% = \frac{C_{\mathrm{i}} - C_{\mathrm{f}}}{C_{\mathrm{i}}} \times 100\% \tag{3.1}$$

where C_{f} and C_{i} represent the final and initial concentration of Cu^{2+} (μg/mL). We also define the adsorption capacity Q (mg/g) as follows.

$$Q = \frac{(C_{\mathrm{i}} - C_{\mathrm{f}}) \times V}{W} \tag{3.2}$$

where W is the mass of silica gel (g) and V is the total volume of copper solution (L).

Desorption of Cu^{2+} and multiple use cycle

In a typical run, 100 mg of copper-imprinted or nonimprinted silica gels were stirred in 100 mL of 64 μg/mL copper solution at pH = 4.5 for 30 min. Then, the silica gels loaded with Cu^{2+} were placed in 100 mL of 1.0 M HCl for 30 min and recovered by vacuum filtration. The amount of Cu^{2+} desorbed from the silica gels and leached to the HCl solution was measured. The recovered silica gels were washed with copious

amounts of deionized water and then dried at 100ºC for 2 h. These procedures were repeated four more times to determine whether the copper-imprinted and nonimprinted silica gels could retain their copper adsorption capacity after several cycles.

Spectrophotometric quantification of Cu^{2+} concentration

Quantification of copper concentration was carried out by measuring the absorbance of a copper solution/dithizone mixture with a UV-vis spectrometer (Cary 50, Varian, Australia). In all experiments, water was used as reference. First, dithizone was dissolved in a hot aqueous solution containing 4% (w/v) of Triton X-100 to a final concentration of 0.1 mM, and the pH was adjusted to 1.4 with concentrated sulfuric acid (~ 1.0 M). Next, 3.5 mL of the dithizone solution was pipetted into a standard quartz cuvette and aliquots of copper solution were added and equilibrated for a few minutes. Finally, the absorbance at 506 nm at 25°C was measured and the concentration of Cu^{2+} was obtained by comparing the absorbance value with a calibration curve. More details regarding the spectrophotometric method can be found elsewhere (Kumar et al., 1991).

3.1.3 Results and Discussion

Validation of the spectrophotometric method for determining Cu^{2+} concentration

First, we validated the methodology of using UV-vis spectroscopy to quantify the concentration of Cu^{2+}. As shown in Figure 3.1a, the absorbance at 506 nm increased

linearly with the Cu^{2+} concentration up to 350 μg/mL, and the correlation coefficient of the fitting line was 0.99896. This result suggests that the concentration of Cu^{2+} can be determined quantitatively by measuring the absorbance at 506 nm. In addition, we also investigated the influence of competing ions, such as Ca^{2+} and Mg^{2+} on the accuracy of this method. It was found that with the presence of 200 μg/mL of Mg^{2+} or

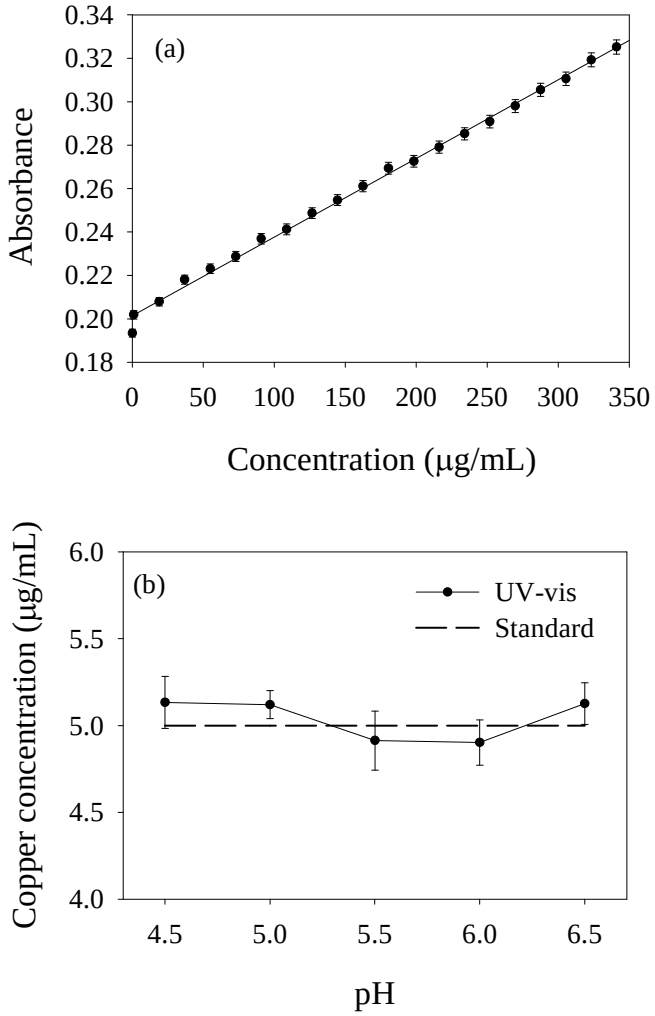

Figure 3.1 (a) Absorbance (at 506 nm) of various aqueous solutions containing 0.1 mM of dithizone, 4% of Triton X-100, and different concentration of Cu^{2+} (0 – 350 μg/mL). The fitting line was used as a calibration curve for the determination of Cu^{2+} concentration. (b) Comparison of Cu^{2+} concentrations obtained from UV-vis spectroscopy and the standard concentration at different pH.

360 μg/mL of Ca^{2+}, the absorbance at 506 nm still increased linearly with the concentration of Cu^{2+} (data not shown). Thus, we can exclude the interferences from Mg^{2+} and Ca^{2+} in the measurement. We further confirm the methodology by measuring the concentration of a standard Cu^{2+} solution (5.0 μg/mL) at different pH by using the UV-vis spectroscopy. As shown in Figure 3.1b, the differences in the measured concentrations and the actual concentration is found to be 2.67% for pH = 4.5, 2.40% for pH =5.0, 1.73% for pH = 5.5, 1.96% for pH = 6.0, and 2.53% for pH = 6.5. We conclude that the spectrophotometric method can be used to determine the concentration of Cu^{2+} with a high accuracy.

Characterization of modified silica gel

To quantify the surface densities of glycine, diglycine and triglycine immobilized on the silica gel, elemental analysis was employed to monitor the contents of carbon, hydrogen, and nitrogen of silica gel after each chemical modification step. First, the results in Table 3.1 indicate that after reacting with APES, the contents of carbon, hydrogen and nitrogen of the silica gel increased to 5.45%, 1.17% 1.65%, respectively. If we assume all three ethoxy groups of APES hydrolyze before reacting with surface silanol groups, each immobilized APES has three carbon atoms. Based on this assumption and the total surface area of the silica gel (320 m^2/g), we estimate the surface density of immobilized APES to be 4.73 μmol/m^2. Because this value is close to the ideal surface density of silanol groups (4.49 μmol/m^2), we hypothesize that a complete monolayer of APES is formed on silica surfaces (Krasnoslobodtsev et

al., 2002). From Table 3.1, we also calculate the surface density of aldehyde groups after the immobilized APES reacted with glutaraldehyde. Coincidentally, the results show that the surface density of glutaraldehyde is also 4.73 μmol/m^2. Thus, we assume that each amino group of the immobilized APES reacts with one aldehyde group of a glutaraldehyde molecule on the surface.

Table 3.1 Elemental analysis data showing the weight percentage of chemical composition (C, H, N) of silica gel after each chemical modification step.

	C%	H%	N%	Density based on C (μmol/m^2)
Silica gel	0.17	1.04	0.02	--
APES	5.45	1.17	1.65	4.73
Glutaraldehyde	14.53	1.92	1.52	4.73
Glycine				
Nonimprinted	14.62	1.92	1.49	3.81
Copper-imprinted	14.20	1.38	1.24	3.70
Diglycine				
Nonimprinted	14.86	1.88	1.73	3.22
Copper-imprinted	14.65	1.40	1.62	3.18
Triglycine				
Nonimprinted	15.69	1.81	1.80	2.92
Copper-imprinted	15.37	1.64	1.66	2.86

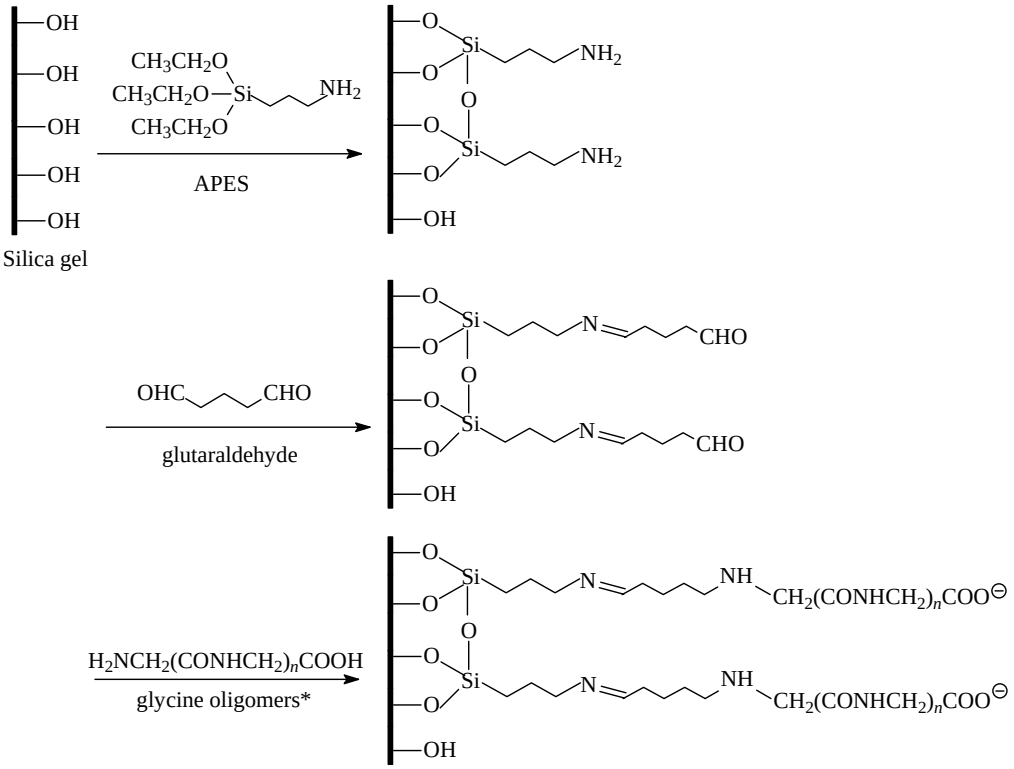

* n = 0, 1, 2 for glycine, diglycine, and triglycine.

Scheme 3.1 Procedure for chemical modification of silica gel with APES, glutaraldehyde, and glycine oligomers.

Next, we compared the chemical composition of glycine, diglycine, and triglycine functionalized silica gels which were not imprinted by Cu^{2+}. If we assume each immobilized glutaraldehyde reacts with one glycine, diglycine or triglycine as shown in Scheme 3.1, the theoretical %C ratio for the glycine, diglycine and triglycine functionalized surface should be 1:1.2:1.4. However, our results show that %C ratio for glycine, diglycine and triglycine is 1:1.02:1.07. The discrepancy from the experimental data suggests that some ethoxy groups from APES might not hydrolyze completely, or some glutaraldehyde did not react with glycine, diglycine or triglycine. Moreover, because glycine is smaller than diglycine and triglycine, it can diffuse into

the micropores of the silica gel more easily, leading to a higher immobilization efficiency. This effect will also cause the %C ratio for the diglycine and triglycine functionalized silica gels lower than 1.2 and 1.4, respectively. Similarly, the theoretical %N ratio for the glycine, diglycine, and triglycine functionalized surface should be 1:1.5:2. Once again, our experimental %N is only 1:1.16:1.21, possibly because of the incomplete hydrolysis of APES, unreacted glutaraldehyde and the higher diffusivity of glycine and its higher immobilization efficiency.

From the analysis of %C and %N shown above, we also find that %N is more sensitive to the surface densities of glycine, diglycine and triglycine. Therefore, to evaluate the influence of the ion-imprinting procedure on the surface densities of functional groups, we compared the nitrogen content of the copper-imprinted and nonimprinted silica gels. From Table 3.1, it is found that the nitrogen content of the copper-imprinted glycine functionalized silica gel is lower than that of the nonimprinted silica gel, which suggests that the density of immobilized glycine on the copper-imprinted silica gel is lower. The lower glycine density on the copper-imprinted silica gel led us to propose a model to explain the difference between the copper-imprinted and nonimprinted silica gels.

As shown in Scheme 3.2, when the glycine is immobilized on the surface without the presence of Cu^{2+}, most of the surface aldehyde group reacts with one glycine molecule. In contrast, in the presence of Cu^{2+}, two glycine molecules complex one Cu^{2+} in the solution as shown in Scheme 3.2c. When these two glycine molecules

react with surface aldehyde groups and immobilize on the surface, the intermolecular distance of two glycine molecules is limited by the presence of Cu^{2+} as shown in Scheme 3.2b. As a result, the distance between the two immobilized glycine is larger than that in Scheme 3.2a.

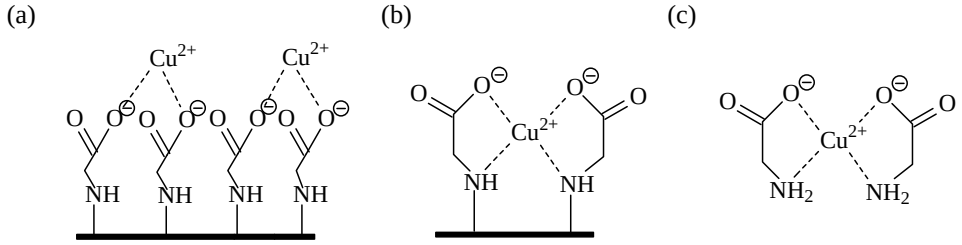

Scheme 3.2 A proposed model of glycine-Cu^{2+} complexes formed on silica surfaces decorated with glycine or in the glycine solution. (a) Complexation of Cu^{2+} with carboxylate groups. (b) Complexation of Cu^{2+} with carboxylate-O and amine-N. (c) The proposed glycine-Cu^{2+} complex in the glycine solution.

Similarly, nonimprinted silica gels functionalized with diglycine and triglycine also have higher nitrogen contents compared to copper-imprinted silica gels, similar to the case of glycine-functionalized silica gel. Thus, we propose a similar model for the copper-imprinted silica gels functionalized with diglycine and triglycine. In the solution phase, diglycine and triglycine form stable metal complexes with Cu^{2+} as shown in Scheme 3.3e, 3.3f and Scheme 3.4f. The metal complexes therefore define the intermolecular distances between diglycine and triglycine when they are immobilized on the surface.

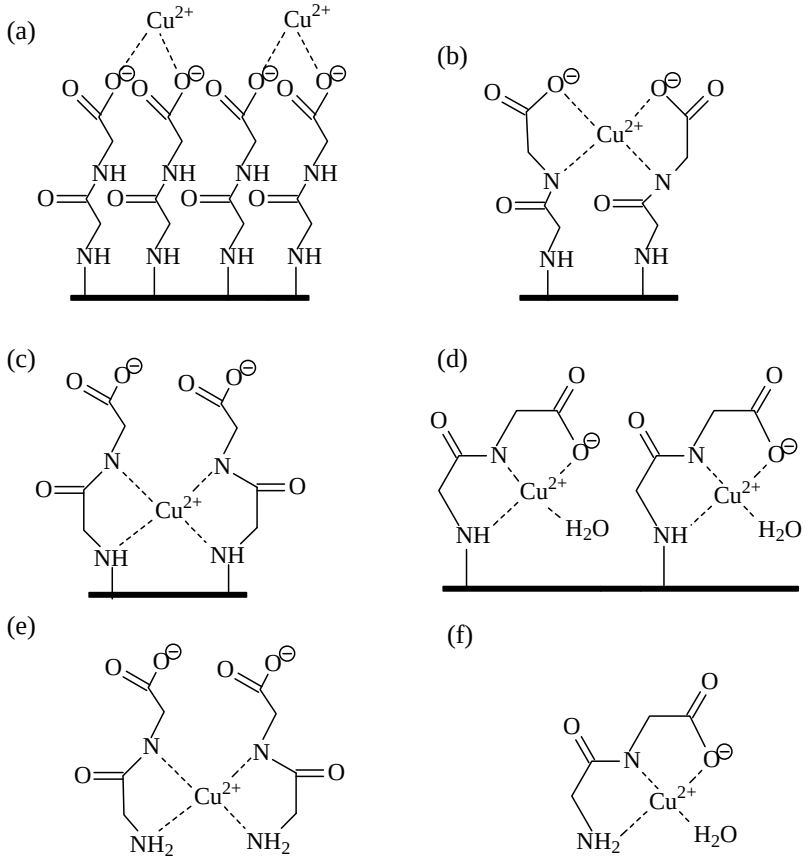

Scheme 3.3 A proposed model of diglycine-Cu^{2+} complexes formed on silica surfaces decorated with diglycine or in the diglycine solution. (a) Complexation of Cu^{2+} with carboxylate groups. (b) Complexation of Cu^{2+} with carboxylate-O and amide-N. (c) Complexation of Cu^{2+} with two amine-N and two amide-N. (d) Complexation of Cu^{2+} with diglycine to form 1:1 complex. (e) and (f) are the proposed diglycine-Cu^{2+} complexes in the diglycine solution.

Effect of ion-imprinting on Cu^{2+} adsorption

To evaluate how much Cu^{2+} can be adsorbed by the copper-imprinted and nonimprinted silica gels, we performed several dynamic adsorption experiments at different pH and obtained the percentage of Cu^{2+} adsorption by using silica gels functionalized with glycine, diglycine and triglycine, respectively. We can draw several conclusions from the results shown in Figure 3.2a. First, the amounts of Cu^{2+}

adsorbed onto the glycine-functionalized silica gel generally decreased with the decreasing of pH for both copper-imprinted and nonimprinted silica gels, which is consistent with many past studies showing the protons compete with Cu^{2+} for adsorption sites effectively at low pH. Second, at pH = 6.0, nonimprinted silica gel adsorbed more Cu^{2+} than the one imprinted with Cu^{2+}. The higher adsorption percentage can be attributed to the higher surface density of glycine on the nonimprinted silica gel as shown in Table 3.1. When the pH was lowered to 4.5, however, only 34.29% of Cu^{2+} was adsorbed by the nonimprinted silica gel whereas 60.98% of Cu^{2+} was adsorbed by the copper-imprinted silica gel. This result suggests the copper imprinting during the immobilization of glycine is able to increase the percentage of Cu^{2+} adsorption at low pH. We can explain the imprinting effect by using Scheme 3.2a and 3.2b. For nonimprinted silica gel, the complexation of Cu^{2+} and glycine is formed because of the electrostatic attraction between carboxylate and Cu^{2+}. When pH is lowered to 4.5, part of the carboxylate groups are protonated and cause the destabilization of the metal complex. In contrast, for copper-imprinted silica gel, the cavity formed between two glycine molecules allow them to chelate a Cu^{2+} not only through their carboxylate groups but also through amide nitrogen as shown in Scheme 3.2b. Because the coordination between nitrogen and Cu^{2+} is more stable than the ionic interactions between carboxylate and Cu^{2+}, the Cu^{2+} complex shown in Scheme 3.2b is more stable at low pH and results in a higher adsorption percentage of Cu^{2+}.

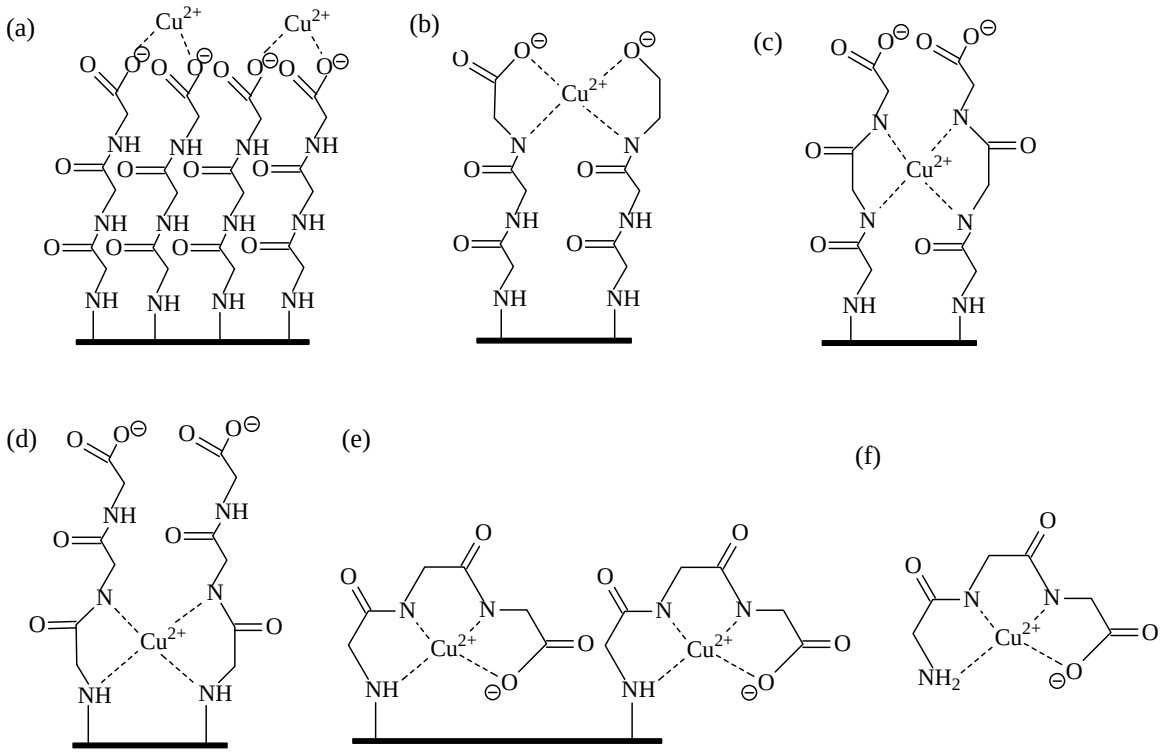

Scheme 3.4 A proposed model of triglycine-Cu^{2+} complexes formed on silica surfaces decorated with triglycine or in triglycine solution. (a) Complexation of Cu^{2+} with carboxylate groups. (b) Complexation of Cu^{2+} with carboxylate-O and amide-N. (c) Complexation of Cu^{2+} with four amide-N. (d) Complexation of Cu^{2+} with two amine-N and two amide-N. (e) Complexation of Cu^{2+} with triglycine to form 1:1 complex. (f) triglycine-copper complex in the triglycine solution.

Next, we performed similar Cu^{2+} adsorption experiments with diglycine-functionalized silica gel at different pH. As shown in Figure 3.2b, the percentage of Cu^{2+} adsorption for nonimprinted silica gel modified with diglycine was generally higher than the silica gel modified with glycine. We propose that the higher capacity can be attributed to the complexation of Cu^{2+} to the amide nitrogen of diglycine. Scheme 3.3a and 3.3b reveal that the immobilized diglycine does not only allow the complexation with Cu^{2+} through the carboxylate-O, but also through the amide-N. We point out that the complexation shown in Scheme 3.3b is possible without the ion-imprinting procedure because of the flexibility of the diglycine

molecules. Two immobilized diglycine may slightly separate apart and allow the entrance of Cu^{2+} to the binding site, which is prohibited for a shorter molecule such as glycine. In addition, we note that the copper-imprinting procedure on diglycine-functionalized silica gel also led to a higher adsorption percentage than the one without the copper imprinting. Based on this observation, we propose that when the copper imprinting procedure is employed, diglycine is likely to form two different complexes with Cu^{2+} in the aqueous solution as shown in Scheme 3.3e and 3.3f. As a result, the two immobilized diglycine with proper intermolecular distance may form Cu^{2+} complex as shown in Scheme 3.3c and 3.3d, which are more stable than the Cu^{2+} complexes shown in Scheme 3.3a and 3.3b because of the addition stability offered by the coordination with N (Gooding et al., 2001).To further support our proposition, we point out that if the diglycine is immobilized on surface as shown in Scheme 3.3c and 3.3d, the surface density of diglycine should be lower compared to Scheme 3.3a and 3.3b, which is consistent with our elemental analysis results in Table 3.1. Therefore, we believe that the higher Cu^{2+} adsorption capacity of the copper imprinted silica gel at low pH comes from the additional stability provided by the metal complexes shown in Scheme 3.3c and 3.3d.

Furthermore, Figure 3.2a – 3.2c show that for both copper-imprinted and nonimprinted silica gels, the one functionalized with triglycine provided the highest percentage of Cu^{2+} adsorption among the glycine, diglycine and triglycine-functionalized silica gels. To explain this phenomenon, we have the following propositions. First, when nonimprinted silica gel is used, the immobilized

triglycine complex with Cu^{2+} as shown in Scheme 3.4a – 3.4c. Once again, we believe Scheme 3.4b and 3.4c are possible because of the flexibility of triglycine molecules permits the entrance of Cu^{2+} to the binding site. The complex shown in Scheme 3.4c is very stable because it involves the coordination with four nitrogen atoms; the high stability of the complex is consistent with the higher copper adsorption capacity observed at low pH. Second, because triglycine is a tetradentate ligand which is able to complex a Cu^{2+} with one amine-N, two amide-N and one carboxylate group, we propose that when copper imprinting is employed, the immobilized triglycine molecule can form a very stable 1:1 complex with Cu^{2+} as shown in Scheme 3.4e. Another possible metal complex can be formed on the surface is shown in Scheme 3.4d, which involves four nitrogen from two adjacent immobilized triglycine molecules. Metal complex shown in Scheme 3.4d is very stable because the two immobilized molecules can act as a single tetradentate ligand. This phenomenon is known as "surface-chelating effect" (Major et al., 2003). However, we hypothesize that, to form metal complexes as shown in Scheme 3.4d and 3.4e requires a proper intermolecular distance. For example, if the surface is functionalized with high-density of triglycine as shown in Scheme 3.4a, the complex as shown in Scheme 3.4e will not form because of the steric hindrance from the adjacent molecules. As a result, we believe that the higher adsorption capability obtained from the copper imprinting procedure at low pH can be ascribed to the formation of highly-stable metal complexes as shown in Scheme 3.4d and 3.4e.

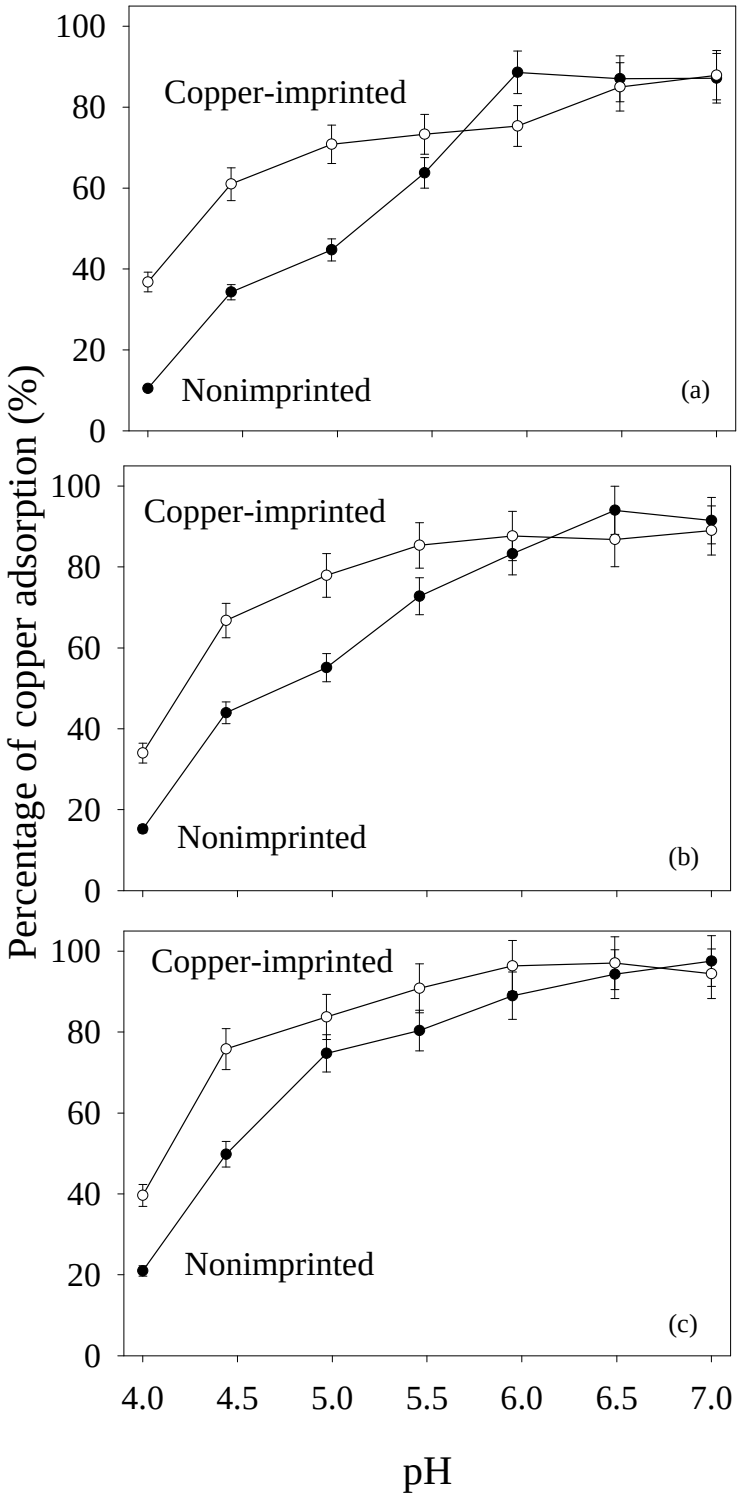

Figure 3.2 Effect of pH on the percentage of Cu^{2+} adsorption by using copper-imprinted and nonimprinted silica gels functionalized with (a) glycine (b) diglycine and (c) triglycine. The concentration of Cu^{2+} was 4.0 μg/mL.

Copper adsorption capacity of imprinted and nonimprinted silica gel

From Figure 3.2a – 3.2c, we observe that copper-imprinted silica gel consistently exhibits a higher percentage of Cu^{2+} adsorption than the one without imprinting, except when pH > 6.0. In addition, it is found that copper-imprinted and nonimprinted silica gels show greatest difference in the percentage of Cu^{2+} adsorption at pH = 4.5. Therefore, in our next experiments, we tested the adsorption capacity of Cu^{2+} by using the imprinted and nonimprinted silica gels at this pH. To measure the Cu^{2+} adsorption capacity, we varied the initial Cu^{2+} concentration from 0.4 to 320 μg/mL. The results in Figure 3.3 show that the amounts of Cu^{2+} adsorbed by silica gels increase with the initial Cu^{2+} concentration until a maximum is reached, which is defined as the total adsorption capacity. The total adsorption capacities of the copper-imprinted and nonimprinted silica gels are summarized in Figure 3.4. The result shows that the adsorption capacity of the copper-imprinted silica gel is approximately 50% higher than that of the nonimprinted silica gel, and the total adsorption capacity increases in the order of triglycine > diglycine > glycine.

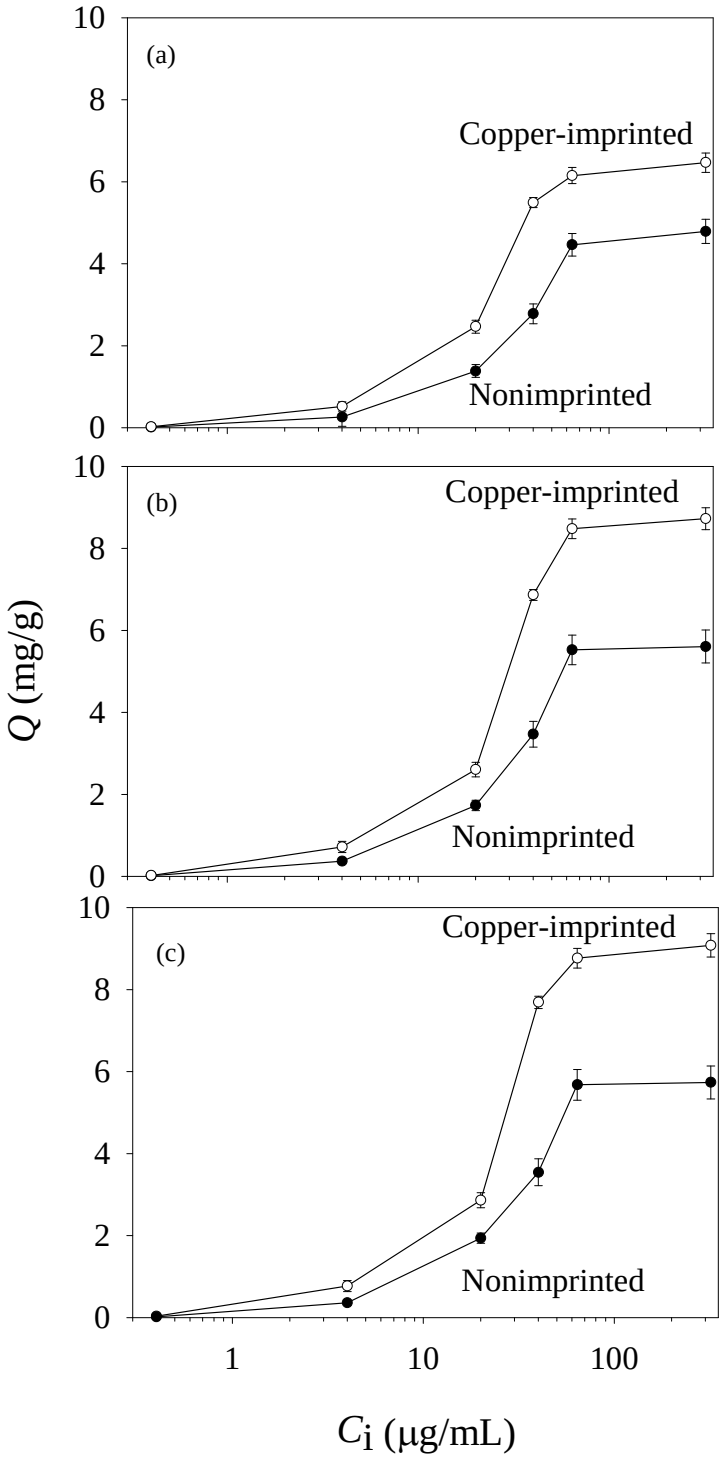

Figure 3.3 Amounts of Cu^{2+} adsorbed per unit mass of copper-imprinted and nonimprinted silica gels functionalized with (a) glycine, (b) diglycine and (c) triglycine as a function of Cu^{2+} concentration at pH = 4.5.

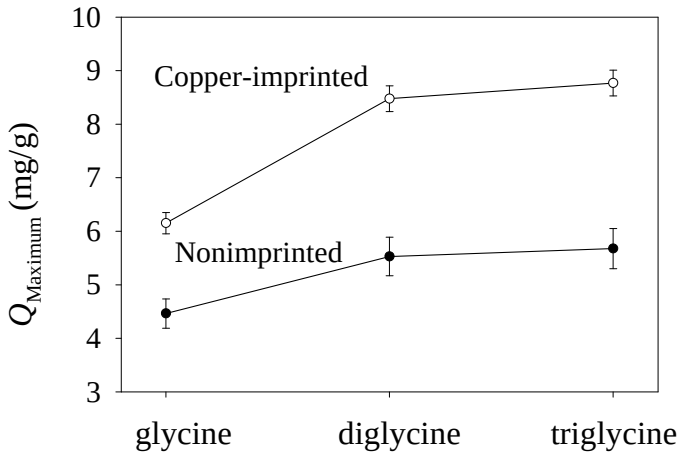

Figure 3.4 Comparison of total Cu^{2+} adsorption capacities of copper-imprinted and nonimprinted silica gels at pH = 4.5. The silica gels were functionalized with glycine, diglycine and triglycine, respectively.

Selectivity for metal ions

The above results clearly illustrate that the copper-imprinted silica gel has a higher Cu^{2+} adsorption capacity than the nonimprinted silica gel. In the following experiments, we further investigated whether the copper-imprinted silica gel still has a higher adsorption capacity for Cu^{2+} in the presence of competing metal ions, such as Mg^{2+} and Ca^{2+}. First, we performed the competitive adsorption experiments by using a solution containing 4.0 μg/mL of Cu^{2+} and 200 μg/mL of Mg^{2+}. We chose Mg^{2+} not only because it is a divalent metal ion but it also has a similar ionic radius as Cu^{2+}. Figure 3.5 shows the adsorption percentage of Cu^{2+} as a function of pH by using silica gels functionalized with glycine, diglycine and triglycine, respectively. Apparently, all copper-imprinted silica gels exhibit higher adsorption percentage than their nonimprinted counterparts for all pH tested in this experiment. By comparing the results in the presence of Mg^{2+} (Figure 3.5) and without the Mg^{2+} (Figure 3.2), it is

found that the percentage of Cu^{2+} adsorbed onto nonimprinted silica gel in Figure 3.5 is lower than in Figure 3.2, which suggests that the Mg^{2+} is capable of competing with Cu^{2+} for the adsorption sites at carboxylate groups. This competition is consistent with an electrostatic attraction between the positively-charged Mg^{2+} and negatively-charged carboxylate groups. However, for the copper-imprinted silica gel, the percentage of Cu^{2+} adsorption did not show a significant decrease in the presence of Mg^{2+}, especially at low pH. This is because Mg^{2+} is unable to coordinate with amide-N or amine-N as Cu^{2+}, and the Cu^{2+} adsorbed onto the copper-imprinted silica gel through the stable coordination with N as shown in Scheme 3.2b, 3.3c, 3.3d, 3.4d and 3.4e cannot be replaced by Mg^{2+}. Therefore, the percentage of Cu^{2+} adsorption for copper-imprinted silica gel is less affected by the presence of Mg^{2+}. In fact, the presence of Mg^{2+} only makes the imprinting effect more pronounced.

To further investigate the selectivity of the copper-imprinted silica gel, we used a second divalent metal ion, Ca^{2+}, as the competing ion. The results shown in Figure 3.6 were obtained by using a solution containing 4.7 μg/mL of Cu^{2+} and 360 μg/mL of Ca^{2+}. Once again, we find that the percentage of Cu^{2+} adsorption was higher for all pH when the copper-imprinted silica gel was used. This finding further confirms that the copper-imprinted silica gel show high selectivity for Cu^{2+} over metal ions which do not form coordination complexes with nitrogen.

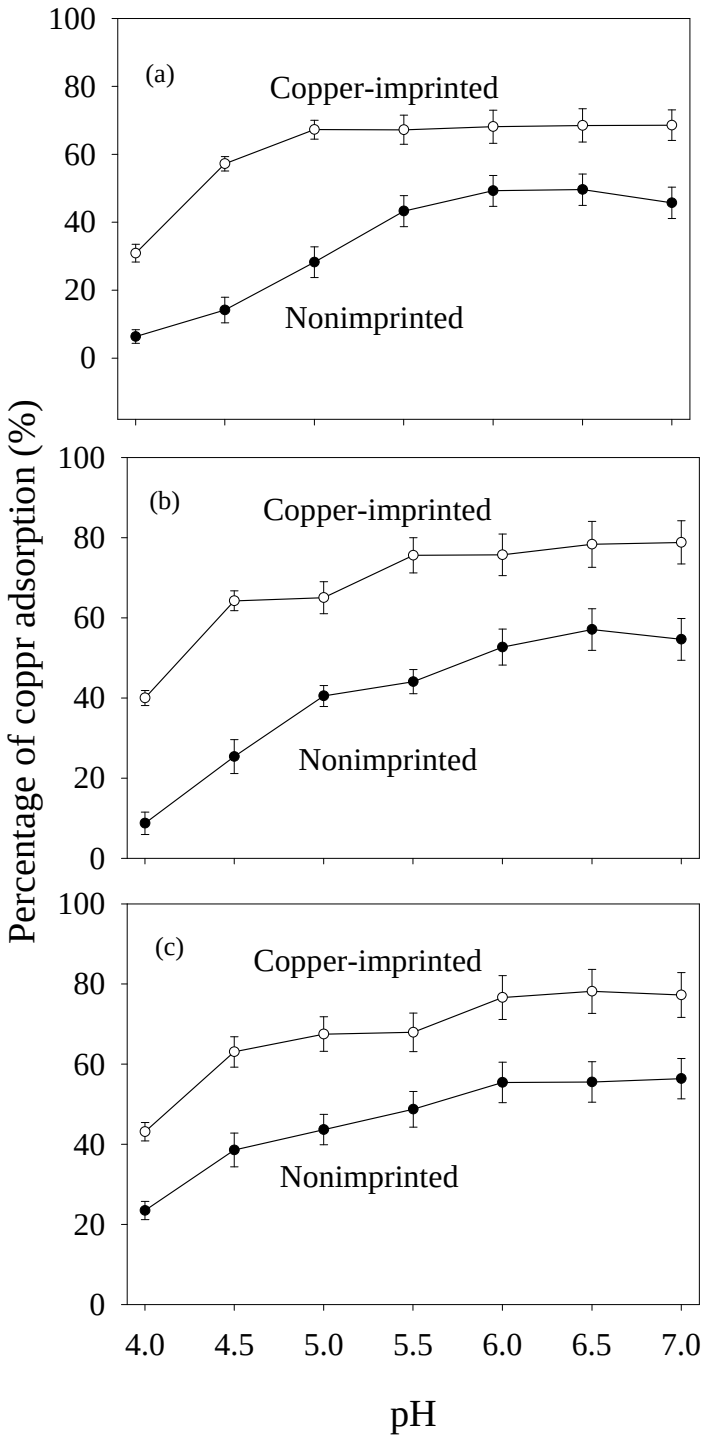

Figure 3.5 Percentage of Cu^{2+} adsorption by using copper-imprinted and nonimprinted silica gels functionalized with (a) glycine (b) diglycine and (c) triglycine at different pH. In all of the adsorption experiments, Mg^{2+} was added to the Cu^{2+} solution as a competing metal ion. The concentration of Cu^{2+} and Mg^{2+} were 4.0 μg/mL and 200 μg/mL, respectively.

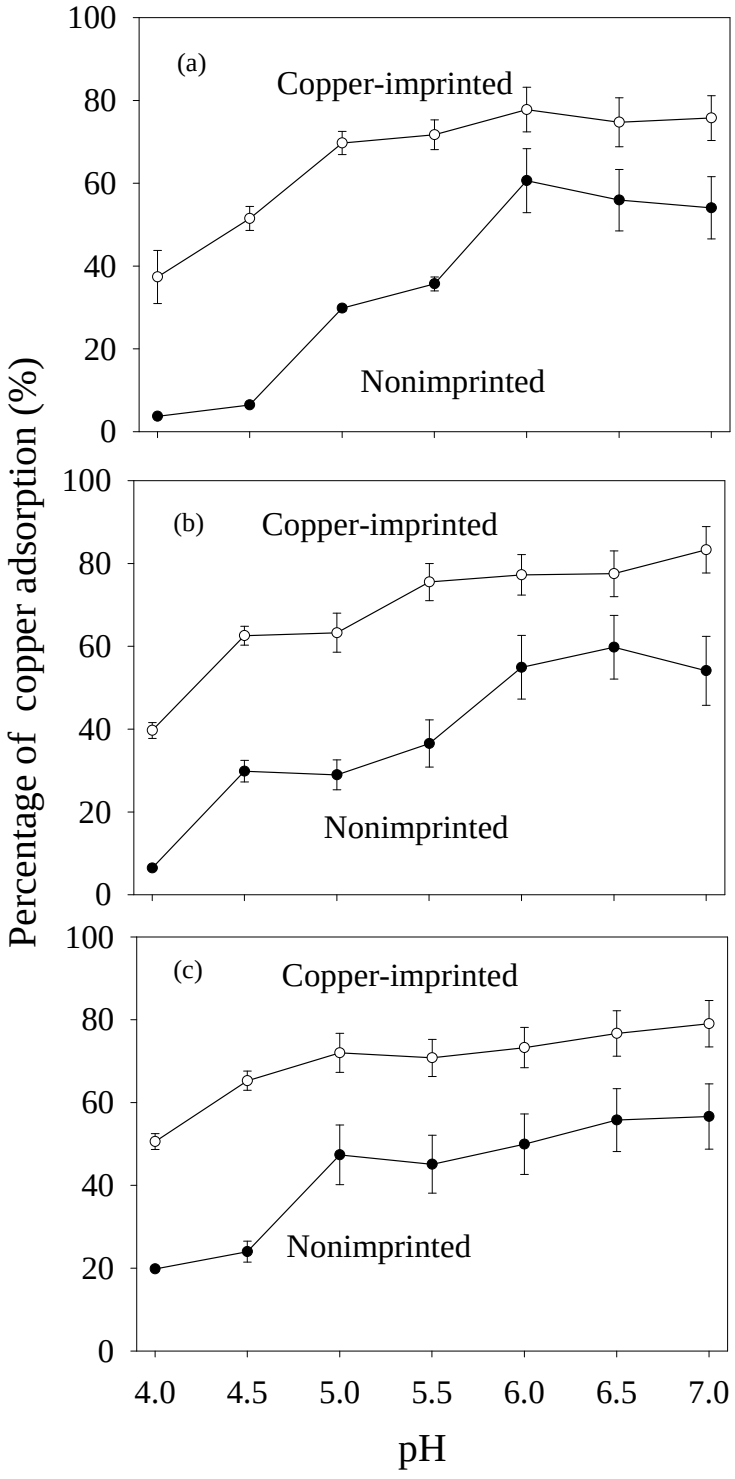

Figure 3.6 Percentage of Cu^{2+} adsorption by using copper-imprinted and nonimprinted silica gels functionalized with (a) glycine (b) diglycine and (c) triglycine at different pH. In all of the adsorption experiments, Ca^{2+} was added to the Cu^{2+} solution as a competing metal ion. The concentration of Cu^{2+} and Ca^{2+} were 4.7 µg/mL and 360 µg/mL respectively.

Desorption of Cu^{2+} and reusability of the silica gel

To evaluate the reusability of the copper-imprinted and nonimprinted silica gels for Cu^{2+} adsorption, we first performed desorption experiments with copper-imprinted and nonimprinted silica gels functionalized with glycine, diglycine, and triglycine, respectively, by rinsing the copper-loaded silica gel with 1.0 M of HCl for 30 min. The percentage of Cu^{2+} desorption from different silica gels in Figure 3.7 reveals that the acidic HCl solution can effectively desorb the absorbed Cu^{2+} from the copper-imprinted and the nonimprinted silica gels.

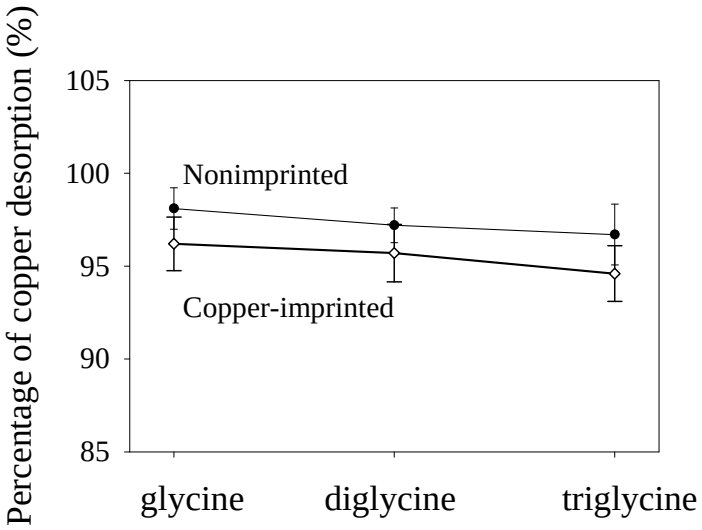

Figure 3.7 Percentage of Cu^{2+} desorption from the copper-imprinted and nonimprinted silica gels functionalized with glycine, diglycine, and triglycine. The copper-loaded silica gel was incubated in 1.0 M of HCl for 30 min to desorb the Cu^{2+}.

It is found that the percentage of Cu^{2+} desorption from copper-imprinted silica gel functionalized with triglycine is the lowest, while the nonimprinted silica gel functionalized with glycine is the highest. This result is consistent with the high stability of triglycine- Cu^{2+} complex on the surface of copper-imprinted silica gel. We

also conclude that a single stage of washing with 1.0 M HCl is able to remove more than 94.5% of Cu^{2+}.

Next, we performed several adsorption/desorption experiments in which the copper-loaded silica gel was rinsed with 1.0 M HCl and reused for Cu^{2+} adsorption. Due to the number of steps involved, approximately 5% of the total mass of silica gel was lost in each cycle. Therefore, the amount of the initial Cu^{2+} solution was also reduced by 5% in each cycle, i.e. 95 mL of Cu^{2+} solution in the second cycle, and 90.25 mL in the third cycle, etc. Figure 3.8 shows the Cu^{2+} adsorption capacities for both copper-imprinted and nonimprinted silica gels for five consecutive cycles. It can be found that the adsorption capacities of both copper-imprinted and nonimprinted silica gels decrease slightly after each cycle. Despite the small decrease, the adsorption capacity of copper-imprinted silica gel is still 50% higher than that of nonimprinted silica gel until the final cycle.

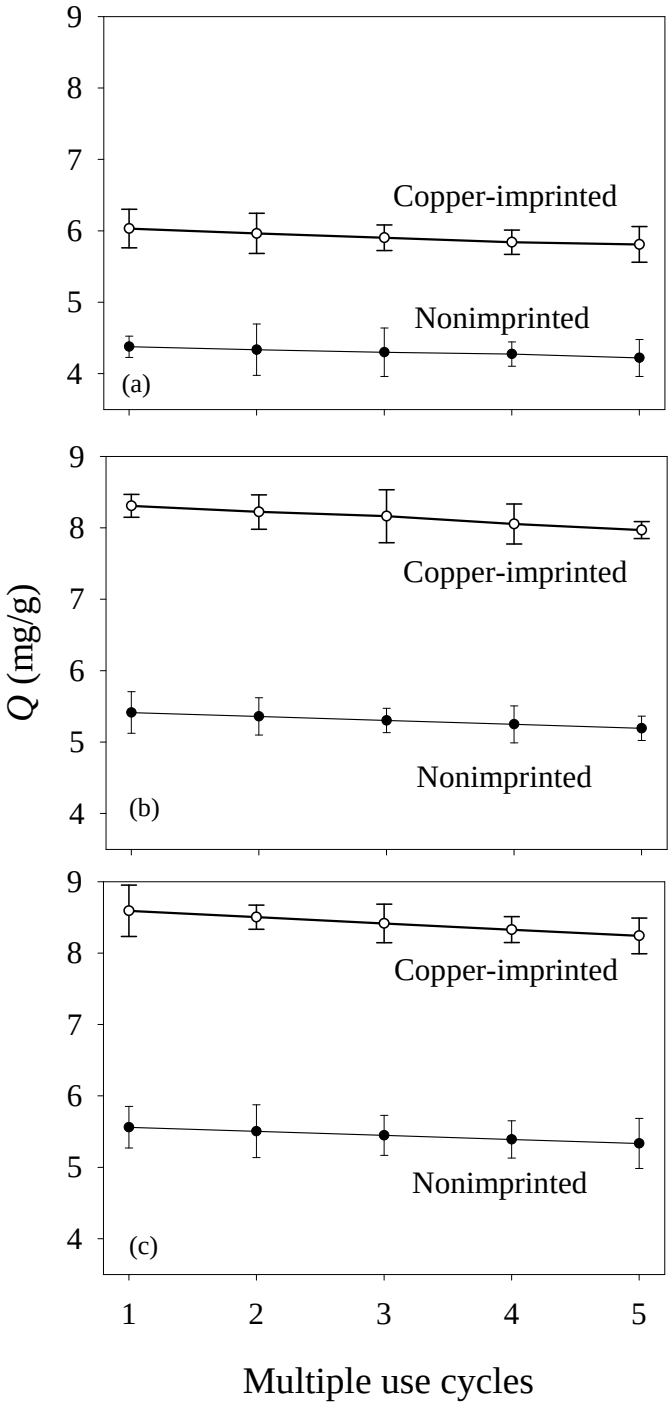

Figure 3.8 Multiple use cycles of copper-imprinted and nonimprinted silica gels functionalized with (a) glycine, (b) diglycine and (c) triglycine.

3.1.4 Conclusions

In this study, we have demonstrated that the copper-imprinted silica gels functionalized with glycine, diglycine and triglycine have higher adsorption capacity for Cu^{2+} than the nonimprinted silica gels. The imprinting effect is more significant at low pH. For example, at pH = 4.5, the adsorption capacity of the copper imprinted silica gel is 50% higher than nonimprinted silica gel whereas at pH = 6.0, the adsorption capacity of the nonimprinted silica gel is slightly higher than copper-imprinted silica gel. We attribute the higher adsorption capacity of copper-imprinted silica gel at low pH to two factors. First, two immobilized molecules can chelate Cu^{2+} as a multi-dentate ligand if the intermolecular distance between these two molecules is appropriate. This phenomenon is known as the surface chelating effect. Second, for a single immobilized diglycine and triglycine, they can form very stable 1:1 complex with Cu^{2+} if the surface is not over-crowded. By using copper imprinting during the immobilization procedure, both proper intermolecular distance and intermediate density of the immobilized molecules suitable for chelating Cu^{2+} can be achieved. Finally, it is also found that the difference between the copper-imprinted and nonimprinted silica gel becomes more pronounced in the presence of competing ions. When 200 μg/mL (50-fold) of Mg^{2+} or 360 μg/mL (76-fold) of Ca^{2+} are used as competing ions, the adsorption capacity of the copper-imprinted silica gel is nearly unaffected. In contrast, the nonimprinted silica gel exhibits lower adsorption capacity of Cu^{2+} in the presence of Mg^{2+} or Ca^{2+}.

3.2 Interactions Between Ion-Imprinted Silica Surfaces with Cu^{2+}

3.2.1 Introduction

It is well-known that proteins or peptides form secondary structures through the formation of hydrogen bonds between adjacent amide groups and functional side chains (Branden et al., 1999). In addition, more and more studies show that metal ions also can induce conformational changes in polypeptides or oligopeptides, leading to the formation of secondary structures. For example, when a Cu^{2+} binds to a pentapeptide HAKCE, it triggers the formation of an α-helix structure as demonstrated by Wang et al. (Wang et al., 2003). Another example is when Cu^{2+} binds to an oligopeptide, AEAEAKAKAEAEAKAKGGH, it causes the conformation of the oligopeptide to change from α-helix/random coil to β-sheet (Yang et al., 2006). In these examples, Cu^{2+} binds to metal-coordinating amino acid residues such as cysteine (C) or histidine (H). Furthermore, Cu^{2+} also can bind to the amide groups (Sigel et al., 1982; Burger et al., 1990) and change the conformations of oligopeptides or small molecules. For example, when triglycine complexes with Cu^{2+}, it forms a loop structure through the metal complexation with an amino group, a carboxylate group, and two amide groups (Kim et al., 1966 and 1969) The Cu^{2+} is able to deprotonate the amide nitrogen when pH > 4, making the triglycine-Cu^{2+} complex form a very stable loop structure as shown in Scheme 3.5. On the other hand, for those metal ions which cannot deprotonate the amide nitrogen of triglycine, they cannot form stable complexes with triglycine.

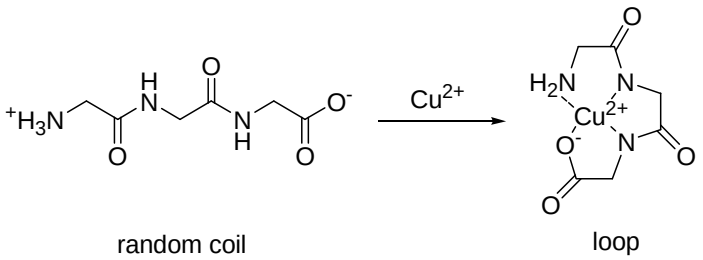

Scheme 3.5 Formation of triglycine-Cu^{2+} complex in aqueous solution.

Although conformational changes of oligopeptides caused by metal ions in aqueous solutions have been studied extensively, the influence of metal ions on the conformations of oligopeptides immobilized on solid surfaces is less known. However, an increasing number of researchers are taking advantages of the interactions between metal ions and immobilized oligopeptides for designing useful sensor devices or growing nanocrystals. For example, Takehara et al. (Takehara et al., 1994) exploited the conformational changes of glutathione induced by lanthanide ions to regulate the reduction/oxidization of ferrocyanide ions near an electrode decorated with glutathione. This principle was used as a sensing mechanism for detecting lanthanide ions. More recently, Banerjee et al. (Banerjee et al., 2003) used an oligopeptide, HGGGHGHGGGHG and its folded conformation induced by Cu^{2+} to control the growth of copper nanocrystals. In our previous work (Bi et al., 2007), we also observed that Cu^{2+} binds to tripeptides GGH and GGG immobilized on surfaces with high affinity. However, it was not clear whether the Cu^{2+} induced conformational changes of these tripeptides when they bound to Cu^{2+}. Because different conformations of immobilized peptides may lead to different binding capacity or selectivity for metal ions, it would be interesting to characterize the conformations of

these immobilized tripeptides and understand how these conformations influence the selectivity for metal ions.

Past studies have established that Fourier Transformation Infrared (FTIR) spectroscopy is a very useful analytical tool for characterizing protein conformations, because the ratio of amide I band (1600-1700 cm^{-1}) to amide II band (1500-1580 cm^{-1}) of a particular protein can be used to determine the proportion of its secondary structures (Oberg et al., 1998; Onodera et al., 2007; Zhang et al., 2005; Rigler et al., 2003; Liley et al., 1997; Surewicz et al., 1993; Hirashima et al., 2005; Maeda et al., 2000). However, FTIR in the transmission mode is not sensitive enough to study a single layer of molecules adsorbed on a solid surface. To address the sensitivity issue, FTIR with a horizontal attenuated total reflectance (HATR) attachment can be used. This configuration provides sensitivity high enough to study a single layer of molecules adsorbed on solid surfaces, because the signal-to-noise ratio is improved by increasing numbers of internal reflection (Stefan et al., 2000; Hind et al., 1997; Rigler et al., 2004). In the past, Onodera et al. has used this technique to study protein-protein specific and nonspecific interactions by combining FTIR with secondary structure analysis (Onodera et al., 2007), but it has never been used to study immobilized oligopeptides before. In this study, we used HATR-FTIR to characterize triglycine immobilized on the surfaces and investigate the effects of metal ions on the conformation of triglycine.

3.2.2 Experimental Section

Materials

Same as those in 3.1.2.

Surface modifications of silicon wafers

Silicon wafers (dummy grade, 0.6 mm thick, one-side polished, obtained from Wellbond, Singapore) were cut into small pieces (~ 2 cm × 1 cm) and cleaned in freshly prepared piranha solution (70% H_2SO_4 and 30% H_2O_2) at 80°C for 1 h to remove all organic contaminants. *Warning: Piranha solution reacts strongly with organic compounds and should be handled with extreme caution.* Subsequently, these cleaned wafers were washed with copious amount of deionized water and immersed in an aqueous solution containing 5% (v/v) of APES at 50ºC for 1 h. After removing the wafers from the aqueous solution, they were rinsed thoroughly with deionized water and acetone, blown dry with nitrogen and then baked in a vacuum oven (100ºC) for 15 min to promote the crosslinking of silanol groups to form siloxane networks. Subsequently, the APES-modified silicon wafers were immersed in an aqueous solution containing 5% (v/v) of glutaraldehyde and 10 mM of $NaBH_3CN$ for 2 h at 25ºC. The aldehyde-decorated silicon wafers were washed with excessive deionized water and acetone to remove residual glutaraldehyde and blown dry with nitrogen.

Immobilization of triglycine on solid surfaces

The aldehyde-decorated silicon wafers were reacted with 1 mM of triglycine in 0.5 M carbonate buffer (pH = 10) containing 10 mM of $NaBH_3CN$ at 50°C for 4 h. After the reaction, the silicon wafers were washed with copious amount of deionized water and blown dry with nitrogen to obtain **1** in Scheme 3.6. Alternatively, the aldehyde-decorated silicon wafers were reacted in an aqueous solution containing 1 mM triglycine, 1 mM copper nitrate and 10 mM $NaBH_3CN$ at 50°C for 4 h to obtain **3**. To remove Cu^{2+}, the silicon wafers were immersed in 1 M nitric acid for 5 min. Then, they were washed with copious amount of deionized water and blown dry with nitrogen to obtain **4**.

Complexation with Cu^{2+}

MES buffer (10 mM, pH = 6) was used to prepare copper solutions with various concentrations. Silicon wafers functionalized with triglycine were immersed in each copper solution for 15 min. Then, the silicon wafers were rinsed with ethanol and blown dry under nitrogen.

Ellipsometry

The ellipsometric thicknesses of triglycine, which was immobilized on the surfaces of silicon wafers, were measured using a Stokes Ellipsometer LSE (Gaertner in Skokie, IL, USA) at a wavelength of 632 nm and a fixed angle of 70°. Ellipsometric constants, *n* and *k*, of each cleaned silicon wafer were obtained using the computer

software provided by the manufacturer. The ellipsometric thicknesses of the surface organic layers were determined by assuming a single reflective index of 1.46 for a one-layer model. Each thickness represents an average thickness of five different spots.

XPS characterization

X-ray photoelectron spectroscopy (XPS) data were obtained utilizing an ultra-high vacuum XPS system AXIS HIS (Kratos, UK), which is equipped with a monochromotized Al Kα X-ray source (1486.6 eV) with a constant dwell time of 100 ms and a pass energy of 40 eV. The samples to be tested were mounted on standard studs using double-sided adhesive tapes. The pressure in the analysis chamber was maintained at 10^{-8} Torr or lower. All binding energies were referenced to the C1s hydrocarbon peak at 284.6 eV.

HATR-FTIR

A Fourier Transformation Infrared Spectroscopy (FTIR) spectrophotometer (IRPrestige-21, Shimadzu in Tokyo, Japan) equipped with a liquid nitrogen-cooled, mercury-cadmium-telluride (MCT) detector was employed for all measurements. Prior to each measurement, the silicon trough plate (PIKE Technologies, Madison, WI, USA) was polished with AUTOSOL®, followed by a thorough rinsing with deionized water. The surface modification of silicon trough plates is the same as that of silicon wafers. For each spectrum, the resolution was maintained at 4 cm^{-1} and 256

scans were accumulated between 1500 and 3100 cm^{-1}. All spectra were smoothed by using a procedure described by Onodera et al. (2007).

The effects of Cu^{2+} on the triglycine conformation in aqueous phase were investigated in situ by injecting aliquots of copper nitrate into triglycine solution (buffered to pH 6 with MES). Spectrum recorded in a copper-free triglycine solution was used as the reference. The immobilization of triglycine on surfaces and the copper-induced triglycine conformation were investigated by recording the spectra on dry silicon trough plates.

3.2.3 Results and Discussion

Cu^{2+}-induced conformational changes of triglycine in solution

Our first goal was to study the effect of Cu^{2+} on the triglycine conformation in aqueous solutions. Figure 3.9 shows the HATR-FTIR spectra of the triglycine solution with different concentrations of Cu^{2+} (a triglycine solution without Cu^{2+} was used as a reference). The peak at 1620 cm^{-1} is mainly due to amide C=O stretching whereas the peak at 1541 cm^{-1} is due to amide N-H bending (Surewicz et al., 1993; Hirashima et al., 2005; Maeda et al., 2000). These two peaks are the so-called amide I and amide II peaks, which are very sensitive to the protein secondary structures. Interestingly, although the triglycine concentration remains constant, when the Cu^{2+} concentration is increased, intensities of amide I and amide II peaks at 1620 cm^{-1} and 1541 cm^{-1} also increase. This result is consistent with an earlier IR study showing that the intensity of triglycine's amide I peak increased when more and more triglycine

molecules formed complexes with Cu^{2+} at increasing pH (Kim et al., 1966). Therefore, since we know that (1) triglycine forms a loop structure when it complexes with Cu^{2+}, and (2) the formation of a loop structure can lead to an increase in the amide I and amide II peaks (Prestrelski et al., 1991; Wilder et al., 1992), we propose that the increase of amide I and amide II peaks in Figure 3.9 can be attributed to the formation of loop-structured triglycine-Cu^{2+} complex.

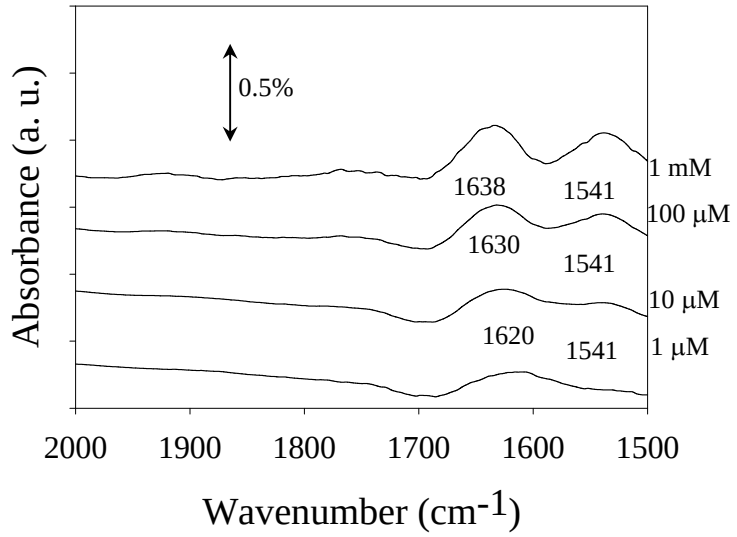

Figure 3.9 HATR-FTIR spectra of MES buffer (10 mM, pH = 6) containing 1 mM of triglycine and different concentrations of Cu^{2+}. Cu-free triglycine solution was used as a reference.

Characterization of triglycine immobilized on surfaces

Next, we investigated the effects of Cu^{2+} on the conformation of triglycine immobilized on solid surfaces. To increase the sensitivity of the HATR-FITR method, triglycine was directly immobilized on an aldehyde-decorated silicon trough plate. The HATR-FTIR spectrum in Figure 3.10 shows four characteristic peaks. Two strong peaks at 2857 cm^{-1} and 2930 cm^{-1} are assigned to symmetric and asymmetric

stretching of CH_2 (Asanuma et al., 2005) and peaks at 1625 cm^{-1} and 1556 cm^{-1} are assigned to amide I and amide II, respectively. These four peaks indicate that triglycine has been immobilized on the surface.

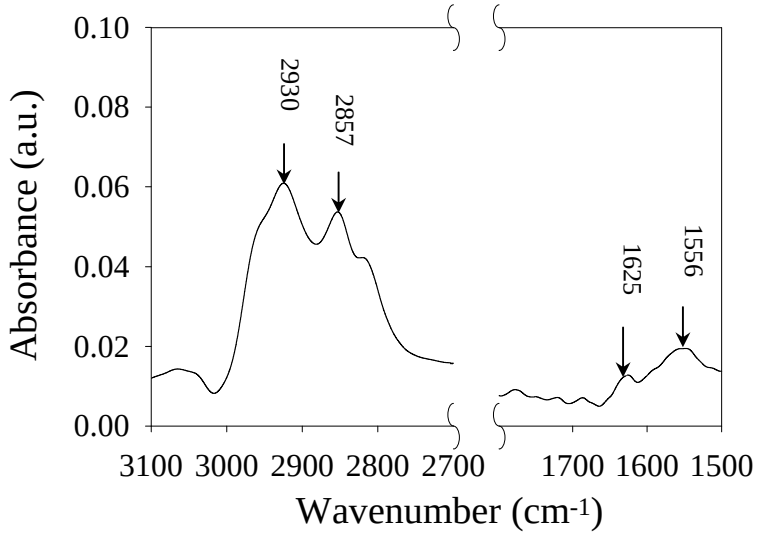

Figure 3.10 HATR-FTIR spectra of an aldehyde-decorated silicon trough plate with triglycine immobilized on the surface. The aldehyde-decorated surface was used as a reference.

We refer to this type of surface as **1** (Scheme 3.6). After we immersed **1** in aqueous solutions containing different concentrations of Cu^{2+} for 15 min and rinsed the surface with ethanol, we characterized the surface with XPS to detect the presence of Cu^{2+}. The XPS spectrum in Figure 3.11a for 100 μM of Cu^{2+} shows two peaks at 933 eV and 953 eV, which can be attributed to $Cu2p_{3/2}$ and $Cu2p_{1/2}$, respectively. These results suggest that triglycine immobilized on **1** start to complex with Cu^{2+} when the Cu^{2+} concentration is 100 μM. Then, by using HATR-FTIR, we investigated whether the complexation of Cu^{2+} also affected the conformation of immobilized triglycine.

As shown in Figure 3.11b, two peaks at amide I and amide II appeared when the Cu^{2+} concentration was as low as 1 μM.

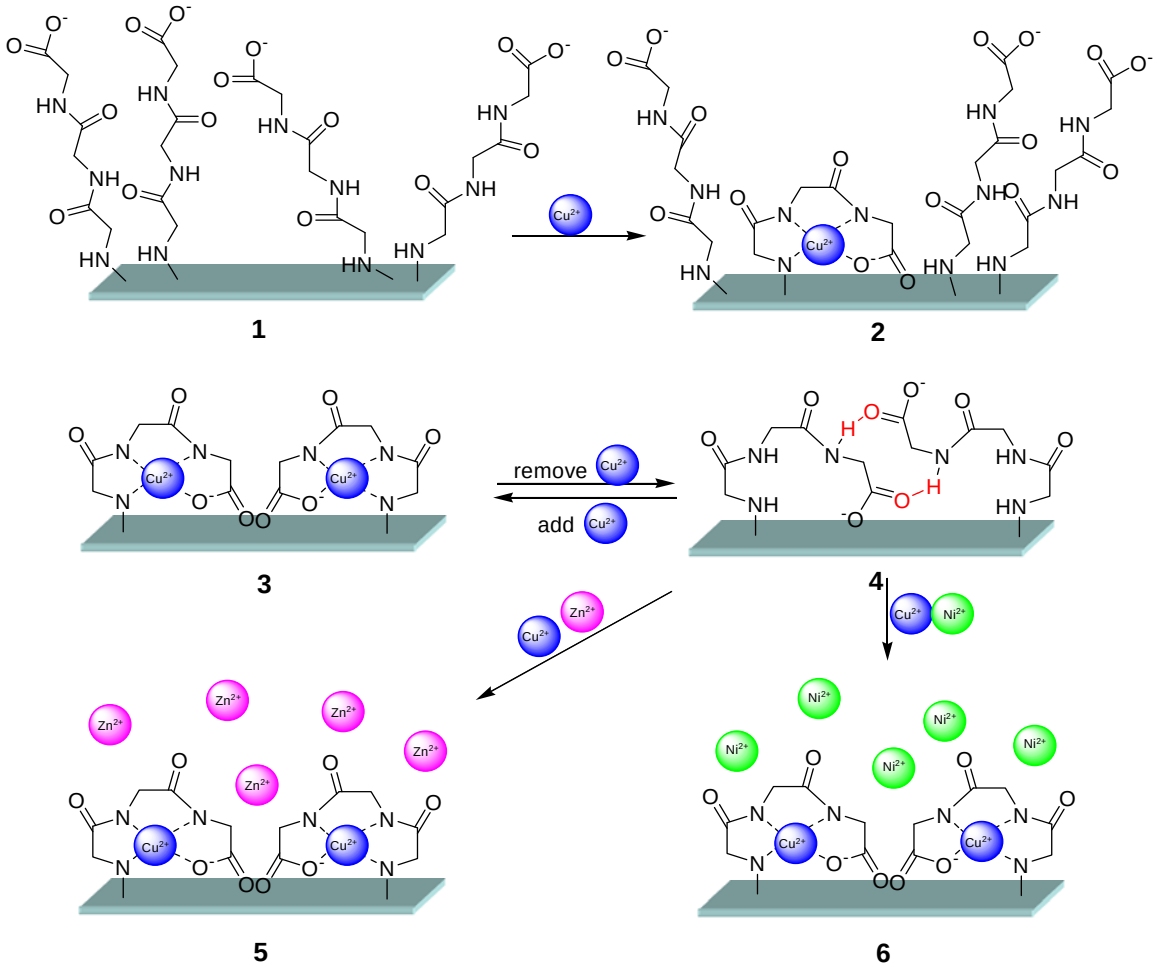

Scheme 3.6 Cu^{2+}-induced conformational changes of immobilized triglycine on surfaces. **1** is prepared by direct immobilization of triglycine from solution, whereas **3** is prepared by immobilization of triglycine-Cu^{2+} complex from solution. **4** is prepared by removing Cu^{2+} from **3**. The immobilized triglycine on **4** can complex exclusively with Cu^{2+} in the presence of Zn^{2+} (**5**) and Ni^{2+} (**6**).

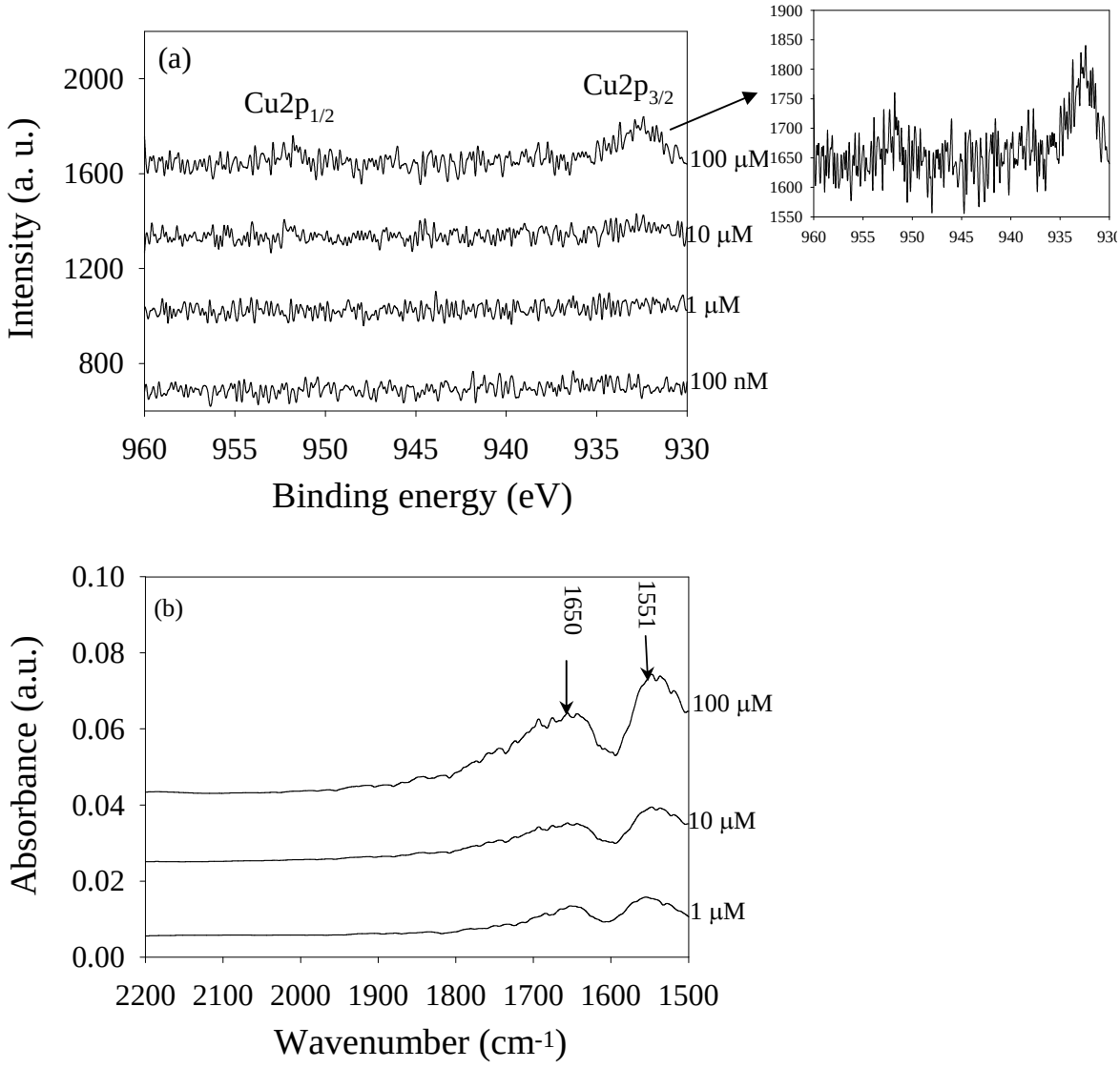

Figure 3.11 (a) XPS spectra (Cu2p) and (b) HATR-FTIR spectra of **1** after it was immersed in different concentrations of Cu^{2+} solutions at pH 6 and blown dry with nitrogen. The spectrum of **1** before exposing to Cu^{2+} solutions was used as a reference in (b). The enlarge spectrum for 100 μM Cu^{2+} in (a) was shown on the right-hand side.

By comparison of Figure 3.10 and 3.11b, we found that the amide I peak shifted from 1625 to 1650 cm^{-1}. This is consistent with the formation of a loop structure of triglycine-Cu^{2+} complex on the surface as shown in **2** in Scheme 3.6. However, the peak areas only increased slightly when we increased the concentration from 1 μM to 10 μM. This is probably because the steric hindrance between adjacent triglycine

molecules prevents the formation of a loop-structured triglycine-Cu^{2+} complex. When we further increased the Cu^{2+} concentration to 100 μM, the peak areas increased again. One possible explanation for this phenomenon is that some triglycine molecules do not experience steric hindrance when they form loop-structured Cu^{2+} complexes; therefore, they can complex Cu^{2+} at a concentration as low as 1 μM. In contrast, other immobilized triglycine molecules are too close to one another to form loop-structured Cu^{2+} complexes.

To avoid the steric hindrance mentioned above, we attempted to optimize the surface density of triglycine by immobilizing triglycine-Cu^{2+} complex from the aqueous solution directly onto an aldehyde-decorated surface. Because the formation constant of triglycine-Cu^{2+} complex in aqueous solution is large (log K = 6.72) (Martell et al.), we can assume that the loop structure of the triglycine-Cu^{2+} complex is preserved (as shown in **3**) after the immobilization. Then, we removed Cu^{2+} from the surface by immersing the surface in 1 M nitric acid for 5 min, leaving free triglycine on the surface as shown in **4**. (The complete removal of Cu^{2+} from the surface was confirmed by XPS.) Characterization of surfaces **3** and **4** with FTIR allowed us to draw some conclusions. First, as shown in Figure 3.12, peak areas of CH_2 group are smaller than that in Figure 3.10, suggesting that the surface density of triglycine on **3** and **4** is lower than **1**. In addition, we also found that the ellipsometric thicknesses of **1** and **4** are 20 ± 3 Å and 16 ± 2 Å, respectively, which also supports a lower surface density of triglycine on **4**. Second, despite the lower surface density of triglycine on **3**, the peak area between 1500 cm^{-1} and 1700 cm^{-1} in Figure 3.12 is much larger than

that in Figure 3.10. As we point out earlier, when triglycine forms a loop structure, the intensities of the amide I and amide II peaks increase significantly. Thus, the larger peak area between 1500- 1700 cm^{-1} in Figure 3.12 could be due to the loop structure of the triglycine-Cu^{2+} complex immobilized on the surface. Surprisingly, even after Cu^{2+} were completely removed from the surface, the peak area between 1564 cm^{-1} and 1654 cm^{-1} in Figure 3.13 did not decrease. A possible explanation is that although the loop structure is no longer holding up by a Cu^{2+}, multiple hydrogen bonds are formed between adjacent triglycine molecules and stabilize the loop structure as shown in Scheme 3.6 (**4**).

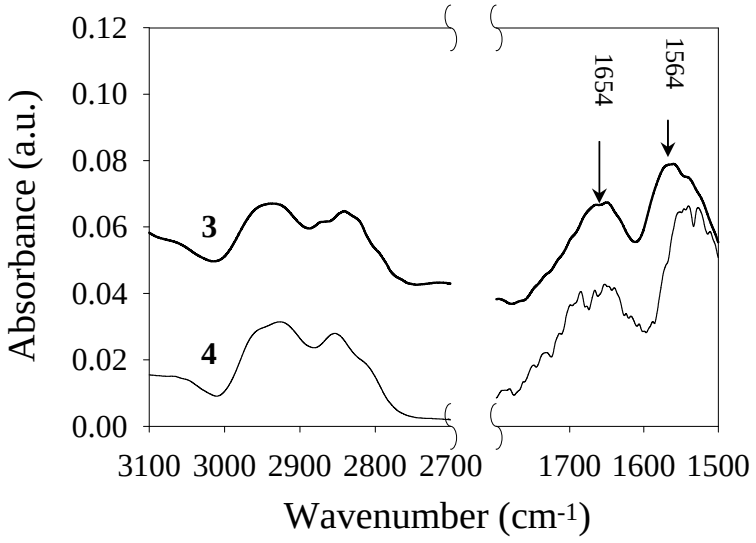

Figure 3.12 HATR-FTIR spectra for **3** and **4**. Surface **4** was obtained by immersion of **3** into 1 M HNO_3 for 5 min to remove copper ions. The spectrum of the aldehyde-decorated silicon trough plate was used as a reference.

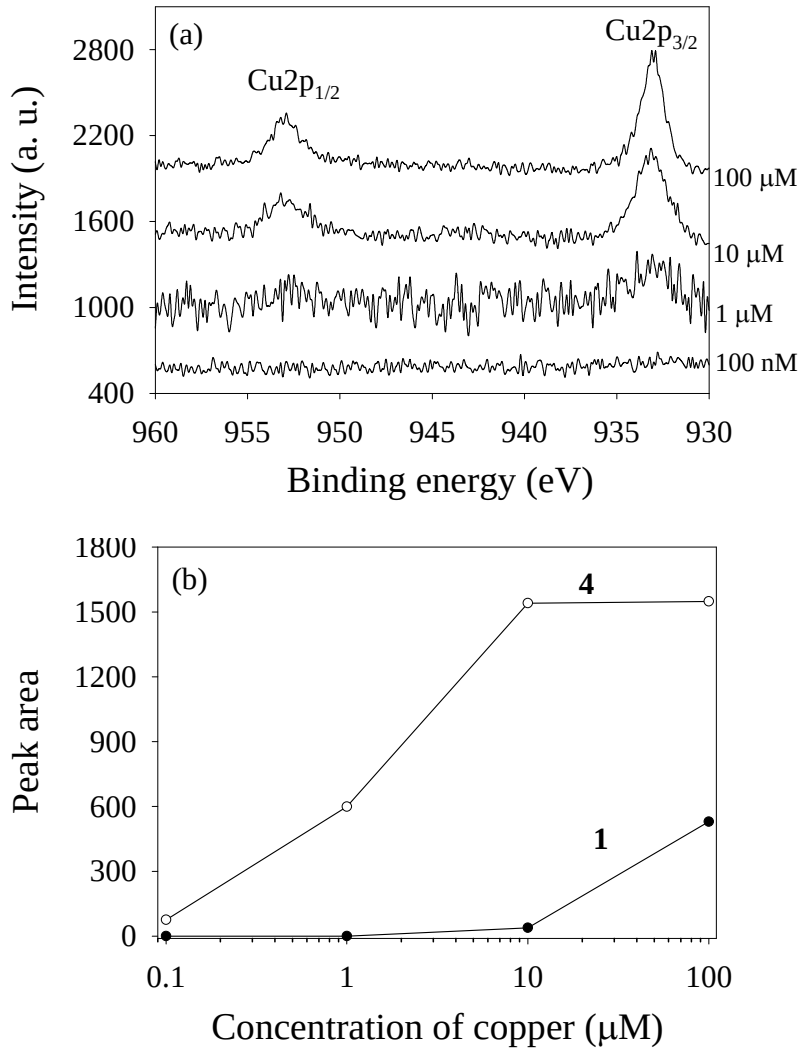

Figure 3.13 (a) XPS spectra (Cu2p) of **4** after it was immersed in different concentrations of copper solutions at pH 6 and blown dry with nitrogen. (b) XPS peak areas of Cu2p for **1** and **4**, after they were immersed in the copper solutions with various concentrations. The peak areas were calculated from Figure 3.18a and 4.20a.

Although surfaces **1** and **4** are now both functionalized with free triglycine, their surface densities are very different as the intermolecular distance of triglycine on **4** is defined by the Cu^{2+}-triglycine complex whereas **1** is determined by the surface density of amine groups. This difference may affect their abilities to complex with Cu^{2+} if the steric hindrance is taken into account. To compare the Cu^{2+} complexation

capability of **1** and **4**, we immersed **4** in different concentrations of Cu^{2+}. As shown in Figure 3.13a, Cu2p peaks start to appear after **4** was immersed in a Cu^{2+} concentration as low as 1 μM, which is 100-times lower than the lowest detectable Cu^{2+} concentration (100 μM) on surface **1** (Figure 3.11a). Comparison of the peak areas of Cu2p on **1** and **4** also reveal that the intensities of Cu2p for **4** are much higher than that of **1** for all Cu^{2+} concentrations (Figure 3.13b). In terms of conformation of triglycine on **4**, no significant changes in the amide I and amide II peaks in Figure 3.14 were observed when we increased the Cu^{2+} concentration from 1 μM to 100 μM. These results suggest that these triglycine molecules probably maintain their loop structures on the surface when they bind to Cu^{2+}.

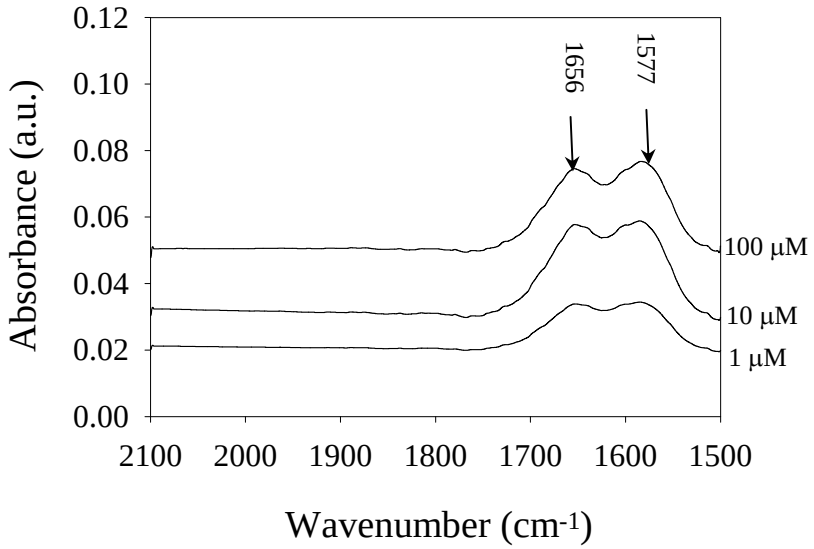

Figure 3.14 HATR-FTIR spectra of **4** after it was immersed in different concentrations of Cu^{2+} solutions at pH 6 and blown dry with nitrogen. The spectrum of **4** before exposing to Cu^{2+} solutions was used as a reference.

Because a proper intermolecular distance between two adjacent triglycine molecules is essential to increase the Cu^{2+} complexation capability, we also sought to control the

spatial density of immobilized triglycine by using a spacer molecule glycine. To make a fair comparison with our previous system, we employed tetraglycine instead of triglycine in this experiment because the additional glycine unit can be used to compensate for the height of the spacer molecule while the other three glycine units can complex Cu^{2+} like a triglycine molecule. We used four different tetraglycine percentages (i.e. 0%, 50%, 75% and 100%) in tetraglycine/glycine binary mixtures to obtain different density of tetraglycine. After we exposed these four surfaces to 10 μM of Cu^{2+}, the peak intensities of Cu2p for surfaces functionalized with 50% and 75% tetraglycine are much higher than those functionalized with 0% and 100% of tetraglycine as shown in Figure 3.15.

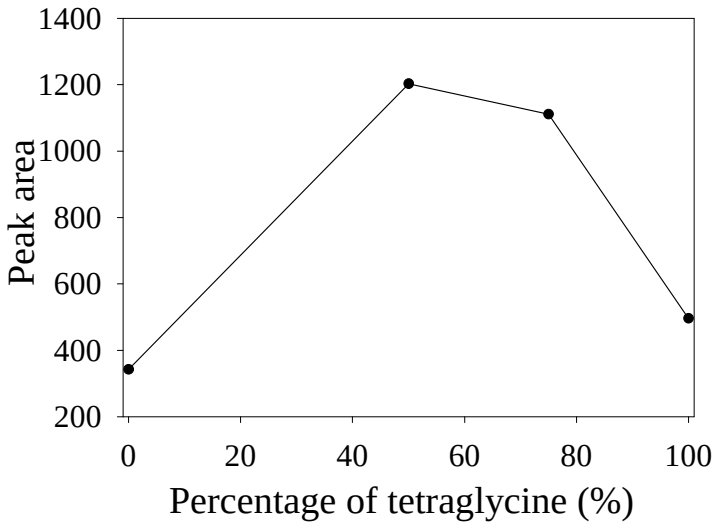

Figure 3.15 XPS Cu2p peak areas showing the amounts of Cu^{2+} adsorbed on four different surfaces with different ratios of tetraglycine/glycine immobilized on the surfaces. These surfaces were incubated in 10 μM of Cu^{2+} solutions (pH = 6), rinsed with ethanol and blown dry before spectra were taken.

These results again suggest that the capabilities of tetraglycine to complex Cu^{2+} increase significantly when there is a spacer between two adjacent tetraglycine

molecules. We believe that the additional room provided by the spacer helps reduce steric hindrance when immobilized tetraglycine undergoes a conformation change and forms a loop structure on a crowded surface.

Selectivity for Cu^{2+}

The above results clearly illustrate that the copper complexation capability of immobilized triglycine can be increased significantly by choosing immobilization procedures that give an optimal surface density of triglycine. In the following experiments, we investigated further whether surface **4** has a higher Cu^{2+} selectivity in the presence of competing metal ions, such as Zn^{2+} and Ni^{2+}. First, we performed the competitive complexation experiment using Cu^{2+} and Zn^{2+}. Figure 3.16a and 3.16b shows the XPS spectra of Cu2p and Zn2p, respectively, after the surface was immersed in a mixed solution containing 10 μM of Cu^{2+} and 1 mM of Zn^{2+}. Two Cu2p peaks in Figure 3.16a indicate that **4** can complex with Cu^{2+}. In contrast, no Zn2p peaks appeared in Figure 3.16b. This is surprising because triglycine is able to complex with Zn^{2+} in the solution with its carboxylate and amine groups. However, in this experiment, only Cu^{2+} can complex with triglycine exclusively on the surface **4** to give **5**, even if the Zn^{2+} concentration is 100-times higher than that of Cu^{2+}.

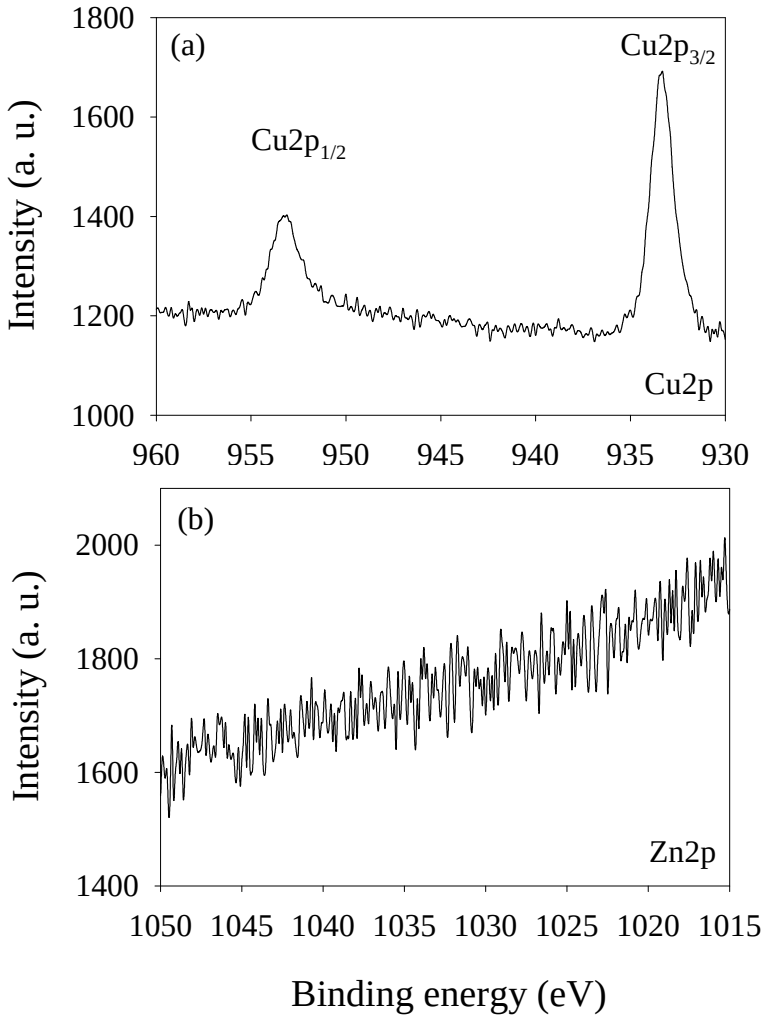

Figure 3.16 XPS spectra of **4**, after it was immersed in a solution containing 10 μM copper and 1 mM zinc and rinsed with ethanol, (a) Cu2p and (b) Zn2p.

To understand the origin of the high selectivity for Cu^{2+}, we also immersed **1** in the same solution containing Cu^{2+} and Zn^{2+}. XPS results in Figure 3.17 show that two Cu2p peaks and two Zn2p peaks at 1021 eV and 1044 eV are clearly visible (Moffitt et al., 2001), indicating that **1** can complex with both Cu^{2+} and Zn^{2+}. Comparing the XPS results for **1** and **4** led us to conclude that the unusual selectivity of **4** for Cu^{2+} can be ascribed to the immobilization procedure and the conformation of triglycine on

the surface. When the triglycine molecules are immobilized on the surface and form loop structures, the selectivity for Cu^{2+} is increased. In addition, the peak intensities of Cu2p in Figure 3.16a is higher than that in Figure 3.17a, supporting again the higher capability of Cu^{2+} complexation on the surface **4** than **1**.

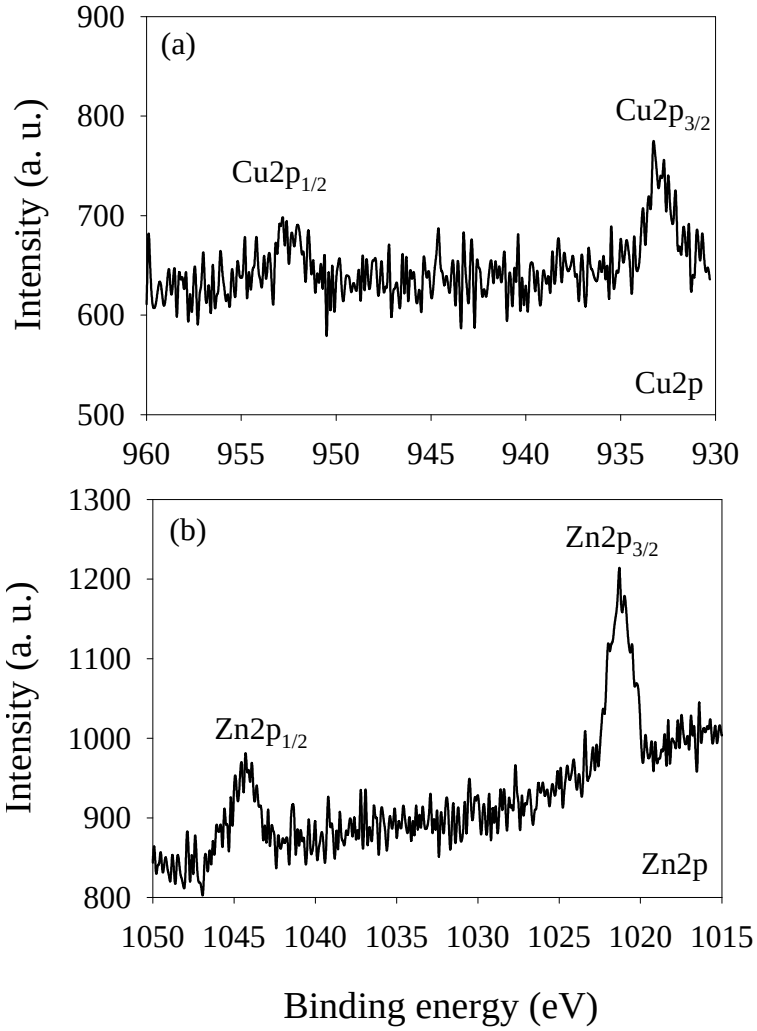

Figure 3.17 XPS spectra of **1**, after it was immersed in a solution containing 10 μM copper and 1 mM Zn^{2+} and rinsed with ethanol, (a) Cu2p and (b) Zn2p.

Finally, we chose Ni^{2+} as another competitive metal ion and determine if surface **4** can selectively bind to Cu^{2+} in the presence of Ni^{2+}. When we immersed **4** in a mixed solution containing 10 μM of Cu^{2+} and 1 mM of Ni^{2+}, Cu2p peaks appeared in Figure

3.18a, whereas no Ni2p peaks appeared in Figure 3.18b. This implies that the surface immobilized triglycine molecules only complex with Cu^{2+}, as shown in Scheme 3.6 (**6)**. This finding is also consistent with our previous result showing that **4** has higher selectivity for Cu^{2+} in the presence of Zn^{2+}.

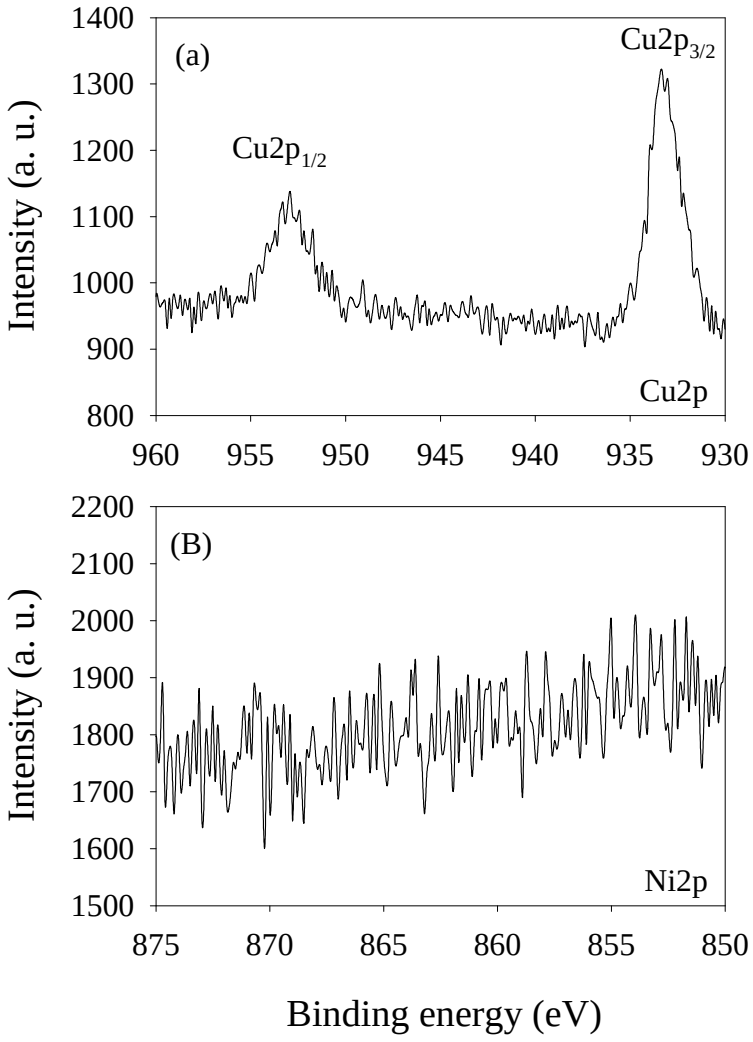

Figure 3.18 XPS spectra of **4**, after it was immersed in a solution containing 10 μM copper and 1 mM Ni^{2+} and rinsed with ethanol, (a) Cu2p and (b) Ni2p.

3.2.4 Conclusions

The principal conclusion of the investigation reported in this study is that the loop structure of triglycine-Cu^{2+} complex formed in aqueous solution can be preserved when it is immobilized on a solid surface; this loop structure of triglycine is maintained even after Cu^{2+} is completely removed from the triglycine-Cu^{2+} complex. We attribute the retention of triglycine conformation to the formation of hydrogen bonds between adjacent triglycine molecules. Our study also demonstrates that the conformations of triglycine on the surface caused by different immobilization procedures can lead to superior complexation capability and selectivity for Cu^{2+}. For example, the surface concentration of Cu^{2+} on a surface functionalized with triglycine having a loop structure is much higher than that on a surface with triglycine with random conformations, when both surfaces were immersed in Cu^{2+} solutions. It is also found that in the presence of 100-times of interfering ions such as Zn^{2+} and Ni^{2+}, triglycine still preferentially binds to Cu^{2+}. This study may shed lights on the influence of metal ions on the conformations of triglycine and may provide useful information for the design of metal ion sensors by using oligopeptides as a sensing element.

CHAPTER 4
COMPLEXATION OF Cu^{2+} WITH HISTIDINE-CONTAINING TRIPEPTIDES

4.1 Introduction

Protein complex with metal ions play an essential role in many biological processes (Sanna et al., 2004). One common element in the protein-metal complex systems is that one or more peptide motif in proteins bind metal ions with high specificity. These peptide motifs are often arranged in a special sequence of residues to ensure the high affinity between the metal ions and donor atoms from the peptide backbones or functional side groups. In the past, many peptide motifs that show both high affinity and specificity to metal ions have been reported (Deschamps et al., 2005; Kozlowski et al., 2005; Daniele et al., 1991; Lau et al., 1974). These peptides motifs often contain metal-complex residues such as histidine (His), because the imidazole moiety in His residue contains a pyridine-like nitrogen atom, which is a good ligand for metal ions. In addition, the position of His residue in a peptide motif also determines the stability of the metal complexes. An example is a tripeptide that contains two glycine (Gly) and one His. Depending on whether the His residue is in the first (His-Gly-Gly) or the last position (Gly-Gly-His), the tripeptides either form 2:1 (ligand:metal) or 1:1 copper complexes as shown in Scheme 4.1. For His-Gly-Gly, because the imidazole-N is a very efficient donor atom that hinders the deprotonation of the amide nitrogen, the dimeric complexes are formed with the imidazole-N as a bridging

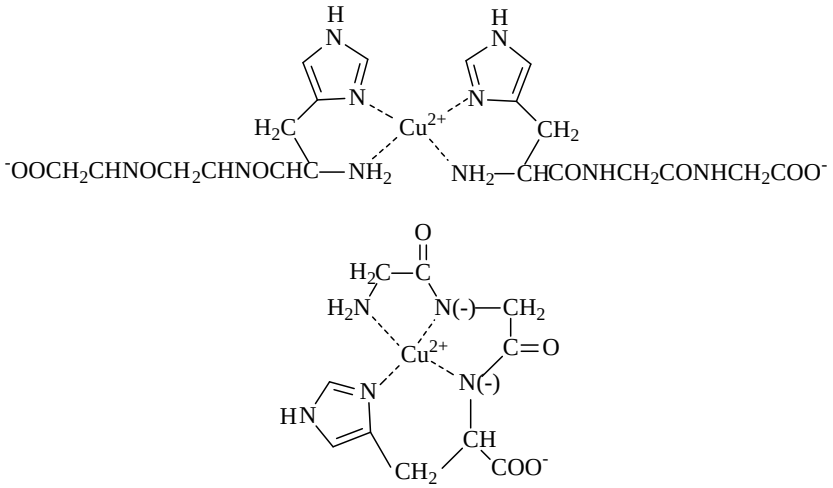

Scheme 4.1 Structures of major copper complexes with (a) His-Gly-Gly, and (b) Gly-Gly-His in aqueous solutions.

ligand. In contrast, Gly-Gly-His is able to form three fused chelate rings that saturate the coordination plane of a copper ion (Kozlowski et al., 1999). Therefore, the resulting copper complex is very stable. While most of previous studies were focused on the complexes formed between His-containing peptides and metal ions in aqueous solutions, His-containing peptides immobilized on solid surfaces coupled to a transducer represents a more useful system for chemical sensing applications (Yang et al., 2001 and 2003; Gooding et al., 1998; Forzani et al., 2005). In these systems, the behaviors of immobilized His-containing peptides are usually assumed to be similar to those in the aqueous solutions. However, more and more studies have proven that molecules immobilized on solid surfaces behave very differently from those in the solution phases. Examples of these studies include the immobilization and hybridization of DNA on solid surfaces (Hong et al., 2005), the coordination of metal ions to surface functional groups, such as carboxylate (Evans et al., 1991; Major et al.,

2003), and the dissociation of carboxylic acids in self-assembled monolayers (Gershevitz et al., 2004). It has been proposed that the "surface effects" originate from several factors (Liu et al., 1998; Feng et al., 1997; Lam et al., 2006), such as the extensive intermolecular hydrogen bonding on surfaces, the interactions between immobilized molecules and surfaces, and the steric hindrance caused by the adjacent molecules. In view of the conformation changes when the immobilized Gly-Gly-His complex with copper ions as shown in Scheme 4.2, an adjacent molecule could prevent the stable 4N complexes from forming and result in a smaller stability constant for

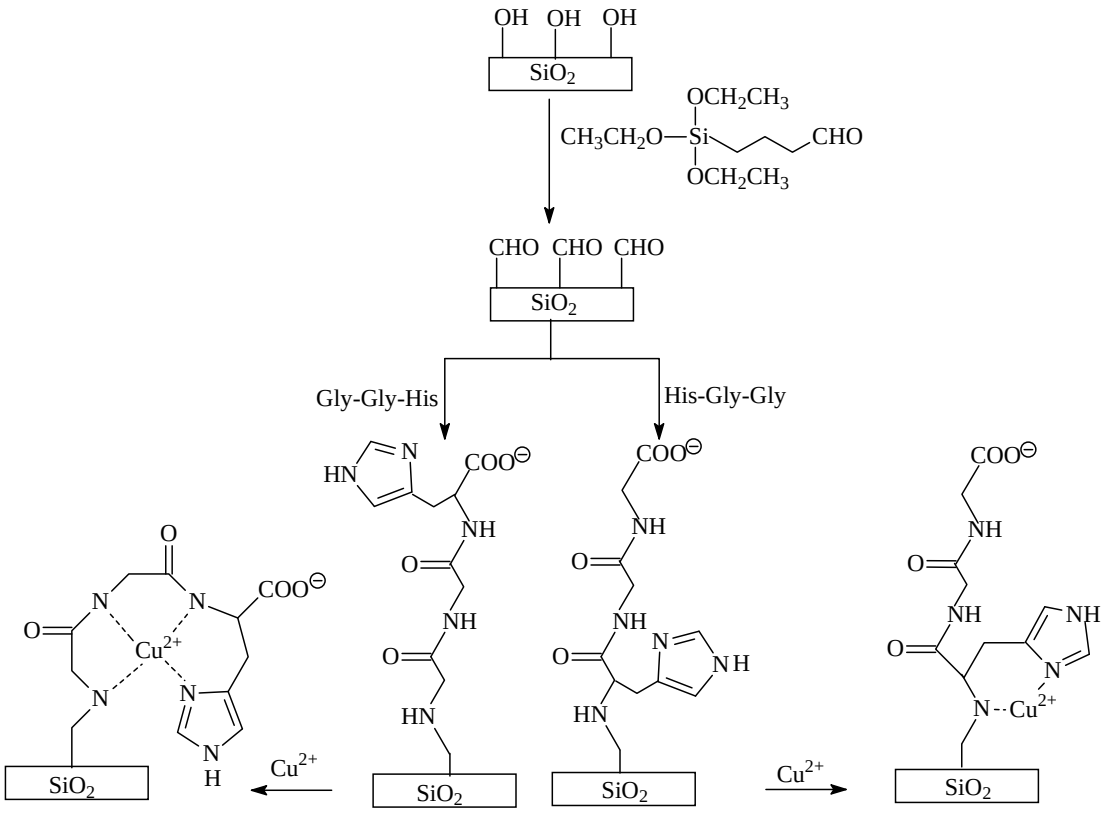

Scheme 4.2 Procedure for the chemical modifications of silicon wafers with TEA, followed by the immobilization of tripeptides Gly-Gly-His and His-Gly-Gly.

the copper complex. As a result, we propose that when the His-containing tripeptides are immobilized on solid surfaces with a high density, they experience strong steric hindrance which affects their complexation with copper ions. We also propose that these surface effects could be minimized by controlling the surface densities of these tripeptides. One of the promising solutions to control the surface crowdedness of immobilized peptides is through two-dimensional (2D) ion-imprinting method. In a typical 2D imprinting method, the ligands (usually organosilanes or thiols) are self-assembled on the surface of an inorganic matrix in the presence of templates. After the removal of the templates, the resulting cavities on the monolayers can be used to adsorb molecules with similar size and shape as the templates. Hence, 2D imprinting sorbents provide high affinity and good selectivity for the templates.

4.2 Experimental Section

Materials

Tripeptides including glycyl-glycyl-histidine (Gly-Gly-His) and histidyl-glycyl-glycine (His-Gly-Gly) were purchased from Bachem (Switzerland). Triethoxysilane aldehyde (TEA) was purchased from United Chemical Technologies (Bristol, PA, USA). Other chemicals are the same as those in **Chapter 3**.

Preparation of silicon substrates and surface functionalization

Silicon wafers were cleaned following the procedure mentioned in **Chapter 3**. Subsequently, cleaned wafers were rinsed with methanol, and immersed into a

methanolic solution containing 2% (v/v) of TEA at 25ºC for 1 h. After the wafers were removed from the solution, they were washed with copious amounts of methanol. Finally, the wafers were blown dry with nitrogen and heated at 100ºC in a vacuum oven for 15 min to promote the crosslinking of silanol groups to form siloxane networks.

Immobilization of tripeptides on the aldehyde-decorated surface

We prepared the tripeptides modified surface following the procedure shown in Scheme 4.2. First, we mixed two 500 mM $(NH_4)_2CO_3$ solutions together, one containing 2 mM of Gly-Gly-His or His-Gly-Gly, and the other containing 20 mM of $NaBH_3CN$, in a 1:1 volumetric ratio. Next, we immersed the aldehyde-decorated silicon wafers into the solution. After reacting at 25°C for 1 h (we defined this sample as **GGH-1h** or **HGG-1h**) or 2 h (**GGH-2h** or **HGG-2h**), the modified wafers were washed thoroughly with copious amounts of deionized water, dried under purified nitrogen and heated at 100°C in a vacuum oven for 15 min. To create a copper-imprinted silicon wafer surface (**Imprinted GGH)**, we mixed two aqueous solutions together, one containing 2 mM of Gly-Gly-His and 2 mM of copper nitrite, and the other containing 20 mM of $NaBH_3CN$, in a 1:1 volumetric ratio. Then, we immersed the aldehyde-decorated silicon wafers into the mixed solution at 25°C for 2 h. After this, we rinsed **Imprinted GGH** with 1 M of HNO_3 for 5 min and copious amounts of deionized water sequentially to remove Cu^{2+}. We checked **Imprinted GGH** by XPS to ensure there was no Cu^{2+} left on the surface after the rinsing

procedure. Finally, the copper-imprinted surfaces were blown dry with purified nitrogen.

UV-vis absorption spectroscopy

The absorption spectra were obtained with a UV-vis spectrometer (Cary 50, Varian, Australia). In all experiments, water was used as reference. The Cu^{2+} titration was performed by adding aliquots of a $Cu(NO_3)_2$ stock solution (70 mM) to 0.3 mM of peptide solution in MES buffer (pH = 6.0).

Complexation with Cu^{2+}, ellipsometry, and XPS

Following the procedure mentioned in **Chapter 3**.

4.3 Results and Discussion

Complexation of Cu^{2+} in aqueous solutions

First, we investigate the complexation of Cu^{2+} with 0.3 mM of His-Gly-Gly or Gly-Gly-His in MES buffer (pH = 6). As shown in Figure 4.1a, the addition of 0.15 mM Cu^{2+} (final concentration) to the His-Gly-Gly solutions results in a new peak at 633 nm, which is attributed to the formation of a 1:2 Cu^{2+} complex with His-Gly-Gly as shown in Scheme 4.1a. However, when the Cu^{2+} concentration was further increased to 0.3 mM then to 0.6 mM, the peak at 633 nm also increased slowly. The small increase suggests that either the stability constant of the dimeric Cu^{2+} complex is not large enough (such that some unbound His-Gly-Gly remained in the solution

after the addition of 0.15 mM of Cu^{2+}), or other types of Cu^{2+} complexes (such as monomeric complex) also forms when the Cu^{2+} concentration is higher. In contrast, the addition of 0.15 mM of Cu^{2+} to the Gly-Gly-His solutions resulted in a new peak around 520 nm (Figure 4.1b), which corresponds to the formation of a 1:1 Cu^{2+} complex with Gly-Gly-His.

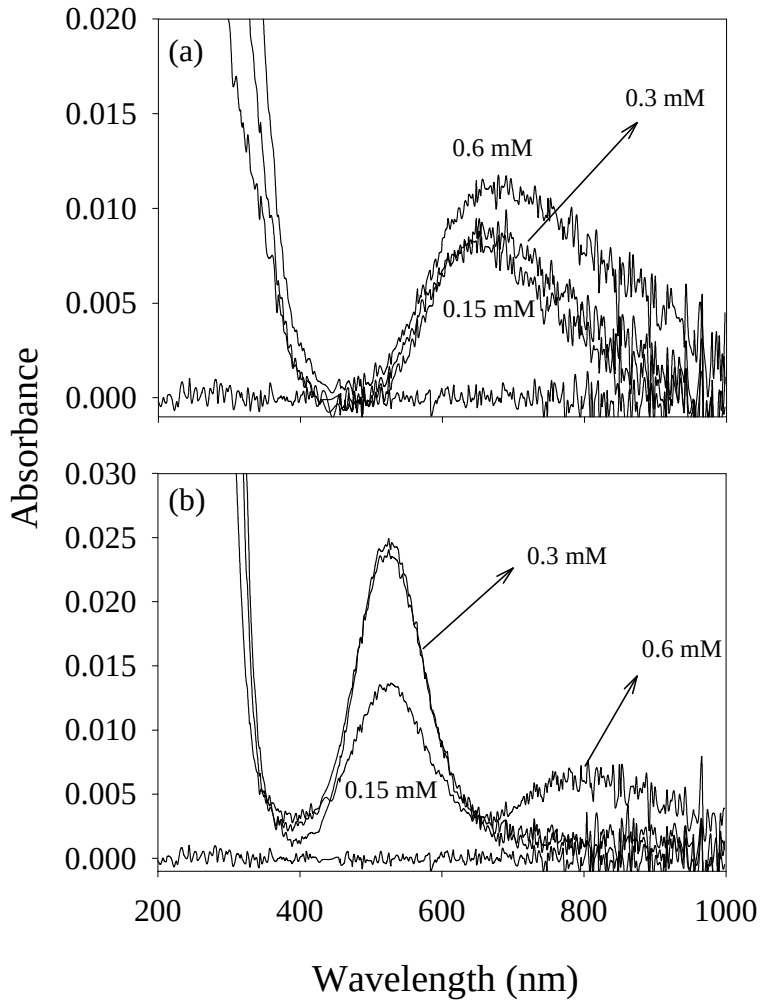

Figure 4.1 Titrating 0.3 mM of (a) His-Gly-Gly, and (b) Gly-Gly-His in MES buffer (pH = 6.0) with copper nitrate solutions. The number indicates the final copper concentrations in the solution.

When 0.3 mM of Cu^{2+} was added to the solution, the peak height at 520 nm also doubled. Eventually, when the Cu^{2+} concentration was increased to 0.6 mM, there was

no further increase in the peak height at 520 nm. Meanwhile, a second peak near 800 nm corresponding to free Cu^{2+} appeared (Yang et al., 2006). The above observation is consistent with a large stability constant of the Cu^{2+} complex with Gly-Gly-His (log *K* = 7.59). The results also confirm that it is more favorable for Cu^{2+} to form complexes with Gly-Gly-His than His-Gly-Gly.

Effect of buffer concentration and reaction time on the tripeptide immobilization

Next, we immobilized His-Gly-Gly and Gly-Gly-His on aldehyde-decorated silicon wafers to study their complexation with Cu^{2+} on surfaces. To ensure high surface packing densities of these tripeptides immobilized on surfaces, we first investigated the influence of two important factors, i.e. the concentration of buffer and reaction time, on the surface densities of immobilized tripeptides. Figure 4.2a shows the ellipsometric thicknesses on the surfaces of silicon wafers after the immobilization of Gly-Gly-His and His-Gly-Gly in different concentrations of buffer. It is found that the ellipsometric thickness increases with the increase of buffer concentration from 0 M to 0.5 M. Our results suggest that a high buffer concentration can be used to screen electrostatic repulsions between negatively charged carboxylate groups during immobilization and hence increase the immobilization efficiency of Gly-Gly-His and His-Gly-Gly. Figure 4.2a also shows that the ellipsometric thickness of Gly-Gly-His is higher than that of His-Gly-Gly. This phenomenon implies that the immobilization efficiency of Gly-Gly-His on the aldehyde-decorated surface is higher than

His-Gly-Gly, possibly because the Gly residue in N-terminal has less steric hindrance than His residue.

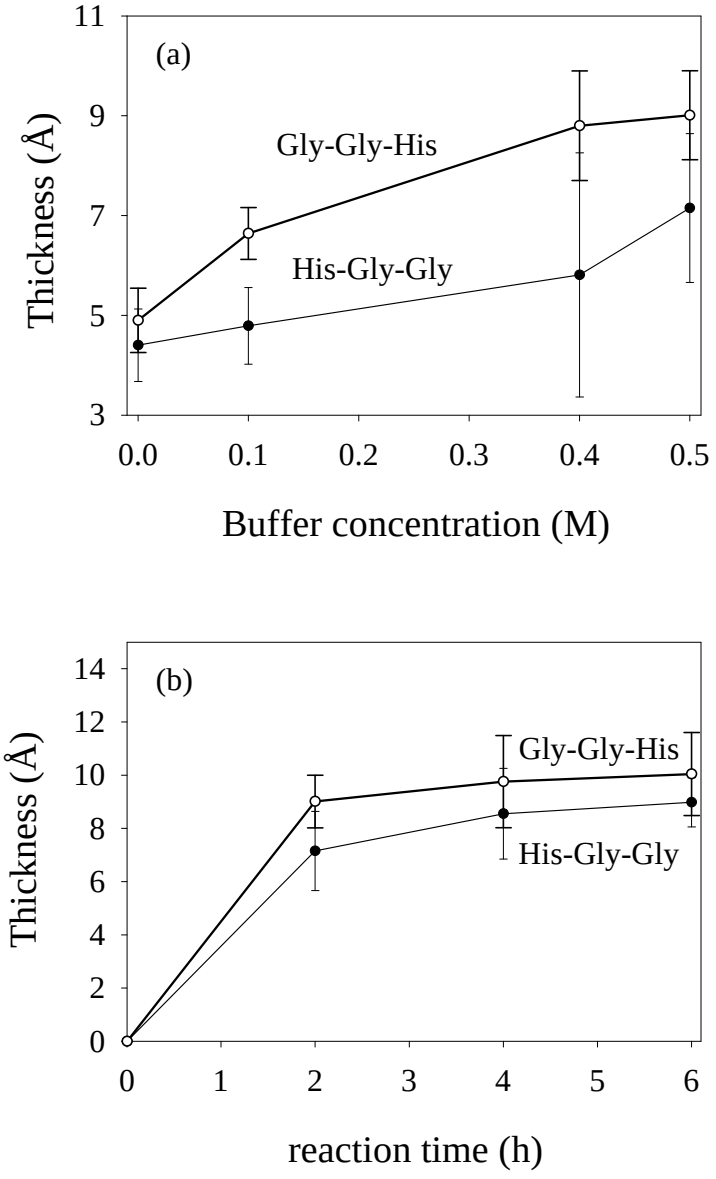

Figure 4.2 Effect of (a) buffer concentration and (b) reaction time on the immobilization of 1 mM of Gly-Gly-His or His-Gly-Gly in 0.5 M carbonate buffer on aldehyde-decorated silicon wafer. The results show that the ellipsometric thickness increases with the buffer concentration and the reaction time.

Subsequently, we explored the effect of reaction time on the immobilization of Gly-Gly-His and His-Gly-Gly. Figure 4.2b shows the ellipsometric thicknesses of the aldehyde- decorated silicon wafers after they were functionalized with Gly-Gly-His or His-Gly-Gly for different reaction times. It is found that the ellipsometric thickness increases by 7 ± 1 Å and 9 ± 1 Å for His-Gly-Gly and Gly-Gly-His, respectively, after 2 h. Then, the ellipsometric thicknesses increase only slightly if the reaction time is increased from 2 h to 6 h, which suggests that the coupling reaction between tripeptides molecules and TEA molecules on surface is almost complete after 2 h. We conclude from above results that 0.5 M of ammonium carbonate buffer and a reaction time of 2 h are sufficient for the immobilization of Gly-Gly-His and His-Gly-Gly with near maximum packing densities.

We further performed XPS to obtain chemical compositions of the samples functionalized with Gly-Gly-His and His-Gly-Gly under the experimental condition stated above. Figure 4.3a shows that the N1s spectrum of an aldehyde-decorated silicon wafer does not contain any nitrogen. After the immobilization of Gly-Gly-His or His-Gly-Gly on the surface, three peaks appeared in Figure 4.3b and 4.3c, respectively. The main peak at 400.1 eV is the amide nitrogens of His-Gly-Gly or Gly-Gly-His, whereas the peaks at 398.8 eV and 401.2 eV are the C=N-C and C-N-C nitrogen of the imidazole group on the side chain of His residue (Liu et al., 2006). As shown in Figure 4.3b and 4.3c, the ratios of three peak areas at 398.8, 400.1 and 401.2 eV are 1:3.31:1 for His-Gly-Gly and 1:3.16:1 for Gly-Gly-His. These ratios are in reasonable agreement with the stoichiometric ratio of N (1:3:1) for these two

molecules immobilized on the surfaces. In addition, we obtained the N ratio of Gly-Gly-His to His-Gly-Gly functionalized surface was 1.07 based on the total N1s peak areas. This result reveals that Gly-Gly-His either has a slightly higher or a similar surface density as His-Gly-Gly.

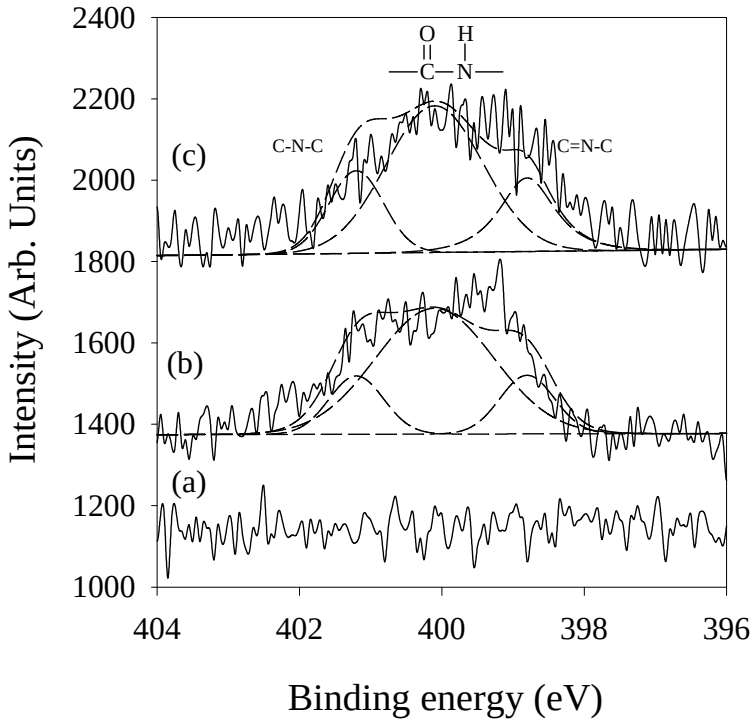

Figure 4.3 XPS spectra (N1s) for (a) TEA, (b) His-Gly-Gly, and (c) Gly-Gly-His functionalized silicon wafers.

Complexation of Cu^{2+} on surfaces with immobilized tripeptides

Our next goal is to investigate the Cu^{2+} complexation with the immobilized Gly-Gly-His and His-Gly-Gly. Figure 4.4 shows the XPS spectra of Cu2p after Gly-Gly-His or His-Gly-Gly functionalized silicon wafer was immersed in copper nitrate solutions with various concentrations. We used the $Cu2p_{3/2}$ peak at 933 eV and the $Cu2p_{1/2}$ peak at 953 eV for comparing of the amounts of Cu^{2+} complexed on

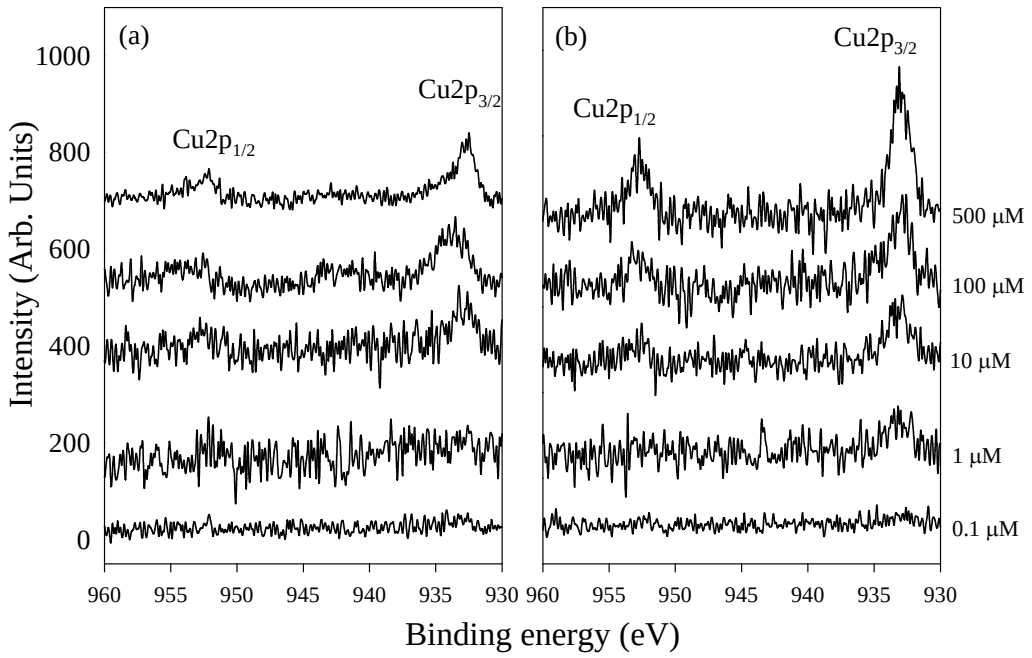

Figure 4.4 XPS spectra (Cu2p) for (a) His-Gly-Gly and (b) Gly-Gly-His functionalized silicon wafers, after they were immersed in copper nitrate solutions with various concentrations and cleaned with ethanol.

these surfaces. It was found that for the His-Gly-Gly functionalized surface, Cu^{2+} can be detected if the Cu^{2+} concentration is more than 10 μM. After this, the intensity of $Cu2p_{3/2}$ peak increases slowly with the increasing Cu^{2+} concentrations. For the Gly-Gly-His functionalized surface, Cu^{2+} still can be detected even if the Cu^{2+} concentration is as low as 1 μM, which is ten-times lower than the detection limit for His-Gly-Gly. In addition, we compared the peak areas of $Cu2p_{3/2}$ for both tripeptides-functionalized surfaces. As shown in Figure 4.5, the peak area of $Cu2p_{3/2}$ for the Gly-Gly-His-functionalized surface is much higher than the His-Gly-Gly-functionalized surface. It is also found that the $Cu2p_{3/2}$ peak area for Gly-Gly-His-functionalized surface increases significantly with the Cu^{2+} concentration until 100 μM is reached, then continue to increase slowly with the Cu^{2+}

concentration until 500 μM. On the other hand, the peak area for His-Gly-Gly-functionalized surface increases dramatically with the concentration of Cu^{2+} up to 10 μM and then increases slightly for higher concentrations of Cu^{2+}.

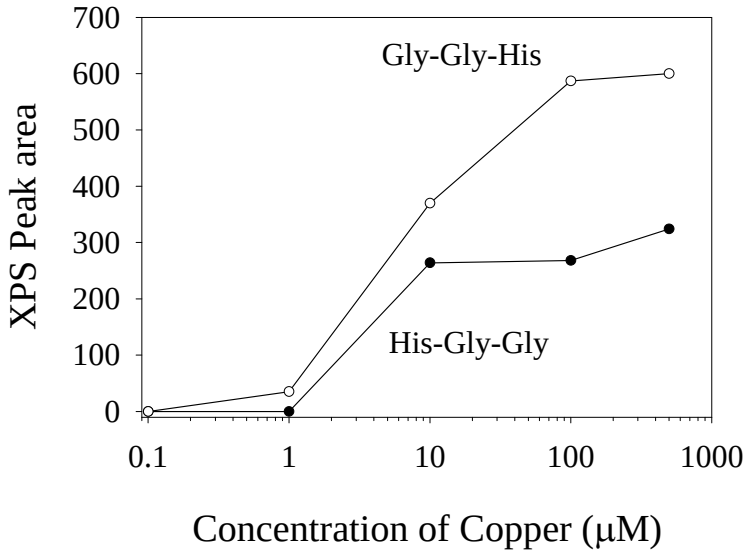

Figure 4.5 XPS Peak areas of $Cu2p_{3/2}$ for silicon wafers functionalized with Gly-Gly-His or His-Gly-Gly. The peak areas were calculated by using Figure 4.4.

We can draw two principle conclusions from Figure 4.4 and 4.5. First, the Gly-Gly-His functionalized surface has a higher Cu^{2+} binding capability, because it starts to complex with Cu^{2+} at a concentration as low as 1 μM whereas the His-Gly-Gly functionalized surface can only complex with Cu^{2+} at 10 μM. Another evidence that supports this conclusion is that although the densities of Gly-Gly-His and His-Gly-Gly are similar on the surface, the total amounts of Cu^{2+} that complex with Gly-Gly-His are higher than His-Gly-Gly. A similar conclusion based on the study of Cu^{2+} binding with cysteamine/COOH-His-Gly-Gly-NH_2 and 11-mercaptoundecanoic acid/NH_2-Gly-Gly-His-COOH immobilized on gold surfaces

was also reported before. Second, immobilized Gly-Gly-His does not behave the same way as it is in the aqueous solution. For example, after a Gly-Gly-His functionalized silicon wafer was incubated in 10 μM of Cu^{2+}, the N1s/Cu2p ratio is 9.86 ± 0.68. This is almost two times of the ideal ratio, i.e. 5.0, if one Cu^{2+} binds with one Gly-Gly-His molecule as shown in Scheme 4.1b.

If the stability constant of Cu^{2+} complex with Gly-Gly-His in the solution can be applied to the immobilized Gly-Gly-His, we expect most of the immobilized Gly-Gly-His complexed with Cu^{2+} when the Cu^{2+} concentrations reaches 10 μM. Apparently, this is not the case in our experiment. In Figure 4.4b, the $Cu2p_{3/2}$ peak continues to rise until the Cu^{2+} concentration reaches 500 μM, suggesting that the stability constant of the Cu^{2+} complex with Gly-Gly-His immobilized using the method reported herein is much lower than that in the solution phase. To account for the lower stability constant we observed in our experiment, we propose that the high packing density of Gly-Gly-His may prevent the formation of the most stable tetragonal Cu^{2+} complexes (Scheme 4.1b) and cause the formation of other less stable Cu^{2+} complexes on the surface.

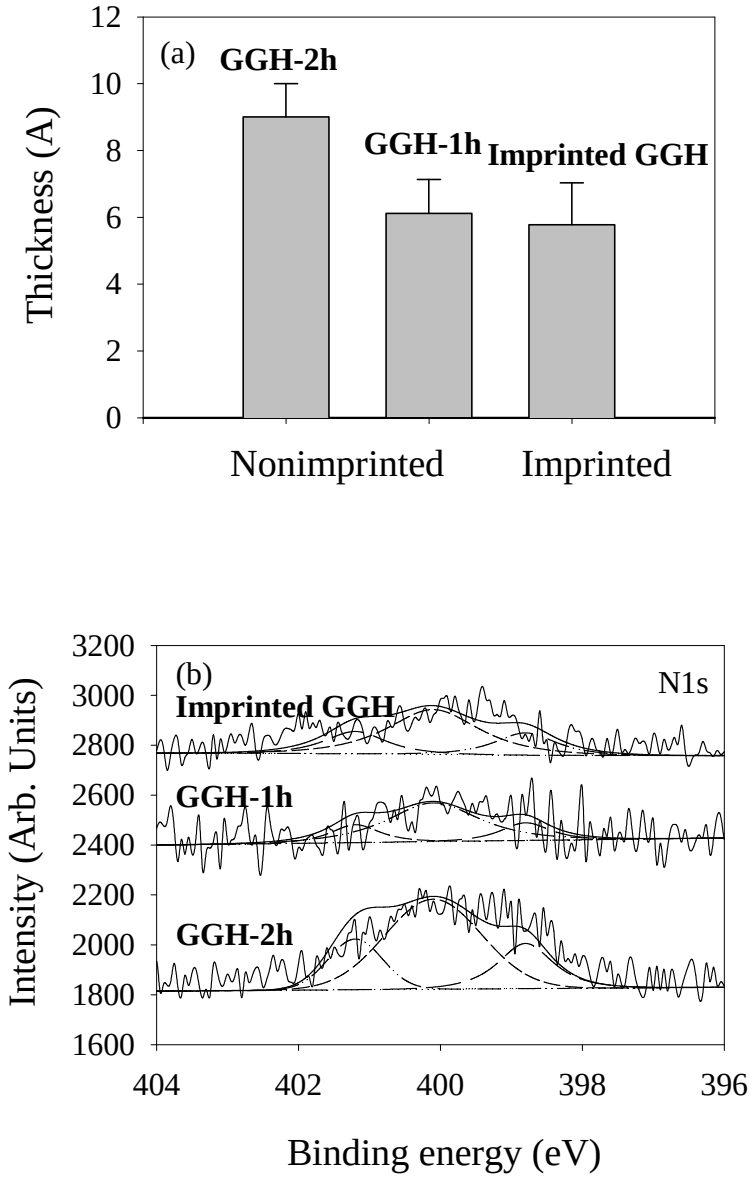

Figure 4.6 (a) Ellipsometric thicknesses of the thin organic layers on **GGH-2h**, **GGH-1h**, and **Imprinted GGH**. (b) XPS spectra (N1s) for **GGH-2h**, **GGH-1h**, and **Imprinted GGH**. The measurements were taken after the silicon wafers were immersed in a 10 μM copper nitrate solution and cleaned with ethanol.

To examine our proposition and investigate whether the high surface density of Gly-Gly-His affects the Cu^{2+} complexation, we lower the packing density of Gly-Gly-His on the surface by decreasing the reaction time from 2 h (**GGH-2h**) to 1 h

(**GGH-1h**). In Figure 4.6a, we observe that the ellipsometric thickness decreases with the decreasing of reaction time, which is also confirmed by XPS. As shown in Figure 4.6b, the N1s peak area decreases by 46% when 1 h was used as the reaction time instead of 2 h. Interestingly, although **GGH-2h** has a higher packing density of Gly-Gly-His than **GGH-1h**, when we incubated these two samples in 10 μM of Cu^{2+}, the intensity of Cu2p peak for **GGH-1h** is higher than that for **GGH-2h** (Figure 4.7a), suggesting that the low packing density actually leads to an increase in the amounts of Cu^{2+} bound to the surface. This is probably because the surface crowdedness on **GGH-2h** hinders the complexation of Cu^{2+} with the immobilized Gly-Gly-His. Quantitative analysis of the $Cu2p_{3/2}$ peak areas of **GGH-1h** and **GGH-2h** in Figure 4.7b shows that the peak area of **GGH-1h** is 31% higher than that of **GGH-2h**. To better understand the complexation mode of Cu^{2+} to the surface with a low packing density, we calculated the N1s/Cu2p ratio for **GGH-1h** after it was incubated in 10 μM of copper nitrate solution. The ratio is 6.92 ± 0.73, which is lower than the ratio for **GGH-2h** (9.86 ± 0.68). This value is between the ratio of 5.0 (corresponds to one Cu^{2+} binding with one Gly-Gly-His molecule) and 10.0 (corresponds to one Cu^{2+} binding with two Gly-Gly-His molecules), suggesting some other complexation modes may also exist on the surface of **GGH-1h**. For example, some Gly-Gly-His may not bind to any $Cu^{2+,}$ or two Gly-Gly-His molecules may bind to one Cu^{2+} through the carboxylate groups and forms a 2:1 complex.

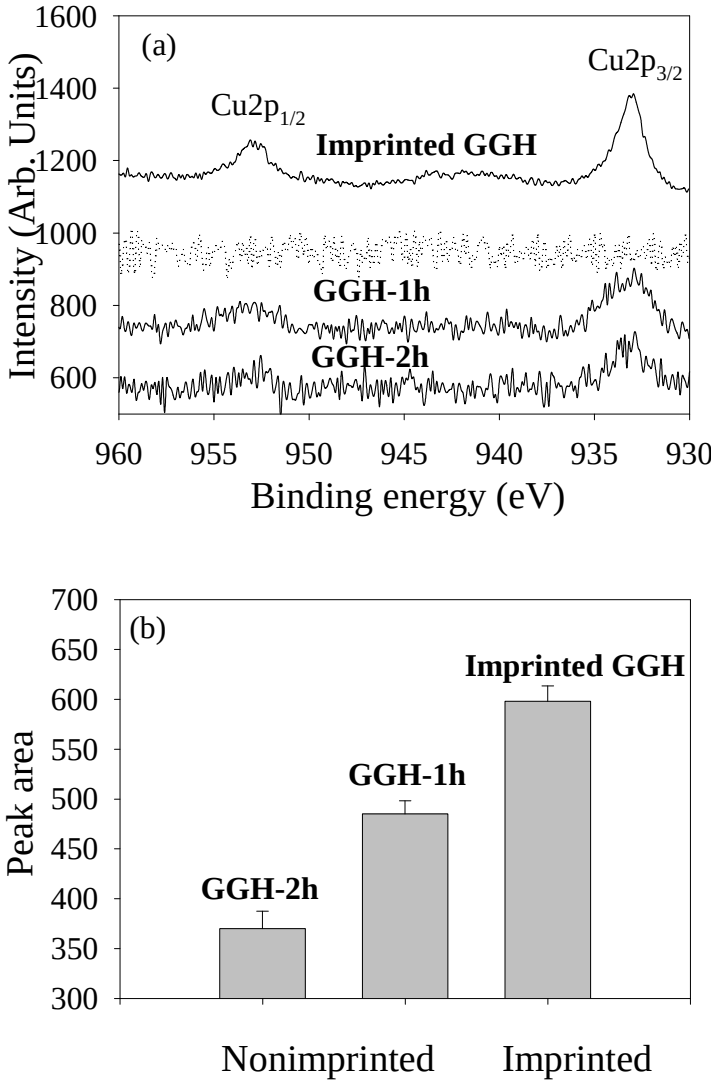

Figure 4.7 (a) XPS spectra (Cu2p) and (b) $Cu2p_{3/2}$ peak area for **GGH-2h**, **GGH-1h**, and **Imprinted GGH**. The measurements were taken after the silicon wafers were immersed in a 10 μM copper nitrate solution and cleaned with ethanol. The dotted line is **Imprinted GGH** before its immersion into the copper nitrate solution. It shows that no Cu^{2+} left on the surface after the ion-imprinting procedure.

2D ion-imprinting

Although we have shown that the Cu^{2+} complexing capability can be enhanced by lowering the surface density, it is difficult to control the surface density by changing the reaction time. To create a surface with a high packing density of peptide

molecules without compromising their Cu^{2+} complexation capabilities, we exploit the 2D ion-imprinting technique in this study. First, we compared the ellipsometric thicknesses of copper-imprinted (**Imprinted GGH**) and nonimprinted (**GGH-1h** and **GGH-2h**) surfaces functionalized with Gly-Gly-His by using ellipsometry. Figure 4.6a clearly indicates that the surface density of Gly-Gly-His immobilized on the **Imprinted GGH** is lower than that on the **GGH-2h**. We also performed XPS to compare the N1s signal on the surface of **Imprinted GGH** and **GGH-2h**. As shown in Figure 4.6b, the N1s peak areas obtained on the surface of **Imprinted GGH** is also lower than **GGH-2h**. Our explanation for the low density of **Imprinted GGH** is that with the ion-imprinting procedure, Gly-Gly-His forms a stable metal complex with a Cu^{2+} in the solution (Scheme 4.1b) before the immobilization. The metal complex then defines the intermolecular distances between two Gly-Gly-His molecules when they are immobilized on the surface. As a consequence, the surface density of **Imprinted GGH** is lower than that of **GGH-2h**.

Next, we compare the Cu^{2+} complexation with **Imprinted GGH** and **GGH-2h** to study whether the extra intermolecular space obtained from the ion-imprinting will affect the Cu^{2+} complexation capability. Although the intensity of N1s for **Imprinted GGH** is lower than **GGH-2h** as shown in Figure 4.6b, the intensity of Cu2p for **Imprinted GGH** is higher than **GGH-2h** in Figure 4.7a, suggesting **Imprinted GGH** has a higher Cu^{2+} complexation capability. In addition, based on the Cu2p and N1s peak intensities, the N/Cu ratio for **Imprinted GGH** is 4.77 ± 0.5. This result agrees well with the theoretical N/Cu ratio of 5, which is expected when one Cu^{2+} atom binds

to one Gly-Gly-His molecule, forming a Cu^{2+} complex as shown in Scheme 4.1b. As shown in Figure 4.7b, when we incubated both **GGH-2h** and **Imprinted GGH** in 10 μM of copper nitrate solution, the $Cu2p_{3/2}$ peak area for **Imprinted GGH** is 62% higher than **GGH-2h**. These results, when combined, imply that maintaining proper intermolecular distances among immobilized Gly-Gly-His is an important factor for the formation of the most stable Cu^{2+} complexes. If the surface is too crowded, there is not enough space for the immobilized Gly-Gly-His to undergo a conformation change and form the Cu^{2+} complex as shown in Scheme 4.1b.

4.4 Conclusions

In this study, we immobilize His-containing tripeptides (His-Gly-Gly and Gly-Gly-His) on aldehyde-decorated silicon wafers and study the effect of packing density of these tripeptides on their abilities to complex Cu^{2+}. It is concluded that a buffer concentration of 0.5 M and a reaction time of 2 h can lead to the formation of a dense monolayer of tripeptide on the surface. When the tripeptides-functionalized surfaces are incubated in a copper nitrate solution, the complexation of tripeptides with Cu^{2+} highly depends on the position of His residue in the tripeptide sequence. For example, Gly-Gly-His functionalized surface has a higher complexation capability to Cu^{2+} than His-Gly-Gly functionalized surface, a finding that can be attributed to the different binding mode of the two tripeptides. Our results also show that the surface crowdedness might lower the Cu^{2+} binding capability. One solution to overcome this limitation is using the so-called 2D ion-imprinting technique. It is

found that the Cu^{2+} complexation capability of a copper-imprinted surface functionalized with Gly-Gly-His is 62% higher than a nonimprinted surface, because more stable Cu^{2+} complexes whose formation requires the proper intermolecular distance of two immobilized tripeptide molecules can be obtained when the ion-imprinting technique is employed. This study may shed lights on the complexation of metal ions with immobilized peptides on surfaces and provides a useful guideline for increasing the sensitivity of metal ion sensors by using ion-selective peptides.

CHAPTER 5
DEVELOPMENT OF SILICON NANOWIRE BASED Cu^{2+} SENSORS

5.1 Introduction

Nanoscale sensor systems attract a lot of attention in recent years because of their high sensitivity and simple detection scheme (Cui et al., 2001; Risveden et al., 2007; Zheng et al., 2005; Alivisatos et al., 2004). Up to date, many types of semiconductor nanowires or carbon nanotubes configured as field-effect transistors (FETs) have been applied for chemical and biological sensing (Li et al., 2004; Stern et al., 2007; Nguyen et al., 2002; Li et al., 2005; Law et al., 2002; Curreli et al., 2005). Among them, silicon nanowires (SiNWs) show great promise due to their biocompatibility, vast surface-to-bulk ratio, tunable electrical properties, and fast response (Kim et al., 2007; Patolsky et al., 2004; Wang et al., 2005; Zhang et al., 2008; Im et al., 2007). Therefore, previous studies have demonstrated the applications of SiNW sensors for the detection of ions (Cui et al., 2001), proteins (Zheng et al., 2005), virus (Patolsky et al., 2004), and cells (Patolsky et al., 2006a,b).

Fabricating SiNW sensors for the detection of chemical and biological molecules requires the modification of SiNW surfaces with molecular receptors that only recognize and bind target molecules. Such binding events often result in changes in the conductance of SiNWs, which can be measured and correlates with the concentration of target molecules. In the case of metal ion biosensors, several

recognizing elements based on proteins (Darwish et al., 2002), peptides (Yang et al., 2001 and 2003; Deo et al., 2000; Shults et al., 2003; Forzani et al., 2005), enzymes (Thompson et al., 1996), and DNA/RNA (Lu et al., 2003) have been developed. For example, Cui et al. immobilized a calcium-binding protein, calmodulin onto SiNW surfaces as a sensitive layer to detect calcium ions. They found that the system has good specificity and reversibility. However, immobilized proteins on surfaces lack long-term stability, which may limit its applications.

From the literature, peptides with optimal amino acid sequences are considered as attractive molecular receptors for metal ion recognition. Among all amino acid residues, the imidazole nitrogen in histidine (His) is an efficient donor atom, and hence His-containing oligopeptides are good metal ions chelators (Sanna et al., 2004). However, the position of His residue in oligopeptide chain also plays an important role in the formation of Cu^{2+} complexes (Lau et al., 1974; Varnagy et al., 2000). Outstanding metal binding ability was reported for the X-Y-His sequence. In this study, we demonstrate the selective detection of Cu^{2+} by combining SiNWs with highly selective His-containing tripeptide, Gly-Gly-His, as a Cu^{2+} recognition element.

5.2 Experimental Section

Materials

Copper nitrite, sodium cyanoborohydride, sodium bicarbonate, and

4-morpholinoethanesulfonic acid (MES) were purchased from Sigma Aldrich (Singapore). His-containing oligopeptides including glycyl-glycyl-histidine (Gly-Gly-His) and glycyl-histidyl-glycine (Gly-His-Gly) were purchased from Bachem (Switzerland).

Sensor fabrication and surface modification

Silicon-on-insulator wafers, which have 50 nm thick silicon oxide and 80 nm thick silicon, were used as substrates. First, fin structures (150 nm wide) were patterned on the wafers by using standard DUV lithography and reactive ion etching. Then, they were oxidized in dry O_2 at 900ºC. After 2 - 6 h, 40 - 50 nm wide SiNWs surrounded by 20 - 50 nm of SiO_2 were formed during a self-limiting oxidization process. Next, the central part of the SiNWs were doped with phosphorous (~1e18 cm^{-3}) to form *n*-type SiNWs, and both ends (source and drain) were connected to a metal pad (AlSiCu, with 1% silicon and 0.5% copper, on top of a TaN layer). Finally, the entire chip was passivated with silicon nitride (Si_3N_4) except for the active sensor area and metal pads. For a single chip, it usually consists of 36 SiNW clusters, and each cluster has 5 individually addressable SiNWs (Agarwal, et al., 2008).

Before surface modifications, the SiNW arrays were immersed in 0.5% HF for 12 min, washed with copious deionized water and left it in air overnight. The HF treatment etches away the surface SiO_2 layer, exposing a fresh SiO_2 for subsequent immobilization. After the cleaned chip was immersed in 2% (v/v) TEA methanolic solution for 2 h, they were rinsed thoroughly with methanol, blown dry with nitrogen

and then baked in a vacuum oven (100ºC) for 15 min. Finally, the chip was immersed in carbonate buffer (500 mM, pH = 10) containing 10 mM of $NaBH_3CN$ and 1 mM of tripeptide (either Gly-Gly-His or Gly-His-Gly), and stored in a sealed chamber at room temperature for 4 h. After the reaction, the chips were washed with deionized water and blown dry with nitrogen.

Electrical conductance measurement

The conductance of each SiNW was measured by using a semi-automatic probe station Alessi REL 6100 (Cascade Microtech, USA) and a semiconductor parameter analyzer, Hewlett Packard 4156 A. Conductance measurements were performed between –0.5 V to 0.5 V with a stepwise increment of 20.0 mV and a compliance of 100 mA. Conductance of a particular SiNW was then calculated from the slope of current-voltage characteristic curve between -0.1 V and 0.1 V.

5.3 Results and Discussion

In our experiments, linear current (*I*) versus voltage (*V*) behavior was observed, suggesting the ohmic nature of the electrical contacts and no SiNW/metal electrode contact issues (Gao et al., 2007). Figure 5.1a shows the changes in the conductance after Gly-Gly-His- and Gly-His-Gly-modified SiNWs were immersed in MES buffer (100 mM, pH = 6.0) containing different concentrations of Cu^{2+}. Here, we define the percentage of change in conductance, *G*%, as follows.

$$G\% = \frac{G_{Cu} - G_{buffer}}{G_{buffer}} \times 100\% \quad (5.1)$$

where G_{Cu} and G_{buffer} represent the conductance of the Gly-Gly-His-modified SiNW in MES buffer with and without Cu^{2+}, respectively. As shown in Figure 5.1a, the conductance increased by 55.7% when the Cu^{2+} concentration was only 1 nM. The increase in the conductance can be explained by the formation of Gly-Gly-His-Cu complex on the surface of the SiNW. Because Cu^{2+} is positively charged, it can act as positive gate potential and increases the conductance of *n*-type SiNWs. When we further increased the Cu^{2+} concentration, the conductance also increased almost linearly with the logarithm of the Cu^{2+} concentration. If we assume that immobilized Gly-Gly-His forms 1:1 Cu^{2+} complex, the formation of Gly-Gly-His-Cu complex can be described by an overall equilibrium constant β:

$$\beta = \frac{[\text{Gly-Gly-His-Cu}^+][\text{H}^+]}{[\text{Gly-Gly-His-H}][\text{Cu}^{2+}]} \quad (5.2)$$

where [Gly-Gly-His-Cu^+] and [Gly-Gly-His-H] represent the surface concentrations of Gly-Gly-His-Cu and Gly-Gly-His, respectively, while [Cu^{2+}] and [H^+] represent the localized concentration of Cu^{2+} and H^+, respectively. By using Possion-Boltzmann equations (Hunter et al., 1993) and assuming high ionic strength in the solution, we can obtain the following relationship between the conductance G and the bulk concentration of Cu^{2+} $[Cu]_b$:

$$G \propto \psi_0 = \frac{2.303kT}{2e}\{\log[\text{Cu}^{2+}]_b + \log\beta + \text{pH}\} \quad (5.3)$$

where *k* is Boltzmann constant, *T* is the temperature, *e* is the elementary charge. This equation suggests that both surface potential and conductance of the SiNW increases linearly with $\log[Cu^{2+}]_b$, which is consistent with our experimental data. On the other hand, when aldehyde-terminated SiNWs (without Gly-Gly-His) were immersed in the same solution, the conductance almost unchanged. These results suggest that the presence of a Gly-Gly-His layer on the SiNW is critical for the realization of a Cu^{2+} sensor. The conductance response towards Cu^{2+} on Gly-His-Gly-modified SiNWs was also studied. Similar trends, but much smaller conductance changes than those achieved by Gly-Gly-His-modified SiNWs were observed (Figure 5.1a). By comparison of the conductance response towards a certain concentration of Cu^{2+} on Gly-Gly-His- and Gly-His-Gly-modified surface, it was found that the conductance changes due to Cu^{2+} binding on the former surface are 3 ~ 4 times higher than on the latter surface. We attributed this phenomenon to a more effective Cu^{2+} binding on Gly-Gly-His-modified surface.

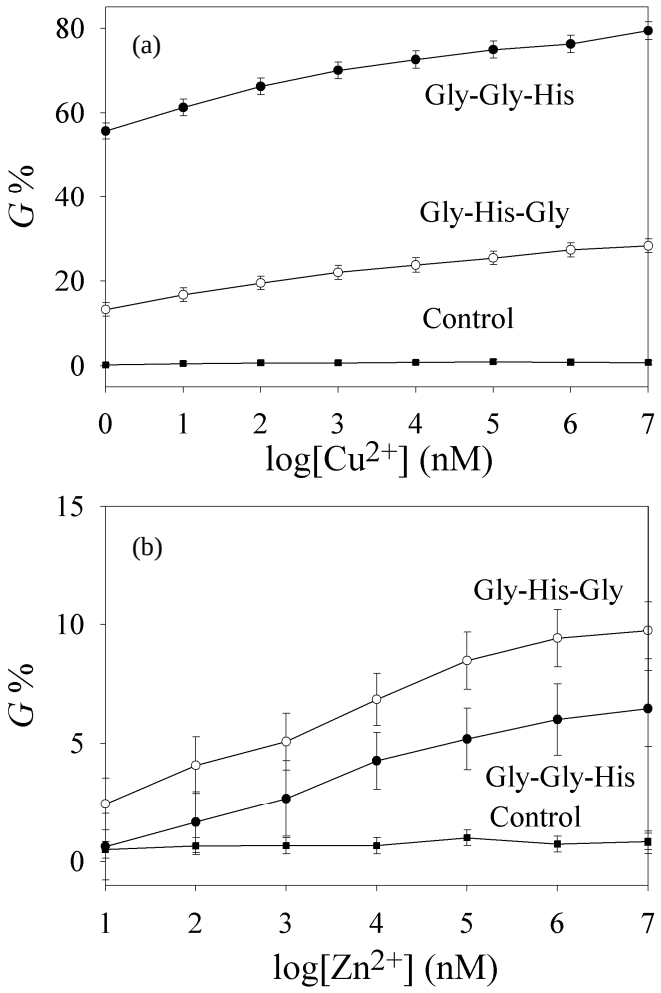

Figure 5.1 Effect of (a) Cu^{2+} concentration and (b) Zn^{2+} concentration on the conductance change of two tripeptides-modified SiNWs and aldehyde-terminated SiNWs (control experiment). The conductance increased almost linearly with the logarithm of the metal ion concentration for both Gly-Gly-His- and Gly-His-Gly-modified SiNWs, which can be attributed to metal ion binding on the tripeptides-modified surfaces. All solutions were prepared in MES buffer (100 mM, pH = 6).

To use the Gly-Gly-His-modified SiNWs-based sensors for Cu^{2+} detection, a number of other factors, including interferences, response time, and reversibility must be considered. To determine the interference from other metal ions, we chose Zn^{2+} as the interfering ions because it is one of the metal ions that have the most similar

properties to Cu^{2+}. First, we measured the conductance responses of Gly-Gly-His- and Gly-His-Gly-modified SiNWs caused by Zn^{2+} alone. As shown in Figure 5.1b, exposing Gly-Gly-His-modified SiNWs to buffer solutions containing 10 mM of Zn^{2+} only lead to small conductance changes (< 7%), suggesting that the formation Gly-Gly-His-Cu complex is more favorable than Gly-Gly-His-Zn complex. Next, we investigated the interferences from Zn^{2+} in mixed solutions containing both Zn^{2+} and Cu^{2+} (the Zn^{2+}/Cu^{2+} molar ratio was maintained at 100 for all Cu^{2+} concentrations tested). As shown in Figure 5.2a, the conductance changes caused by Cu^{2+} in the presence of Zn^{2+} were close to those caused by Cu^{2+} alone at all concentrations. The maximum difference in the conductance change between the mixed and pure Cu^{2+} solutions is only 2% if the Cu^{2+} concentration is higher than 20 μM. This observation suggests that Zn^{2+} causes minimal interferences in this system. Therefore, we can conclude that Gly-Gly-His-modified SiNWs have good selectivity for Cu^{2+} even in the presence of 100-fold of Zn^{2+}.

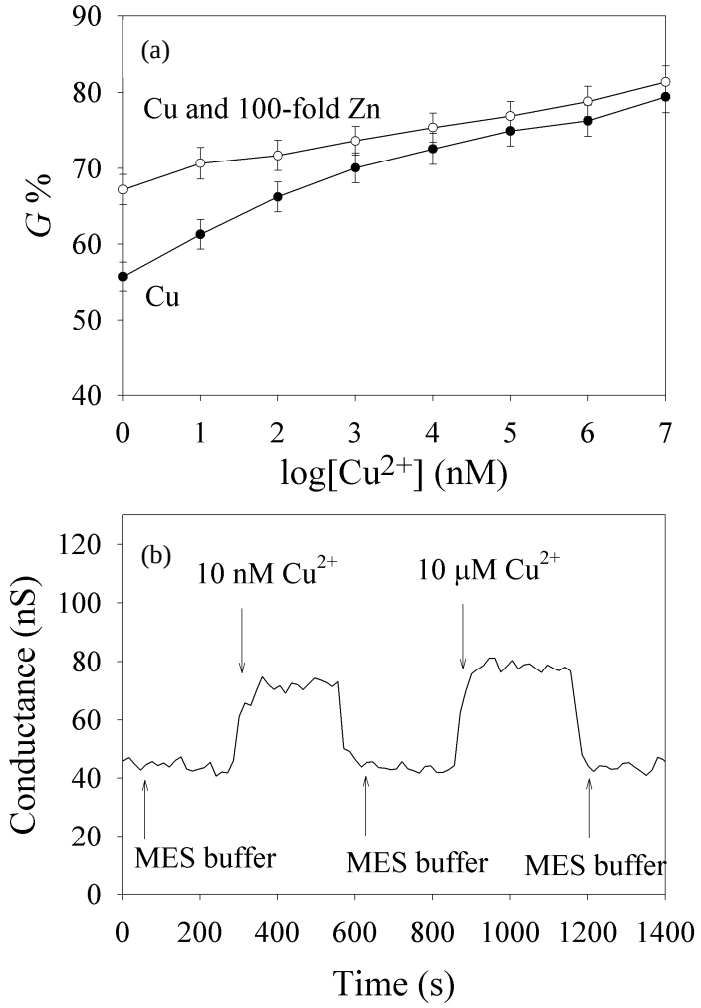

Figure 5.2 (a) Changes in the conductance of Gly-Gly-His-modified SiNWs immersed in solutions containing different concentrations of Cu^{2+} (from 1 nM to 10 mM) or mixed solutions containing both Cu^{2+} and Zn^{2+}. The Zn^{2+} concentration was 100 times higher than the Cu^{2+} concentration. (b) Kinetic behavior of the conductance of a Gly-Gly-His-modified SiNW exposed to MES buffer and Cu^{2+} solutions, alternatively.

Finally, we investigated the response time and reversibility of the Gly-Gly-His modified SiNW sensor. Figure 5.2b show that the conductance of the SiNW increases from 44.3 ± 2.0 nS to 70.7 ± 3.5 nS within few seconds after the injection of 10 nM Cu^{2+} solution and then remained stable for the next 300 s. This result suggests that the binding of Cu^{2+} to the immobilized Gly-Gly-His and the diffusion of Cu^{2+} to the

surface are both fast processes (in the scale of few seconds). Moreover, when we replaced the Cu^{2+} solution with fresh MES buffer (without Cu^{2+}), the conductance quickly decreased back to 44.4 ± 2.3 nS. The process can be repeated several cycles without losing much sensitivity, suggesting that the formation of Gly-Gly-His-Cu is a reversible process.

5.4 Conclusions

It is demonstrated that the Gly-Gly-His-modified SiNWs can be used as a channel in an FET configuration to detect the presence of Cu^{2+} with high sensitivity and specificity. The conductance changes of the modified SiNWs increase linearly with the logarithm of the Cu^{2+} concentrations, which can be attributed to the formation of a stable complexation between Cu^{2+} and Gly-Gly-His. We also compared the performance of Gly-Gly-His- and Gly-His-Gly-modified SiNWs and found that only Gly-Gly-His-modified SiNWs show high selectivity and sensitivity for Cu^{2+}. Even in the presence of 100-fold Zn^{2+} as interfering ions, the SiNW-based sensor shows real-time and reversible responses for Cu^{2+} as low as 1 nM.

CHAPTER 6
SILICON NANOWIRE ARRAYS AS MULTICHANNEL METAL ION SENSORS

6.1 Introduction

In **Chapter 5**, the fabricated SiNWs can only be used for the detection of Cu^{2+}. In this Chapter, a multichannel metal ion sensor is reported by using the SiNW arrays.

Currently, most SiNW sensors reported in the literatures are fabricated either by using "bottom-up" or "top-down" methods. In the former, SiNWs were synthesized in bulk, and one of the SiNWs was selected and connected to metallic contacts. However, it is often difficult to fabricate a SiNW sensor array with multiple channels following this method because the integration process is quite complicated. In contrast, the "top-down" method permits the production of hundreds of identical SiNWs in an array format. Therefore, each SiNW can serve as an individual sensor which can respond to its own target analyte. Although such a SiNW-based multichannel sensor array fabricated by "top-down" approach shows great promise, to the best of our knowledge, it has not been demonstrated in the literatures before. Most of the SiNW sensor array reported so far, can only respond to one kind of target, such as calcium (Bi et al., 2008) or copper ion (see **Chapter 5**) or DNA target (Li et al., 2004 and 2005). One of the major challenges is the lack of a suitable sensitive layer which exhibits high specificity for its target. At the same time, the sensitive layer must be thin enough such that the induced electric field can be detected by the SiNW.

Detecting multiple metal ions and quantifying their concentrations in aqueous solutions in a real-time manner is an important analytical problem. Although ion-selective electrodes are readily available for detecting specific metal ions, they can only detect one type of metal ion, and they are difficult to be miniaturized. On the other hand, atomic adsorption spectrometry (Bannon et al., 1994; Parsons and Slavin, 1993; Tahan et al., 1994) and inductively coupled plasma mass spectrometry (Aggarwal et al., 1994; Liu et al., 1999; Bowins and McNutt, 1994) can be used to detect and quantify multiple metal ions simultaneously, but they are not real-time and the instruments are expensive. Considering the limitation of existing technologies in metal ion detection, we exploited oligopeptide-modified SiNW arrays (fabricated by "top-down" approach) for detecting Cu^{2+} and Pb^{2+} simultaneously at two different channels. The high sensitivity, selectivity, small size and fast response makes the SiNW based sensors an ideal alternative for detecting trace metal ions in water, food and biological samples.

6.2 Experimental Section

Materials

Pb^{2+}-selective oligopeptide (Cys-Asp-Arg-Val-Tyr-Ile-His-Pro-Phe-His-Leu, purity > 90%) was synthesized by Research Biolabs (Singapore). The oligopeptide solution was prepared in sodium phosphate buffer (100 mM, pH = 7.0). Other chemicals are the same as those used in **Chapter 5**.

Sensor fabrication and surface modification

In this Chapter, we used the same sensor as that in **Chapter 5**. After modifying the SiNW surface with TEA, 0.5 μL of sodium phosphate buffer containing 10 μM of Pb^{2+}-selective oligopeptide and 0.5 μL of sodium carbonate buffer containing 10 μM of Cu^{2+}-selective oligopeptide (with 1 mM of $NaBH_3CN$) were spotted onto two different SiNW clusters, respectively, by using a micropipette. Pb^{2+}-selective oligopeptide was immobilized through a reaction between the N-terminal cysteine of the oligopeptide and a surface aldehyde group while Cu^{2+}-selective oligopeptide was immobilized through a reaction between the N-terminal amine of the oligopeptide and a surface aldehyde group. To prevent the evaporation of the oligopeptide solutions, the chip was stored in a sealed and humid chamber at room temperature for 12 h. Finally, the chip was washed with deionized water and blown dry with nitrogen.

Complexation with metal ions and electrical conductance measurement

First, different concentrations of Pb^{2+} were prepared in 100 mM of MES buffer (adjusted to pH = 6.0 with 1 M NaOH). Then, the oligopeptide-modified SiNWs were covered with 10 μL of Pb^{2+} solution. Conductance measurements were performed following the procedure mentioned in **Chapter 5**.

Surface characterization

The microscopic features of SiNWs were observed with a field-emission scanning electron microscope (FESEM, model: JSM-6700F) from JEOL (Japan). Surface chemical compositions on the SiNWs were analyzed with an energy dispersive X-ray (EDX) attachment.

6.3 Results and Discussion

To obtain good reproducibility in our experiments, a current-voltage (*I*-*V*) curve for each SiNW was obtained before any surface modifications were performed. SiNWs which did not give linear *I*-*V* curves were discarded. Figure 6.1 shows a linear *I*-*V* curve for 5 SiNWs in a cluster, suggesting that the electrical contacts are ohmic. Figure 6.1 also shows that the 5 SiNWs exhibit slightly different intrinsic conductance. Therefore, we used an average conductance of 15 SiNWs (from 3 different clusters) to minimize the experimental errors in the following experiments.

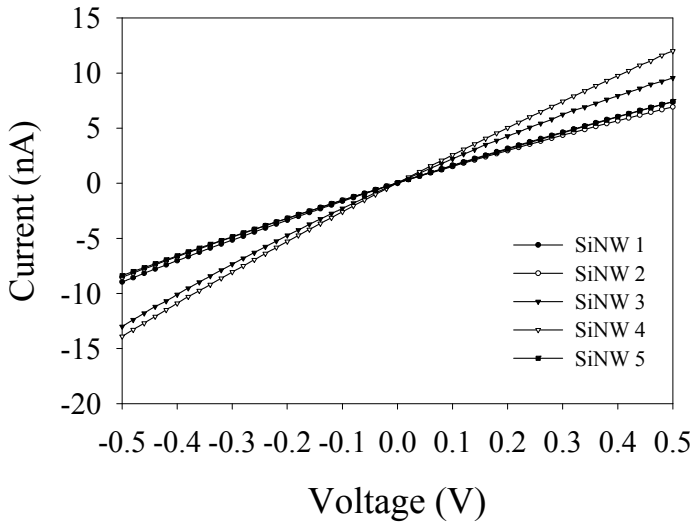

Figure 6.1 Typical *I*-*V* curves for 5 different SiNWs in one cluster.

Figure 6.2a shows an optical image of 3 SiNW clusters (100-μM long for each) on a chip. The surface of the first SiNW cluster was modified with Cys-Asp-Arg-Val-Tyr-Ile-His-Pro-Phe-His-Leu, which is a Pb^{2+}-selective oligopeptide (Hu and Loo, 1995; Loo et al., 1994) and the second SiNW cluster was

modified with Gly-Gly-His, a Cu^{2+}-selective oligopeptide (Yang et al., 2001). The last cluster was not modified with oligopeptides such that its surface remained aldehyde-terminated. The schematic of the immobilization procedure is shown in Figure 6.2b. Thereafter, we immersed these SiNW clusters in a solution containing 100 nM Pb^{2+} and 100 nM Cu^{2+}. After rinsing and drying, SEM-EDX was employed to characterize the surface.

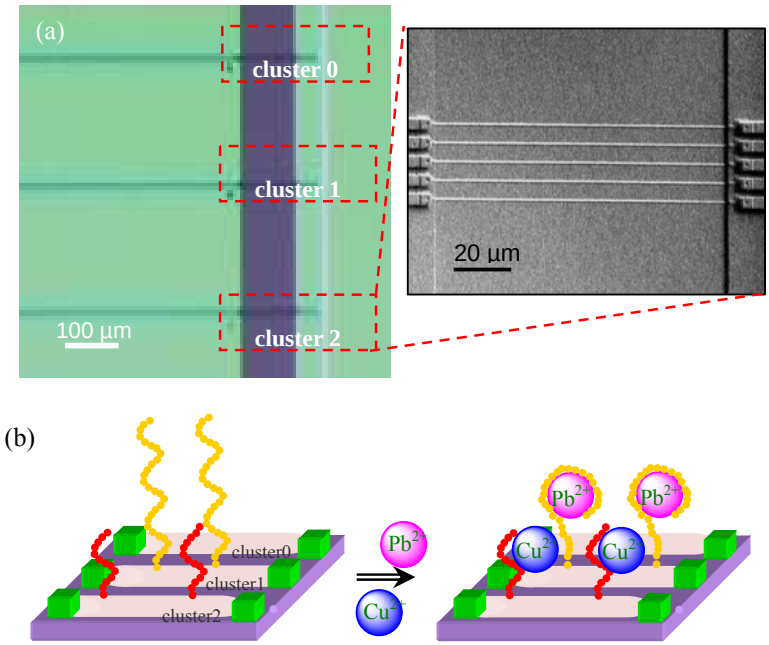

Figure 6.2 (a) Optical image of three SiNW clusters (each cluster has 5 SiNWs). Zoom-in SEM image showing 5 SiNWs in one cluster. (b) Schematic illustration of the surface modification of aldehyde-terminated SiNW clusters (cluster0) with oligopeptides specific for Pb^{2+} (Cys-Asp-Arg-Val-Tyr-Ile-His-Pro-Phe-His-Leu, cluster1) and Cu^{2+} (Gly-Gly-His, cluster2), respectively.

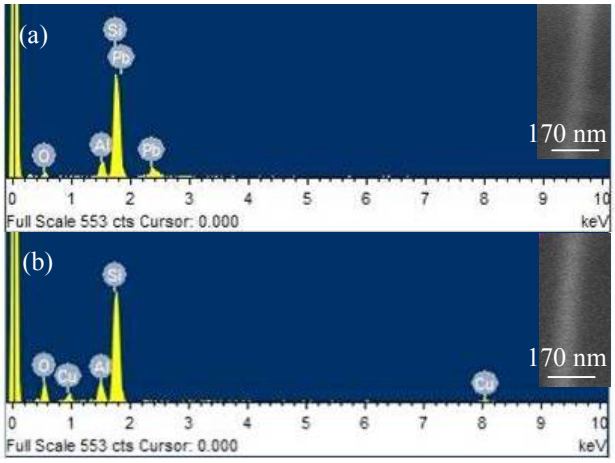

Figure 6.3 SEM-EDX spectroscopy of SiNWs modified with (a) Cys-Asp-Arg-Val-Tyr-Ile-His-Pro-Phe-His-Leu and (b) Gly-Gly-His, respectively, after they were immersed into a mixed solution containing 100 nM Pb^{2+} and 100 nM Cu^{2+}. Inset shows the SEM image.

Figure 6.3 shows that only Pb was detected on the first SiNW cluster modified with Cys-Asp-Arg-Val-Tyr-Ile-His-Pro-Phe-His-Leu while only Cu was detected on the second SiNW cluster modified with Gly-Gly-His. These results suggest that the oligopeptides binds metal ions with high selectivity. We can also conclude that Cys-Asp-Arg-Val-Tyr-Ile-His-Pro-Phe-His-Leu binds Pb^{2+} more strongly than Cu^{2+} while Gly-Gly-His binds Cu^{2+}more strongly than Pb^{2+}. The high selectivity of Cys-Asp-Arg-Val-Tyr-Ile-His-Pro-Phe-His-Leu for Pb^{2+} is probably because Pb^{2+} complexes with one of the His residues and two adjacent carbonyl groups. Another possible mechanism is that both His7 and His10 are responsible for complex with Pb^{2+} (Hu and Loo, 1995; Loo et al., 1994). Similarly, the high selectivity of Gly-Gly-His for Cu^{2+} can be attributed to the formation of three fused chelate rings and a flat 4N coordination plane around Cu^{2+} (see **Chapter 4**).

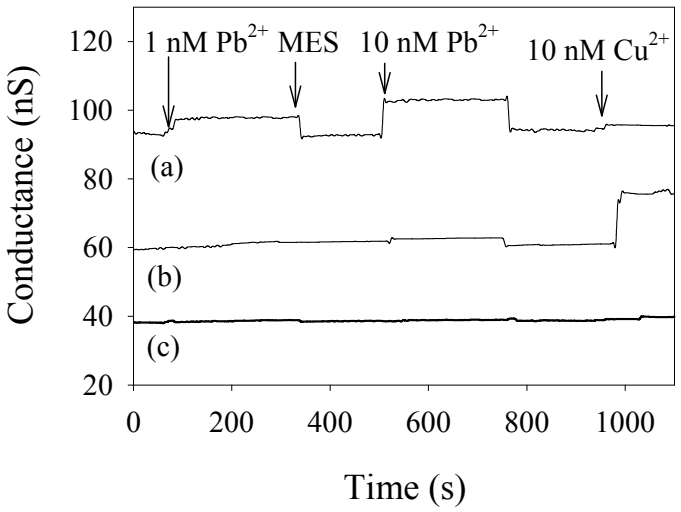

Figure 6.4 Conductance versus time data recorded simultaneously in three different SiNW clusters. The surfaces of these clusters were modified with (a) Cys-Asp-Arg-Val-Tyr-Ile-His-Pro-Phe-His-Leu, (b) Gly-Gly-His, and (c) aldehyde, respectively. The arrows indicate the sequential introduction of 1 nM Pb^{2+}, MES, 10 nM Pb^{2+}, MES, and then 10 nM Cu^{2+} on the SiNW clusters.

Then, we monitored the conductance of each SiNW in these clusters when aqueous solutions containing different concentrations of Pb^{2+} or Cu^{2+} were delivered to the chip. As shown in Figure 6.4, after the injection of 1 nM Pb^{2+}, the conductance of SiNW modified with Cys-Asp-Arg-Val-Tyr-Ile-His-Pro-Phe-His-Leu increases by 5 nS within few seconds and then remains stable, whereas the conductance of both SiNWs modified with Gly-Gly-His and aldehyde do not change. These results demonstrate the following points. First, the increase in the conductance of SiNW modified with Cys-Asp-Arg-Val-Tyr-Ile-His-Pro-Phe-His-Leu is caused by an increase in the positive gate potential after the formation of oligopeptide-Pb complex on the SiNW surface. Second, the formation of oligopeptide-Pb complex reaches equilibrium within a few seconds, and this process is not limited by the diffusion of

Pb^{2+}, probably because of the small dimensions of our SiNW sensor. Third, no Pb^{2+} binds to Gly-Gly-His-modified or aldehyde-terminated SiNW. This result suggests that Pb^{2+} only binds to Cys-Asp-Arg-Val-Tyr-Ile-His-Pro-Phe-His-Leu, and that is also consistent with our SEM-EDX results. Moreover, when we replaced Pb^{2+} solution with fresh MES buffer, the conductance of the SiNW modified with Cys-Asp-Arg-Val-Tyr-Ile-His-Pro-Phe-His-Leu quickly decreased to its original value, which implies that formation of the oligopeptide-Pb complex is fully reversible. Similar behavior was also observed after the addition of 10 nM Pb^{2+}, except that the change in conductance was larger. In contrast, when we injected 10 nM of Cu^{2+} to the chip, the conductance of Gly-Gly-His-modified SiNW exhibited a significant increase. However, the conductance of SiNW modified with Cys-Asp-Arg-Val-Tyr-Ile-His-Pro-Phe-His-Leu and aldehyde remained almost unchanged. These results, when combined with SEM-EDX results, verify that Cys-Asp-Arg-Val-Tyr-Ile-His-Pro-Phe-His-Leu binds Pb^{2+} and Gly-Gly-His binds Cu^{2+} with high specificity. They also demonstrate that one can modify each SiNW cluster with a different oligopeptide such that a SiNW array containing different clusters can be used as a multichannel metal ion sensor.

Finally, we examined the performance of SiNWs modified with Cys-Asp-Arg-Val-Tyr-Ile-His-Pro-Phe-His-Leu in solutions containing only Pb^{2+} and in solutions containing both Pb^{2+} and Cu^{2+}. For the solution containing only Pb^{2+}, a plot of the conductance versus Pb^{2+} concentration (Figure 6.5) shows that the conductance increases almost linearly with the logarithm of Pb^{2+} concentration from 1

nM to 10 μM. We can model these data by using Langmuir adsorption isotherm:

$$\frac{G}{G_{\max}} = \frac{C}{C+K_{\mathrm{d}}} \tag{6.1}$$

where G and $G_{\max}$ are the normalized conductance change ($\Delta G/G_0 \times 100\%$, where ΔG is the conductance change and G_0 is the initial conductance) and the normalized maximum conductance change, respectively, C is the concentration of Pb^{2+}, and K_{d} is the dissociation constant. We estimated $G_{\max}$ = 21.19% and K_{d} = 33.66 nM from Equation (6.1) by using a least-square fitting method. If the smallest reliable conductance change of our instrument is 0.1%, then the lowest Pb^{2+} concentration can be detected by using the SiNW sensor is 1.0 nM, which is lower than that of the fluorosensor (10 nM) demonstrated by Li and Lu (Li and Lu, 2000). On the other hand, the value of K_{d} gives an indication of the affinity of the immobilized oligopeptide for Pb^{2+}, which is consistent with the value determined previously (Chow et al., 2005).

Figure 6.5 also shows that after the injection of the Pb^{2+} solution containing 50 μM of Cu^{2+}, the change in conductance is larger than that at the same Pb^{2+} concentration without Cu^{2+}, especially when the Pb^{2+}concentration is low (from 1 to 100 nM). We also point out that the influence of Cu^{2+} decreases when the concentration of Pb^{2+} is increased. For example, the difference is less than 10% if the concentration of Pb^{2+} is higher than 480 nM (when the blood Pb^{2+} concentration exceeds this level, it is considered harmful). In addition, Figure 6.5 shows that if the concentration of Pb^{2+} is above 1000 nM (the concentration ratio of Cu^{2+} to Pb^{2+} is 50), no interference is

observed.

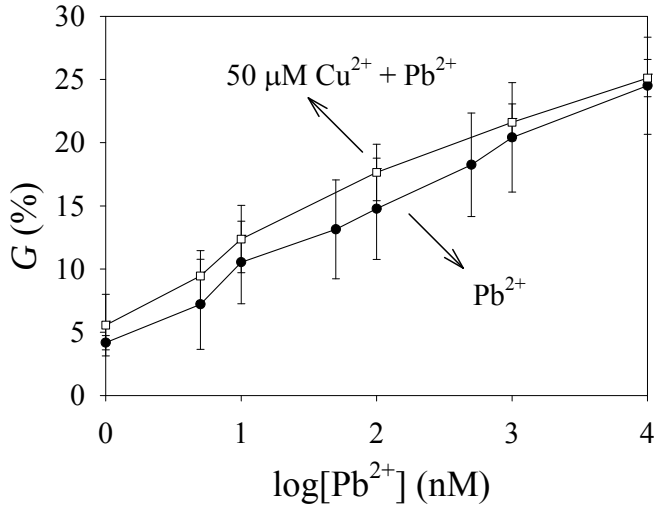

Figure 6.5 Effects of Pb^{2+} concentration on the conductance of SiNWs (modified with Cys-Asp-Arg-Val-Tyr-Ile-His-Pro-Phe-His-Leu) under two conditions: in solutions containing only Pb^{2+} (no Cu^{2+}) and in solutions containing Pb^{2+} and 50 μM Cu^{2+}. The error bars are standard deviations of conductance for 15 SiNWs in different clusters. In the absence of Cu^{2+}, the conductance increases almost linearly with the logarithm of the Pb^{2+} concentration.

6.4 Conclusions

In summary, we have developed a multichannel metal ion sensor by using SiNW arrays, which can be manufactured by using "top-down" semiconductor processes. After two different oligopeptides were immobilized on two independently addressable SiNW clusters, both Pb^{2+} and Cu^{2+} can be detected simultaneously and quantitatively. The simplicity, high sensitivity, capability of selective multiplexed detection of different metal ions suggest that the SiNW arrays can move beyond current metal ion sensing technologies and have the potential for environmental monitoring, waste water treatment, and clinical toxicology caused by heavy metal ions.

CHAPTER 7
CONTROLLING ORIENTATIONS OF IMMOBILIZED OLIGOPEPTIDES USING N-TERMINAL CYSTEINE LABELS

7.1 Introduction

Immobilization of peptides or proteins on surfaces with well-defined orientations is critical to prevent protein denaturation and to keep the function of immobilized proteins or peptides (Seong and Choi, 2003; Lesaicherre et al., 2002a, b; Luk et al., 2004). However, controlling the orientations of immobilized proteins or peptides remains a big challenge because most immobilization strategies rely on the crosslinking of reactive residues, such as lysine (MacBeath and Schreiber, 2000; Zhu et al., 2000; Huang et al., 1996; Nakanishi et al., 1996) or cysteine (Sasaki et al., 1997), in a nonspecific manner. In contrast, several reactions, such as Staudinger ligation (Köhn et al., 2003; Soellner et al., 2003 and 2006) or Diels-Alder reaction (Houseman et al., 2002) can be used to immobilize proteins or peptides with high specificity. However, these immobilization strategies require labeling peptides with an unnatural moiety, such as phosphinothioester or cyclopentadiene. Meanwhile, some other methods only require natural amino acid labels, such as histidine (Zhu et al., 2001; Cha et al., 2004) or cysteine (Shen et al., 2005; Lee et al., 2007), because the former is able to complex with nickel ions and the latter can form an Au-S bond on a gold surface. The use of natural amino acids is advantageous because additional

amino acids can be introduced into target proteins or peptides through genetic engineering (Sambrook et al., 1989). However, these methods are not site-specific because any histidine or cysteine residues, regardless of their positions in the peptides or proteins, can bind nickel ions or react with gold. To address this issue, we consider a site-specific immobilization reaction between aldehyde and N-terminal cysteine (Liu and Tam, 1994a, b; Shao and Tam 1995), in which free aldehyde group reacts with the mercaptoethylamine moiety of cysteine and forms a stable thiazolidine ring (Zatsepin et al., 2002; Spetzler and Tam, 1995). In the past, Falsey et al. reported the immobilization of cysteine-terminated peptides on an aldehyde-terminated surface (Falsey et al., 2001). However, it is well-known that aldehyde can also react with N-terminal amine or lysine under certain conditions, especially in the presence of reducing agents. Thus, whether the peptides are immobilized on aldehyde-terminated surfaces through the N-terminal cysteine or lysine depends on the competition between the formation of thiazolidines and imines. In this Chapter, we study the competition between these two reactions and evaluate whether an N-terminal cysteine label can be used to control the orientations of immobilized oligopeptides effectively.

7.2 Experimental Section

Materials

Tripeptides Cys-Gly-Gly and Gly-Gly-Cys, pentapeptide Cys-Gly-Gly-Gly-Lys, and oligopeptide Cys-Ser-Asn-Lys-Tyr-Arg-Ile-Asp-Glu-Ala-Asn-Asn-Lys-Ala-Tyr-Lys-Met-Leu (with a purity of > 90%) were synthesized by 1st Base and Research Biolabs

(Singapore). Trypsin was purchased from Sigma Aldrich (Singapore).

Oligopeptides immobilization

First, aldehyde-terminated silicon wafers were prepared as described in **Chapter 4**. Then, oligopeptides (10 μM) were immobilized on the aldehyde-terminated surfaces by using either 0.1 M phosphate buffer (pH = 7.0) or 0.1 M carbonate buffer (pH = 10.0) containing 1 mM of $NaBH_3CN$. After reactions, the oligopeptide-modified surfaces were washed with 2×SSPE buffer (300 mM NaCl, 23 mM NaH_2PO_4, 2.8 mM EDTA) with 1% Triton-100 for 30 min to remove unreacted oligopeptides.

Quartz crystal microbalance (QCM)

All QCM experiments were performed by using an Affinity Detection System manufactured by ANT technology (Taipei, Taiwan). For each measurement, 300 μL of sample solution was injected into the flow system and delivered to an amine-terminated gold sensor chip by using a peristaltic pump. Teflon tubings with an internal diameter of 0.5 mm were used to connect each component of the system. PBS (phosphate buffer saline) was used as the running buffer and the flow rate was fixed at 30 μL/min. After each measurement, the used sensor chip was cleaned by incubating gold surfaces in 10 μL dichromate acid for at least 15 min and then rinsed thoroughly with copious amounts of deionized water. Finally, the cleaned chip was incubated in 10% 1-octadecanthiol for 5 min and 10% PEI (polyethyleneimine) for 30 min to regenerate the sensor chip.

HATR-FTIR

A Fourier Transformation Infrared (FTIR) spectrophotometer (model: IRPrestige-21, from Shimadzu, Tokyo, Japan) equipped with a liquid nitrogen-cooled, mercury-cadmium-telluride (MCT) detector was employed for all measurements. Prior to each measurement, a Ge trough plate (PIKE Technologies, Madison, WI, USA) was polished with AUTOSOL®, and then rinsed thoroughly with deionized water. Surface modifications of the Ge trough plates are the same as that of silicon wafers. For each spectrum, the resolution was maintained at 4 cm^{-1} and 256 scans were accumulated.

Cleavage of surface immobilized oligopeptides

Surface-immobilized oligopeptides were exposed to 100 nM trypsin in trypsin buffer (50 mM Tris-HCl, 20 mM $CaCl_2$, pH = 8.0) at 37°C for 30 min. Excess trypsin and cleaved oligopeptides were removed by incubating the substrate in 2×SSPE buffer and 1% Triton-100 for 30 min.

Fluorescence microscopy

The peptide-modified surface was incubated in 1 mg/mL fluorescein isothiocyanate (FITC) for 2 h. The images were observed with a fluorescence microscope (Eclipse E200, Nickon, Tokyo, Japan). A fluorescein/enhanced green fluorescent protein (FITC/EGFP) filter set from Chroma Technology (Brattleboro, VT, USA) was used. The same parameters were used for all images.

7.3 Results and Discussion

First, we designed two simple cysteine-containing tripeptides Cys-Gly-Gly (with an N-terminal cysteine) and Gly-Gly-Cys (with a C-terminal cysteine) to study the effect of cysteine position on the immobilization reaction. After incubating aldehyde-terminated silicon wafers in phosphate buffer (pH = 7.0) containing 10 μM Cys-Gly-Gly or Gly-Gly-Cys, we characterized both surfaces with ellipsometry periodically. Figure 7.1 shows that the ellipsometric thickness of the immobilized Cys-Gly-Gly increases to 8 ± 0 Å after 5 h whereas that of the immobilized Gly-Gly-Cys shows no increase even after 20 h.

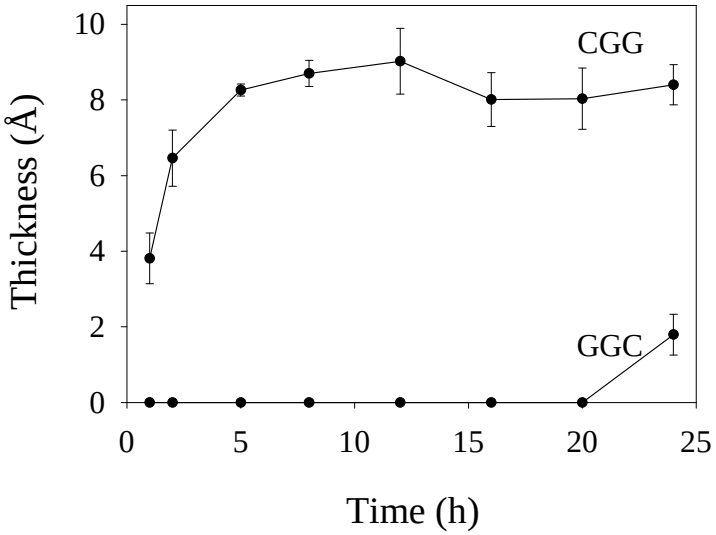

Figure 7.1 Ellipsometric thicknesses of immobilized tripeptides (Cys-Gly-Gly or Cys-Gly-Gly) on aldehyde-terminated surfaces as a function of incubation time (in 0.1 M phosphate buffer). Cys-Gly-Gly and Cys-Gly-Gly are immobilized on the surface through the formation of thiazolidine ring and secondary amine, respectively.

These results clearly suggest that the position of the cysteine in a tripeptide plays an important role in the formation of thiazolidine. Only the N-terminal cysteine is

capable of forming thiazolidine with aldehyde whereas the C-terminal cysteine cannot undergo such a reaction.

The formation of thiazolidine was also confirmed by our ATR-FTIR results. A broad peak at 1128 cm^{-1} appeared after the immobilization of Cys-Gly-Gly on an aldehyde-terminated surface (Figure 7.2). This peak can be assigned to the C-N group in the thiazolidine ring. In contrast, no new peak can be observed when Gly-Gly-Cys was immobilized. Although N-terminal amine groups of oligopeptides are known to react with aldehydes and form imines under certain conditions, the failure to immobilize Gly-Gly-Cys on the aldehyde-terminated surface implies that no imines are formed, probably because all imines hydrolyze and become amine and aldehyde again (Peelen and Smith, 2005; Lemieux et al., 1998).

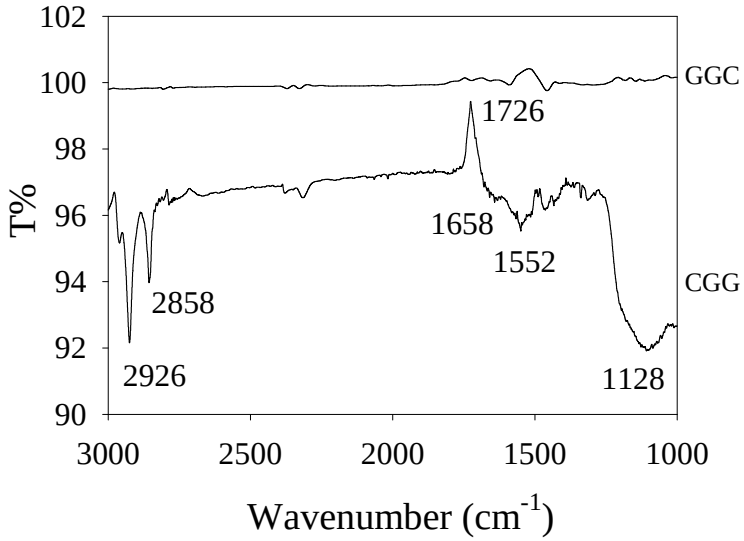

Figure 7.2 FTIR spectra of an aldehyde-terminated Ge trough plate after the immobilization of Cys-Gly-Gly and Gly-Gly-Cys, respectively, in the phosphate buffer for 5 h. The aldehyde-terminated Ge trough plate was used as reference.

This proposition can be tested, because imines can be reduced to stable secondary amines by adding a reducing agent such as $NaBH_3CN$ (This particular reducing agent only reduces imines without affecting aldehydes). As expected, when we immobilized 10 μM Cys-Gly-Gly and Gly-Gly-Cys on the aldehyde-terminated surface in the presence of 1 mM $NaBH_3CN$ (in carbonate buffer, pH = 10.0), the ellipsometric thicknesses of both tripeptides increased to 6 Å after 5 h (Figure 7.3). Unlike the formation of thiazolidine ring which requires an N-terminal cysteine, the immobilization of tripeptides via secondary amine linkage is nonspecific. Any primary amines in a peptide will react with surface aldehyde groups in the presence of reducing agents.

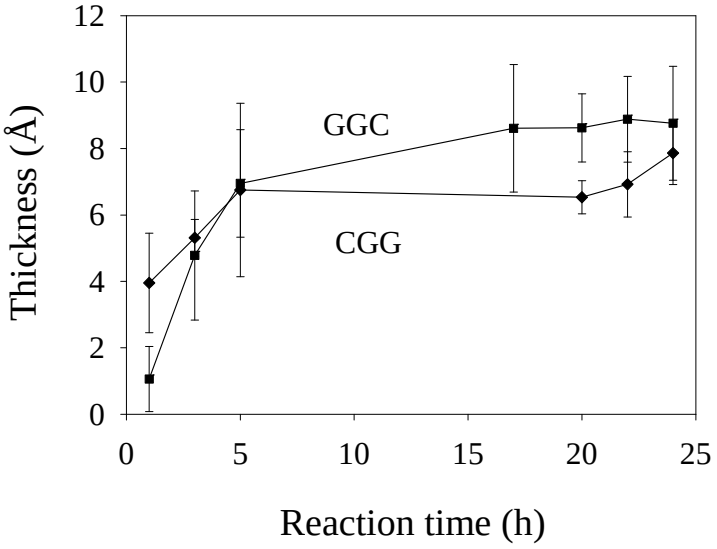

Figure 7.3 Ellipsometric thicknesses of the immobilized tripeptide (Cys-Gly-Gly or Gly-Gly-Cys) on the aldehyde-decorated silicon wafers in 0.1 M carbonate buffer with 1 mM $NaBH_3CN$.

To further investigate these two competing reactions, we used quartz crystal microbalance (QCM) to study the reaction kinetics. In this experiment, we increased

the concentration of Cys-Gly-Gly and Gly-Gly-Cys to 100 μM to get a reasonable signal. As shown in Figure 7.4a, injection of 100 μM Cys-Gly-Gly (in phosphate buffer) leads to a 226 Hz decrease in the frequency, whereas the injection of Gly-Gly-Cys does not lead to any changes in frequency (Figure 7.4b). These results once again support the proposition that only N-terminal cysteine can form thiazolidine rings with aldehyde groups. To consider a "worst-case scenario" in which N-terminal amines may react with aldehydes, we added 1 mM $NaBH_3CN$ to the Gly-Gly-Cys solution. In this case, the frequency only decreased by 16 Hz (Figure 7.4c), which was much smaller than the 226 Hz shift after Cys-Gly-Gly was injected. Therefore, we conclude that the formation of thiazolidine is not only site-specific, but also faster than the formation of imine even in the presence of reducing agent.

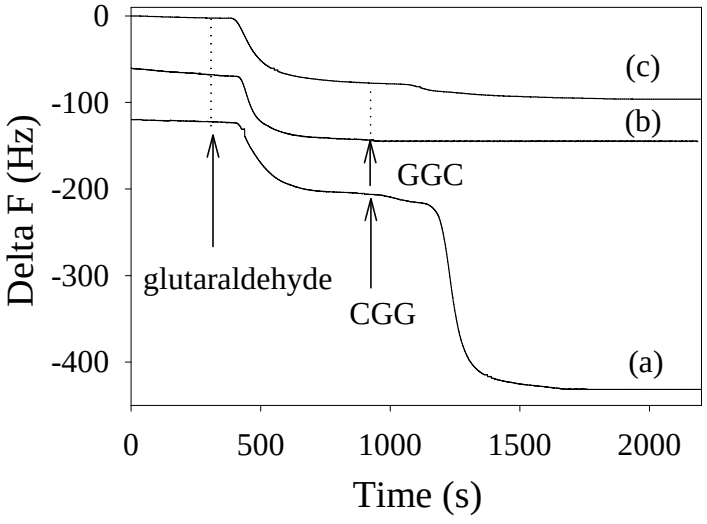

Figure 7.4 Frequency changes of the QCM due to the reaction with 5% glutaraldehyde and the immobilization of (a) 100 μM Cys-Gly-Gly in phosphate buffer, (b) 100 μM Gly-Gly-Cys in phosphate buffer, and (c) 100 μM Gly-Gly-Cys in carbonate buffer containing 1 mM of $NaBH_3CN$.

Based on the relative reactivities of N-terminal cysteine and primary amines with aldehydes, we hypothesize that for an oligopeptide containing both N-terminal cysteine and lysine, the formation of thiazolidines is much faster than the reaction between lysine and aldehyde in phosphate buffer (without reducing agent). To test this hypothesis, we designed a new pentapeptide, Cys-Gly-Gly-Gly-Lys, which contains one N-terminal cysteine label and one lysine. We expect that the free amine will be left on the surface if surface aldehydes only react with the N-terminal cysteine. Otherwise, if both cysteine and lysine react with aldehyde, no free amine will be left.

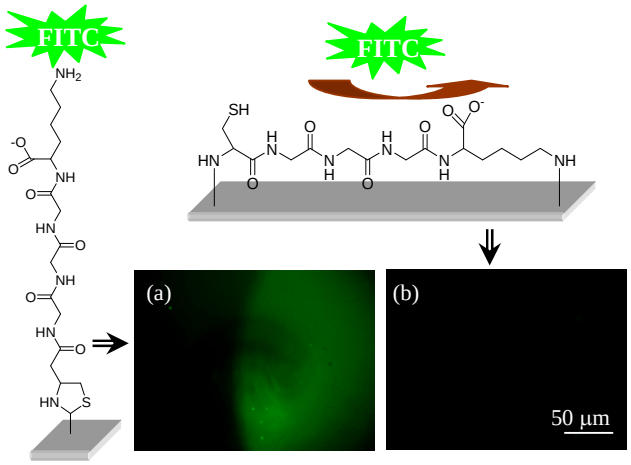

Figure7.5 Fluorescence images of Cys-Gly-Gly-Gly-Lys-modified silicon wafers prepared in (a) phosphate buffer without reducing agent, and (b) carbonate buffer with reducing agent. The green fluorescence indicates the presence of FITC which reacts with free amine (from lysine) on the surface after the immobilization of Cys-Gly-Gly-Gly-Lys.

After immobilizing Cys-Gly-Gly-Gly-Lys by using phosphate buffer (without reducing agent) and carbonate buffer (with reducing agent), we used fluorescein isothiocyanate (FITC) as a free amine marker to probe both surfaces. Figure 7.5

shows that the fluorescence intensity of the former is indeed stronger than the latter, which supports our hypothesis that lysine does not react with surface aldehydes in the absence of reducing agent.

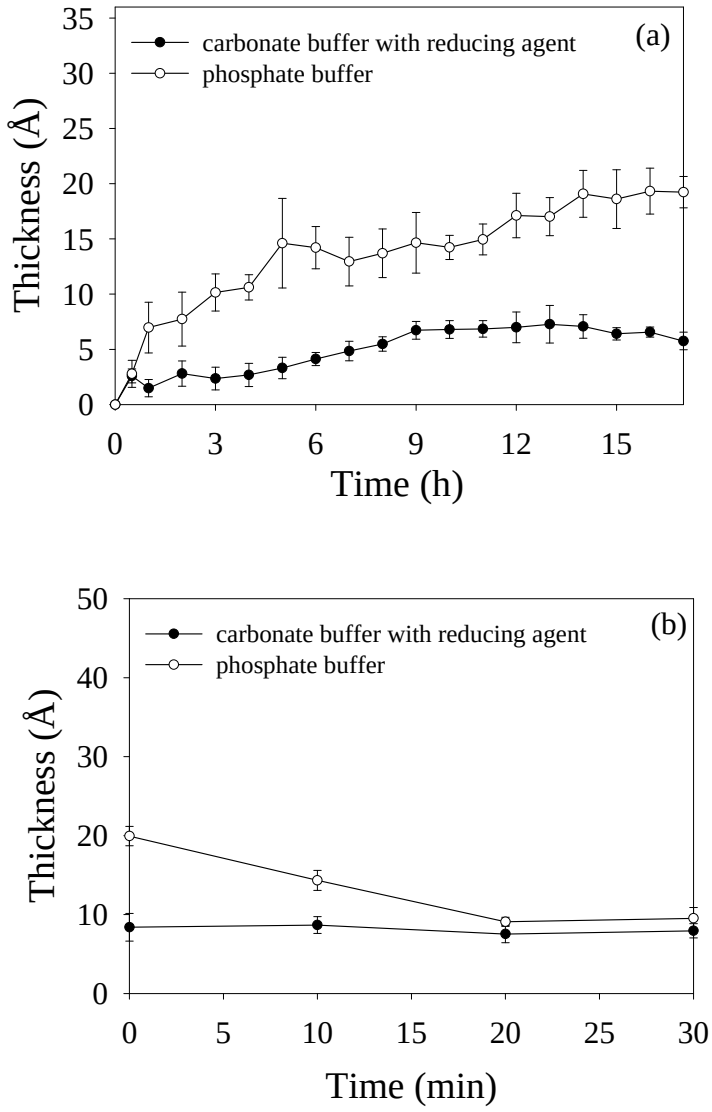

Figure 7.6 Ellipsometric thickness of (a) after 10 μM of the 18-mer oligopeptide was immobilized on an aldehyde-terminated surface through different immobilization strategies. (b) after both oligopeptide-modified surfaces were incubated in 100 nM trypsin solution at 37°C.

Finally, we immobilized an oligopeptide (Cys-Ser-Asn-Lys-Tyr-Arg-Ile-Asp-Glu-Ala-

Asn-Asn-Lys-Ala-Tyr-Lys-Met-Leu) that contains 18 residues, including an N-terminal cysteine label and three lysines (at position 4, 13 and 16, respectively) on an aldehyde-terminated surface. We found that when the immobilization was performed in phosphate buffer without reducing agent (we refer to this substrate as **1**) and in carbonate buffer with reducing agent (we refer to this substrate as **2**), the ellipsometric thickness increased by 20 Å and 7 Å, respectively (Figure 7.6).

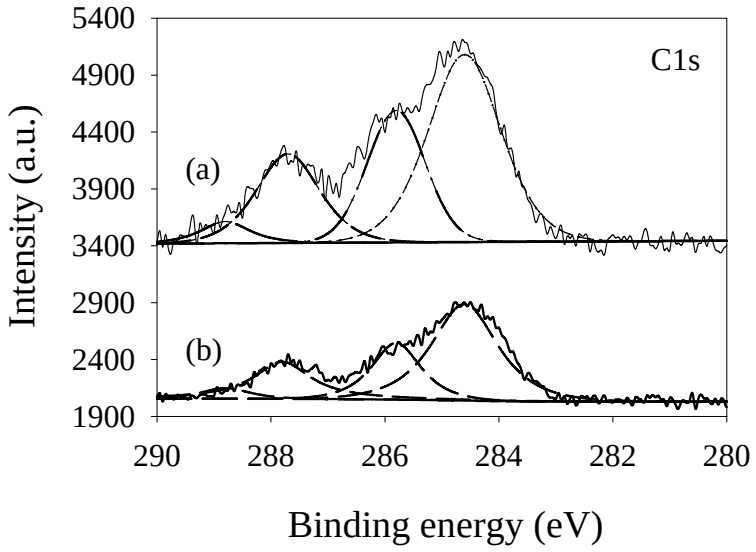

Figure 7.7 XPS spectra (C1s) of a silicon wafer functionalized with 10 μM oligopeptide Cys-Ser-Asn-Lys-Tyr-Arg-Ile-Asp-Glu-Ala-Asn-Asn-Lys-Ala-Tyr-Lys-Met-Leu in phosphate buffer without reducing agent (a) before, and (b) after the oligopeptide-modified surface was incubated in 100 nM of trypsin solution at 37°C for 30 min.

On the basis of the pentapeptide result, we propose that the larger thickness corresponds to a layer of vertically immobilized oligopeptide with only one anchoring point at the N-terminal cysteine, whereas the smaller thickness corresponds to a layer of horizontally immobilized oligopeptide with multiple anchoring points at both

cysteine and lysine residues. To investigate whether different oligopeptide orientations caused by different immobilization strategies can influence enzymatic activities acting on the immobilized oligopeptides, we incubated both substrates **1** and **2** in 100 nM trypsin solution, which can cleave a polypeptide chain at the C-terminal side of arginine and lysine residues (Kemmler et al., 1971; Wang et al., 1989). After 30 min of incubation, we observed that the ellipsometric thickness of **1** decreased from 20 Å to 9 Å. Comparison of XPS spectra in Figure 7.7a and 7.7b also show that the intensities of four C1s peaks (belong to the immobilized oligopeptide) decrease after the incubation, suggesting that the immobilized oligopeptide has been cleaved by trypsin. The cleavage of oligopeptide was also confirmed by the N1s spectra (Figure 7.8), and ATR-FTIR (Figure 7.9).

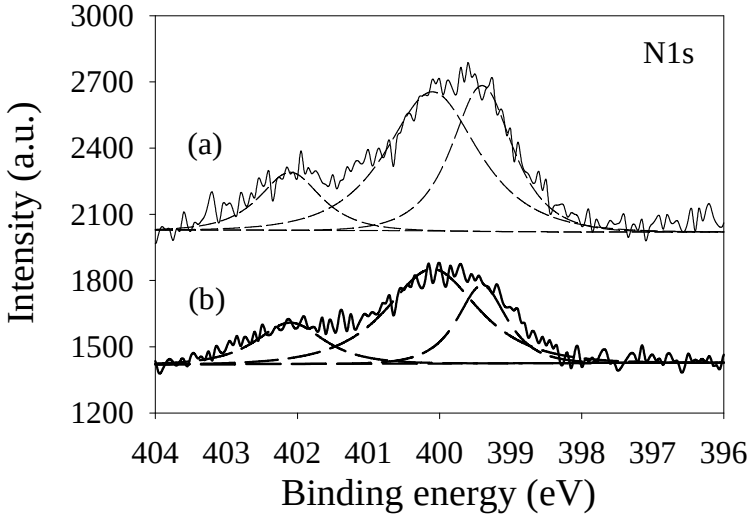

Figure 7.8 XPS spectra (N1s) of a silicon wafer functionalized with 10 μM oligopeptide Cys-Ser-Asn-Lys-Tyr-Arg-Ile-Asp-Glu-Ala-Asn-Asn-Lys-Ala-Tyr-Lys-Met-Leu in phosphate buffer without reducing agent (a) before, and (b) after the oligopeptide-modified surface was incubated in 100 nM of trypsin solution at 37°C for 30 min.

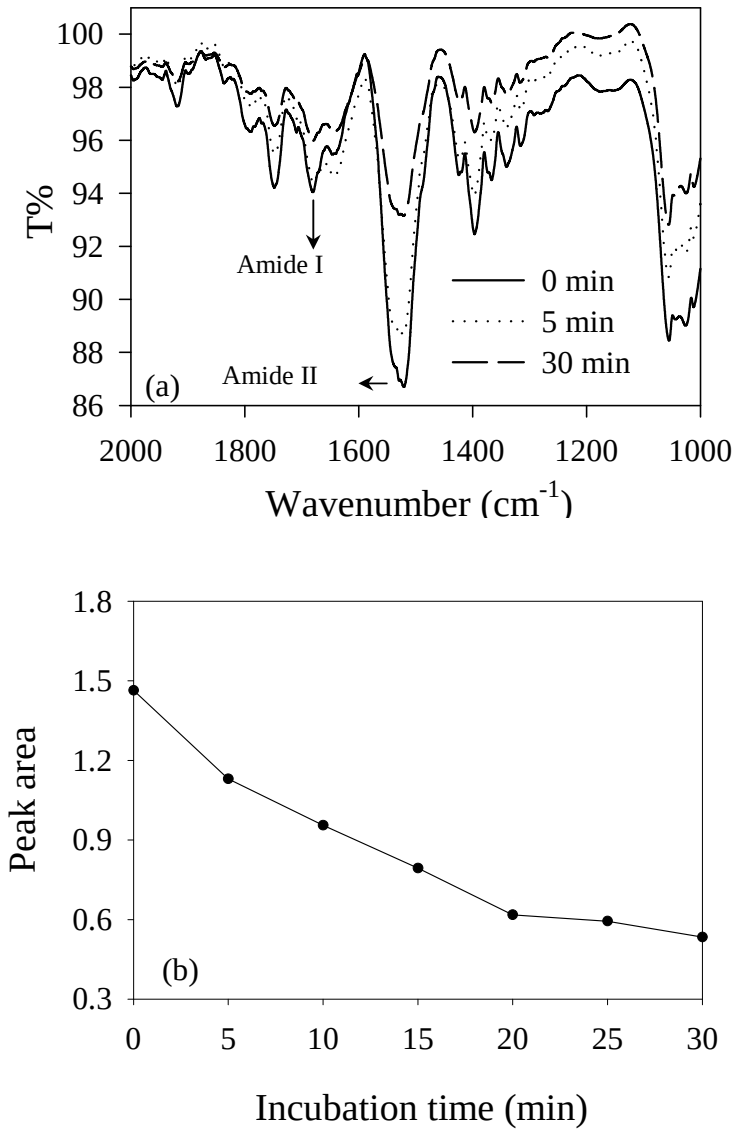

Figure 7.9 (a) FTIR spectra of an aldehyde-terminated Ge trough plate after it was modified with an 18-mer oligopeptide in the phosphate buffer (pH = 7.0). The dotted line and dashed line were the spectra after the oligopeptide-modified Ge trough plate was incubated in 100 nM trypsin solution at 37°C for 5 min and 30 min, respectively. (b) Peak areas ranging from 1420 cm^{-1} to 1580 cm^{-1} after the oligopeptide-modified Ge trough plate was incubated in 100 nM trypsin at 37°C for different time.

On the other hand, when we incubated **2** in 100 nM trypsin solution, we found that both ellipsometric thickness and FTIR peaks remained unchanged. These results, when combined, suggest that **1** is a better enzyme substrate than **2**. There are two possibilities. The first one is because multiple anchoring points at lysine residues cause the immobilized oligopeptide to lay flat on the surface, and that prevents the trypsin from cleaving the immobilized oligopeptide. The second possibility is that the trypsin is able to cleave the immobilized oligopeptide, but the digested oligopeptide fragments do not desorb from the surface as they are confined to the surface through some anchoring points. Hence, the ellipsometric thicknesses and FTIR peaks do not change (Figure 7.10).

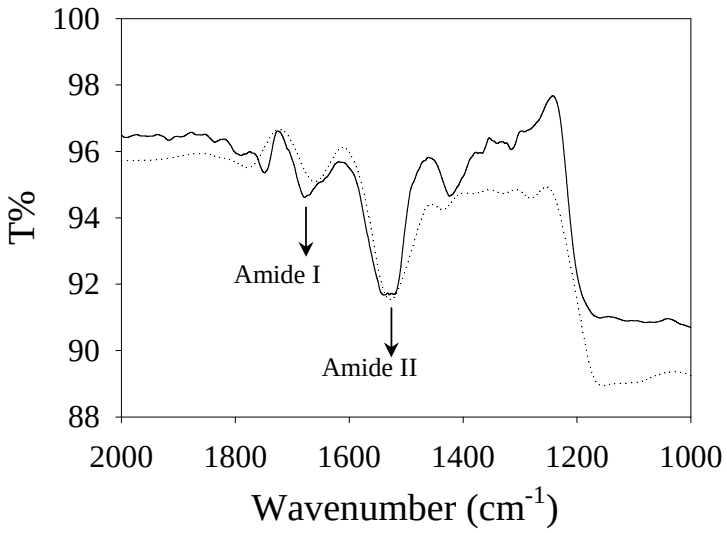

Figure 7.10 FTIR spectra of an aldehyde-terminated Ge trough plate after it was modified with the 18-amino acid oligopeptide in the carbonate buffer (pH = 10.0) with 1 mM $NaBH_3CN$. The dotted line was the spectra after the oligopeptide-modified Ge trough plate was incubated in 100 nM trypsin at 37°C for 30 min.

7.4 Conclusions

In summary, we describe an immobilization strategy which can be used to control the orientations of immobilized oligopeptides through the formation of thiazolidine ring between N-terminal cysteine and surface aldehyde groups. When an oligopeptide with an N-terminal cysteine label and multiple lysines is immobilized on the aldehyde-terminated surface, the N-terminal cysteine quickly reacts with surface aldehydes to form a stable thiazolidine ring, which prevents lysines from reacting with aldehydes. This immobilization strategy can lead to well-defined orientations of immobilized oligopeptide and has a great influence on its ability as an enzyme substrate. By using ellipsometry, XPS, and ATR-FTIR, we conclude that trypsin can cleave the oligopeptide with measurable changes only if the oligopeptide is vertically immobilized on the surface.

CHAPTER 8
DETECTING OLIGOGLYCINES BY USING LIQUID CRYSTALS

From **Chapter 3** to **Chapter 7**, we immobilized the oligopeptides on the surfaces and used them to adsorb metal ions. Based on the complex mechanism between oligopeptides and metal ions, we fabricated silicon nanowire-based metal ion sensors. In the following chapters, we sought to develop a simple and sensitive liquid crystal-based biosensor for monitoring enzymatic activities. In this chapter, we determine the feasibility of using liquid crystal for optical detection of surface immobilized oligopeptides. In **Chapter 9** and **Chapter 10**, we develop LC-based sensors to report the enzymatic activity.

8.1 Introduction

When thermotropic LCs are melting, they undergo a liquid crystalline phase, which is an intermediate state between solid and isotropic liquid. Although mesogens (molecules that form LC phases) can move freely as molecules in a liquid phase, they remain orientated in a certain direction known as director. In the past, the special orientations of mesogens in the liquid crystalline phase, including their response to temperature, pressure, and external stimuli have been widely studied and exploited for the applications of chemical sensors (Novak et al., 1972; Poziomek et al., 1973). For example, past studies have shown that the pitch of cholesteric LCs may increase when the temperature is raised, or when organic vapors diffuse into the layers of cholesteric

LC. As a result, the color of LC changes according to the environmental temperature, or the concentration of organic vapors (Winterbottom et al., 2003).

Recently, more studies have demonstrated an alternative of using LCs to report chemical and biomolecular binding events occurring at a solid interface (Gupta et al., 1998; Shah et al., 2001; Brake et al., 2003; Luk et al., 2004). The detection principle, however, is based on the changes of the anchoring of LCs supported on surfaces, rather than the changes of their bulk properties. Because the anchoring of LCs is determined by interactions between mesogens and surfaces (Gupta et al., 1998; Shah et al., 1999), the anchoring of LCs depends on the chemical compositions and the molecular-level structures of surfaces (Jerome, 1991). Based on the correlations between the anchoring energies and surface properties, subtle changes of the surface properties can lead to the different orientations of LCs supported on the surface. Moreover, these orientations of LCs near surfaces can be propagated and amplified rapidly through the bulk of LCs up to 100 μm away, thanks to the liquid-like mobilities of mesogens. This liquid-crystal based detection method has been exploited to report the protein binding events on nanostructured surfaces (Gupta et al., 1998) and low-level of chemical analytes in the vapor phase (Yang et al., 2005).

In recent years, short oligopeptides have found broad applications in many fields, such as the study of enzymatic activity (Salisbury et al., 2002; Schutkowski et al., 2004), protein binding events (Schulze et al., 2004; Clare et al., 2005), and biological and chemical sensing (Pilloud et al., 1998; Potyrailo et al., 1998; Härtl et al., 2004).

To characterize these short oligopeptides, several analytical methods are readily available. For example, Matrix-Assisted Laser Desorption/Ionization-Time of Flight (MALDI-TOF) mass spectrometry (Bienvenut, 2005) and liquid chromatography-mass spectrometry (LC-MS) (Niessen, 1999) are efficient methods for the characterization and detection of short oligopeptides. However, these methods cannot be used to study the interactions between oligopeptides and other biomolecules. On the other hand, surface-based analytical tools, such as surface plasmon resonance (SPR) (Johnsson et al., 1991) and quartz-crystal microbalance (QCM) (Matsuno et al., 2001) can be used to study the interactions of short oligopeptides with other biomolecules, but these methods require expensive instrumentations. It is also difficult to perform a parallel analysis of multiple oligopeptides simultaneously. In contrast, several past studies have demonstrated that liquid-crystal based sensors can be used to detect multiple oligopeptides on a surface simultaneously with a good spatial resolution. This detection scheme does not require complex instrumentations because the orientational changes of LCs can be easily observed under crossed polarizers due to the birefringent property of LCs. These approaches also have been exploited to study the interactions between oligopeptides and proteins (Clare et al., 2005). However, this system requires an obliquely deposited gold film which needs to be prepared in an expensive high-vacuum system. In addition, a linker such as sulfo-succinimidyl 4-(*N*-maleimidomethyl) cyclohexane-1-carboxylate (SSMCC) is needed to link the thiol groups of the oligopeptides to the amine-terminated self-assembled monolayers on the surface. This

immobilization strategy has some stability issues because both linker and thiol are very reactive. They can be oxidized easily in an ambient environment.

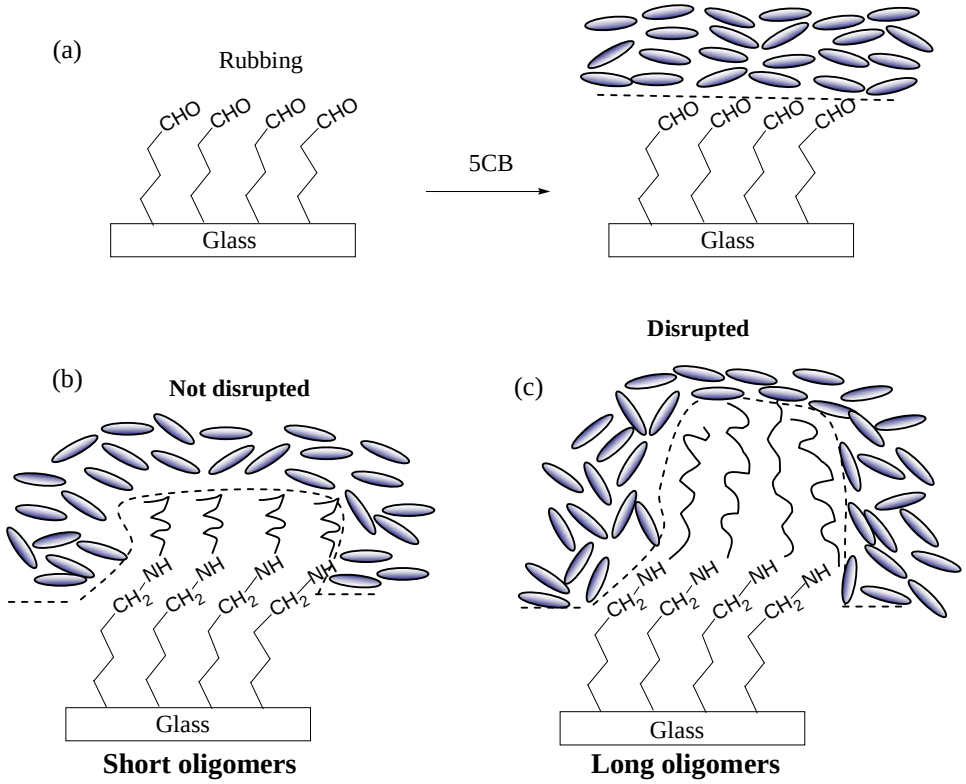

Figure 8.1 Schematic illustrations of (a) uniform orientations of LCs supported on the rubbed surface decorated with TEA; (b) orientations of 5CB supported on a TEA-decorated surface with immobilized short glycine oligomers were not disrupted, and (c) orientations of 5CB supported on the TEA-decorated surface with immobilized long glycine oligomers were disrupted.

In this study, we designed a simpler and more cost-effective system to detect a number of glycine oligomers by using LCs. First, we used glass slides as the solid substrates to replace the expensive gold films. Glass slides can be modified with organic silane linkers, such as commercially available TEA, to introduce aldehyde functional groups for the immobilization of glycine oligomers. Then, the aldehyde-decorated surfaces are rubbed (Figure 8.1a), and induces uniform

orientations of LCs supported on the surfaces (Kim et al., 2001). Finally, we coupled the naturally-occurring amino groups of glycine oligomers directly to the aldehyde-decorated surfaces, without using any linker groups. As shown in Figure 8.1b and 8.1c, we hypothesized that the orientations of 5CB were disturbed when the surface thickness exceeded a critical value, while the orientations of 5CB remained unchanged if the surface thickness was lower than that critical value. If the orientations of LCs are disrupted, the planar orientation of 5CB supported on glycine oligomers modified regions can be readily distinguished from 5CB supported on TEA-decorated surfaces under crossed polarizers.

8.2 Experimental Section

Materials

The glass slides were from Marienfeld (Germany). Sodium cyanoborohydride, sodium carbonate, ammonium carbonate, *N*,*N*-dimethyl-n-octadecyl-3-aminopropyl-trimethoxysilyl chloride (DMOAP), glycine oligomers including glycyl-glycine (diglycine), glycyl-glycyl-glycine (triglycine), glycyl-glycyl-glycyl-glycine (tetraglycine), and glycyl-glycyl-glycyl-glycyl-glycine (pentaglycine) were purchased from Sigma Aldrich (Singapore). LC 4-cyano-4'-pentylbiphenyl (5CB) was purchased from Merck (Singapore).

Preparation of substrates and surface modification

The substrates preparation follows the same procedure as mentioned in **Chapter 3**. Subsequently, cleaned substrates are modified with TEA (See **Chapter 4**). The TEA-decorated slides were then rubbed with a velvet-type cloth and washed with copious amounts of deionized water to remove any contaminants introduced by rubbing. The slides were then blown dried using purified nitrogen and heated at 100°C overnight to promote the crosslinking of silanol groups to form siloxane networks. Next, we mixed two 0.5 M $(NH_4)_2CO_3$ solutions together, one containing glycine oligomers, and the other containing 20 mM of $NaBH_3CN$, in a 1:1 volumetric ratio. Subsequently, we dispensed droplets (~ 2 μL) of the mixed solution onto a TEA-decorated glass slide. After reaction in a sealed chamber at 50°C for 2 h, the modified slides were washed thoroughly with copious amounts of methanol and then sonicated in methanol for 2 min. The slides were then dried under purified nitrogen and heated at 100°C for 1 h.

Preparation of DMOAP-coated glass slides

The cleaned glass slides were immersed into an aqueous solution containing 0.1% (w/v) of DMOAP for 5 min, and then rinsed with copious amounts of deionized water. The DMOAP-coated glass slides were dried under a stream of nitrogen and then heated in a 100°C oven for at least 3 h to allow the crosslinking of DMOAP. The DMOAP-coated glass slides were tested for homeotropic alignment by observing the orientations of 5CB sandwiched between two DMOAP slides. Any slide that did not

induce homeotropic alignment of 5CB was discarded.

Fabrication of LC cells

A hybrid LC cell was made by sandwiching two glass slides with two strips of thin Mylar polyester spacer (~ 6 μm) and two binder clips. The top surface was modified with DMOAP, because 5CB supported on the DMOAP-modified surface assumes a homeotropic orientation (perpendicular to the surface) (Frederic, 1973). The bottom surface was patterned with regions of glycine oligomers on a TEA-decorated glass slide. After the LC cell was made, approximately 3 μL of 5CB was drawn into the cavity formed between the two glass slides by using capillary force. The optical appearance of the sample was observed by using a polarizing optical microscope (Nikon ECLIPSE LV100POL, Tokyo, Japan) in the transmission mode. Each image was captured by a digital camera (Nikon DIGITAL SIGHT DS-U1, Tokyo, Japan) mounted on the microscope with an exposure time of 8 msec.

Ellipsometric thickness

The measurements of ellipsometric thickness follow the same procedure as mentioned in **Chapter 3**.

8.3 Results and Discussion

A fundamental hypothesis in this study is that the thicknesses of the monolayers formed from glycine oligomers are directly proportional to the molecular lengths of these molecules. Therefore, it is important to ensure that a high-quality and

well-ordered monolayer is formed during the immobilization procedure. We have listed a number of factors including buffer solution, concentration of the reducing agent, temperature, and reaction time which may influence the immobilization reaction.

The effect of buffer solution

Our previous experiments have shown that glycine oligomers were effectively immobilized on the aldehyde-decorated surface in Na_2CO_3 buffer (Bi et al., 2007). However, Na_2CO_3 buffer also contaminated the surface for subsequent LC experiments, unless the surface was washed for more than 30 times with deionized water. For this reason, we chose $(NH_4)_2CO_3$ as the reaction buffer in this paper because it has similar properties as Na_2CO_3, but it decomposes at a high temperature and releases gaseous products, which do not contaminate the surface. Figure 8.2a and 8.2b show the optical images of nematic LC 5CB supported on the TEA-decorated surfaces treated with 0.5 M of Na_2CO_3 and 0.5 M of $(NH_4)_2CO_3$, respectively. It was found that the Na_2CO_3 buffer contaminated the surface after washing five times with deionized water, while the orientations of 5CB supported on the TEA-decorated surface were not disrupted by the $(NH_4)_2CO_3$ buffer.

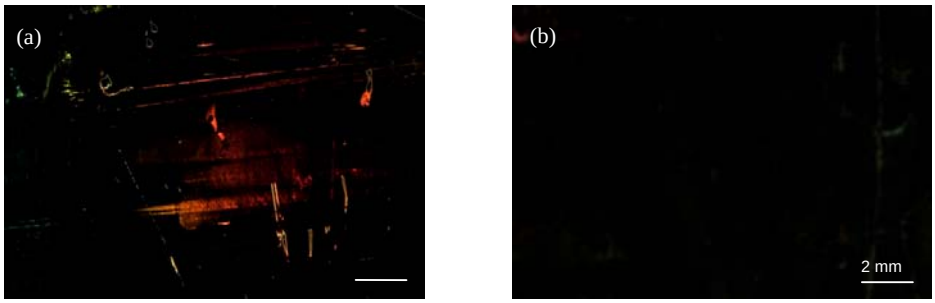

Figure 8.2 Optical textures (crossed polars) of 5CB sandwiched between a DMOAP-coated glass slide (on top) and a TEA-decorated glass slide (at bottom) patterned with a region of (a) 0.5 M of Na_2CO_3, (b) 0.5 M of $(NH_4)_2CO_3$, Each surface was washed five times with deionized water. The results show that Na_2CO_3 buffer may contaminate the surface even after washing five times with deionized water. We have increased the contrast of each of the figure simultaneously.

To compare the differences of these two buffers for the immobilization of glycine oligomers, we performed the immobilization in either 0.5 M of $(NH_4)_2CO_3$ or Na_2CO_3 buffer containing 1 mM of glycine oligomers and 10 mM of $NaBH_3CN$ at 50°C for 2 h. Then, the thicknesses of the surface organic layers before and after the immobilization were measured by using ellipsometry. Figure 8.3 shows the increase of ellipsometric thicknesses after immobilization of glycine oligomers on the TEA-decorated silicon wafers using either Na_2CO_3 or $(NH_4)_2CO_3$ buffers. It can be seen in Figure 8.3 that immobilization performed in both buffers gave similar increase of thicknesses. By comparing the results with theoretical molecular lengths of glycine oligomers (i.e. glycine: 0.46 nm, diglycine: 0.66 nm, triglycine: 0.92 nm, tetraglycine: 1.01 nm and pentaglycine: 1.22 nm[*], we concluded that glycine oligomers nearly formed monolayers on the surfaces in both buffer solutions.

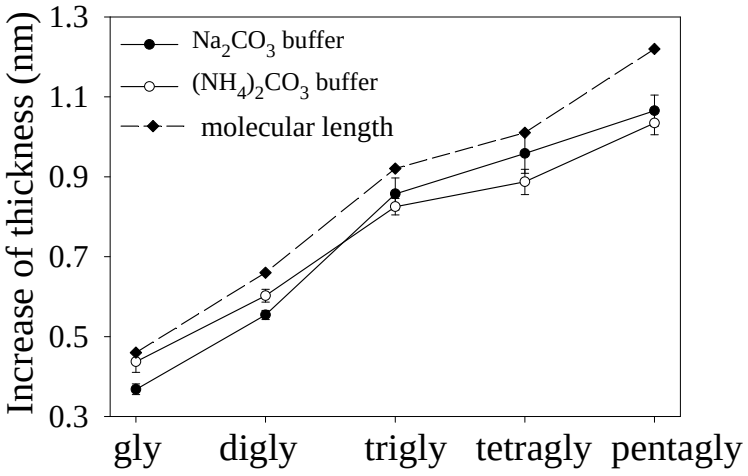

Figure 8.3 Increase of ellipsometric thicknesses of thin organic layers after silicon wafers decorated with TEA incubated in two different buffers, Na_2CO_3 and $(NH_4)_2CO_3$ buffer, both containing 1 mM of glycine oligomers and 10 mM of reducing agent. Theoretical molecular lengths of these oligomers are also shown for comparison (dashed line). We assume monolayers of glycine oligomers are formed when thicknesses of the surface organic layers are equal to their theoretical molecular lengths.

The effect of reducing agent concentration

Our next goal is to investigate the effect of the reducing agent on the immobilization reaction. It is known that the Schiff base formed from the coupling of aldehyde with amine readily undergoes hydrolysis and results in a free amine and an aldehyde group. To address this instability issue, a reducing agent, such as $NaBH_3CN$ is required to [i]reduce the Schiff base and form a stable secondary amine linkage (Peelen et al., 2005). In this experiment, different concentrations of $NaBH_3CN$ (0 mM, 10 mM, and 100 mM) were used when glycine oligomers were immobilized on the TEA-decorated surfaces at 50°C for 2 h. Figure 8.4a shows the ellipsometric thicknesses of the surface organic layers after the immobilization reaction. Inspection of Figure 8.4a reveals that the immobilization of glycine oligomers without $NaBH_3CN$ led to the

smallest surface thickness, suggesting the presence of $NaBH_3CN$ is critical for the

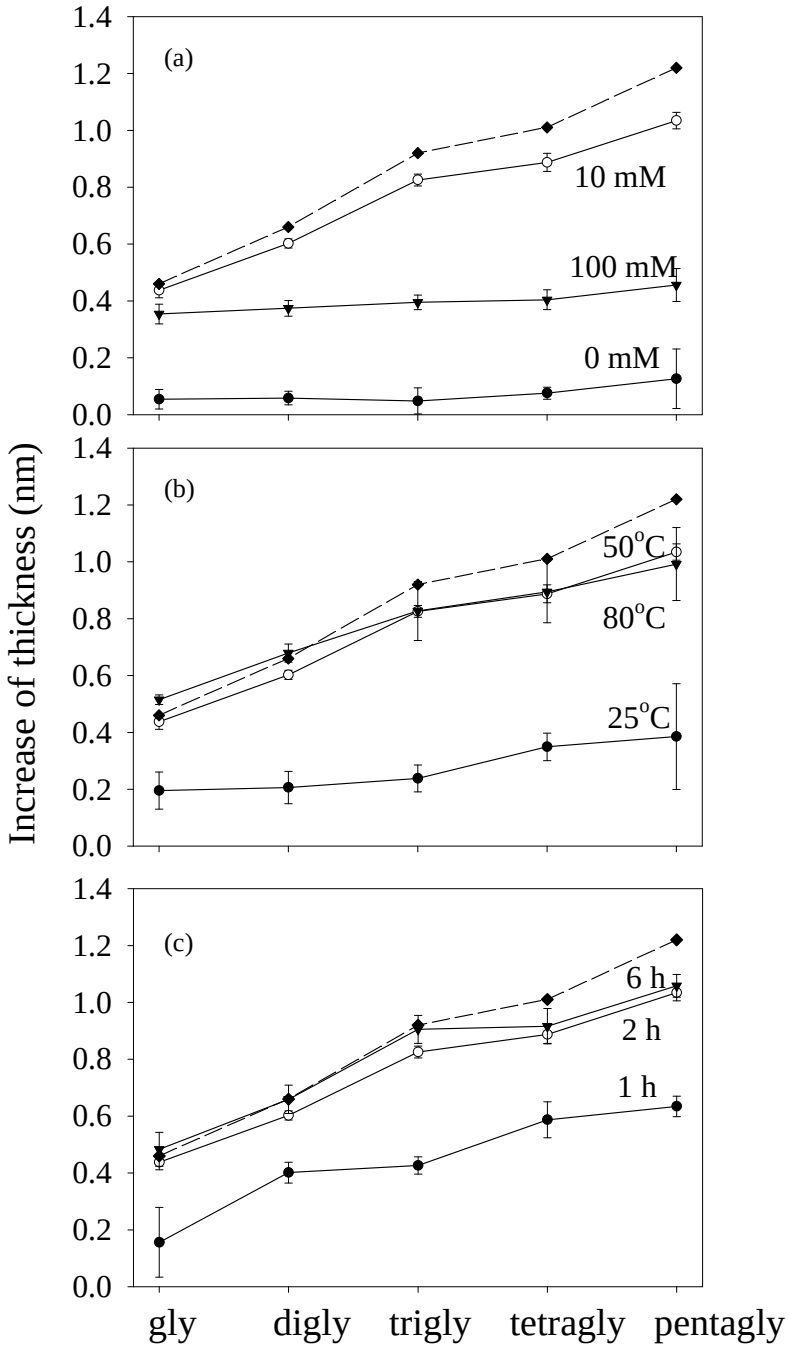

Figure 8.4 Increase of ellipsometric thicknesses of thin organic layers after silicon wafers decorated with TEA incubated in 0.5 M of $(NH_4)_2CO_3$ buffer containing 1 mM of glycine oligomers. (a) Effect of the $NaBH_3CN$ concentration; (b) effect of the immobilization temperature; (c) effect of the reaction time. The dashed lines are the theoretical molecular lengths.

immobilization of glycine oligomers on the aldehyde-decorated surfaces. When the concentration of $NaBH_3CN$ was increased to 10 mM, the surface thicknesses were nearly equivalent to the calculated molecular lengths of glycine oligomers, suggesting monolayers were formed on the aldehyde-decorated surface. However, further increase the concentration of $NaBH_3CN$ to 100 mM resulted in smaller surface thicknesses compared to the ones obtained with 10 mM of $NaBH_3CN$. This is probably because the high concentration of $NaBH_3CN$ reduced the aldehyde groups on the surfaces, and prevented the subsequent reaction with glycine oligomers. Hence, we standardized following experiments with 10 mM of $NaBH_3CN$.

The effect of immobilization temperature

Temperature is expected to be an important factor for the immobilization of glycine oligomers. Higher temperature presumably results in higher reaction rates and faster diffusion of glycine oligomers toward the surface aldehyde groups. To evaluate the effect of temperature, we immobilized glycine oligomers in the presence of 10 mM $NaBH_3CN$ for 2 h at 25°C, 50°C, and 80°C, respectively. Figure 8.4b shows the increase in thicknesses of the surface organic layers after immobilization of glycine oligomers at three different temperatures. Based on the results, it is concluded that a better coupling efficiency can be obtained when a higher temperature is used. However, the most dramatic increase in thickness was achieved when the temperature was increased from 25°C to 50°C. In contrast, there were little changes when the temperature was further increased to 80°C. This is probably because the surface was

already saturated with monolayers of glycine oligomers when 50°C was used. Because higher temperature at 80°C may lead to the hydrolysis of TEA, we fixed the reaction temperature at 50°C for the following experiments.

The effect of reaction time

We also investigated how much reaction time it takes to form a complete monolayer on the surface. In this experiment, we immobilized glycine oligomers on the aldehyde-decorated surface in 10 mM of $NaBH_3CN$ at 50°C for 1 h, 2 h, and 6 h respectively. As shown in Figure 8.4c, the ellipsometric thicknesses of the surface organic layers increased with the reaction time. It can be seen, however, that the effect of reaction time on the ellipsometric thicknesses was marginal when the reaction time was increased from 2 h to 6 h. Hence, we hypothesized that the formation of monolayers was almost complete after 2 h. Although long reaction time can be used to ensure the completeness of the reaction, especially when the concentration of glycine oligomers is low, long reaction time may also lead to the evaporation of small droplets from surfaces. All of the above results indicated that an optimized immobilization of glycine oligomers on the TEA-decorated surfaces can be carried out in a 0.5-M $(NH_4)_2CO_3$ buffer mixed with 10 mM $NaBH_3CN$ at 50°C for 2 h. The subsequent experiments followed these conditions.

Simultaneous detection of multiple glycine oligomers by using LC

Next, we used the optimized experimental conditions (50°C, 2 h, 10 mM of $NaBH_3CN$) to pattern an aldehyde-decorated surface with one blank control and five

glycine oligomers. Subsequently, we fabricated a LC cell with a DMOAP-coated glass slide and the TEA-decorated glass slide patterned with glycine oligomers. As shown in Figure 8.6, it was found that the optical appearances of 5CB supported on the region of blank control remained unchanged, suggesting that the buffer and reducing agent at 10 mM did not influence the orientations of 5CB supported on the TEA-decorated surface. In contrast, 5CB supported on the glycine oligomers modified regions exhibited very distinct birefringence. These results suggest that we can use LC to detect the glycine oligomers on the same surface simultaneously if glycine oligomers formed monolayers on surfaces.

Sensitivity of the detection method

To test the sensitivity of the LC based detection method, we lowered the concentration of glycine oligomers to 100 μM and repeated the same immobilization procedure. The changes in ellipsometric thicknesses of the surface organic layers on the TEA-decorated surface after the immobilization of glycine oligomers are shown in Figure 8.5. The contribution of glycine oligomers to the total ellipsometric thickness was found to be 0.19 nm (glycine), 0.49 nm (diglycine), 0.74 nm (triglycine), 0.87 nm (tetraglycine), and 0.95 nm (pentaglycine) respectively, which are lower than the thicknesses of the surface layers when 1 mM of these glycine oligomers were used.

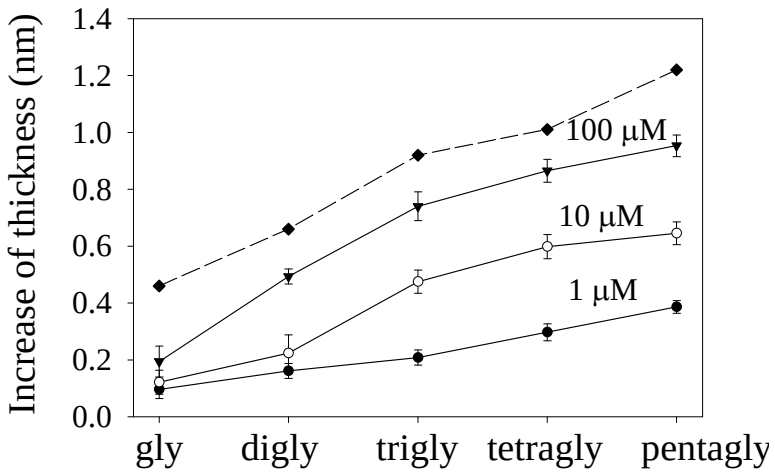

Figure 8.5 Increase of ellipsometric thicknesses of thin organic layers after silicon wafers decorated with TEA incubated in the $(NH_4)_2CO_3$ buffer containing glycine oligomers with various concentrations ranged from 1 μM to 100 μM. The reaction was carried out in a 0.5-M $(NH_4)_2CO_3$ buffer mixed with 10 mM of $NaBH_3CN$ at 50°C for 2 h. The dashed lines are the theoretical molecular lengths.

It was also found that glycine oligomers did not form monolayers on the surfaces if the concentration was 100 μM or below. The optical appearance of a 5CB cell constructed with a 100 μM glycine oligomers-modified surface is shown in Figure 8.6. It shows that the orientations of 5CB supported on tetraglycine and pentaglycine modified regions were significantly disrupted and gave very distinct optical appearance under crossed polarizers. Furthermore, the orientations of 5CB supported on diglycine- and triglycine-modified regions appeared to be less disrupted and gave less birefringence. However, the orientations of 5CB supported on glycine-modified region were unchanged. These observations demonstrated that the surface thicknesses of glycine oligomers influenced the orientations of LCs. The greater the surface thickness, the more LCs changed their orientations.

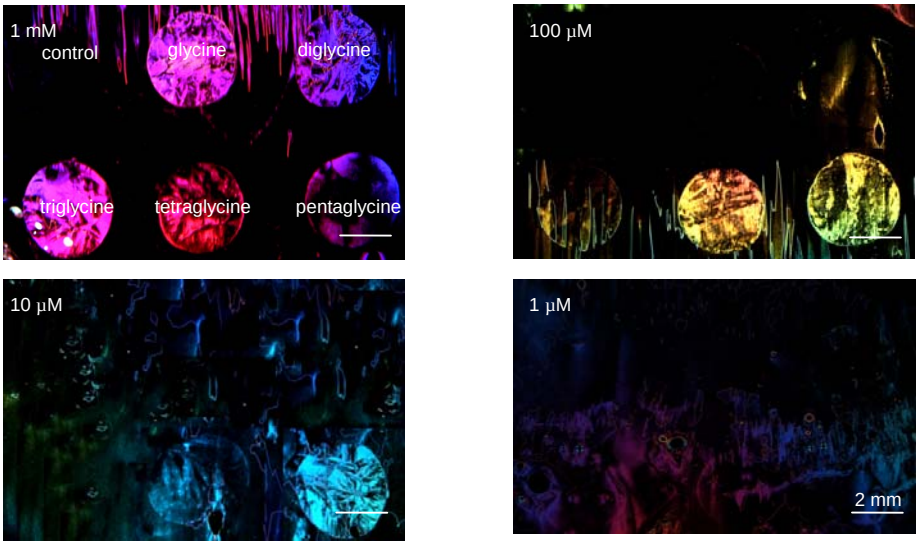

Figure 8.6 Optical textures (crossed polars) of 5CB sandwiched between a DMOAP-coated glass slide (on top) and a TEA-decorated glass slide (at bottom) patterned with regions of glycine oligomers having concentrations of 1 mM, 100 μM, 10 μM, and 1 μM respectively. The immobilization temperature was 50°C, the reaction time was 2 h, and the $NaBH_3CN$ concentration was 10 mM. The positions of immobilized glycine oligomers on all other images are the same as the first one. We have increased the contrast of each of the figure simultaneously.

As shown in Figure 8.5, when the concentrations of glycine oligomers were further reduced to 10 μM, the contribution of glycine oligomers to the total ellipsometric thickness was 0.12 nm for glycine, 0.22 nm for diglycine, 0.48 nm for triglycine, 0.60 nm for tetraglycine, and 0.65 nm for pentaglycine. All of them were less than those formed from 100 μM of glycine oligomers. Inspection of the optical images of a 5CB cell constructed with 10 μM glycine oligomers-modified surface in Figure 8.6 reveals that the orientations of 5CB supported on triglycine, tetraglycine, and pentaglycine modified regions was disrupted. Among them, 5CB supported on pentaglycine modified region appeared the most disrupted and exhibited high level of birefringence. In contrast, the orientations of 5CB supported on glycine and diglycine modified regions remained uniform.

Finally, we further reduced the concentration of glycine oligomers to 1 μM. As shown in Figure 8.5 and 8.6, the increase of thickness for the longest pentaglycine was only 0.39 nm, and the orientations of 5CB supported on all of glycine oligomers modified regions remained unchanged.

The above observations demonstrated that the longer the glycine oligomers, or the higher densities of glycine oligomers immobilized on the surface, the more easily the orientations of 5CB supported on the surface were disrupted. By comparing the ellipsometric thicknesses in Figure 8.5 and the optical appearances of 5CB in Figure 8.6, we concluded that the orientations of 5CB supported on glycine oligomers modified regions were disrupted when the increase of thickness was above 0.5 ± 0.1 nm. The sensitivity of the LC based detection method was 1 mM for glycine, 100 μM for diglycine, and 10 μM for triglycine, tetraglycine and pentaglycine.

8.4 Conclusions

We have demonstrated a surface-based method for simultaneous detection of multiple glycine oligomers by using LCs. Depending on their molecular lengths, the immobilized glycine oligomers on the aldehyde-decorated surfaces contribute to different increases of thicknesses when they form monolayers under an optimal condition, i.e. 50°C, 2 h and with the presence of 10 mM of $NaBH_3CN$. It was found that the orientations of 5CB supported on glycine oligomers modified regions were disrupted if the increase of thickness was above 0.5 ± 0.1 nm. The LC based sensor is simple and can be used to detect glycine oligomers with micromolar concentrations

by immobilizing them on the same surface. The detection limit was found to be 1 mM for glycine, 100 μM for diglycine, and 10 μM for triglycine, tetraglycine and pentaglycine under the proposed experimental conditions.

*http://davapc1.bioch.dundee.ac.uk/ programs/prodrg/

CHAPTER 9
LIQUID CRYSTAL MULTIPLEXED PROTEASE ASSAYS

9.1 Introduction

Proteases are enzymes which can cleave peptide bonds in polypeptides or proteins. They are essential for many important biological processes, such as digestion, blood clotting, and apoptosis (Salisbury et al., 2002; Neff et al., 2007; Leung et al., 2000). Dysfunction of proteases can lead to several well-known diseases including cancers (Beckett et al., 1996; Johnson et al., 1998; Yan et al., 1998), viral infections (e.g. HIV) (Wlodawer et al., 1993; West et al., 1995), and neurodegenerative disorders (e.g. Alzheimer's disease) (Vassar et al., 1999), making them important therapeutic targets. Traditionally, proteases activities are determined by using radioactive or fluorogenic methods. For example, fluorescein isothiocyanate (FITC)-labeled casein was added to a solution containing proteases. Then, enzymatic activities of the proteases were quantified by the increase in the fluorescence. It was demonstrated that this assay can be used to detect approximately 5 ng of trypsin in a 10-μL solution. More examples of traditional proteases assays can be found in the literatures (Twining et al., 1984; Spencer et al., 1973; Schickaneder et al., 1988).

Recently, more and more array-based protease assays have been developed because of their high-throughput nature (Houseman et al., 2002a, b; Schutkowski et al., 2004; Duan et al., 1994; Gan et al., 1999). Unlike traditional protease assays, immobilized

oligopeptides on solid surfaces were used as protease substrates because oligopeptides with well-defined sequences and lengths can be custom-made by using solid-phase synthesis. When these immobilized oligopeptides are exposed to a solution containing proteases, they are recognized and cleaved by proteases, leading to a decrease in the oligopeptide length. Thereafter, surface-sensitive analytical techniques such as phosphorimaging (Houseman et al., 2002), SPR (Markgren et al., 1998; Rich et al., 2000), fluorescence (Salisbury et al., 2002), or MALDI-TOF mass spectrometry (Lequart et al., 1999; Karlsson et al., 2000), are employed to transduce minute changes in surface properties into measurable signals. However, these methods either require labels or complicated instrumentations. Therefore, a convenient and label-free method that is able to report the proteases activities is highly desirable.

As mentioned in **Chapter 8**, LCs have been used to amplify and transduce chemical and biological binding events on surfaces into optical signals (Brake et al., 2003; Park et al., 2006; Tingey et al., 2004; Jang et al., 2006; Luk et al., 2004 Hoogboom et al., 2006; Kim et al., 2005). The LC-based detection principle is viable because the anchoring energy of LCs is so small that an anchoring state of LCs can be easily disrupted by subtle changes on a solid surface. Another advantage of using LCs as imaging materials is that the signal output is in the form of optical signals which are clearly visible with the naked eye. Recently, on the basis of the unique properties of LCs mentioned above, Abbott and coworkers designed a LC-based sensor to report the protease activity of trypsin acting on an oligopeptide substrate (SNKTRIDEANNKATKML), which was covalently immobilized at an aqueous/LC

interface (Park et al., 2006 and 2008). It was found that when the oligopeptide was cleaved by trypsin, the optical textures of the LC underneath changed from bright to dark. Despite the promise of this method, three major challenges remained. First, oligopeptides were immobilized at the aqueous/LC interface by reacting oligopeptides with carboxylic acid-terminated lipids self-assembled at aqueous/LC interfaces. Therefore, the reaction is not site-specific, and that can lead to multiple anchoring points at lysine residues and N-terminal amine of the oligopeptides. Second, the exact mechanism that leads to the disruption of LCs was not fully understood. As reported by the authors, cleavage of some well-known trypsin substrates, such as poly-lysine, did not cause any response in the LCs. Third, this sensor was built upon aqueous/LC interfaces rather than on traditional solid surfaces, which precluded the use of microarray techniques for preparing a high density array with hundreds or thousands of oligopeptide probes.

In this study, we report a LC-based protease assay which can potentially overcome the limitations mentioned above. First, we labeled oligopeptides with an N-terminal cysteine, which can react with aldehyde irreversibly and form thiazolidine. This reaction also proceeds much faster than the one between lysine and aldehydes. Thus, it is possible to immobilize an oligopeptide on an aldehyde-terminated surface with a single anchoring point at the N-terminal cysteine (see **Chapter 7**). Second, the assay was built on a solid substrate in a microarray format. This configuration allows us to immobilize multiple oligopeptides (or the same oligopeptide with different surface densities) on the same surface for probing protease activities simultaneously.

Depending on the oligopeptide sequences, very rich information, such as surface densities of oligopeptides, the protease concentration and incubation time, can therefore be obtained from these microarrays. Third, we combined the unique optical properties of LCs and the microarray techniques to create a multiplexed protease assay. In this assay, we used the orientational transitions of LCs to report the enzymatic activities. The results in **Chapter 8** showed that orientations of LCs supported on glycine oligomers- modified surface were disrupted if the ellipsometric thickness exceeded 5 ± 1 Å. This phenomenon suggests that the orientations of LCs are very sensitive to the length of immobilized oligopeptides and that forms the basis of using LCs for detecting proteases if they can cleave immobilized oligopeptides and decrease their lengths.

9.2 Experimental Section

Materials

Trypsin (from bovine pancreas), α-chymotrypsin (from bovine pancreas, type II), and fluorescein isothiocyanate isomer I (FITC) were purchased from Sigma Aldrich (Singapore). Phosphate buffer saline (PBS) and sodium dodecyl sulfate (SDS) were purchased from 1st Base (Singapore). Oligopeptides including CDRVYIHPFHLK (**P1**), CDRVYIHPFHL (**P2**), CDHVYIHPFHLK (**P3**), CSNKTRIDEANNKATKML (**P4**), CWHWQRPLMPVSI (**P5**), and CDYKDDDDK (**P6**) (with a purity of > 90%) were synthesized by Research Biolabs and Sigma Aldrich (Singapore).

Surface modifications

Glass slides (Sailboat, China) were cleaned following the procedure in **Chapter 8**. Subsequently, the cleaned glass slides were immersed in an aqueous solution containing 0.1% (v/v) of DMOAP for 1 min, and rinsed with copious amounts of deionized water. The DMOAP-coated glass slides were dried under a stream of nitrogen and then heated in a 100°C vacuum oven for 15 min to allow the crosslinking of silanol groups. To introduce aldehyde functional groups to the surface, we immersed the glass slides into a methanolic solution containing 2% (v/v) of TEA for 2 h. After this, the glass slides were rinsed with copious amounts of methanol to remove residual TEA. Finally, they were dried under a stream of purified nitrogen and then heated in a 100°C vacuum oven for 15 min.

Fabrication of oligopeptide microarrays

First, different concentrations of oligopeptides solutions were prepared in PBS buffer (0.1 M, pH = 7.0) containing 0.001 % (w/v) SDS. To prepare an oligopeptide microarray, oligopeptide solutions were dispensed onto an aldehyde-terminated surface by using a spotting robot (Biodot, U.S.A.). There were two types of oligopeptide microarrays used in this study; both of them had 6 rows, each row had 30 spots and each spot had a volume of 100 nL. The first type of microarray had six different concentrations of **P1** in each row and the second type had immobilized oligopeptide **P1**-**P6 (**40 μM) in each row. The sequences of oligopeptides and their enzymatic cleavage sites by trypsin and chymotrypsin, respectively, are shown in

Table 9.1. After oligopeptide solutions were dispensed, these microarrays were incubated in a humid chamber for 12 h, allowing the covalent immobilization of oligopeptides on the surfaces. In the final step, all microarrays were washed thoroughly with PBS buffer to remove unreacted oligopeptides, and dried under a stream of purified nitrogen.

Trypsin microarrays

To prepare a trypsin microarray, different concentrations of trypsin solutions were dispensed onto an aldehyde-terminated surface by using the spotting robot. After this, the microarray was incubated in a humid chamber for 3 h and then washed thoroughly with deionized water and dried under a stream of purified nitrogen.

Table 9.1 Sequences of **P1** ~ **P6** and their cleavage sites for trypsin and chymotrypsin, respectively.[a]

Symbol	Sequence and cleavage site for trypsin ⬇ and chymotrypsin ⇩
P1	Cys-Asp-Arg⬇-Val-Tyr⇩-Ile-His-Pro-Phe⇩-His-Leu-Lys
P2	Cys-Asp-Arg⬇-Val-Tyr⇩-Ile-His-Pro-Phe⇩-His-Leu
P3	Cys-Asp-His-Val-Tyr⇩-Ile-His-Pro-Phe⇩-His-Leu-Lys
P4	Cys-Ser-Asn-Lys⬇-Thr-Arg⬇-Ile-Asp-Glu-Ala-Asn-Asn-Lys⬇-Ala-Thr-Lys⬇-Met⇩-Leu
P5	Cys-Trp⇩-His-Trp⇩-Gln-Arg-Pro-Leu⇩-Met⇩-Pro-Val-Ser-Ile
P6	Cys-Asp-Tyr⇩-Lys⬇-Asp-Asp-Asp-Asp-Lys

[a] Trypsin hydrolyzes a peptide with arginine (Arg) or lysine (Lys) residue in its sequence unless they are followed by proline (Pro). Chymotrypsin hydrolyzes a peptide with tryptophan (Trp), tyrosine (Tyr), phenylalanine (Phe), leucine (Leu), or methionine (Met) residue (Voet et al., 1999; Barrett et al., 2004; Graf et al., 1988; Banerjee et al., 2008).

Characterization of oligopeptide density with fluorescence

The oligopeptide microarray supported on a glass slide was incubated in 10 μg/mL of FITC in PBS buffer for 2 h. After this, the glass slide was washed with 1% SDS in PBS buffer. Fluorescence images of the microarray were then taken with GenePix (4100A) microarray scanner manufactured by Molecular Devices (U.S.A.). Same parameters (PMT gain = 600, pixel size = 10 μm) were used for all images and analysis. The fluorescence profiles were analyzed with Image J.

Cleavage of immobilized oligopeptides

To cleave immobilized oligopeptides with protease, we immersed the oligopeptide microarray in a protease solution by using two different experimental set-ups. In the mode of gradient immersion time, an oligopeptide microarray was mounted vertically inside a small vial (2.62 cm in diameter). Then, trypsin buffer (50 mM Tris-HCl, 20 mM $CaCl_2$, pH = 8.0) with 3 mg/mL of trypsin was delivered to the vial at a flow rate of 70 μL/min for 10 h by using a peristaltic pump. The temperature of the solution was maintained at 37˚C by using a hotplate (Figure 9.1). Under this experimental condition, it took 7.7 min for the trypsin solution level to increase by 1 mm. In the mode of constant immersion time, an oligopeptide microarray was immersed in trypsin or chymotrypsin solutions at 37˚C for 3 h. After the immersion, the oligopeptide was withdrawn from the solution, washed thoroughly with deionized water and dried under a stream of purified nitrogen.

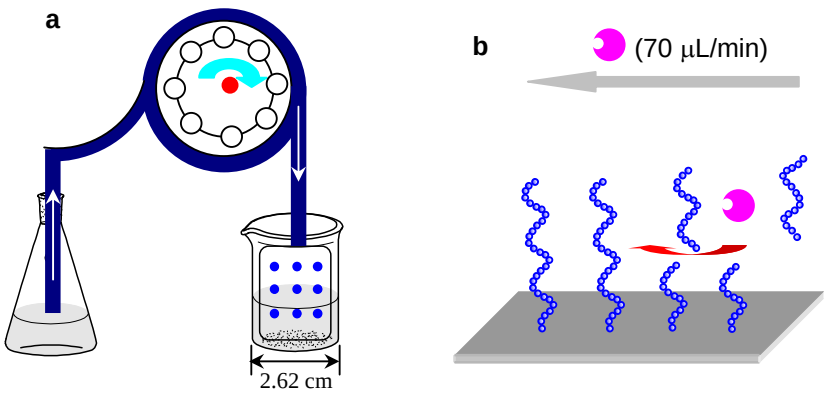

Figure 9.1 (a) Experimental set-up for the gradient immersion time mode (delivery of trypsin solution to **P1** microarray by using the peristaltic pump). (b) Schematic illustrations of the trypsin cleavage on the oligopeptide substrates.

Fabrication of LC cells

The fabrication of LC cells and the observation of optical images of LC follow those mentioned in **Chapter 8**.

9.3 Results and Discussion

Preparation oligopeptide microarrays

Our first goal was to build an oligopeptide microarray with well-orientated, covalently immobilized oligopeptides. The strategy we adopted was to label an oligopeptide **P1** with an N-terminal cysteine. The N-terminal cysteine can react with an aldehyde-decorated surface and formed a thiazolidine ring (in the absence of reducing agents), and prevent lysines from reacting with aldehydes. Figure 9.2a shows the green fluorescence image of the **P1** microarray after it was immersed in FITC solution (as a free amine marker). The green fluorescence in Figure 9.2a confirms the presence

of free lysine groups on the surface and suggests that an oligopeptide with an N-terminal cysteine label can be immobilized on an aldehyde-terminated surface through a single anchoring point at the N-terminal cysteine label. In contrast, when solutions of **P1** were applied to a surface without aldehyde groups, no fluorescence was observed (Figure 9.2b). This observation further confirms that the N-terminal cysteine-label oligopeptide reacted with the surface aldehyde groups. The crosslinking of the N-terminal cysteine label to the surface aldehyde groups was also found in Figure 9.3.

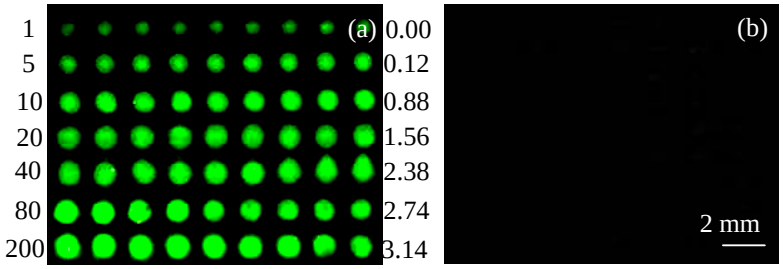

Figure 9.2 Fluorescence images of **P1** microarrays after they were immersed in 10 μg/mL of FITC (as a free lysine marker) for 2 h. These microarrays were built on (a) an aldehyde-terminated surface and (b) a DMOAP-coated surface. Numbers on the left indicate concentrations (μM) of **P1** solution dispensed on the surface; numbers on the right were estimated surface densities of **P1** ($\times 10^{10}$/mm^2) based on a fluorescence intensity calibration curve.

Figure 9.3a shows that the FTIR spectrum exhibits several peaks after the immobilization of **P1** on the aldehyde-terminated surface. Among them, the peak at 3285 cm^{-1} can be assigned to the stretching mode of primary amine (Chiang et al., 1980), suggesting that **P1** was immobilized on the aldehyde-terminated surface. Moreover, the primary amine in lysine residue was free after the immobilization. On the other hand, we also performed the immobilization reaction on DMOAP-coated

silicon trough plate; no new peaks were observed (Figure 9.3b).

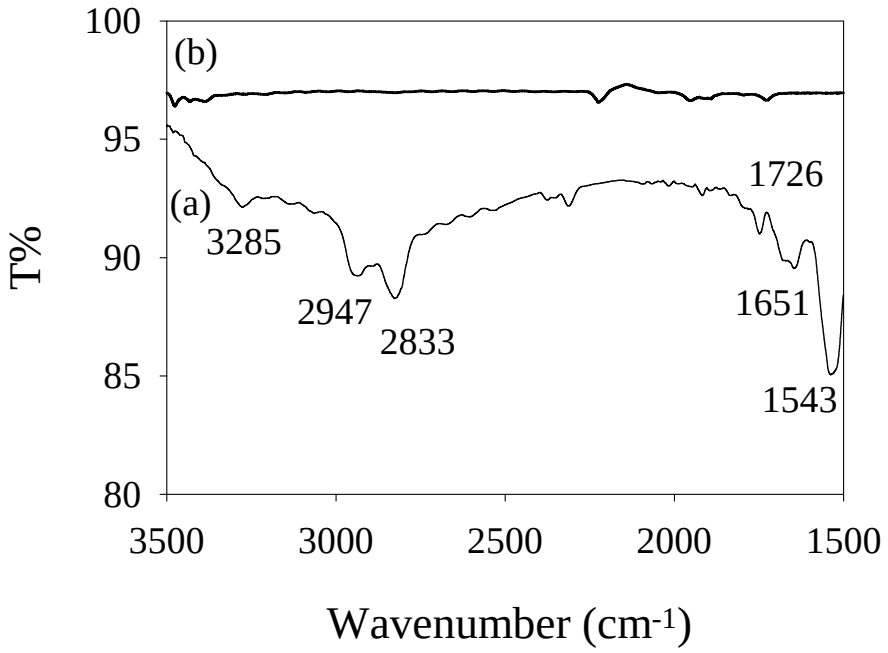

Figure 9.3 HATR-FTIR spectra of silicon trough plates after they were modified with (a) DMOAP for 1 min and then 2% TEA for 2 h and (b) DMOAP for 1 min and then incubated in 50 μM **P1** for 12 h. The aldehyde-terminated and DMOAP-coated silicon trough plates were used as references for (a) and (b), respectively.

Optical textures of LCs supported on oligopeptide microarrays

Figure 9.4a shows an optical image of a LC made from a DMOAP-coated slide and a **P1** microarray, whose pattern is similar to the one shown in Figure 9.2. Unlike the continuous fluorescence profile in Figure 9.2a, the optical image of LC shows a very clear cut-off point when the oligopeptide concentration is below 10 μM, (i.e., when the **P1** concentration is equal to or above 10 μM, 5CB appears bright, but when the **P1** concentration is below 10 μM, 5CB appears dark.) The different optical textures of 5CB can be attributed to different orientations of 5CB supported on the surface. When

the orientations of 5CB are disrupted by the surface immobilized **P1** as shown in Figure 9.4c, they can give strong birefringence under crossed polarizers. In contrast, when orientations of 5CB are not disrupted by **P1** as shown in Figure 9.4d, 5CB gives no birefringence under crossed polarizers. The results in Figure 9.4 suggest that whether 5CB appears bright or dark is determined by the surface density of **P1.** More specifically, we can estimate that when the surface density **P1** exceeds a critical value, $0.88 \times 10^{10}/mm^2$, the surface immobilized **P1** is able to disrupt 5CB. The sharp orientational transition of 5CB at the critical surface density of **P1** can be developed as a mechanism to detect protease, because proteases activities may cause the surface density of **P1** fall below the critical value after the cleavage of **P1**.

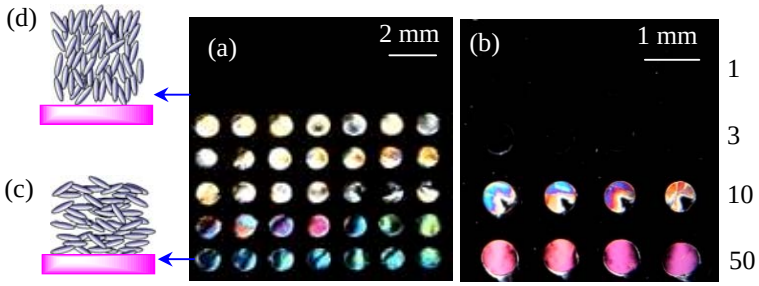

Figure 9.4 Optical textures (under crossed polars) of 5CB sandwiched between two DMOAP-coated glass slides. One of the DMOAP-coated glass slide was also functionalized with TEA and decorated with (a) a **P1** microarray. Concentrations of **P1** are the same as those in Figure 9.2, and (b) trypsin microarray Concentrations of trypsin (μg/mL) are indicated on the right. Schematics on the left are the proposed orientations of 5CB in the (c) bright region and (d) dark region.

Interactions between LCs and proteases

Before developing a LC-based protease assay, we also need to understand the interactions between LC and proteases. Herein, we selected trypsin as a model

protease since it was also used in several past studies. To determine whether trypsin can adsorb on the surface and influence the orientations of LC, we prepared a trypsin microarray on an aldehyde-terminated surface and used it to make a LC cell. As shown in Figure 9.4b, if the concentration of trypsin was higher than 10 μg/mL, the optical texture of 5CB appears bright, suggesting that the orientation of 5CB can be disrupted by trypsin adsorbed on the surface if the initial trypsin concentration is too high. In contrast, 5CB remained dark if trypsin concentration was lower than 3 μg/mL. Therefore, we conclude that to eliminate the influence of trypsin on the orientations of LCs, the maximum concentration of trypsin that can be used in the LC protease assay is 3 μg/mL. If the trypsin concentration is more than 10 μg/mL, it may adsorb on the surface and influence the orientations of LC. In some real applications where the trypsin concentration is too high, it is necessary to dilute it before use.

Cleavage of oligopeptides with trypsin

Because the minimum concentration of **P1** that triggered the orientational transition of 5CB shown in Figure 9.4 was 10 μM (or a surface density of $0.88 \times 10^{10}/mm^2$), we created an oligopeptide microarray with **P1** concentrations ranging from 10 to 500 μM. Figure 9.5a shows that before cleavage of **P1**, the fluorescence images of all of **P1**-modified regions were green. Subsequently, we delivered 3 μg/mL of trypsin solution to the surface following the gradient immersion time procedure. Figure 9.5b shows that the fluorescence images on all of the regions appeared dark after 10 h, suggesting that trypsin cleaved surface immobilized **P1** completely regardless of the

surface density of **P1**. However, when the incubation time was only 2 h, the fluorescence intensities were determined by original surface densities of **P1**. If the concentration of **P1** is lower than 40 μM (which corresponds to a surface density of $2.38 \times 10^{10}/mm^2$), the fluorescence images on **P1**-modified regions appeared dark after cleavage. In contrast, if concentration of **P1** is higher than 80 μM (which corresponds to a surface density of $2.74 \times 10^{10}/mm^2$), the fluorescence images on **P1**-modified regions appeared green after cleavage. These results indicate that trypsin did not cleave all of the surface immobilized **P1** within 2 h when the initial surface density of **P1** is higher than $2.74 \times 10^{10}/mm^2$. To further investigate the influence of incubation time on the cleavage of **P1**, we compared the fluorescence profiles of **P1** with two initial surface densities, $2.74 \times 10^{10}/mm^2$ and $3.47 \times 10^{10}/mm^2$ as a function of different incubation time as shown in Figure 9.6.

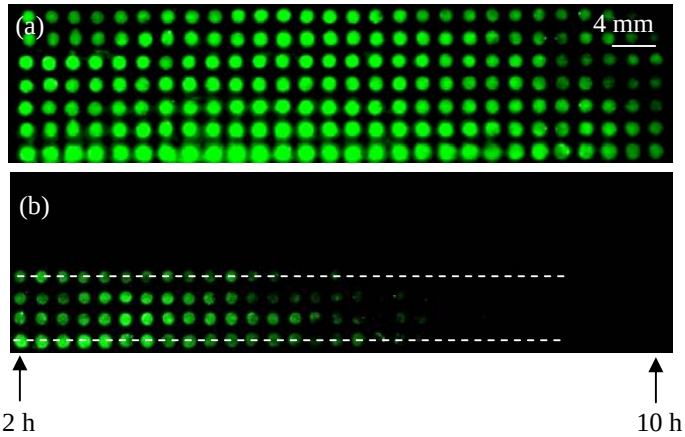

Figure 9.5 Fluorescence images of a complete **P1** microarray (a) before and (b) after 3 μg/mL of trypsin was delivered to the slide from right to left with a peristaltic pump with a flow rate 70 μL/min at 37˚C. Then, it was immersed in 10 μg/mL of FITC for 2 h. The concentrations of **P1** were 10, 20, 40, 80, 160, 320, and 500 μM from the top to down.

If we assume the fluorescence intensity is proportional to the surface density of **P1**,

we can calculate the surface density of **P1** decreased to 0.91 × 10^{10}/mm^2 after 2 h incubation time (Figure 9.6a). In contrast, Figure 9.6b shows that if the initial surface density of **P1** was 3.47 × 10^{10}/mm^2, the surface density of **P1** decreased to 2.70 × 10^{10}/mm^2 after the same incubation time.

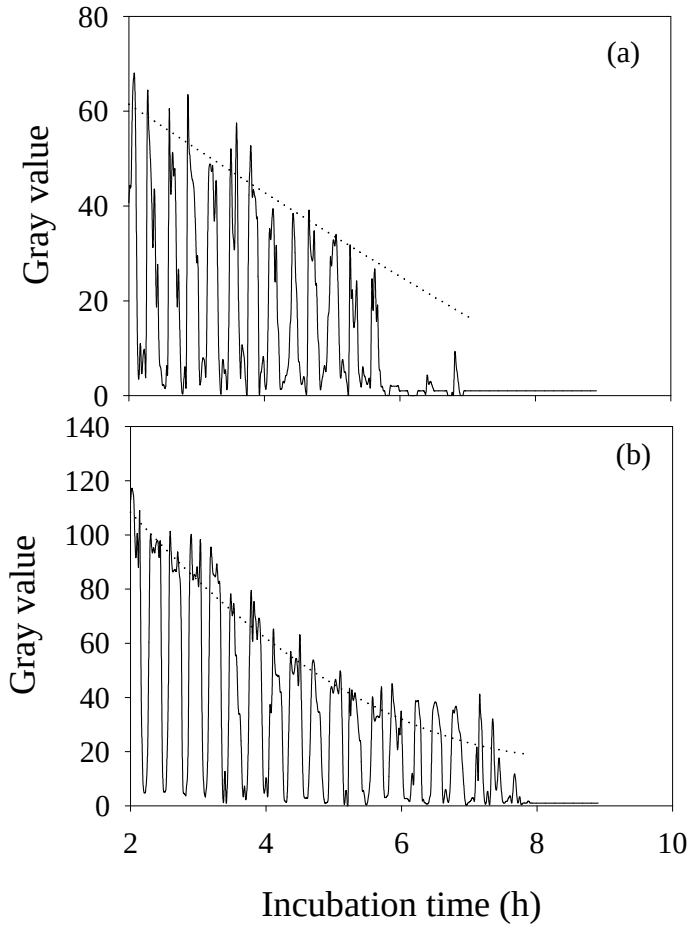

Figure 9.6 Fluorescence intensity profiles obtained along the dashed line shown in Figure 9.5b. (a) 80 μM **P1** (surface density: 2.74 × 10^{10}/mm^2) and (b) 500 μM **P1** (3.47 × 10^{10}/mm^2).

LC protease assays

To demonstrate that LC can be used as an imaging material for the development of a

label-free trypsin assay, we prepared two oligopeptide microarrays with different densities of **P1** immobilized on the surface. One of the microarrays was incubated in trypsin buffer, while the other microarray was incubated in a 3 μg/mL trypsin solution following the gradient immersion time procedure. Figure 9.7a and 9.7b show the images of LC cells made from these two microarrays.

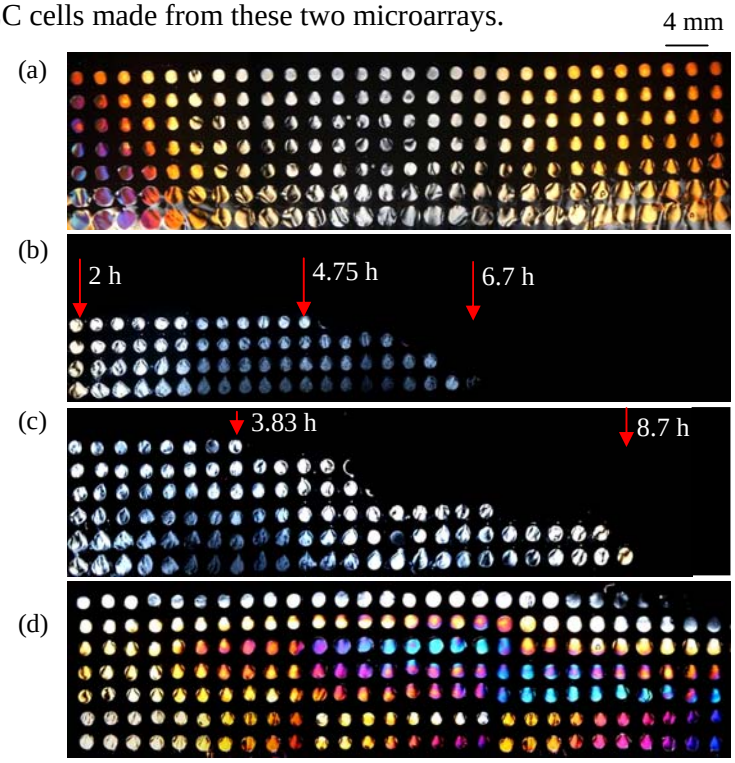

Figure 9.7 Optical textures (under crossed polars) of 5CB sandwiched between two DMOAP-coated glass slides. The bottom slide was also modified with TEA and droplets of **P1** solutions with various concentrations. Then (a) trypsin buffer, (b) 3 μg/mL (c) 0.5 μg/mL, and (d) 0.05 μg/mL of trypsin were delivered to the slide, respectively, from right to left with a peristaltic pump with a flow rate 70 μL/min at 37˚C. Concentrations of **P1** are the same as those in Figure 9.5.

In Figure 9.7a, all **P1** spots remained bright, which suggests that the buffer solution did not affect the immobilized **P1**. In contrast, Figure 9.7b shows that in regions where the incubation time is longer or where the surface density of **P1** is lower, some

of the bright spots disappear. Unlike the continuous profile of fluorescence intensity in Figure 9.6a or 9.6b, the LCs assay in Figure 9.7b exhibits a clear cut-off point in each row. As a result, Figure 9.7b appears like an optical bar chart, which is very useful for determining the incubation time to completely cleave immobilized **P1** with different surface densities. When we decreased the trypsin concentration to 0.5 μg/mL, Figure 9.7c exhibits more bright spots than Figure 9.7b. These results in Figure 9.7b and 9.7c indicate that the optical bar-chart feature of the LC image permits the quantification of trypsin concentration, incubation time, and surface density of **P1**.

Detection limit and quantitative analysis

We also tested the detection limit of the protease assay by decreasing the concentration of trypsin to 0.05 μg/mL. As shown in Figure 9.7d, the images of 5CB supported on 10 μM **P1**-modified regions changed to dark after 8.7 h of incubation time. However, the images of 5CB supported on the other regions modified with **P1** remained bright. Therefore, the detection limit of this assay was found to be at least 0.05 μg/mL, which is better than the sensitivity of a typical fluorescence array (~0.5 μg/mL) (Twining, 1984). Next, we calculated the minimal incubation time needed to cause a spot to change from bright to dark, as a function of **P1** concentration used to prepare the microarray. Figure 9.8 shows that when the trypsin concentration was 0.5 μg/mL, it took 5.4 h to cleave immobilized **P1** having a density of $2.74 \times 10^{10}/mm^2$. In comparison, when the trypsin concentration was 3 μg/mL, only 4.7 h was needed to cleave immobilized **P1** of the same density. We can also use Figure 9.8 to estimate the

concentration of trypsin in an unknown sample. For example, if we incubated a **P1** microarray in an unknown trypsin solution for 6 h and fabricated a LC cell, only the images of 5CB supported on 160, 320, and 500 μM **P1**-modified regions appeared bright. Then, we can estimate that the concentration of trypsin is about 0.5 μg/mL. On the other hand, if the images of 5CB supported on 320 and 500 μM **P1**-modified regions appeared bright, while the images of 5CB supported on 160 μM **P1**-modified regions appeared dark, we can predict that the concentration of trypsin is about 3 μg/mL.

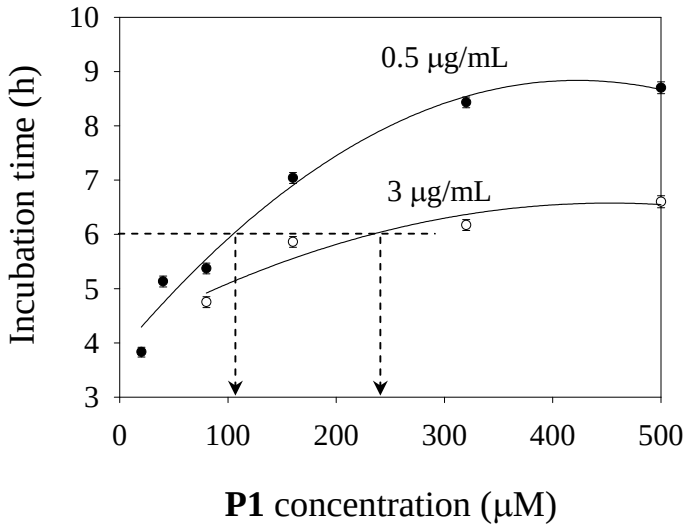

Figure 9.8 Minimum incubation time (in trypsin solution) required for changing a bright LC spot (caused by immobilized **P1**) to dark as a function of **P1** concentrations. Concentrations of trypsin solutions used in this experiment were 0.5 μg/mL and 3 μg/mL, respectively.

Assay specificity

To examine the specificity of the trypsin assay, we prepared another type of oligopeptide microarray containing oligopeptides **P1**-**P6**. Among them, **P2** has the

same sequence as **P1** except that **P2** does not have a C-terminal lysine residue. **P3** is also similar to **P1**, but the arginine residue, which is cleavable by trypsin, is replaced by a non-cleavable histidine residue. **P5** also cannot be cleaved by trypsin because the arginine residue is followed by proline, which prevents the trypsin from cleaving the C-terminal arginine. Both **P4** and **P6** can be cleaved by trypsin (their cleavage sites are detailed in Table 9.1).

After the microarray was prepared, we used it to fabricate a LC cell. Figure 9.9a shows that the only the last row modified with **P6** appears dark, whereas other rows modified with **P1**-**P5** appear bright. This is probably because **P6** only has 9 amino acid residues (which is shorter than **P1**-**P5**) such that it cannot trigger the orientational transitions of LCs when it is immobilized on the surface. Next, we incubated another oligopeptide microarray in 3 μg/mL trypsin solution for 3 h (following the constant immersion time procedure) and then fabricated a LC cell to study whether immobilized oligopeptides **P1**-**P5** can be cleaved as expected and detected by LCs. Figure 9.9b shows that the images of 5CB supported on **P1**, **P2** and **P4** change to dark while the images on **P3** and **P5** remain bright. This result suggests that trypsin cleaved the immobilized **P1**, **P2**, **P4** but did not cleave the immobilized **P3** and **P5** as expected. This result also implies that the cleavages of **P1, P2,** and **P4** by trypsin all lead to changes in the optical textures of 5CB.supported on the oligopeptide microarray. These results, when combined, suggest the following two key features. First, the detection principle of the LC-based protease assay is general. Any oligopeptides containing the specific amino acid residues may be hydrolyzed by the proteases.

Second, the trypsin cleavage on oligopeptides substrates has high selectivity. It can discriminate two oligopeptide substrates (i.e. **P1** and **P3**), which only differ in one amino acid residue.

Detection of chymotrypsin

To further test the generality of the LC-based protease assay, we selected chymotrypsin as our second model proteases. Although chymotrypsin has a similar structure to trypsin, it prefers large hydrophobic residues, including tryptophan, tyrosine, phenylalanine, leucine, and methionine. The cleavage sites of chymotrypsin for different oligopeptides were shown in Table 9.2. Once again, we prepared an oligopeptide microarray with **P1**-**P6** and incubated the oligopeptide microarray in 3 μg/mL of chymotrypsin solution for 3 h before a LC cell was fabricated. Figure 9.9c shows that the images of 5CB supported on **P1**, **P2, P3** and **P5** changed to dark, while the images on **P4** remained bright. This result suggests that chymotrypsin cleaved the immobilized **P1**, **P2, P3** and **P5** as expected. For **P4**, although chymotrypsin can also cleave it from the C-terminal methionine, the cleavage of one amino acid unit from **P4** did not greatly decrease the ellipsometric thickness (from 28 ± 4 Å to 25 ± 5 Å), and thus the orientations of 5CB remained planar. All of these results suggest that the combination of oligopeptide microarray and optical textures of LCs to report the trypsin cleavage on oligopeptide substrate does not require labels, is simple to implement, and can apply for the multiplexed protease assays.

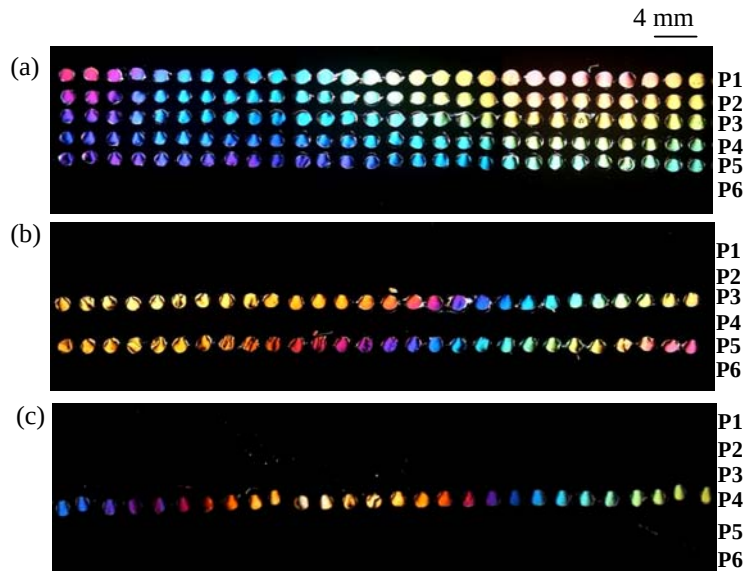

Figure 9.9 Optical textures (under crossed polars) of 5CB sandwiched between two DMOAP-coated glass slides. The bottom slide was also modified with TEA and circular domains of 40 μM **P1**, **P2**, **P3**, **P4**, **P5**, and **P6** in a microarray format and then incubated in (a) trypsin buffer, (b) 3 μg/mL of trypsin solution, and (c) 3 μg/mL of chymotrypsin solution at 37˚C for 3 h.

9.4 Conclusions

In this study, we have successfully demonstrated a simple and label-free LCs-based multiplexed protease assay which can easily report the enzymatic activity. A key element of this assay is an oligopeptide microarray with well-orientated immobilized oligopeptides which were obtained by reacting N-terminal cysteine-labeled oligopeptides with an aldehyde-terminated surface. When the surface density of **P1** exceeded 0.88×10^{10}/ mm^2, it disrupted the orientations of LC supported on the surface and changed the images of LC from dark to bright. The dependence of orientations of LC on the surface densities of **P1** was then exploited to detect protease activities. When a **P1** microarray was immersed in a trypsin solution by using the gradient immersion time mode, an interesting optical bar chart having clear cut-off

points was obtained. This optical bar chart is very different from the continuous intensity profile found in most fluorescence assays and it allows us to determine the concentration of trypsin with high sensitivity and low detection limit (~0.05 μg/mL). This technique reported herein also can be used for detecting other proteases such as chymotrypsin with high specificity or differentiating two oligopeptides with difference only in one of the residues in their sequences.

CHAPTER 10
LIQUID CRYSTAL pH SENSOR FOR MONITORING ENZYMATIC ACTIVITIES

10.1 Introduction

Monitoring pH values are important in many chemical and biological processes, clinical analyses, environmental science, and oceanography. Although pH sensors made from glass electrodes are readily available for monitoring pH values in aqueous solutions, they are not suitable for measuring pH within a small volume. Recently, many novel techniques, including fluorescence (Nishimura et al., 2005; Evangelio et al., 2008) and pH sensitive field-effect transistors (pHFETs) (Janata et al., 1985; Bergveld et al., 1988), have been developed to address this issue. Nevertheless, the pH measured by the pHFET is an average value over the entire sensor surface. Thus, it is often difficult to probe localized pH changes caused by surface reactions. Herein, we sought to exploit optical properties of LCs and design a label-free pH sensor with good spatial resolution for monitoring changes in localized pH and enzymatic activities.

Penicillin G, which is a group of β-lactam antibiotics, has been widely used for the treatment of bacterial infection, such as pneumococcal pneumonia (Austrian et al., 1964; Finland, 1972). However, almost as soon as penicillin was introduced, penicillin-resistant bacteria began to appear (Lee et al., 1944). These bacteria produce an enzyme penicillinase, which is able to catalyze the hydrolysis of penicillin G as

shown in Eq. 10.1. After penicillin G is hydrolyzed, a H^+ is released and the pH value is decreased (Hall et al., 2004; Hassen et al, 2007; Walsh, 2000; Galarneau et al., 2002; Levy et al., 2004; Page et al, 1999; Bush, 1988; Abouzar et al., 2008; Hartl et al., 2008; Caras et al., 1980).

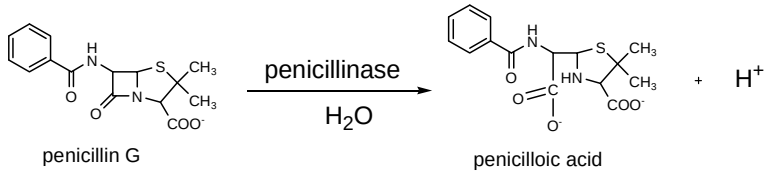

penicillin G penicilloic acid (10.1)

Therefore, detecting penicillinase is possible via pH changes associated with the reaction. Recently, some pioneered studies from Abbott's group have successfully demonstrated the utility of LCs to transduce and amplify molecular events at an aqueous/LC interface into optical images visible with the naked eye (Price et al., 2008; Lockwood et al., 2006 and 2008; Meli et al., 2008; Park et al., 2006 and 2008). The LC based sensor is sufficiently simple, label-free, and provides good spatial resolution (Gupta et al., 1998). Because anchoring of LCs at the aqueous/LC interface is controlled by a fine scale of energetics (10^{-2} to10^{-3} mJ/m^2), it is possible to couple the orientations of LCs to surfactants (Brake et al., 2003 and 2003; Lockwood et al., 2005), lipids (Brake et al., 2003; Hartono et al., 2008), proteins (Brake et al., 2003), and synthetic polymers (Kinsinger et al., 2007) adsorb at the aqueous/LC interface. Moreover, when these surfactants or polymers containing pH sensitive functional groups, a LC based pH sensor can be prepared. For example, Kinsinger et al. designed a polymer-functionalized interface (by conjugate addition of poly(ethylene imine) to *N*-[3-(dimethylamino)propyl] acrylamide) that responded reversibly to pH changes in

the aqueous phase (Kinsinger et al., 2007). They demonstrated that the pH-dependent changes in the orientation and optical appearance of LC arise from the changes in the ordering of the polymer at the interference. However, they only observed different optical appearance of LC at pH = 9.0 and 5.0. Thus, whether this system is suitable for detecting small changes in pH value is unclear. Moreover, the response time is very long (10 h).

To address the need for detecting small pH changes and the slow response issue reported previously, we designed a new LC based pH sensor by doping 5CB with PBA, which has a pH sensitive functional group and a similar structure with 5CB. We also studied the feasibility of using the LC based pH sensor for monitoring H^+ released from enzymatic reactions in real time. The challenge is that because only a small amount of H^+ is released during an enzymatic reaction, it only causes a very small pH change in the bulk solution, especially when the buffer capacity is high. Nevertheless, we hypothesize that the release of H^+ still can lead to localized and temporal pH changes which can be detected by a highly sensitive pH sensor with a good spatial resolution.

10.2 Experimental Section

Reagents

Poly(ethylene imine) (PEI, M.W. = 75,000), sodium chloride (NaCl), penicillin G, ampicillin, penicillinase from *Bacillus Cereus* (K_m = 60 μM, M.W. = 28,000), 4’-pentyl-biphenyl-4-carboxylic acid (PBA), biphenyl-4-carboxylic acid, lauric acid

and acetic acid were purchased from Sigma Aldrich (Singapore).

Immobilization of penicillinase on copper grids

Copper grids (75 mesh, Electron Microscopy Sciences, U. S. A.) were first cleaned in methanol, ethanol, and acetone (sonication for 15 min in each solvent), and heated overnight at 100°C to evaporate residual solvents. Next, the clean grids were immersed in an aqueous solution containing 5% of PEI. After 30 min, the grids were washed thoroughly with deionized water and dried in a 100°C oven. Next, we immersed the grids in an aqueous solution containing 5wt% of glutaraldehyde and 10 mM of sodium cyanoborohydride for 2 h. Finally, the grids were incubated in a buffer (which contained 0.5 mM sodium phosphate and 50 mM sodium chloride and was degassed for at least 1 h before use) containing 0.2 mg/mL of penicillinase for 12 h at 4˚C. For the bar-shaped grid, 0.5 μL of buffer solution containing penicillinase was dispensed onto one side of the grid. To prevent the evaporation of the penicillinase solutions, the grid was stored in a sealed and humid chamber for 12 h at 4˚C. Excess penicillinase was removed by incubating the grid in 2×SSPE buffer (300 mM NaCl, 23 mM NaH_2PO_4, 2.8 mM EDTA) and 1% Triton X-100 for 10 min. All penicillinase-modified grids were kept at 4˚C before use.

Preparation of LC samples

First, DMOAP-coated glass slides were prepared following the procedure as described in **Chapter 9**. Briefly, glass slides were immersed in 0.1wt% DMOAP solution to obtain a layer of DMOAP on the surface. The glass slides were then cut into small

squares (5 mm × 5 mm) and used as substrates for supporting LC. For fabrication of LC based pH sensor, unmodified copper grid was placed on the DMOAP-coated glass slide. Then, approximately 0.3 μL of 0.3wt% PBA-doped 5CB was dispensed onto the grid, and excess LC was removed by using a capillary tube. Finally, the grid containing LC was covered with 300 μL of buffer solutions at different pH. For monitoring enzymatic activities, the unmodified copper grid was replaced by a penicillinase-modified copper grid. Then, after filling the grid with PBA-doped 5CB, the grid was immersed in 300 μL of sodium phosphate buffer (pH = 7.0) with different concentrations of penicillin G. The optical appearances and fluorescence images of these samples were observed by using polarizing optical microscope and fluorescence microscope, respectively.

10.3 Results and Discussion

Orientational response of carboxylic acid-doped 5CB to pH

Our first goal was to develop a LC based pH sensor that gives fast response to small pH changes. Since 5CB does not contain any pH sensitive functional groups, we doped it with 0.3% of PBA. We selected PBA because (1) it has a carboxylic acid moiety which is sensitive to pH in aqueous solutions. (2) We hypothesize that the amphiphilic property of PBA will cause the molecule to self-assemble at the aqueous/LC interface, which is similar to the role of surfactant in the aqueous/LC system reported earlier (Brake et al., 2003 and 2003; Lockwood et al., 2005). (3) PBA has a similar structure to 5CB. Therefore, it has a better chance to interact with 5CB

and influence the orientations of 5CB more effectively. The doped 5CB was then confined in a TEM grid (which prevented the dewetting of 5CB) supported on a DMOAP-coated glass (Brake et al., 2002). When the whole system was immersed in sodium phosphate buffer (pH = 7.0), a dark image was observed under crossed polarizers (Figure 10.1a).

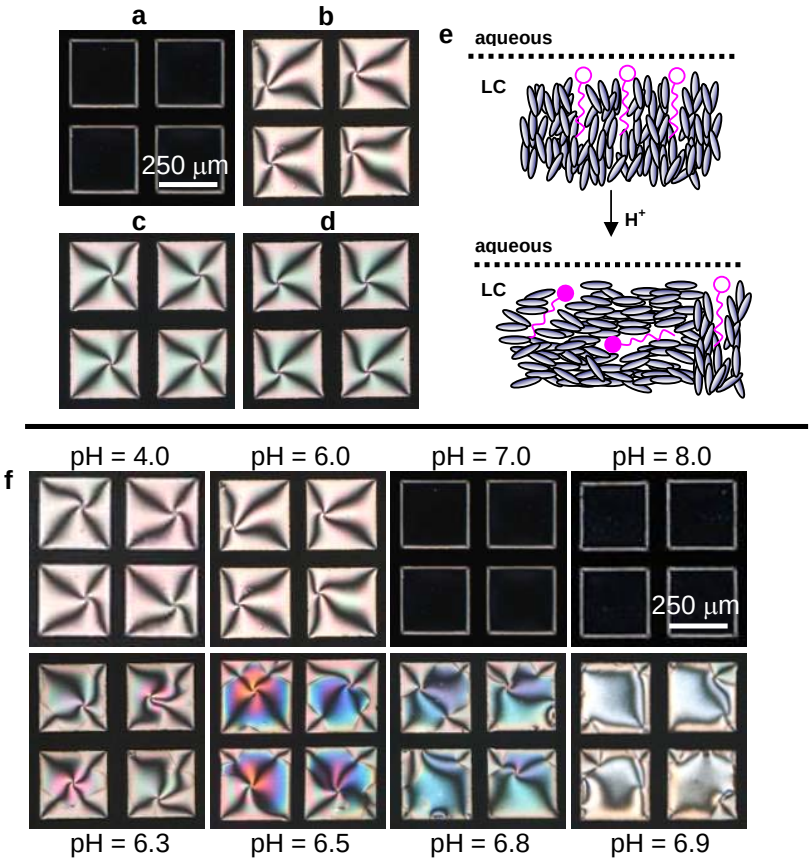

Figure 10.1 Optical images (crossed polars) of copper grids impregnated with (a-b) 0.3% PBA-doped 5CB and (c-d) 5CB, after they were exposed to aqueous solution at (a) and (c) pH = 7.0, (b) and (d) pH = 6.0. (e) The orientational transition of 5CB because of the local pH change. (f) Optical images (crossed polars) of copper grids impregnated with 0.3% PBA-doped 5CB when it was exposed to aqueous solutions at different pH.

Interestingly, when we decreased the pH of the sodium phosphate buffer to 6.0, the

image of LC changed to bright immediately (Figure 10.1b). In contrast, when undoped 5CB was used in this experiment, 5CB appeared bright at pH = 7.0 and 6.0 (Figure 10.1c and 10.1d). From these results, we can conclude that the optical image of 5CB, when doped with PBA, is very sensitive to the pH change between 6.0 and 7.0, and PBA plays an important role in the response to pH.

It is well-known that the dark image of LC was caused by homeotropic orientations of LC at the aqueous/LC interface, and the bright image of LC was caused by plannar orientations. Moreover, past studies have demonstrated that adsorption of surfactants at the aqueous/LC interface often leads to a planar-to-homeotropic transition in the orientation of LC when the density of surfactants exceeds a critical value. In our system, since a similar transition occurred between pH = 6.0 and 7.0, we can postulate that the density of PBA increases with the pH value until it exceeds a critical value at pH = 7.0 as shown in Figure 10.1e , and that causes the dark-to-bright optical response observed in Figure 10.1a and 10.1b. To investigate the response to pH further, we immersed the PBA-doped 5CB in buffer solutions with pH values ranging from 4.0 to 8.0 (Figure 10.1f). We observed that the bright-to-dark optical transition of LC was triggered by a very small pH change (i.e. ~ 0.1). The discontinuous transition between pH = 6.9 and 7.0 also implies that the LC pH sensor is a “all-or-nothing” type of sensor, which can offer many advantages which traditional pH sensors do not have.

Although it is apparent that PBA participates in the orientational response of 5CB, the

actual mechanism that causes the response of LC to pH change is still unclear. To shed lights on the mechanism, we selected other molecules which also contain carboxylic acid groups and studied whether 5CB doped with these molecules also show similar responses to changes in pH. First, we doped 5CB with 0.3% of 4-biphenylcarboxylic acid, which is similar to PBA but without a hydrocarbon tail as PBA. After immersing 4-biphenylcarboxylic acid-doped 5CB in aqueous solutions having different pH (from pH = 2.0 to 8.0), we observed that the images of LC were always bright regardless of the pH (Figure 10.2a). Thus, we can propose that the hydrocarbon chain of PBA plays an important role in controlling the orientations of 5CB. Similarly, acetic acid-doped 5CB also showed no response to changes in pH from 2.0 to 8.0 (Figure 10.2b). This is consistent with the proposition that a long hydrocarbon chain is needed in the molecular structures of dopants for them to couple the orientational behaviors of 5CB to pH. To test this proposition, we doped 5CB with 0.3% of lauric acid which has a carboxylic acid group and a long hydrocarbon chain. Figure 10.2c shows that lauric acid-doped 5CB appears bright at pH = 2.0 and 4.0, but it changes to dark at pH = 5.0 and 8.0. Therefore, this result supports our proposition. We also note that the bright-to-dark transition point occurs around pH 4.0 ~ 5.0, which coincides with the pK_a of lauric acid (~ 4.95). Thus, the bright-to-dark transition can be attributed to the deprotonation/protonation of lauric acid. Because the deprotonated lauric acid is negatively charged, it is more amphiphilic than the protonated one. As a result, the density of deprotonated lauric acid at the aqueous/LC interface increases, leading to the bright-to-dark transition in the appearance of 5CB.

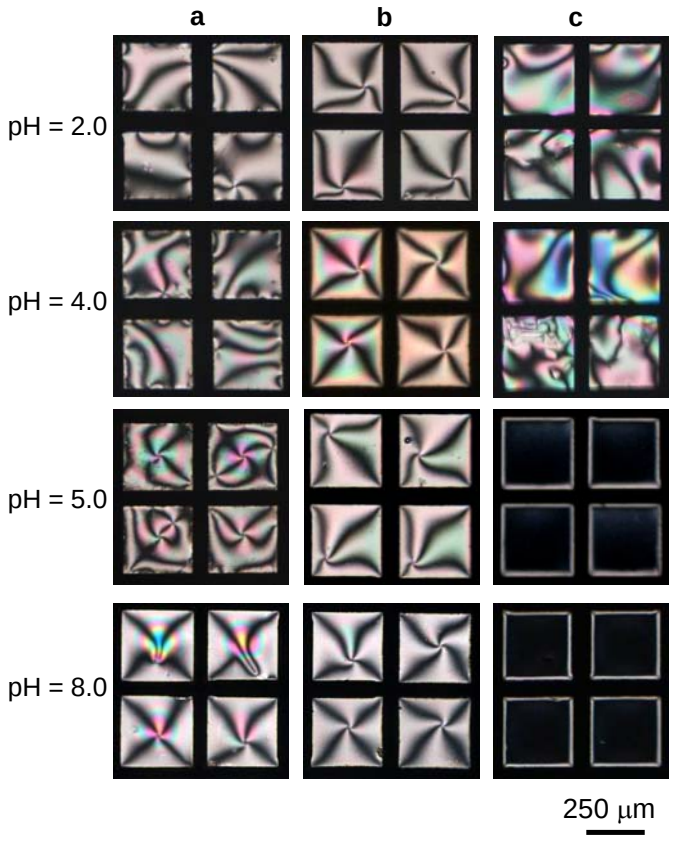

Figure 10.2 Optical images (crossed polars) of 5CB (doped with 0.3% of several carboxylic acid compounds) immersed in aqueous solutions of four different pH values. These compounds are (a) 4-biphenylcarboxylic acid, (b) acetic acid, and (c) lauric acid.

However, the deprotonation/protonation theory may not be sufficient to account for the optical response in the PBA-doped 5CB as shown in Figure 10.1a and 10.1b. Because the pK_a for PBA is 3.46, 99.96% of PBA is already in the deprotonated form at pH = 6.9. Increasing the pH value by 0.1 to pH =7.0 will only cause another 0.01% of PBA to deprotonate and lead to minimal increase in the density of PBA at the aqueous/LC interface. Surprisingly, this small change leads to orientational response of 5CB and the bright-to-dark transition as shown in Figure 10.1a and 10.1b. This is not unusual for 5CB, however. As pointed out by Abbott et al., an undetectable

increase in the density of GM_1 can lead to a similar dark-to-bright transition in 5CB.

Detecting H^+ releasing from enzymatic reactions

Next, we sought to apply the LC based pH sensor to develop a biosensor for detecting H^+ released from an enzymatic reaction. The advantages of the LC based pH sensor include its unusual high sensitivity to pH and its ability to monitor localized pH values in a real-time manner.

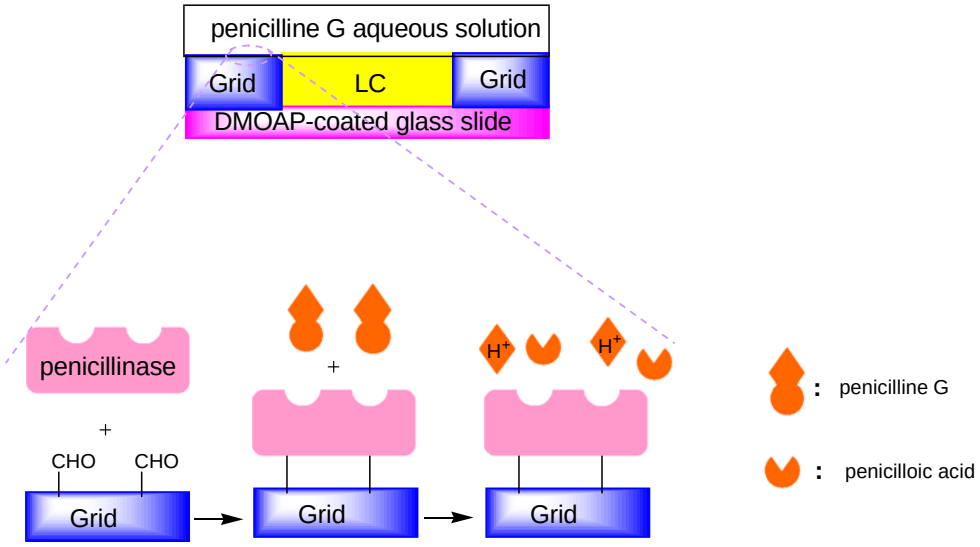

Scheme 10.1 Configuration of the copper grid impregnated with LCs and exposed to penicillin G aqueous solution. Zoom-in: Schematic illustrations showing the immobilization of penicillinase and the enzymatic reaction of penicillinase on the surface of copper grid.

As a proof of concept, we selected the hydrolysis of penicillin G catalyzed by penicillinase as our model enzymatic reaction. As shown in Eq. 10.1, when penicillin G molecules are hydrolyzed, some H^+ will be released, but most H^+ will be neutralized by the buffer. Thus, we hypothesized that the pH change associated with the enzymatic reaction is only temporal and highly localized (near the immobilized

enzyme only). On the basis of this hypothesis, we designed an experimental system as shown in Scheme 10.1.

First, we immobilized penicillinase on the metal bars of a copper grid. Then, the hollow square regions of the grid were filled with PBA-doped 5CB such that the PBA-doped 5CB is in the proximity of the immobilized penicillinase. Finally, the entire system was immersed into sodium phosphate buffer (pH = 7.0) with penicillin G. Figure 10.3a shows that the optical image of LC becomes bright in the presence of penicillin G. For comparison, the same system was immersed in pure sodium phosphate buffer without penicillin G, and the LC remains dark (Figure 10.3b).

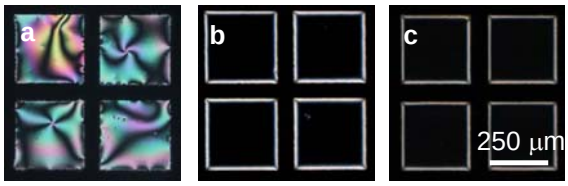

Figure 10.3 Detection of H^+ released from enzymatic reaction of penicillinase. (a-b): copper grids were coated with 0.2 mg/mL penicillinase at 4˚C for 12 h and then exposed to: (a) 1 mM penicillin G in sodium phosphate buffer, and (b) pure sodium phosphate buffer (pH = 7.0). (c): unmodified copper grid was exposed to 1 mM penicillin G in sodium phosphate buffer.

This result implies that penicillin G can be hydrolyzed by immobilized penicillinase on the copper grid and release H^+, lowering the local pH and causing the LC to change to bright. To confirm that the color change was indeed caused by the enzymatic reaction, we also immersed an unmodified copper grid (without penicillinase) in the penicillin G solution. Figure 10.3c shows that the image of LC remains dark, suggesting that penicillin G alone does not change the orientation of

LC.

Enzyme specificity

An important consideration for the development of a biosensor is specificity. Thus, we immersed the LC pH sensor in buffer solutions containing ampicillin and tetraglycine (control), respectively. The former is also a substrate for penicillinase, because it contains a β-lactam ring, which can be hydrolyzed by penicillinase. Figure 10.4a shows that the image of LC in the solution containing 1 mM of ampicillin becomes bright immediately after the immersion, while the one in the tetraglycine solution remains dark (Figure 10.4b).

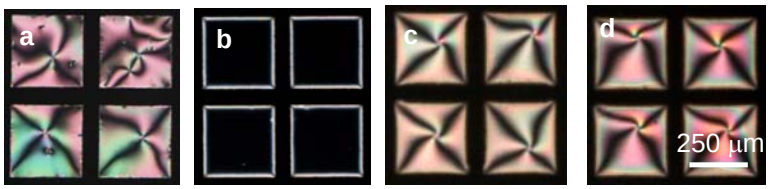

Figure 10.4 Specificity of the LC sensor. (a-c): copper grids were coated with 0.2 mg/mL penicillinase at 4˚C for 12 h and then exposed to: (a) 1 mM ampicillin, (b) 1 mM tetraglycine, and (c) 1 mM HCl. (d): unmodified copper grid was exposed to 1 mM HCl. All of them were dissolved in sodium phosphate buffer (pH = 7.0).

Moreover, because the detection mechanism of the sensor is based on the changes in pH, we also studied the response of the sensor to strong acids. Figure 10.4c shows that the image of LC became bright after the immersion of a penicillinase-modified grid into 1 mM HCl solution. However, when we immersed an unmodified copper grid (with impregnated LC) into the same solution, LC also appeared bright (Figure 10.4d), which is different from the dark appearance of LC when an unmodified grid was

immersed in penicillin G solution (Figure 10.3c). Thus, by comparing the results from penicillinase-modified grid and unmodified grid, one can tell whether the solution contains penicillin G or strong acids.

Kinetics of enzymatic reactions

The above results already demonstrate that our pH sensor can detect some H^+ released from the hydrolysis of penicillin G before they are neutralized by the buffer solution. To determine the detection limit of the system, we compared the dynamic response of LC at different penicillin G concentrations. Figure 10.5a shows that the bright LC region slowly expands from the boundary to the center after the addition of 10 μM penicillin G. After 7 min, the bright region fills the entire square area. Furthermore, Figure 10.5a also shows that when the concentration of penicillin G is lowered to 100 nM and 1 nM, respectively, the time required for the entire square area to appear bright also increases to 10 and 30 min, respectively. We can calculate the ratio of the bright area to the total square area as a function of exposure time for three different penicillin G concentrations as shown in Figure 10.5b. One can use the kinetic behavior of the response to estimate the concentration of penicillin G in the system. However, it is difficult to model the system because of two reasons. First, the diffusion length in the square region is too short (the length of each square is only 283 μm), which prevents us from collecting data over a long period of time. Second, the diffusion of H^+ occurs in a 2-dimensional square geometry.

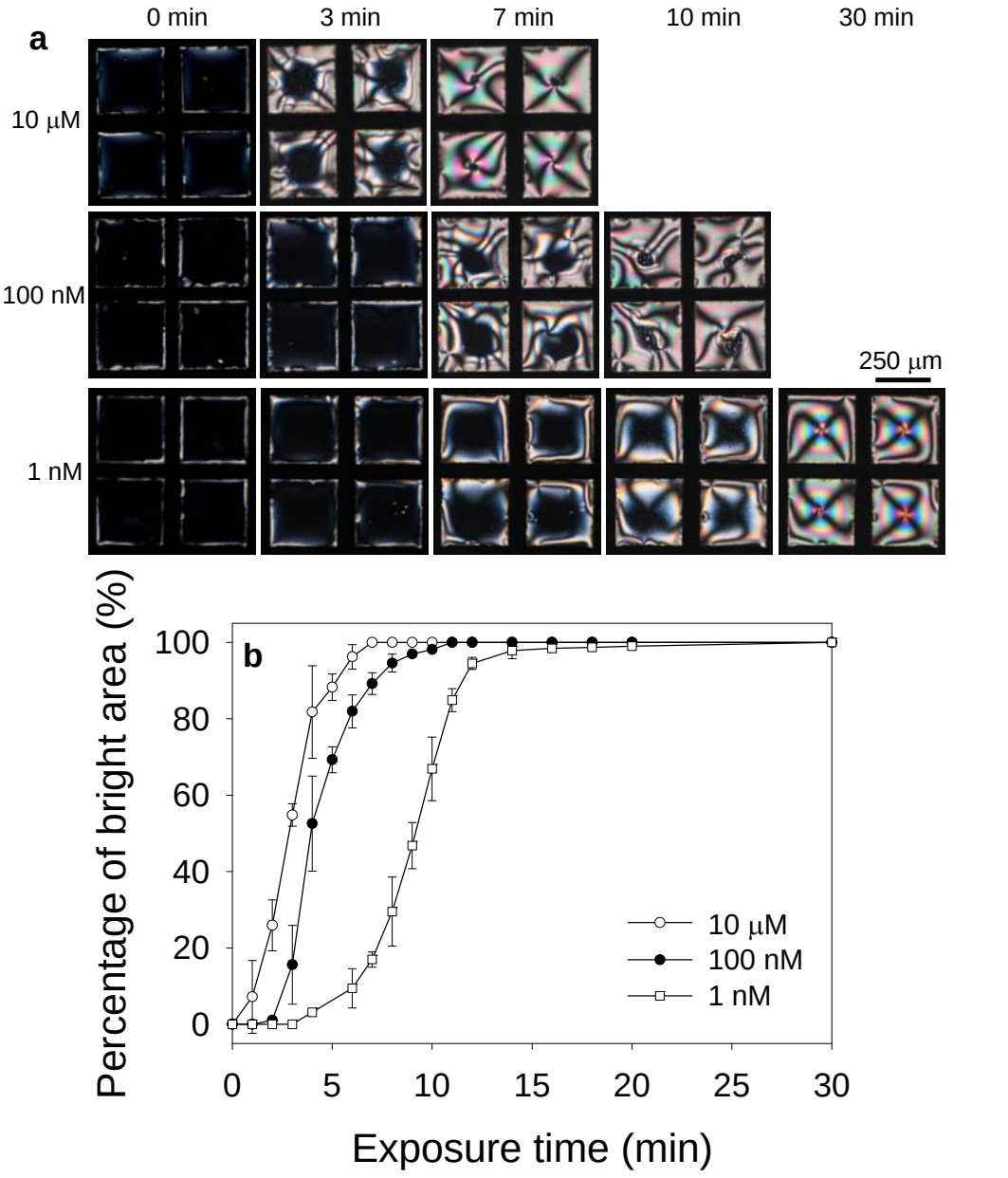

Figure 10.5 (a) Influence of the concentrations of penicillin G on optical images (crossed polars) of 0.3% PBA-doped 5CB confined in copper grids at different time. The copper grids were coated with 0.2 mg/mL penicillinase at 4˚C for 12 h. (b) Increase in planar coverage when 0.3% PBA-doped 5CB confined in copper grids was exposed to different concentrations of penicillin G at different exposure time.

To avoid these problems, we used a bar-shaped grid in the following experiments. We only modified one side of the metal bars of the grid with penicillinase. After we immersed the grid in 100 nM penicillin G solution, the optical image of LC became

bright starting from the side with immobilized penicillinase, and then the bright region extended along the grid (Figure 10.6a). This result suggests that the released H^+ diffuses in one direction within the slit. Figure 10.6b shows that the length of bright region increases with the immersion time at two different penicillin G concentrations.

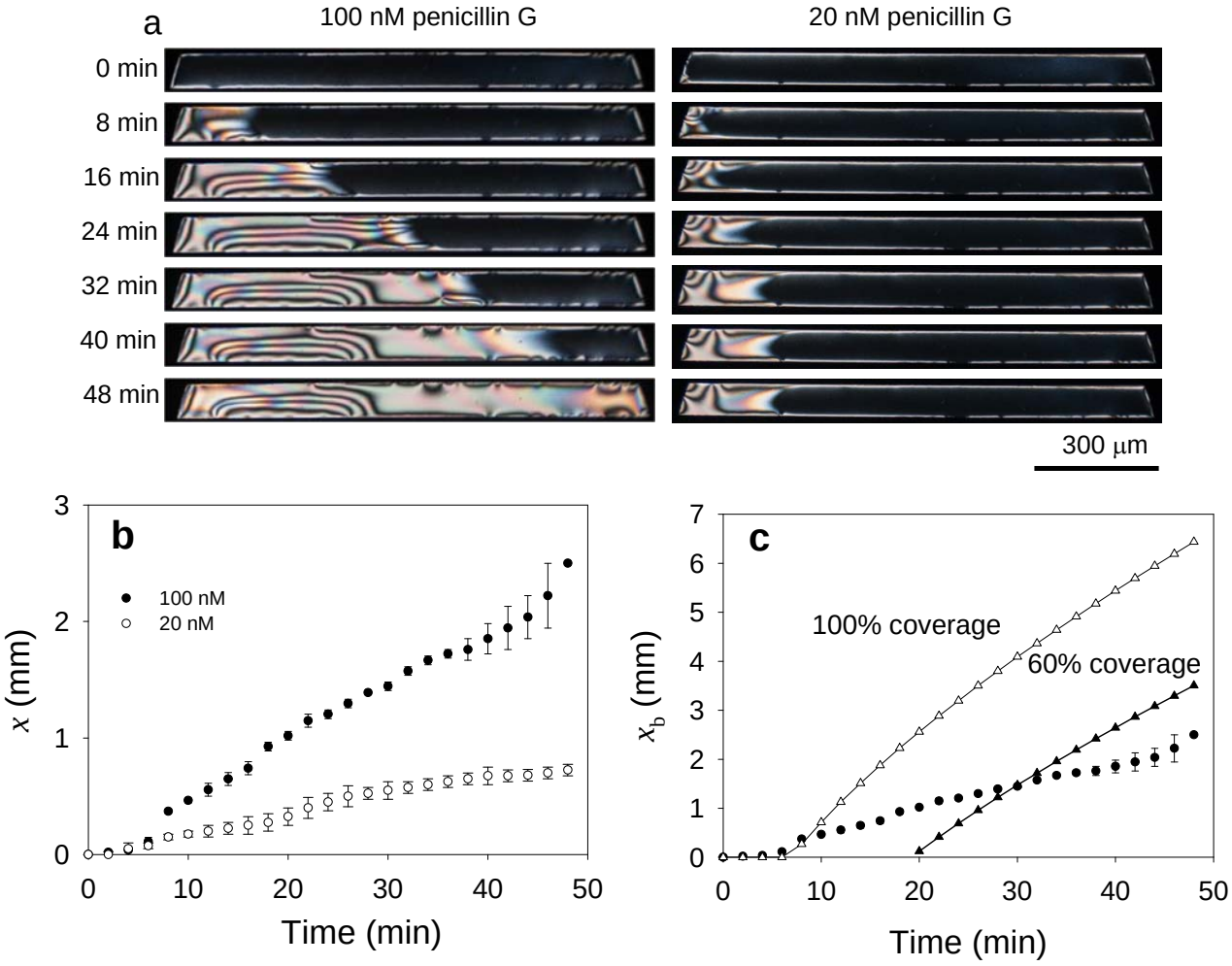

Figure 10.6 (a) Optical images (crossed polars) of 0.3% PBA-doped 5CB confined in a bar-shaped, penicillinase-modified grid after contacting with 20 and 100 nM penicillin G, respectively at different time. (b) Positions of the diffusion front x as a function of immersion time when the grid was contacted with 20 and 100 nM penicillin G. (c) Theoretical positions of the diffusion front x_b as a function of immersion time when penicillinase-modified grid (100% and 60% coverage, respectively) was contacted with 100 nM penicillin G.

In theory, the amount of H^+ released during the enzymatic reaction and the resulting change in pH can be estimated. Because the diameter of a penicillinase molecule is about 6 nm (Munshi et al., 1995), the density of a penicillinase monolayer will be $2.78 \times 10^{10}/mm^2$. Moreover, a single penicillinase molecule can hydrolyze 10^3 penicillin G molecules per second and release equal amount of H^+. Because the diffusion coefficient of H^+ in aqueous solution ($\sim 9.3 \times 10^{-5}$ cm^2/s) (Disalvo et al., 1995), we can estimate that within 1 min, the diffusion length L ($L^2 = 2Dt$) of H^+ is 0.11 cm. By assuming 100% hydrolysis efficiency, the localized pH will decrease to 6.4 after the reaction taking the buffer capacity into consideration. We point out that measuring the small decrease in pH occurs in a localized zone is challenging by using conventional pH meter, but is possible by using the LC based pH sensor.

Moreover, the diffusion of H^+ in the experiment shown in Figure 10.6b can be described by using an unsteady-state one-dimensional diffusion equation (Welty et al., 2000).

$$\frac{\partial[\mathrm{H}^+]}{\partial t} = D\frac{\partial^2[\mathrm{H}^+]}{\partial x^2} \tag{10.2}$$

where $[H^+]$ and D are the concentration and diffusion coefficient of H^+, respectively. t is the diffusion time, and x is the diffusion distance. Because the experiment was conducted at pH = 7.0, the initial condition for Eq. 10.2 is

$$[\mathrm{H}^+](x,0) = 10^{-7} \tag{10.3}$$

and two boundary conditions are

$$x = 0,\ D\frac{\partial[\mathrm{H}^+]}{\partial x} = r_0 \tag{10.4}$$

$$x = \infty, [\mathrm{H}^+] = 10^{-7} \tag{10.5}$$

where r_0 is the generation rate of H^+ in the reaction. The exact solution to Eqs 10.2-10.5 is:

$$[\mathrm{H}^+] - 10^{-7} = \frac{2r_0}{D}\sqrt{Dt}\,\mathrm{erfc}\left(\frac{x}{2\sqrt{Dt}}\right) \tag{10.6}$$

If we assume that the enzymatic reaction follows Michaelis-Menten kinetics (Kuby, 1991; Nishino et al., 2004), then r_0 can be expressed as

$$r_0 = \frac{k_{\mathrm{cat}}[\mathrm{E}]_0[\mathrm{S}]_0}{[\mathrm{S}]_0 + K_{\mathrm{m}}} \tag{10.7}$$

where $[E]_0$ and $[S]_0$ are the initial concentrations of enzyme and substrate, respectively, k_{cat} is catalytic rate constant, and K_m is Michaelis constant. By assuming that the immobilized penicillinase has similar activities as that in the solution, k_{cat} is 114 min^{-1} (Yamaguchi et al., 1983), and K_m is 60 μM (provided by the manusfacturer). If penicillinase forms a monolayer on the surface (density = $2.78 \times 10^{10}/mm^2$), and the initial concentration of penicillin G is 100 nM, then r_0 is 3.68 $nmol/m^2$**.**min in the sodium phosphate buffer.

Furthermore, it has been shown in our experiments that the dark-to-bright transition of 5CB starts when the pH value is lower than 6.9. Thus, we can assume that the $[H^+]$ at

the boundary that separates the bright and dark region in Figure 10.6a is $10^{-6.9}$ M. We can also calculate the position of the moving boundary x_b at different time t. Figure 10.6c shows that the theoretical value of x_b is bigger than the experimental value. The increase is probably because we assumed that penicillinase formed a dense monolayer on the surface. If the surface coverage was 60%, the average error between the theoretical and experimental values is 35%. Another possible reason for the big average error is because the diffusion barrier for penicillin G to the catalytic centers of penicillinase due to the spatial constraints in the case of immobilized enzymes (Hai et al., 2006; Letant et al., 2004). As a result, the values of both k_{cat} and K_m should be lower than those in the case of free penicillinase.

10.4 Conclusions

In conclusion, we developed a highly sensitive and label-free pH sensor by using 5CB doped with PBA. As pH of the aqueous solution changes, orientations of LC undergo a homeotropic-to-planar or planar-to-homeotropic transition, which can be easily visualized as an optical dark or bright image. The pH-driven optical response is attributed to the protonation and deprotonation of PBA at the aqueous/LC interface, which induces the orientational transitions of 5CB. The LC based pH sensor shows great promise in monitoring enzymatic reactions. As a model system, the hydrolysis of β-lactam antibiotics by penicillinase releases a H^+ and decreases pH in the vicinity of penicillinase-modified region. In our experiments, we have observed that the LC based pH sensor shows high sensitivity (1 nM within 7 min) and specificity (only

β-lactam antibiotics can be detected) to monitor the enzymatic reaction.

CHAPTER 11
CONCLUSIONS AND RECOMMENDATIONS

11.1 Conclusions

In this thesis, we have created an oligopeptide-modified surface and exploited its applications in the adsorption of metal ions and the design of chemical and biological sensors.

Firstly, 2D molecular imprinting technique is employed to create a metal ion-imprinted surface exhibiting high adsorption capacity and specificity for Cu^{2+}. The experimental results shows that the adsorption capacity of the copper-imprinted silica gel is 50% higher than nonimprinted silica gel at pH = 4.5. The higher adsorption capacity of copper-imprinted silica gel at low pH is attributed to two factors. First, the two immobilized molecules can chelate Cu^{2+} as a multi-dentate ligand if the intermolecular distance between these two molecules is appropriate. Second, for a single immobilized diglycine and triglycine, they can form very stable 1:1 complex with Cu^{2+} if the surface is not over-crowded. By using copper imprinting during the immobilization procedure, both proper intermolecular distance and intermediate density of the immobilized molecules suitable for chelating Cu^{2+} can be achieved. Moreover, the difference between the copper-imprinted and nonimprinted silica gel is more pronounced in the presence of competing ions. When 50-fold of Mg^{2+} or 76-fold of Ca^{2+} is added, the adsorption capacity of the copper-imprinted

silica gel is nearly unaffected, whereas the nonimprinted silica gel exhibits much lower adsorption capacity.

To better understand the system, the structure of immobilized triglycine in the presence of Cu^{2+} is investigated by using FTIR. The FTIR results show that the loop structure of triglycine is maintained even after Cu^{2+} is completely removed from the triglycine-Cu^{2+} complex. The retention of triglycine conformation is because of the formation of hydrogen bonds between adjacent triglycine molecules. Therefore, the conformations of triglycine on the surface caused by the immobilization procedure can lead to superior complexation capability and selectivity for Cu^{2+}. Similarly, two His-containing tripeptides (His-Gly-Gly and Gly-Gly-His) are immobilized on the surface and the effects of packing density of these tripeptides on their abilities to complex Cu^{2+} are studied. It is concluded that the complexation of tripeptides with Cu^{2+} highly depends on the position of His residue in the tripeptide sequence. Gly-Gly-His functionalized surface has a higher complexation capability to Cu^{2+} than His-Gly-Gly functionalized surface, which can be attributed to the different binding mode of the two tripeptides. In addition, the surface crowdedness might lower the Cu^{2+} binding capability. It is found that the Cu^{2+} complexation capability of a copper-imprinted surface functionalized with Gly-Gly-His is 62% higher than a nonimprinted surface, because more stable Cu^{2+} complexes whose formation requires the proper intermolecular distance of two immobilized tripeptide molecules can be obtained when the ion-imprinting technique is employed.

Secondly, the oligopeptide-modified SiNWs can be used as a channel in an FET configuration to detect the presence of metal ions in aqueous solution. When the SiNWs modified with Gly-Gly-His are exposed to Cu^{2+} solution, the conductance changes of the SiNWs increase linearly with the logarithm of the Cu^{2+} concentrations. This can be attributed to the formation of a stable complexation between Cu^{2+} and Gly-Gly-His. Moreover, Gly-Gly-His-modified SiNWs show higher selectivity and sensitivity for Cu^{2+} than the Gly-His-Gly-modified ones. Even in the presence of 100-fold Zn^{2+} as interfering ions, the SiNW-based sensor shows real-time and reversible responses for Cu^{2+} as low as 1 nM. Moreover, because the SiNWs can be fabricated by using "top-down" method, each SiNW can serve as an individual sensor. Therefore, we develop a multichannel metal ion sensor by immobilizing two different oligopeptides (copper- and lead-selective oligopeptide) on two distinct addressable SiNW arrays. Both Pb^{2+} and Cu^{2+} can be simultaneously and quantitatively detected by using this sensor. The simplicity, high sensitivity, capability of selective multiplexed detection of different metal ions suggests that the SiNWs arrays can move beyond current technologies and have the potential for environmental monitoring, waste water treatment, and clinical toxicology caused by heavy metal ions.

Thirdly, to control the orientations of immobilized oligopeptides, we develop an immobilization strategy through the formation of thiazolidine ring between N-terminal cysteine and surface aldehyde groups. When an oligopeptide with an N-terminal cysteine label and multiple lysines is immobilized on the

aldehyde-terminated surface, the N-terminal cysteine quickly reacts with surface aldehydes to form a stable thiazolidine ring, which prevents lysines from reacting with aldehydes. This immobilization strategy can lead to well-defined orientations of immobilized oligopeptide and has great influence on its ability as an enzyme substrate. Based on ellipsometry, XPS, and ATR-FTIR results, we conclude that trypsin can cleave the oligopeptide with measurable changes only if the oligopeptide is vertically immobilized on the surface.

Next, when glycine oligomers are immobilized on the surface, they contribute to different increases of thicknesses depending on their molecular lengths. When a thin layer of LC 5CB is supported on the surface, the orientations of 5CB are disrupted if the increase of thickness is above 0.5 ± 0.1 nm. This phenomenon suggests that the orientations of LC are very sensitive to the lengths or surface densities of the immobilized oligopeptides. This phenomenon also forms the basis of using LC for detecting proteases because they can cleave immobilized oligopeptides and decrease their lengths or densities. Therefore, we develop a simple and label-free LCs-based multiplexed protease assay which easily reports the enzymatic activity. When an oligopeptide microarray is immersed in a trypsin solution by using the gradient immersion time mode, an interesting optical bar chart having clear cut-off points can be obtained. This optical bar chart is very different from the continuous intensity profile found in most fluorescence assays and it allows us to determine the concentration of trypsin with high sensitivity and low detection limit (~0.05 μg/mL). This technique also can be used for detecting other proteases such as chymotrypsin

with high specificity or differentiating two oligopeptides with difference only in one of the residues in their sequences.

Finally, if the LC 5CB is doped with PBA, it undergoes a dark-to-bright optical transition within a very small pH range (between 7.0 and 6.9). Therefore, the LC-based sensor can be used for pH detection. The optical transition of 5CB can be understood in terms of the orientational transitions induced by the competition between protonation and deprotonation of PBA at the aqueous/LC interface. This high pH sensitivity of the LC based sensor would have great promise for monitoring local pH change resulting from some enzymatic reactions. As a proof of concept, penicillinase is used as the model system to detect penicillin G down to 1 nM in 7 min. The LC-based pH sensor is also a useful tool for the kinetic studies of penicillinase. The good spatial resolution and capability of LC based sensor for sensitive, specific, and quantitative monitoring enzymatic reactions can be exploited for array-based screening and therapeutic applications.

11.2 Recommendations

Based on the conclusions obtained in our previous work, recommendations are given below.

First of all, the peptide-based microarrays have been developed as a powerful tool to study a variety of interactions, including peptide-enzyme, peptide-protein, peptide-DNA, peptide-small molecule, and peptide-cell over the past few years, the full potential of the peptide microarray technology has not been realized. To produce

an effective peptide microarray, the attachment of peptides on the surface through covalent reactions should be further developed in the future such that the oligopeptides can be immobilized on various surfaces, such as carboxylic acid-, epoxy-, and isothiocyanate-functionalized surfaces, etc.

Second, detecting and quantifying the concentrations of metal ions with high specificity are important analytical problems. Outstanding Cu^{2+} binding ability has been reported for His-containing tripeptide, Gly-Gly-His, in chapter 4 and 5. Since Ni^{2+} also binds to Gly-Gly-His with similar tetragonal geometry as Cu^{2+}, Ni^{2+} would be a good choice for testing its interference against Cu^{2+}.

Moreover, it is known that the "top-down" semiconductor processing permits the production of hundreds of identical SiNWs in an array format, and thus each SiNW can serve as an individual sensor which can respond to its own target analyte. By attaching different peptides to the nanowire surfaces, SiNWs can be converted to multiplexed sensors for high-throughput immunoassay. As a proof of concept, the peptides with sequences of CDYKDDDDK (FLAG epitope tag), CDAKDDDDK, CDYADDDDK, and CDYKDADDK can be immobilized on four SiNW clusters. If antibody solutions are delivered to the SiNW surfaces, the interactions of the FLAG epitope tag and monoclonal anti-FLAG M_2 can be monitored by the conductance changes of SiNWs.

On the other hand, since the LC-based detection approaches are highly sensitive, real-time, and label-free, the development of an LC-based sensor is important. Previous studies of ours and others have demonstrated that the anchoring energy of

LCs is very small, so a molecular alignment of LCs can be easily influenced by the introduction of ionizable groups to surfaces or the addition of electrolytes to LCs. If we dope LCs with a long hydrocarbon chain-terminated function, such as lauric aldehyde, LCs will assume a homeotropic orientation at the aqueous/LC interface. Moreover, the aldehyde groups presented at the aqueous/LC interface can react with the peptides and form a peptide-decorated (including CDYKDDDDK, CDAKDDDDK, CDYADDDDK, and CDYKDADDK) interface. The monoclonal anti-FLAG M_2 can be detected based on the orientational transitions of LCs.

Finally, the LC-based technology will provide a great contribution to the design of biomolecular interfaces based on orientational transitions of LCs at which interactions involving enzymes, proteins, cells, viruses, DNA, and other biological species can be investigated. It is known that dengue virus is a single-stranded RNA flavivirus which is the causative agent associated with many severe diseases in humans. Infection by dengue virus may cause dengue hemorrhagic fever or dengue shock syndrome. Unfortunately, up to date, there is no causative antiviral chemotherapy available for the cure of severe forms of dengue diseases. Dengue virus genome encodes three structural (C, prM, and E) and seven non-structural (NS1, NS2A, NS2B, NS3, NS4A, NS4B, and NS5) proteins. One of the most promising methods of an effective antiviral therapy is the development of small molecule inhibitors directed against the viral NS3 serine protease, which is an essential component for the maturation of the dengue virus polyprotein. NS3 protease displays a marked sensitivity to product inhibition by peptides. Therefore, reliable monitoring product inhibition is regarded as an attractive

therapeutic target for the dengue virus infections. In the future, the LC-based biosensor can be developed to monitor NS3 protease relevant to dengue virus because of its sensitivity to product inhibition by peptides. The mechanism of cleavage of peptides by NS3 protease is shown in Figure 11.1. Because proton is consumed in this process and it will cause pH to increase. Therefore, we hypothesize that the developed LC-based assay based on the penicillinase-penicillin system in **Chapter 10** can also be used to monitor the NS3 protease inhibition.

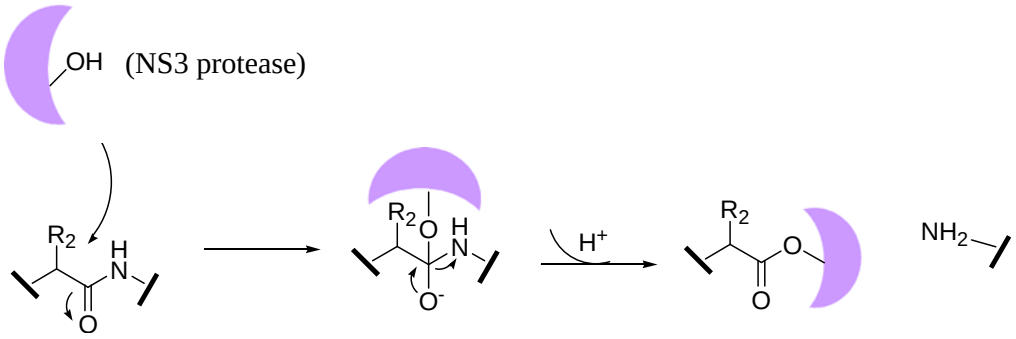

Figure 11.1 NS3 Protease cleavage mechanism.

REFERENCES

1. Abouzar, M. H.; Poghossian, A.; Razavi, A.; Besmehn, A.; Bijnens, N.; Williams, O. A.; Haenen, K.; Wagner, P.; Schoning, M. J. Penicillin detection with nanocrystalline-diamond field-effect sensor. *phys. stat. sol. (a)* **2008**, *205*, 2141-2145.
2. Agarwal, A., Buddharaju, K., Lao, I. K., Singh, N., Balasubramanian, N., Kwong, D. L. Silicon nanowire sensor array using top–down CMOS technology. *Sens. Actuator A* **2008**, *145-146*, 207-213.
3. Aggarwal, S. K.; Kinter, M.; Herold, D. A**.** Determination of lead in urine and whole blood by stable isotope dilution gas chromatography-mass spectrometry**.** *Clin. Chem.* **1994**, *40*, 1494-1502.
4. Alivisatos, P. The use of nanocrystals in biological detection. *Nat. Biotechnol.* **2004**, *22*, 47-52.
5. Andersson, L. I.; Müller, R.; Vlatakis, G.; Mosbach, K. Mimics of the binding sites of opioid receptors obtained by molecular imprinting of enkephalin and morphine. *Proc. Natl. Acad. Sci, U. S. A.* **1995**, *92*, 4788-4792.
6. Arrigan, D. W. M.; Bihan, L. L. A study of L-cysteine adsorption on gold *via* electrochemical desorption and copper (II) ion complexation. *Analyst* **1999**, *124*, 1645-1649.
7. Asanuma, H.; Lopinski, G. P.; Yu, H. Z. Kinetic control of the photochemical reactivity of hydrogen-terminated silicon with bifunctional molecules. *Langmuir* **2005**, *21*, 5013-5018.
8. Austrian, R.; Gold, J. Pneumococcal bacteremia with especial reference to bacteremic pneumococcal pneumonia. *Ann. Intern. Med.* **1964**, *60*, 759-766.
9. Banerjee, I. A.; Yu, L.; Matsui, H. Cu nanocrystal growth on peptide nanotubes by biomineralization: size control of Cu nanocrystals by tuning peptide conformation. *Proc. Natl. Acad. Sci. USA* **2003**, *100*, 14678-14682.
10. Banerjee, D.; Srivastava, S. K.; Pal, S. K. Spectroscopic studies on ligand-enzyme interactions: complexation of α-chymotrypsin with 4',6-diamidino-2-phenylindole (DAPI). *J. Phys. Chem. B* **2008**, *112*, 1828-1833.
11. Barrett, A. J.; Rawlings, N. D.; Woessner, J. F. *Handbook of proteolytic enzyme*, Vol. 2, 2nd Ed. Elsevier: London, **2004**.
12. Bannon, D. I.; Murashchik, C.; Zapf, C. R.; Farfel, M. R.; Chisolm Jr., J. J. Graphite furnace atomic absorption spectroscopic measurement of blood lead in matrix-matched standards**.** *Clin. Chem.* **1994**, *40*, 1730-1734.

13. Beckett, R. P.; Davidson, A. H.; Drummond, A. H.; Huxley, P.; Whittaker, M. Recent advances in matrix metalloproteinase inhibitor research. *Drug Discov. Today* **1996**, *1*, 16-26.

14. Bergveld, P.; Sibbald, A. *Analytical and biomedical applications of ion selective field effect transistors*, Elsevier, Amsterdam. **1988**

15. Berridge, M. J.; Bootman, M. D.; Lipp, P. Calcium- a life and death signal. *Nature* **1998**, *395*, 645-648.

16. Bi, X.; Yang, K. L. Immobilization of oligoglycines on aldehyde-decorated surfaces and its influence on the orientations of liquid crystals. *Colloids Surf. A* **2007**, *302***,** 573-580.

17. Bi, X.; Wong, W. L.; Ji, W.; Agarwal, A.; Balasubramanian, N.; Yang, K. L. Development of electrochemical calcium sensors by using silicon nanowires modified with phosphotyrosine. *Biosens. Bioelectron.* **2008**, *23*, 1442-1448.

18. Bi, X.; Yang, K. L. On-line monitoring imidacloprid and thiacloprid in celery juice using quartz crystal microbalance. *Anal. Chem.* **2009**, *81*, 527-532.

19. Bienvenut, W. V. in *Acceleration and improvement of protein identification by mass spectrometry*. Dordrecht Springer Science & Business Media **2005**.

20. Blackburn, G. F. in *Biosensors Fundamentals and applications*, Turner, A. P. F.; Karube, I.; Wilson, G. S. Eds. Oxford Univ. Press, Oxford, **1987**.

21. Bowins, R. J.; McNutt, R. H. Electrothermal isotope dilution inductively coupled plasma mass spectrometry method for the determination of sub-ng ml^{-1} levels of lead in human plasma. *J. Anal. At. Spectrom.* **1994**, *9*, 1233-1236.

22. Brake, J. M.; Abbott, N. L. An experimental system for imaging the reversible adsorption of amphiphiles at aqueous-liquid crystal interfaces. *Langmuir* **2002**, *16*, 6101-6109.

23. Brake, J. M.; Daschner, M. K.; Luk, Y. Y.; Abbott, N. L. Biomolecular interactions at phospholipid-decorated surfaces of liquid crystals. *Science* **2003a**,*302*, 2094-2097.

24. Brake, J. M.; Mezera, A. D.; Abbott, N. L. Active control of the anchoring of 4'-pentyl-4-cyanobiphenyl (5CB) at an aqueous-liquid crystal interface by using a redox-active ferrocenyl surfactant. *Langmuir* **2003b**, *19*, 8629-8637.

25. Branden, C.; Tooze, J. *Introduction to Protein Structure* (2^{nd} Ed.); Garland Publishing: New York, **1999**.

26. Bunimovich, Y. L.; Shin, Y. S.; Yeo, W. S.; Amori, M.; Kwong, G.; Heath, J. R. Quantitative real-time measurements of DNA hybridization with alkylated nonoxidized silicon nanowires in electrolyte solution. *J. Am. Chem. Soc.* **2006**, *128*, 16323-16331.

27. Burger, K. et. al. In *Biocoordination Chemistry: Coordination Equilibria in Biologically Active Systems* Ellis Horwood, **1990**.

28. Bush, K. β-lactamase inhibitors from laboratory to clinic. *Clin. Microbiol. Rev.* **1988**, *1*, 109-123.

29. Bussow, K.; Cahill, D.; Nietfeld, W.; Bancroft, D.; Scherzinger, E.; Lehrach, H.; Walter, G. A method for global protein expression and antibody screening on high-density filters of an arrayed cDNA library. *Nucleic Acids Res.* **1998**, *26*, 5007-5008.

30. Caras, S. D.; Janata, J. Field effect transistor sensitive to penicillin. *Anal. Chem.* **1980**, *52*, 1935-1937.

31. Cha, T.; Guo, A.; Jun, Y.; Pei, D.; Zhu, X. Y. Immobilization of orientated protein molecules on poly(ethylene glycol)-coated Si(111). *Proteomics* **2004**, *4*, 1965-1976.

32. Chailapakul, O.; Crooks, R. M. Synthesis and characterization of simple self-assembling, nanoporous monolayer assemblies: a new strategy for molecular recognition. *Langmuir* **1993**, *9*, 884-888.

33. Chidsey, C. E. D.; Bertozzi, C. R.; Putvinski, T. M.; Mujsce, A. M. Coadsorption of ferrocene-terminated and unsubstituted alkanethiols on gold: electroactive self-assembled monolayers. *J. Am. Chem. Soc.* **1990**, *112*, 4301-4306.

34. Chow, E.; Hibbert, D. B.; Gooding, J. J. Electrochemical detection of lead ions via the covalent attachment of human angiotensin I to mercaptopropionic acid and thioctic acid self-assembled monolayers. *Anal. Chim. Acta*, **2005a**, *543*, 167-176.

35. Chow, E.; Hibbert, D. B.; Gooding, J. J. His-Ser-Gln-Lys-Val-Phe as a selective ligand for the voltammetric determination of Cd^{2+}. *Electrochem. Commun.* **2005b**, *7*, 101-106.

36. Chow, E.; Wong E. L. S.; Bocking, T.; Nguyen, Q. T.; Hibbert, D. B.; Gooding, J. J. Analytical performance and characterization of MPA-Gly-Gly-His modified sensors. *Sens. Actuators B* **2005c**, *111-112*, 540-548.

37. Chow, E.; Gooding, J. J. Peptide-modified electrodes as electrochemical metal ion sensors. *Electroanalysis* **2006**, *18*, 1437-1448.

38. Clare, B. H.; Abbott, N. L. Orientations of nematic liquid crystals on surfaces presenting controlled densities of peptides: amplification of protein-peptide binding events. *Langmuir* **2005**, *21*, 6451-6461.

39. Collings, P. J. *Liquid Crystal*, Princeton University Pr. **2002**.

40. Collins, P. G.; Arnold, M. S.; Avouris, P. Engineering carbon nanotubes and nanotube circuits using electrical breakdown. *Science* **2001**, *292*, 706-709.

41. Cui, Y.; Duan, X.; Hu, J.; Lieber, C. M. Doping and electrical transport in silicon nanowires. *J. Phys. Chem. B* **2000**, *104*, 5213-5216.

42. Cui, Y.; Wei, Q.; Park, H.; Lieber, C. M. Nanowire nanosensors for highly sensitive and selective detection of biological and chemical species. *Science* **2001a**, *293*, 1289-1292.

43. Cui, Y.; Lieber, C. M. Functional nanoscale electronic devices assembled using silicon nanowire building blocks. *Science* **2001b**, *291*, 851-853.

44. Curreli, M.; Li, C.; Sun, Y.; Lei, B.; Gundersen, M. A.; Thompson, M. E.; Zhou, C. Selective functionalization of In_2O_3 nanowire mat devices for biosensing applications. *J. Am. Chem. Soc.* **2005**, *127*, 6922-6923.

45. Dai, S.; Burleigh, M. C.; Shin, Y.; Morrow, C. C.; Barnes, C. E.; Xue, Z. Imprint coating: a novel synthesis of selective functionalized ordered mesoporous sorbents. *Angew. Chem. Int. Ed.* **1999**, *38*, 1235-1239.

46. Daniele, P. G.; Zerbinati, O.; Zelano, V.; Ostacoli, G. Thermodynamic and spectroscopic study of copper (II)-glycyl-$_L$-histidylglycine complexes in aqueous solution. *Dalton Trans.* **1991**, 2711-2715.

47. Darwish, I. A.; Blake, D. A. Development and validation of a one-step immunoassay for determination of cadmium in human serum. *Anal. Chem.* **2002**, *74*, 52-58.

48. Deo, S.; Godwin, H. A. A selective, ratiometric fluorescent sensor for Pb^{2+}. *J. Am. Chem. Soc.* **2000**, *122*, 174-175.

49. Deschamps, P.; Kulkarni, P. P.; Gautam-Basak, M.; Sarkar, B. The saga of copper (II)-$_L$-histidine. *Coord. Chem. Rev.* **2005**, *249*, 895-909.

50. Disalvo, E. A.; Simon, S. A. Ed. CRC Press, **1995**.

51. Domansky, K.; Janata, J.; Josowicz, M.; Petelenz, D. Present state of fabrication of chemically sensitive field effect transistors- plenary lecture. *Analyst* **1993**, *118*, 335-340.

52. Duan, Y. J.; Laursen, R. A. Protease substrate specificity mapping using membrane-bound peptides. *Anal. Biochem.* **1994**, *216*, 431-438.

53. Duan, X.; Wang, J.; Lieber, C. M. Synthesis and optical properties of gallium arsenide nanowires. *Appl. Phys. Lett.* **2000a**, *76*, 1116.

54. Duan, X.; Lieber, C. M. Laser-assisted catalytic growth of single crystal GaN nanowires. *J. Am. Chem. Soc.* **2000b**, *122*, 188-189.

55. Duan, X.; Lieber, C. M. General synthesis of compound semiconductor nanowires. *Adv. Mater.* **2000c**, *12*, 298-302.

56. Duan, X.; Huang, Y.; Cui, Y.; Wang, J.; Lieber, C. M. Indium phosphide nanowires as building blocks for nanoscale electronic and optoelectronic devices. *Nature* **2001**, *409*, 66-69.

57. Edsall, J. T.; Felsenfeld, G.; Goodman, D. S.; Gurd, F. R. N. The association of imidazole with the ions of zinc and cupric copper[1a,b,c]. *J. Am. Chem. Soc.* **1954**, *76*, 3054-3061.

58. Evangelio, E.; Hernando, J.; Imaz, I.; Bardaji, G. G.; Alibes, R.; Busque, F.; Ruiz-Molina, D. Catechol derivatives as fluorescent chemosensors for wide-range pH detection. *Chem. Eur. J.* **2008**, *14*, 9754-9763.

59. Evans, S. D.; Ulman, A.; Goppert-Berarducci, K. E.; Gerenser, L. J. Self-assembled multilayers of omega-mercaptoalkanoic acids: selective ionic interactions. *J. Am. Chem. Soc.* **1991**, *113*, 5866-5868.

60. Falsey, J. R.; Renil, M.; Park, S.; Li, S.; Lam, K. S. Peptide and small molecule microarray for high throughput cell adhesion and functional assays. *Bioconjugate Chem.* **2001**, *12*, 346-353.

61. Fang, G. Z.; Tan, J.; Yan, X. P. Synthesis and evaluation of an ion-imprinted functionalized sorbent for selective separation of cadmium ion. *Sep. Sci. Technol.* **2005a**, *40*, 1597-1608.

62. Fang, G. Z.; Tan, J.; Yan, X. P. An ion-imprinted functionalized silica gel sorbent prepared by a surface imprinting technique combined with a sol-gel process for selective solid-phase extraction of cadmium (II). *Anal. Chem.* **2005b**, *77*, 1734-1739.

63. Feng, X.; Fryxell, G. E.; Wang, L.-Q.; Kim, A. Y.; Liu, J.; Kemner, K. M. Functionalized monolayers on ordered mesoporous supports. *Science* **1997**, *276*, 923-926.

64. Finland, M. Adventures with antibacterial drugs. *Clin. Pharmacol. Ther.* **1972**, *13*, 469-511.

65. Forzani, E. S.; Zhang, H.; Chen, W.; Tao, N. Detection of heavy metal ions in drinking water using a high-resolution differential surface plasmon resonance sensor. *Environ. Sci. Technol.* **2005**, *39*, 1257-1262.

66. Galarneau, A.; Primeau, M.; Trudeau, L. E.; Michnick, S. W. β-Lactamase protein fragment complementation assays as *in vivo* and *in vitro* sensors of protein-protein interactions. *Nat. Biotechnol.* **2002**, *20*, 619-622.

67. Gan, Z. B.; Marquardt, R. R.; Xiao, H. Protease and protease inhibitor assays using biotinylated casein coated on a solid phase. *Anal. Biochem.* **1999**, *268*, 151-156.

68. Gao, Z.; Agarwal, A.; Trigg, A. D.; Singh, N.; Fang, C.; Tung, C. H.; Fan, Y.; Buddharaju, K. D.; Kong, J. Silicon nanowire arrays for label-free detection of DNA. *Anal. Chem.* **2007**, *79*, 3291-3297.

69. Gershevitz, O.; Sukenik, C. N. In situ FTIR-ATR analysis and titration of carboxylic acid-terminated SAMs. *J. Am. Chem. Soc.* **2004**, *126*, 482-483.

70. Gooding, J. J.; Praig, V. G.; Hall, E. A. H. Platinum-catalyzed enzyme

electrodes immobilized on gold using self-assembled layers. *Anal. Chem.* **1998**, *70*, 2396-2402.

71. Gooding, J. J.; Hibbert, D. B.; Yang, W. Electrochemical metal ion sensors. Exploiting amino acids and peptides as recognition elements. *Sensors* **2001**, *1*, 75-90.

72. Graf, L.; Jancso, A.; Szilagyi, L.; Hegyi, G.; Pinter, K.; Naray-Szabo, G.; Hepp, J.; Medzihradszky, K.; Rutter, W. J. Electrostatic complementarity within the substrate-binding pocket of trypsin. *Proc. Natl. Acad. Sci. USA* **1988**, *85*, 4961-4965.

73. Gupta, V. K.; Skaife, J. J.; Dubrovsky, T. B.; Abbott, N. L. Optical amplification of ligand-receptor binding using liquid crystals. *Science* **1998**, *279*, 2077-2080.

74. Haab, B. B.; Dunham, M. J.; Brown, P. O. Protein microarrays for highly parallel detection and quantitation of specific proteins and antibodies in complex solutions. *Genome Biol.* **2001**, *2*, 0004.

75. Hafeman, D. G.; Parce, J. W.; McConnell, H. M. Light-addressable potentiometric sensor for biochemical system. *Science* **1988**, *240*, 1182-1185.

76. Hahm, J. I.; Lieber, C. M. Direct ultrasensitive electrical detection of DNA and DNA sequence variations using nanowire nanosensors. *Nano Lett.* **2004**, *4*, 51-54.

77. Hai, A.; Ben-Haim, D.; Korbakov, N.; Cohen, A.; Shappir, J.; Oren, R.; Spira, M. E.; Yitzchaik, S. Acetylcholinesterase-ISFET based system for the detection of acetylcholine and acetylcholinesterase inhibitors. *Biosens. Bioelectron.* **2006**, *22*, 605-612.

78. Hall, B. G. Predicting the evolution of antibiotic resistance genes. *Nat. Rev. Microbiol.* **2004,** *2*, 430-435.

79. Hartl, A.; Schmich, E.; Garrido, J. A.; Hernando, J.; Catharino, S. C. R.; Walter, S.; Feulner, P.; Kromka, A.; Steinmüller, D.; Stutzmann, M. Protein-modified nanocrystalline diamond thin films for biosensor applications. *Nat. Mater.* **2004**, *3*, 736-742.

80. Hartl, A.; Baur, B.; Stutzmann, M.; Garrido, J. A. Enzyme-modified field effect transistors based on surface-conductive single-crystalline diamond. *Langmuir* **2008***, 24*, 9898-9906.

81. Hartono, D.; Bi, X.; Yang, K. L.; Yung, L. Y. L. An air-supported liquid crystal system for real-time and albel-free characterization of phospholipases and their inhibitors. *Adv. Funct. Mater.* **2008**, *18*, 2938-2945.

82. Hassen, W. M.; Abdelghani, A.; Vonna, L.; Cherif, K.; Boussaid, M.; Maaref, M. A. Electrochemical properties and topology of gold electrodes with adsorbed penicillin G for biosensor applications. *Sens. Actuators B* **2007**, *120*, 621-627.

83. Haupt, K. Peer reviewed: molecularly imprinted polymers: the next generation. *Anal. Chem.* **2003**, *75*, 376A-383A.

84. Hillberg, A. L.; Brain, K. R.; Allender, C. J. Molecular imprinted polymer sensors: implications for therapeutics. *Adv. Drug Delivery Rev.* **2005**, *57*, 1875-1889.

85. Hind, A. R.; Bhargava, S. K.; Grocott, S. C. Attenuated total reflection fourier transform infrared spectroscopic investigation of the solid/aqueous interface of low surface area, water-soluble solids in high ionic strength, highly alkaline, aqueous media. *Langmuir* **1997a**, *13*, 3483-3487.

86. Hind, A. R.; Bhargava, S. K.; Grocott, S. C. Adsorption of quaternary ammonium compounds on the surface of sodium oxalate: FTIR/ATR investigation under high-ionic-strength, highly alkaline conditions. *Langmuir* **1997b**, *13*, 6255-6259.

87. Hirashima, Y.; Sato, H.; Suzuki, A. ATR-FTIR spectroscopic study on hydrogen bonding of poly(*N*-isopropylacrylamide-*co*-sodium acrylate) gel. *Macromolecules* **2005**, *38*, 9280-9286.

88. Hong, B. J.; Oh, S. J.; Youn, T. O.; Kwon, S. H.; Park, J. W. Nanoscale-controlled spacing provides DNA microarrays with the SNP discrimination efficiency in solution phase. *Langmuir* **2005**, *21*, 4257-4261.

89. Hoogboom, J.; Velonia, K.; Rasing, T.; Rowan, A. E.; Nolte, R. J. M. LCD-based detection of enzymatic action. *Chem. Commun.* **2006**, 434-435.

90. Horton, R. C.; Herne, T. M.; Myles, D. C. Aldehyde-terminated self-assembled monolayers on gold: immobilization of amines onto gold surfaces. *J. Am. Chem. Soc*. **1997**, *119*, 12980-12981.

91. Houseman, B. T.; Huh, J. H.; Kron, S. J.; Mrksich, M. Peptide chips for the quantitative evaluation of protein kinase activity. *Nat. Biotechnol.* **2002**, *20*, 270-274.

92. Hu, P.; Loo, J. A. Gas-phase coordination properties of Zn^{2+}, Cu^{2+}, Ni^{2+}, and Co^{2+} with histidine-containing peptides. *J. Am. Chem. Soc.* **1995**, *117*, 11314-11319.

93. Hu, J.; Ouyang, M.; Yang, P.; Lieber, C. M. Controlled growth and electrical properties of heterojunctions of carbon nanotubes and silicon nanowires. *Nature* **1999**, *399*, 48-51.

94. Huang, S. C.; Caldwell, K. D.; Lin, J. N.; Wang, H. K.; Herron, J. N. Site-specific immobilization of monoclonal antibodies using spacer-mediated antibody attachment. *Langmuir* **1996**, *12*, 4292-4298.

95. Hunter, R. J. *Introduction to modern colloid science (1st Ed.)*, Oxford university press. **1993**.

96. Im, H.; Huang, X. J.; Gu, B.; Choi, Y. K. A dielectric-modulated field-effect transistor for biosensing. *Nature Nanotechnology* **2007**, *2*, 430-434.

97. Israelachvili, J. *Intermolecular and surface forces*. Academic Press: London, **1985**.

98. Jaffrezic-Renault, N.; Chovelon, J. M.; Perrot, H.; Perchec, P. L.; Chevalier, Y. Ion-sensitive field-effect transistor sensors with a covalently bound monolayer membrane: example of calcium detection. *Sens. Actuators B* **1991**, *5*, 67-70.

99. Jal, P. K.; Patel, S.; Mishra, B. K. Chemical modification of silica surface by immobilization of functional groups for extractive concentration of metal ions. *Talanta* **2004**, *62*, 1005-1028.

100. Janata, J. Historical review. Twenty years of ion-selective field-effect transistors. *Analyst* **1994**, *119*, 2275-2278.

101. Janata, J.; Huber, R. J. *Solid state chemical sensors*. Academic Press. **1985**.

102. Jang, C. H.; Cheng, L. L.; Olsen, C. W.; Abbott, N. L. Anchoring of nematic liquid crystals on viruses with different envelop structures. *Nano Lett.* **2006**, *6*, 1053-1058.

103. Jensen, K. K.; Orum, H.; Nielsen, P. E.; Norden, B. Kinetics for hybridization of peptide nucleic acids (PNA) with DNA and RNA studied with the BIAcore technique. *Biochemistry* **1997**, *36*, 5072-5077.

104. Jerome, B. Surface effects and anchoring in liquid crystals. *Rep. Prog. Phys.* **1991**, *54*, 391-452.

105. Johnsson, B.; Lofas, S.; Lindquist, G. Immobilization of proteins to a carboxymethyldextran-modified gold surface for biospecific interaction analysis in surface Plasmon resonance sensors. *Anal. Biochem.* **1991**, *198*, 268-277.

106. Johnson, L. L.; Dyer, R.; Hupe, D. J. matrix metalloproteinases. *Curr. Opin. Chem. Biol.* **1998**, *2*, 466-471.

107. Kahn, F. J. Orientation of liquid crystals by surface coupling agents. *Appl. Phys. Lett.* **1973**, *22*, 386.

108. Karlsson, H., Larsson, T., Karlsson, K. A., Miller-Podraza, H. Polyglycosylceramides recognized by *Helicobacter pylori*: analysis by matrix-assisted laser desorption/ionization mass spectrometry after degradation with wndo-β-galactosidase and by fast atom bombardment mass spectrometry of permethylated undegraded material. *Glycobiology*, **2000**, *10*, 1291-1309.

109. Kemmler, W.; Peterson, J. D.; Steiner, D. F. Studies on the conversion of proinsulin to insulin. I. Conversion *in vitro* with trypsin and carboxypeptidase B. *J. Biol. Chem.* **1971**, *246*, 6786-6791.

110. Kim, M. K.; Martell, A. E. Copper (II) complexes of triglycine and

tetraglycine. *J. Am. Chem. Soc.* **1966**, *88*, 914-918.

111. Kim, M. K.; Martell, A. E. Proton nuclear magnetic resonance study of metal-glycine peptide complexes. Copper (II) and nickel (II) complexes. *J. Am. Chem. Soc.* **1969**, *91*, 872-878.

112. Kim, S. R.; Abbott, N. L. Rubbed films of functionalized bovine serum albumin as substrates for the imaging of protein-receptor interactions using liquid crystals. *Adv. Mater.* **2001**, *13*, 1445-1449.

113. Kim, H. R.; Kim, J. H.; Kim, T. S.; Oh, S. W.; Choi, E. Y. Optical detection of deoxyribonucleic acid hybridization using an anchoring transition of liquid crystal alignment. *Appl. Phys. Lett.* **2005**, *87*, 143901.

114. Kim, A.; Ah, C. S.; Yu, H. Y.; Yang, J. H.; Baek, I. B.; Ahn, C. G.; Park, C. W.; Jun, M. S.; Lee, S. Ultrasensitive, label-free, and real-time immunodetection using silicon field-effect transistors. *Appl. Phys. Lett.* **2007,** *91*, 103901.

115. Kinsinger, M. I.; Sun, B.; Abbott, N. L.; Lynn, D. M. Reversible control of ordering transitions at aqueous/liquid crystal interfaces using functional amphiphilic polymers. *Adv. Mater.* **2007**, *19*, 4208-4212.

116. Köhn, M.; Wacker, R.; Peters, C.; Schröder, H.; Soulère, L.; Breinbauer, R.; Niemeyer, C. M.; Waldmann, H. Staudinger ligation: a new immobilization strategy for the preparation of small-molecule arrays. *Angew. Chem. Int. Ed.* **2003**, *42*, 5830-5834.

117. Kong, J.; Franklin, N. R.; Zhou, C.; Chapline, M. G.; Peng, S.; Cho, K.; Dai, H. Nanotube molecular wires as chemical sensors. *Science* **2000**, *287*, 622-625.

118. Kozlowski, H.; Bal, W.; Dyba, M.; Kowalik-Jankowska, T. Specific structure-stability relations in metallopeptides. *Coord. Chem. Rev.* **1999**, *184*, 319-346.

119. Kozlowski, H.; Kowalik-Jankowska, T.; Jezowska,-Bojczuk, M. Chemical and biological aspects of Cu^{2+} interactions with peptides and aminoglycosides. *Coord. Chem. Rev.* **2005**, *249*, 2323-2334.

120. Krasnoslobodtsev, A. V.; Smirnov, S. N. Effect of water on silanization of silica by trimethoxysilanes. *Langmuir* **2002**, *18*, 3181-3184.

121. Kuby, S. A. Ed. A study of enzymes. vol. 1, CRC Press: Boca Raton, Florida, **1991**.

122. Kuchen, W.; Schram, J. Metal-ion-selective exchange resins by matrix imprint with methacrylates. *Angew. Chem. Int. Ed. Engl.* **1988**, *27*, 1695-1697.

123. Kumar, B.; Singh, H. B.; Katyal, M.; Sharma, R. L. *Mikrochim. Acta* **1991**, *III*, 79.

124. Lam, K. F.; Yeung, K. L.; McKay, G. A rational approach in the design of selective mesoporous adsorbents. *Langmuir* **2006**, *22*, 9632-9641.

125. Lau, S. J.; Kruck, T. P. A.; Sarkar, B. A peptide molecule mimicking the copper (II) transport site of human serum albumin. A comparative study between the synthetic site and albumin. *J. Biol. Chem.* **1974**, *249*, 5878-5884.

126. Law, M.; Kind, H.; Messer, B.; Kim, F.; Yang, P. Photochemical sensing of NO_2 with SnO_2 nanoribbon nanosensors at room temperature. *Angew. Chem. Int. Ed.* **2002**, *41*, 2405-2408.

127. Lee, S. W.; Foley, E. J.; Epstein, J. A. Mode of action of penicillin I. Bacterial growth and penicillin activity-*Staphylococcus aureus* FDA. *J. Bacteriol.* **1944**, *48*, 393-399.

128. Lee, J. M.; Park, H. K.; Jung, Y.; Kim, J. K.; Jung, S. O.; Chung, B. H. Direct immobilization of protein G variants with various numbers of cysteine residues on a gold surface. *Anal. Chem.* **2007**, *79*, 2680-2687.

129. Lemieux, G. A.; Bertozzi, C. R. Chemoselective ligation reactions with proteins, oligosaccharides and cells. *Trends Biotechnol.* **1998**, *16*, 506-513.

130. Lequart, C.; Nuzillard, J. M.; Kurek, B.; Debeire, P. Hydrolysis of wheat bran and straw by an endoxylanase: production and structural characterization of cinnamoyl-oligosaccharides. *Carbohydr. Res.* **1999**, *319*, 102-111.

131. Lesaicherre, M. L.; Uttamchandani, M.; Chen, G. Y. J.; Yao, S. Q. Developing site-specific immobilization strategies of peptides in a microarray. *Bioorg. Med. Chem. Lett.* **2002a**, *12*, 2079-2083.

132. Lesaicherre, M. L.; Uttamchandani, M.; Chen, G. Y. J.; Yao, S. Q. Antibody-based fluorescence detection of kinase activity on a peptide array. *Bioorg. Med. Chem. Lett.* **2002b**, *12*, 2085-2088.

133. Letant, S. E.; Hart, B. R.; Kane, S. R.; Hadi, M. Z.; Shields, S. J.; Reynolds, J. G. Enzyme immobilization on porous silicon surfaces. *Adv. Mater.* **2004**, *16*, 689-693.

134. Leung, D.; Abbenante, G.; Fairlie, D. P. Protease inhibitors: current status and future prospects. *J. Med. Chem.* **2000**, *43*, 305-341.

135. Levy, S. B.; Marshall, B. Antibacterial resistance worldwide: causes, challenges and responses. *Nat. Med.* **2004**, *10*, S122-S129.

136. Li, C.; Curreli, M.; Lin, H.; Lei, B.; Ishikawa, F. N.; Datar, R.; Cote, R. J.; Thompson, M. E.; Zhou, C. Complementary detection of protease-specific antigen using In_2O_3 nanowires and carbon nanotubes. *J. Am. Chem. Soc.* **2005**, *127*, 12484-12485.

137. Li, X.; Husson, S. M. Two-dimensional molecular imprinting approach to produce optical biosensor recognition elements. *Langmuir* **2006**, *22*, 9658-9663.

138. Li, Z.; Rajendran, B.; Kamins, T. I.; Li, X.; Chen, Y.; Williams, R. S. Silicon nanowires for sequence-specific DNA sensing: device fabrication and simulation. *Appl. Phys. A* **2005**, *80*, 1257-1263.

139. Li, Z.; Chen, Y.; Li, X.; Kamins, T. I.; Nauka, K.; Williams, R. S. Sequence-specific label-free DNA sensors based on silicon nanowires. *Nano Lett.* **2004**, *4*, 245-247.

140. Liley, M.; Keller, T. A.; Duschl, C.; Vogel, H. Direct observation of self-assembled monolayers, ion complexation, and protein conformation at the gold/water interface: an FTIR spectroscopic approach. *Langmuir* **1997**, *13*, 4190-4192.

141. Lin, I. H.; Meli, M. V.; Abbott, N. L. Ordering transitions in micrometer-thick films of nematic liquid crystals driven by self-assembly of ganglioside GM_1. *J. Colloid Interface Sci.* **2009**, *336*, 90-99.

142. Liu, C. F.; Tam, J. P. Peptide segment ligation strategy without use of protecting groups. *Proc. Natl. Acad. Sci. USA* **1994a**, *91*, 6584-6588.

143. Liu, C. F.; Tam, J. P. Chemical ligation approach to form a peptide bond between unprotected peptide segments. Concept and model study. *J. Am. Chem. Soc.* **1994b**, *116*, 4149-4153.

144. Liu, J.; Feng, X.; Fryxell, G. E.; Wang, L.-Q,; Kim, A. Y.; Gong, M. Hybrid mesoporous materials with functionalized monolayers. *Adv. Mater.* **1998**, *10*, 161-165.

145. Liu, A. C.; Chen, D. C.; Lin, C. C.; Chou, H. H.; Chen, C. H. Application of cysteine monolayers for electrochemical determination of sub-ppb copper (II). *Anal. Chem.* **1999a**, *71*, 1549-1552.

146. Liu, H. W.; Jiang, S. J.; Liu, S. H. Determination of cadmium, mercury and lead in seawater by electrothermal vaporization isotope dilution inductively coupled plasma mass spectrometry. *Spectrochim. Acta B* **1999b**, *54*, 1367-1375.

147. Liu, J.; Shin, Y.; Nie, Z.; Chang, J. H.; Wang, L. Q.; Fryxell, G. E.; Samuels, W. D.; Exarhos, G. J. Molecular assembly in ordered mesoporosity: a new class of highly functional nanoscale materials. *J. Phys. Chem. A* **2000**, *104*, 8328-8339.

148. Liu, G. ; Nguyen, Q. T. ; Chow, E. ; Böcking, T. ; Hibbert, D. B.; Gooding, J. J. Study of factors affecting the performance of voltammetric copper sensors based on Gly-Gly-His modified glassy carbon and gold electrodes. *Electroanalysis* **2006**, 1141-1151.

149. Lockwood, N. A.; Abbott, N. L. Self-assembly of surfactants and phosphlipids at interfaces between aqueous phases and thermotropic liquid crystals. *Curr. Opin. Colloid Interface Sci.* **2005**, *10*, 111-120.

150. Lockwood, N. A.; Cadwell, K. D.; Caruso, F. Abbott, N. L. Formation of polyelectrolyte multilayer films at interfaces between thermotropic liquid crystals and aqueous phases. *Adv. Mater.* **2006**, *18*, 850-854.

151. Lockwood, N. A.; Gupta, J. K.; Abbbott, N. L. Self-assembly of amphiphiles, polymers and proteins at interfaces between thermotropic liquid crystals and aqueous phases. *Surf. Sci. Rep.* **2008**, *63*, 255-293.

152. Loo, J. A.; Hu, P.; Smith, R. D. Interaction of angiotensin peptides and zinc metal ions probed by electrospray ionization mass spectrometry. *J. Am. Soc. Mass Spectrom.* **1994**, *5*, 959-965.

153. Lotierzo, M.; Henry, O. Y. F.; Piletsky, S.; Tothill, I.; Cullen, D.; Kania, M.; Hock, B.; Turner, A. P. F. Surface plasmon resonance sensor for domoic acid based on grafted imprinted polymer. *Biosens. Bioelectron.* **2004**, *20*, 145-152.

154. Love, J. C.; Estroff, L. A.; Kriebel, J. K.; Nuzzo, R. G.; Whitesides, G. M. Self-assembled monolayers of thiolates on metals as a form of nanotechnology. *Chem. Rev.* **2005**, *105*, 1103-1170.

155. Lu, Y. K.; Yan, X. P. An imprinted organic-inorganic hybrid sorbent for selective separation of cadmium from aqueous solution. *Anal. Chem.* **2004**, *76*, 453-457.

156. Lu, Y.; Liu, J. W.; Li, J.; Bruesehoff, P. J.; Pavot, C. M. B.; Brown, A. K. New highly sensitive and selective catalytic DNA biosensor for metal ions. *Biosens. Bioelectron.***2003**, *18*, 529-540.

157. Luk, Y. Y.; Tingey, M. L.; Dickson, K. A.; Raines, R. T.; Abbott, N. L. Imaging the binding ability of proteins immobilized on surfaces with different orientations by using liquid crystals. *J. Am. Chem. Soc.* **2004a**, *126*, 9024-9032.

158. Luk, Y. Y.; Yang, K. L.; Cadwell, K.; Abbott, N. L. Deciphering the interactions between liquid crystals and chemically functionalized surfaces: role of hydrogen bonding on orientations of liquid crystals. *Surface Science* **2004b**, *570*, 43-56.

159. MacBeath, G.; Schreiber, S. L. Printing proteins as microarrays for high-throughput function determination. *Science*, **2000**, *289*, 1760-1763.

160. Maeda, Y.; Higuchi, T.; Ikeda, I. Change in hydration state during the coil-globule transition of aqueous solutions of poly(*N*-isopropylacrylamide) as evidenced by FTIR spectroscopy. *Langmuir* **2000**, *16*, 7503-7509.

161. Major, R. C; Zhu, X. Y. The surface chelate effect. *J. Am. Chem. Soc.* **2003**, *125*, 8454-8455.

162. Markgren, P. O.; Hamalainen, M.; Danielson, U. H. Screening of compounds interacting with HIV-1 proteinase using optical biosensor technology. *Anal. Biochem.* **1998**, *265*, 340-350.

163. Martell, A. E.; Smith, R. M. *NIST standard reference database 46 version 8.0*, Gaithersburg, MD, USA.

164. Matsuno, H.; Niikura, K.; Okahata, Y. Design and characterization of asparagine- and lysine-containing alanine-based helical peptides that bind selectively to A•T base pairs of oligonucleotides immobilized on a 27 MHz quartz crystal microbalance. *Biochemistry* **2001**, *40*, 3615-3622.

165. Mejare, M.; Ljung, S.; Bulow, L. Selection of cadmium specific hexapeptides and their expression as OmpA fusion proteins in *Escherichia coli*. *Protein Eng.* **1998**, *11*, 489-494.

166. Meli, M. V.; Lin, I. H.; Abbott, N. L. Preparation of microscopic and planar oil-water interfaces that are decorated with prescribed densities of insoluble amphiphiles. *J. Am. Chem. Soc.* **2008**, *130*, 4326-4333.

167. Miller, A. W.; Robyt, J. F. Sodium cyanoborohydride in the immobilization of proteins to glutaraldehyde-activated aminoalkyl silica. *Biotechnology and Bioengineering* **1983**, *25*, 2795-2800.

168. Mirsky, V. M.; Hirsch, T.; Piletsky, S. A.; Wolfbeis, O. S. A spreader-bar approach to molecular architecture: formation of stable artificial chemoreceptors. *Angew. Chem. Int. Ed.* **1999**, *38*, 1108-1110.

169. Moffitt, C. E.; Wieliczka, D. M.; Yasuda, H. K. An XPS study of the elemental enrichment on aluminum alloy surfaces from chemical cleaning. *Surf. Coating Tech.* **2001**, *137*, 188-196.

170. Morales, A. M.; Lieber, C. M. A laser ablation method for the synthesis of crystalline semiconductor nanowires. *Science* **1998**, *279*, 208-211.

171. Mosbach, K. Molecular imprinting. *Trends Biochem. Sci.* **1994**, *19*, 9-14.

172. Moss, S. D.; Johnson, C. C.; Janata, J. Hydrogen, calcium, and potassium ion-sensitive FET transducers: a preliminary report. *IEEE Trans. Biomed. Eng.* **1978**, *25*, 49-54.

173. Munshi, N.; Chakarvorty, K.; De, T. K.; Maitra, A. N. Activity and stability studies of ultrafine nanoencapsulated catalase and penicillinase. *Colloid Polym. Sci.* **1995**, *273*, 464-472.

174. Nakanishi, K.; Muguruma, H.; Karube, I. A novel method of immobilizing antibodies on a quartz crystal microbalance using plasma-polymerized films for immunosensors. *Anal. Chem.* **1996**, *68*, 1695-1700.

175. Neff, P. A.; Serr, A.; Wunderlich, B. K.; Bausch, A. R. Label-free electrical determination of trypsin activity by a silicon-on-insulator based thin film resistor. *ChemPhysChem* **2007**, *8*, 2133-2137.

176. Nguyen, C. V.; Delzeit, L.; Cassell, A. M.; Li, J.; Han, J.; Meyyappan, M. Preparation of nucleic acid functionalized carbon nanotube arrays. *Nano Lett.* **2002**, *2*, 1079-1081.

177. Nielsen, P. E.; Egholm, M.; Berg, R. H.; Buchardt, O. Sequence-selective recognition of DNA by strand displacement with a thymine-substituted polyamide. *Science* **1991**, *254*, 1497-1500.

178. Niessen, W. M. A. *Liquid Chromatography-Mass Spectrometry, Chromatographic Science, V. 80, New York Marcel Dekker.* **1999**.

179. Niiler, E. Bioterrorism- biotechnology to the rescue? *Nat. Biotechnol.* **2002**, *20*, 21-25.

180. Nishimura, G.; Shiraishi, Y.; Hirai, T. A fluorescent chemosensor for wide-range pH detection. *Chem. Commun.* **2005**, 5313-5315.

181. Nishino, H.; Nihira, T.; Mori, T.; Okahata, Y. Direct monitoring of enzymatic glucan hydrolysis on a 27-MHz quartz-crystal microbalance. *J. Am. Chem. Soc.* **2004***, 126*, 2264-2265.

182. Novak, T. J.; Poziomek, E. J.; Mackay, R. A. Use of anisotropic materials as chemical detectors. *Anal. Lett.* **1972**, *5*, 187-192.

183. Oberg, K. A.; Fink, A. L. A new attenuated total reflectance fourier transform infrared spectroscopy method for the study of proteins in solution. *Anal. Biochem.* **1998**, *256*, 92-106.

184. Onodera, K.; Hirano-Iwata, A.; Miyamoto, K.; Kimura, Y.; Kataoka, M.; Shinohara, Y.; Niwano, M. Label-free detection of protein−protein interactions at the GaAs/water interface through surface infrared spectroscopy: discrimination between specific and nonspecific interactions by using secondary structure analysis. *Langmuir* **2007**, *23*, 12287-12292.

185. Page, M. I. The reactivity of β-lactams, the mechanism of catalysis and the inhibition of β-lactamases. *Curr. Pharm. Des.* **1999**, *5*, 895-913.

186. Park, J. S.; Teren, S.; Tepp, W. H.; Beebe, D. J.; Johnson, E. A.; Abbott, N. L. Formation of oligopeptide-based polymeric membranes at interfaces between aqueous phases and thermotropic liquid crystals. *Chem. Mater.* **2006**, *18*, 6147-6151.

187. Park, J. S.; Abbott, N. L. Ordering transitions in thermotropic liquid crystals induced by the interfacial assembly and enzymatic processing of oligopeptide amphiphiles. *Adv. Mater.* **2008**, *20*, 1185-1190.

188. Parsons, P. J.; Slavin, W. A rapid Zeeman graphite furnace atomic absorption spectrometric method for the determination of lead in blood. *Spectrochim. Acta B* **1993,** *48*, 925-939.

189. Patolsky, F.; Zheng, G.; Hayden, O.; Lakadamyali, M.; Zhuang, X.; Lieber, C. M. Electrical detection of single viruses. *Proc. Natl. Acad. Sci. USA* **2004,** *101*, 14017-14022.

190. Patolsky, F.; Zheng, G.; Lieber, C. M. Fabrication of silicon nanowire devices for ultrasensitive, lebel-free, real-time detection of biological and chemical species. *Nature Protocols* **2006a**, *1*, 1711-1724.

191. Patolsky, F.; Timko, B. P.; Yu, G.; Fang, Y.; Greytak, A. B.; Zheng, G.; Lieber, C. M. Detection, stimulation, and inhibition of neuronal signals with high density nanowire transistor arrays. *Science* **2006b**, *313*, 1100-1104.

192. Peelen, D.; Smith, L. M. Immobilization of amine-modified oligonucleotides on aldehyde-terminated alkanethiol monolayers on gold. *Langmuir* **2005**, *21*, 266-271.

193. Piletsky, S. A.; Piletskaya, E. V.; Elgersma, A.; Yano, K.; Karube, I.; Parhometz, Y. P.; El'skaya, A. V. Atrazine sensing by molecularly imprinted membranes. *Biosens. Bioelectron.* **1995**, *10*, 959-964.

194. Piletsky, S. A.; Piletskaya, E. V.; El'skaya, A. V.; Levi, R.; Yano, K.; Karube, I. Optical detection system for triazine based on molecularly-imprinted polymers. *Anal. Lett.* **1997**, *30*, 445-455.

195. Piletsky, S. A.; Piletskaya, E. V.; Panasyuk, T. L.; El'skaya, A. V.; Levi, R.; Karube, I.; Wulff, G. Imprinted membranes for sensor technology: opposite behavior of covalently and noncovalently imprinted membranes. *Macromolecules* **1998**, *31*, 2137-2140.

196. Piletsky, S. A.; Piletskaya, E. V.; Sergeyeva, T. A.; Panasyuk, T. L.; El'skaya, A. V. Molecularly imprinted self-assembled films with specificity to cholesterol. *Sens. Actuators B* **1999**, *60*, 216-220.

197. Pilloud, D. L.; Rabanal, F.; Gibney, B. R.; Farid, R. S.; Dutton, P. L.; Moser, C. C. Self-assembled monolayers of synthetic hemoproteins on silanized quartz. *J. Phys. Chem. B* **1998**, *102*, 1926-1937.

198. Potyrailo, R. A.; Conrad, R. C.; Ellington, A. D.; Hieftje, G. M. Adapting selected nucleic acid ligands (aptamers) to biosensors. *Anal. Chem.* **1998**, *70*, 3419-3425.

199. Poziomek, E. J.; Novak, T. J.; Mackay, R. A. Use of liquid crystals as vapor detectors. *Mol. Cryst. Liq. Cryst.* **1973**, *27*, 175-185.

200. Prestrelski, S. J.; Byler, D. M.; Liebman, M. N. Comparison of various molecular forms of bovine trypsin: correlation of infrared spectra with x-ray crystal structures. *Biochemistry* **1991**, *30*, 133-143.

201. Prestrelski, S. J.; Arakawa, T.; Kenney, W. C.; Byler, D. M. The secondary structure of two recombinant human growth factors, platelet-derived growth factor and basic fibroblast growth factor, as determined by fourier-transform infrared spectroscopy. *Arch. Biochem. Biophys.* **1991**, *285*, 111-115.

202. Price, A. D.; Schwartz, D. K. DNA hybridization-induced reorientation of liquid crystal anchoring at the nematic liquid crystal/aqueous interface. *J. Am. Chem. Soc.* **2008**, *130*, 8188-8194.

203. Ramström, O.; Ye, L.; Mosbach, K. Artificial antibodies to corticosteroids prepared by molecular imprinting. *Chemistry & Biology* **1996**, *3*, 471-477.

204. Rich, R. L., Myszka, D. G. Advances in surface plasmon resonance biosensor analysis. *Curr. Opin. Biotechnol.* **2000**, *11*, 54-61.

205. Rigler, P.; Ulrich, W. P.; Vogel, H. Controlled immobilization of membrane proteins to surfaces for fourier transform infrared investigations. *Langmuir* **2004**, *20*, 7901-7903.

206. Rigler, P.; Ulrich, W.-P.; Hoffmann, P.; Mayer, M.; Vogel, H. Reversible immobilization of peptides: surface modification and in situ detection by attenuated total reflection FTIR spectroscopy. *ChemPhysChem* **2003**, *4*, 268-275.

207. Risveden, K.; Pontén, J. F.; Calander, N.; Willander, M.; Danielsson, B. The region ion sensitive field effect transistor, a novel bioelectronic nanosensor. *Biosens. Bioelectron.* **2007**, *22*, 3105-3112.

208. Sagiv, J. Organized monolayers by adsorption. 1. Formation and structure of oleophobic mixed monolayers on solid surfaces. *J. Am. Chem. Soc.* **1980**, *102*, 92-98.

209. Salisbury, C. M.; Maly, D. J.; Ellman, J. A. Peptide microarrays for the determination of protease substrate specificity. *J. Am. Chem. Soc.* **2002**, *124*, 14868-14870.

210. Sambrook, J.; Fritsch, E. F.; Maniatis, T. *Molecular Cloning*: Cold Spring Harbor Laboratory Press: New York, **1989**.

211. Sanna, D.; Micera, G.; Kállay, C.; Rigó, V.; Sóvágó, I. Copper (II) complexes of N-terminal protected tri- and tetra-peptides containing histidine residues. *Dalton Trans.* **2004**, 2702-2707.

212. Sasaki, Y. C.; Yasuda, K.; Suzuki, Y.; Ishibashi, T.; Satoh, I.; Fujiki, Y.; Ishiwata, S. Two-dimensional arrangement of a functional protein by cysteine-gold interaction: enzyme activity and characterization of a protein monolayer on a gold substrate. *Biophys. J.* **1997**, *72*, 1842-1848.

213. Schickaneder, E.; Hosel, W.; Eltz, H. v. d.; Geuβ, U. Casein-resorufon, a new substrate for a highly sensitive protease. *Fresenius Z Anal. Chem.* **1988**, *330*, 360.

214. Schulze, W. X.; Mann, M. A novel proteomic screen for peptide-protein interactions. *J. Biol. Chem.* **2004**, *279*, 10756-10764.

215. Shults, M. D.; Pearce, D. A.; Imperiali, B. Modular and tunable chemosensor scaffold for divalent zinc. *J. Am. Chem. Soc.* **2003**, *125*, 10591-10597.

216. Schutkowski, M.; Reimer, U.; Panse, S.; Dong, L.; Lizcano, J. M.; Alessi, D. R.; Schneider-Mergener, J. High-content peptide microarrays for deciphering kinase specificity and biology. *Angew. Chem. Int. Ed.* **2004**, *43*, 2671-2674.

217. Sehgal, D.; Vijay, I. K. A method for the high efficiency of water-soluble carbodiimide-mediated amidation. *Anal. Biochem.* **1994**, *218*, 87-91.

218. Seker, F.; Meeker, K.; Kuech, T. F.; Ellis, A. B. Surface chemistry of prototypical bulk II-IV and III-V semiconductors and implications for chemical sensing. *Chem. Rev.* **2000**, *100*, 2505-2536.

219. Seong, S. Y.; Choi, C. Y. Current status of protein chip development in terms of fabrication and application. *Proteomics* **2003**, *3*, 2176-2189.

220. Shah, R. R. Abbott, N. L. Principles for measurement of chemical exposure based on recognition-driven anchoring transitions in liquid crystals. *Science* **2001**, *293*, 1296-1299.

221. Shah, R. R.; Abbott, N. L. Using liquid crystals to image reactants and products of acid-base reactions on surfaces with micrometer resolution. *J. Am. Chem. Soc.* **1999**, *121*, 11300-11310.

222. Shao, J.; Tam, J. P. Unprotected peptides as building blocks for the synthesis of peptide dendrimers with oxime, hydrazone, and thiazolidine linkages. *J. Am. Chem. Soc.* **1995**, *117*, 3893-3899.

223. Shen, Z.; Stryker, G. A.; Mernaugh, R. L.; Yu, L.; Yan, H.; Zeng, X. Single-chain fragment variable antibody piezoimmunosensors. *Anal. Chem.* **2005**, *77*, 797-805.

224. Sigel, H.; Martin, R. B. Coordinating properties of the amide bond. Stability and structure of metal ion complexes of peptides and related ligands. *Chem. Rev.* **1982**, *82*, 385-426.

225. Soellner, M. B.; Dickson, K. A.; Nilsson, B. L.; Raines, R. T. Site-specific protein immobilization by Staudinger ligation. *J. Am. Chem. Soc.* **2003**, *125*, 11790-11791.

226. Soellner, M. B.; Nilsson, B. L.; Raines, R. T. Reaction mechanism and kinetics of the traceless Staudinger ligation. *J. Am. Chem. Soc.* **2006**, *128*, 8820-8828.

227. Spencer, R. D.; Toledo, F. B.; Williams, B. T.; Yoss, N. L. Design, construction, and two applications for an automated flow-cell polarization fluorometer with digital read out: enzyme-inhibitor (antitrypsin) assay and antigen-antibody (insulin-insulin antiserum) assay. *Clin. Chem.* **1973**, *19*, 838-844.

228. Spetzler, J. C.; Tam, J. P. Unprotected peptides as building blocks for branched peptides and peptide dendrimers. *Int. J. Pept. Protein Res.* **1995**, *45*, 78-85.

229. Stadler, K.; Masignani, V.; Eickmann, M.; Becker, S.; Abrignani, S.; Klenk, H. D.; Rappuoli, R. SARS-beginning to understand a new virus. *Nat. Rev. Microbiol.* **2003**, *1*, 209-218.

230. Stern, E.; Klemic, J. F.; Routenberg, D. A.; Wyrembak, P. N.; Turner-Evans, D. B.; Hamilton, A. D.; LaVan, D. A.; Fahmy, T. M.; Reed, M. A. Label-free immunodetection with CMOS-compatible semiconducting nanowires. *Nature* **2007**, *445*, 519-522.

231. Stefan, I. C.; Scherson, D. A. Attenuated total reflection infrared studies of bilayers self-assembled onto a germanium prism. *Langmuir* **2000**, *16*, 5945-5948.

232. Surewicz, W. K.; Mantsch, H. H.; Chapman, D. Determination of protein secondary structure by fourier transform infrared spectroscopy: a critical assessment. *Biochemistry* **1993**, *32*, 389-394.

233. Tahan, J. E.; Granadillo, V. A.; Romero, R. A. Electrothermal atomic absorption spectrometric determination of Al, Cu, Fe, Pb, V and Zn in clinical samples and in certified environmental reference materials. *Anal. Chim. Acta* **1994**, *295*, 187-197.

234. Takehara, K.; Aihara, M.; Ueda, N. An ion-gate response of a glutathione monolayer assembly highly sensitive to lanthanide ions. *Electroanalysis* **1994**, *6*, 1083-1086.

235. Tans, S. J.; Verschueren, A. R. M.; Dekker, C. Room-temperature transistor based on a single carbon nanotube. *Nature* **1998**, *393*, 49-52.

236. Thompson, R. B.; Ge, Z.; Patchan, M.; Huang, C. C.; Fierke, C. A. Fiber optic biosensor for Co(II) and Cu(II) based on fluorescence energy transfer with an enzyme transducer. *Biosens. Bioelectron.* **1996**, *11*, 557-564.

237. Tingey, M. L.; Snodgrass, E. J.; Abbott, N. L. Patterned orientations of liquid crystals on affinity microcontact printed proteins. *Adv. Mater.* **2004**, *16*, 1331-1336.

238. Twining, S. S. Fluorscein isothiocyanate-labeled casein assay for proteolytic enzymes. *Anal. Biochem.* **1984**, *143*, 30-34.

239. Varnagy, K.; Szabo, J.; Sovago, I.; Malandrinos, G.; Hadjiliadis, N.; Sanna, D.; Micera, G. Equilibrium and structural studies on copper (II) complexes of tetra-, penta- and hexa-peptides containing histidyl residues at the C-termini. *Dalton Trans.* **2000**, 467-472.

240. Vassar, R.; Bennett, B. D.; Babu-Kahn, S.; Kahn, S.; Mendiaz, E. A.; Denis, P.; Teplow, D. B.; Ross, S.; Amarante, P.; Loeloff, R.; Luo, Y.; Fisher, S.; Fuller, J.; Edenson, S.; Lile, J.; Jarosinski, M. A.; Biere, A. L.; Curran, E.; Burgess, T.; Louis, J. C.; Collins, F.; Treanor, J.; Rogers, G.; Citron, M. β-secretase cleavage of Alzheimer's amyloid precursor protein by the transmembrane aspartic protease BACE. *Science* **1999**, *286*, 735-741.

241. Vezenov, D. V.; Noy, A.; Rozsnyai, L. F.; Lieber, C. M. Force titrations and ionization state sensitive imaging of functional groups in aqueous solutions by chemical force microscopy. *J. Am. Chem. Soc.* **1997**, *119*, 2006-2015.

242. Vlatakis, G.; Andersson, L. I.; Muller, R. Mosbach, K. Drug assay using antibody mimics made by molecular imprinting. *Nature* **1993**, *361*, 645-647.

243. Voet, D.; Voet, J. G.; Pratt, C. W. *Fundamentals of Biochemistry*, Wiely: New York, **1999**.

244. Walsh, C. Molecular mechanisms that confer antibacterial drug resistance. *Nature* **2000**, *406*, 775-781.

245. Wang, H. Y.; Kobayashi, T.; Fukaya, T.; Fujii, N. Molecular imprint membranes prepared by the phase inversion precipitation technique. 2. Influence of coagulation temperature in the phase inversion process on the encoding in polymeric membranes. *Langmuir* **1997**, *13*, 5396-5400.

246. Wang, M.; Scott, W. A.; Rao, K. R.; Udey, J.; Conner, G. E.; Brew, K. Recombinant bovine α-lactalbumin obtained by limited proteolysis of a fusion protein expressed at high levels in *Escherichia coli*. *J. Biol. Chem.* **1989**, *264*, 21116-21121.

247. Wang, J.; Palecek, E.; Nielsen, P. E.; Rivas, G.; Cai, X.; Shiraishi, H.; Dontha, N.; Luo, D.; Farias, P. A. M. Peptide nucleic acid probes for sequence-specific DNA biosensors. *J. Am. Chem. Soc.* **1996,** *118*, 7667-7670.

248. Wang, J.; Luthey-Schulten, Z. A.; Suslick, K. S. Is the olfactory receptor a metalloprotein? *Proc. Natl. Acad. Sci. USA* **2003**, *100*, 3035-3039.

249. Wang, W. U.; Chen, C.; Lin, K.; Fang, Y.; Lieber, C. M. Label-free detection of small-molecule-protein interactions by using nanowire nanosensors. *Proc. Natl. Acad. Sci. U.S.A.* **2005**, *102*, 3208-3212.

250. Welty, J. R.; Wicks, C. E.; Wilson, R. E.; Rorrer, G. Fundamentals of momentum, heat, and mass transfer. John Wiley & Son, USA, **2000**.

251. West, M. L.; Fairlie, D. P. Targeting HIV-1 protease: a test of drug-design methodologies. *Trends Pharmacol. Sci.* **1995**, *16*, 67-75.

252. Wilder, C. L.; Friedrich, A. D.; Potts, R. O.; Daumy, G. O.; Francoeur, M. L. Secondary structural analysis of two recombinant murine proteins, interleukins 1α and 1β: Is infrared spectroscopy sufficient to assign structure? *Biochemistry* **1992**, *31*, 27-31.

253. Winterbottom, D. A.; Narayanaswamy, R.; Raimundo Jr., I. M. Cholesteric liquid crystals for detection of organic vapours. *Sens. Actuators B* **2003**, *90*, 52-57.

254. Wlodawer, A.; Erickson, J. W. Structure-based inhibitors of HIV-1 protease. *Annu. Rev. Biochem.* **1993**, *62*, 543-585.

255. Wulff, G. Molecular imprinting in cross-linked materials with the aid of molecular templates- a way towards artificial antibodies. *Angew. Chem. Int. Ed. Engl.* **1995**, *34*, 1812-1832.

256. Wulff, G. Enzyme-like catalysis by molecularly imprinted polymers. *Chem. Rev.* **2002**, *102,* 1-28.

257. Yamaguchi, A.; Hirata, T.; Sawai, T. Kinetic studies on inactivation of *citrobacter freundii* cephalosporinase by sulbactam. *Antimicrob. Agents Chemother.* **1983**, *24*, 23-30.

258. Yan, S.; Sameni, M.; Sloane, B. F. Cathepsin B and human tumor progression. *Biol. Chem.* **1998**, *379*, 113-125.

259. Yang, W.; Gooding, J. J.; Hibbert, D. B. Redoc voltammetry of sub-parts per billion levels of Cu^{2+} at polyaspartate-modified gold electrodes. *Analyst* **2001a**, *126*, 1573-1577.

260. Yang, W. R.; Jaramillo, D.; Gooding, J. J; Hibbert, D. B.; Zhang, R.; Willett, G. D.; Fisher, K. J. Sub-ppt detection limits for copper ions with Gly-Gly-His modified electrodes. *Chem. Commun.* **2001b**, 1982-1983.

261. Yang, W. R.; Chow, E.; Willett, G. D.; Hibbert, D. B.; Gooding, J. J. Exploring the use of the tripeptide Gly-Gly-His as a selective recognition element for the fabrication of electrochemical copper sensors. *Analyst* **2003**, *128*, 712-718.

262. Yang, H. H.; Zhang, S. Q.; Tan, F.; Zhuang, Z. X.; Wang. X. R. Surface molecularly imprinted nanowires for biorecognition. *J. Am. Chem. Soc.* **2005a**, *127*, 1378-1379.

263. Yang, W. R.; Hibbert, D. B.; Zhang, R.; Willett, G. D.; Gooding, J. J. Stepwise synthesis of Gly-Gly-His on gold surfaces modified with mixed self-assembled monolayers. *Langmuir*, **2005b**, *21*, 260-265.

264. Yang, K. L.; Cadwell, K.; Abbott, N. L. Use of self-assembled monolayers, metal ions, and smectic liquid crystals to detect organophosphonates. *Sens. Actuators B* **2005c**, *104*, 50-56.

265. Yang, H. ; Pritzker, M. ; Fung, S. Y. ; Sheng, Y. ; Wang, W. ; Chen, P. Anion effect on the nanostructure of a metal ion binding self-assembling peptide. *Langmuir* **2006**, *22*, 8553-8562.

266. Zammatteo, N.; Jeanmart, L.; Hamels, S.; Courtois, S.; Louette, P.; Hevesi, L.; Remacle, J. Comparison between different strategies of covalent attachment of DNA to glass surfaces to build DNA microarrays. *Anal. Biochem.* **2000**, *280*, 143-150.

267. Zatsepin, T. S.; Stetsenko, D. A.; Arzumanov, A. A.; Romanova, E. A.; Gait, M. J.; Oretskaya, T. S. Synthesis of peptide-oligonucleotide conjugates with single and multiple peptides attached to 2'-aldehydes through thiazolidine, oxime, and hydrazine linkages. *Bioconjugate Chem.* **2002**, *13*, 822-830.

268. Zemel, J. N. Ion-sensitive field effect transistors and related devices. *Anal. Chem.* **1975**, *47*, 255A-268A.

269. Zhang, G. J.; Zhang, G.; Chua, J. H.; Chee, R. E.; Wong, E. H.; Agarwal, A.; Buddharaju, K. D.; Singh, N.; Gao, Z.; Balasubramanian, N. DNA sensing by silicon nanowire: charge layer distance dependence. *Nano Lett.* **2008**, *8*, 1066-1070.

270. Zhang, J.; Yan, Y. B. Probing conformational changes of proteins by quantitative second-derivative infrared spectroscopy. *Anal. Biochem.* **2005**, 340, 89-98.

271. Zheng, G.; Patolsky, F.; Cui, Y.; Wang, W. U.; Lieber, C. M. Multiplexed electrical detection of cancer markers with nanowire sensor arrays. *Nat. Biotechnol.* **2005**, *23*, 1294-1301.

272. Zhu, H.; Klemic, J. F.; Chang, S.; Bertone, P.; Casamayor, A.; Klemic, K. G.; Smith, D.; Gerstein, M.; Reed, M. A., Snyder, M. Analysis of yeast protein kinases using protein chips. *Nat. Genet.* **2000**, *26*, 283-289.

273. Zhu, H.; Bilgin, M.; Bangham, R.; Hall, D.; Casamayor, A.; Bertine, P.; Lan, N.; Jansen, R.; Bidlingmaier, S,; Houfek, T.; Mitchell, T.; Miller, P.; Dean, R. A.; Gerstein, M.; Snyder, M. Global analysis of protein activities using proteome chips. *Science* **2001**, *293*, 2101-2105.

274. Zimmerman, S. C.; Lemcoff, N. G. Synthetic hosts *via* molecular imprinting-are universal synthetic antibodies realistically possible? *Chem. Commun.* **2004**, 5-14.

LIST OF PUBLICATIONS

1. **Xinyan Bi**, Kun-Lin Yang, "Immobilization of oligoglycines on aldehyde-decorated surfaces and its influence on the orientations of liquid crystals", *Colloids Surf. A* **2007**, *302***,** 573-580**.**

2. **Xinyan Bi**, Shisheng Huang, Deny Hartono, Kun-Lin Yang, "Liquid-crystal based optical sensors for simultaneous detection of multiple glycine oligomers with micromolar concentrations" *Sens. Actuators B* **2007**, *127*, 406-413.

3. **Xinyan Bi**, Rong Jia Lau, Kun-Lin Yang, "Preparation of ion-imprinted silica gel functionalized with glycine, diglycine and triglycine and their adsorption properties for copper ions" *Langmuir* **2007**, *23*, 8079-8086.

4. **Xinyan Bi**, Kun-Lin Yang, "Complexation of copper ions with histidine-containing tripeptides immobilized on solid surfaces" *Langmuir* **2007**, *23*, 11067-11073.

5. **Xinyan Bi**, Kun-Lin Yang, "A principle of detecting and differentiating dialdehydes from monoaldehydes by using surface reactions and Liquid Crystals" *J. Phys. Chem. C* **2008**, *112*, 1748-1750.

6. **Xinyan Bi**, Wan Ling Wong, Wenjun Ji, Ajay Agarwal, N. Balasubramanian, Kun-Lin Yang, "Development of electrochemical calcium sensors by using silicon nanowires modified with phosphotyrosine" *Biosens. Bioelectron.* **2008**, *23*, 1442-1448.

7. **Xinyan Bi**, Deny Hartono, Kun-Lin Yang, "Controlling orientations of immobilized oligopeptides using N-terminal cysteine labels" *Langmuir* **2008**, *24*, 5238-5240.

8. **Xinyan Bi**, Chee Hua Heng, Kun-Lin Yang, "A method of obtaining high selectivity for copper ions on triglycine decorated surfaces" *J. Phys. Chem. C* **2008**, *112*, 12887-12893.

9. **Xinyan Bi**, Kun-Lin Yang, "Real-time liquid crystal based glutaraldehyde sensor" *Sens. Actuators B* **2008**, *134*, 432-437.

10. **Xinyan Bi**, Ajay Agarwal, N. Balasubramanian, Kun-Lin Yang, "Tripeptide-modified silicon nanowire based field-effect transistors as real-time copper ion sensors" *Electrochem. Commun.* **2008**, *10*, 1868-1871.

11. **Xinyan Bi**, Kun-Lin Yang, "On-line monitoring imidacloprid and thiacloprid in celery juice using quartz crystal microbalance" *Anal. Chem.* **2009**, *81*, 527-532.

12. **Xinyan Bi,** Huan Xu, Siok Lian Lai, Kun-Lin Yang, "Bifunctional oligo(ethylene glycol) decorated surfaces which permit covalent protein immobilization and resistance to protein adsorption" *Biofouling* **2009**, *25*, 435-444.

13. **Xinyan Bi**, Ajay Agarwal, Kun-Lin Yang, "Oligopeptide-modified silicon nanowire arrays as multichannel metal ion sensors" *Biosens. Bioelectron.* **2009**, *24*, 3248-3251.

14. **Xinyan Bi**, Siok Lian Lai, Kun-Lin Yang, "Liquid crystal multiplexed protease assays reporting enzymatic activities as optical bar charts" *Anal. Chem.* **2009**, *81*, 5503-5509.

15. **Xinyan Bi**, Deny Hartono, Kun-Lin Yang, “Real-time liquid crystal pH sensor for monitoring enzymatic activities of penicillinase” *Adv. Funct. Mater.* **2009**, *19*, 3760-3765.

16. **Xinyan Bi**, Kun-Lin Yang, “Liquid crystals decorated with linear oligopeptide FLAG for applications in immunobiosensors” *Biosens. Bioelectron.* **2010**, accepted.

17. Deny Hartono, **Xinyan Bi**, Kun-Lin Yang, Lin-Yue Lanry Yung, “An air-supported liquid crystal system for real-time and label-free characterization of phospholipases and their inhibitors” *Adv. Funct. Mater.* **2008**, *18*, 2938-2945.

18. Huan Xu, **Xinyan Bi**, Xuanming Ngo, Kun-Lin Yang, “Principles of detecting vaporous thiols using liquid crystals and metal ion microarrays” *Analyst*, **2009**, *134*, 911-915.

19. Siok Lian Lai, Shisheng Huang, **Xinyan Bi**, Kun-Lin Yang, “Optical imaging of surface immobilized oligonucleotide probes on DNA microarrays using liquid crystals” *Langmuir*, **2009**, *25*, 311-316.

20. Yadong Wang, Shook Hui Goh, **Xinyan Bi**, Kun-Lin Yang, “Replication of DNA submicron arrays by combining nanoimprint lithography and contact printing” *J. Colloid Interface Sci.*, **2009**, *333*, 188-194.

21. Kun-Lin Yang, **Xinyan Bi** “Transparent polymer films that change colors upon exposure to hydrogen sulfide” US patent 61018736.